

ABSTRACT

Title of Dissertation: LIPOPHILIC G-QUADRUPLEXES: STRUCTURAL STUDIES, POST-ASSEMBLY MODIFICATION, AND COVALENT CAPTURE.

Mark Steven Kaucher, Doctor of Philosophy, 2006

Dissertation directed by: Professor Jeffery T. Davis
Department of Chemistry and Biochemistry

New nanostructures and functional materials are built through the self-assembly of guanosine. Both the size and regiochemistry of these noncovalent structures are controlled. Lipophilic G-quadruplexes are further stabilized through covalent capture techniques. These new nanostructures demonstrate the ability to bind cations and transport monovalent cation through phospholipid membranes.

Diffusion NMR is demonstrated as a valuable technique in characterizing the size

of lipophilic G-quadruplexes. Control over the size of self-assembled G-quadruplexes is demonstrated through modifying the guanosine nucleosides and the cation concentration. The solution structure of $[G \mathbf{8}]_{16} \cdot 4K^+ \cdot 4pic^-$ is determined to be a hexadecamer using diffusion NMR. Additionally, G **24** is also shown to form a hexadecamer G-quadruplex, which has an octameric intermediate structure. Two different octamers, a singly and doubly charged octamer, formed by G **29** are elucidated by diffusion NMR. The information gained from the diffusion NMR technique allowed for a better understanding of the self-assembly processes, especially regarding the roles of cation, anion and solvent.

The use of a kinetically controlled exchange reaction to effect regioselective modification of a hydrogen-bonded assembly is discussed. The pseudo-regioselective exchange of isotopically labeled G **35-d** into $[G \mathbf{8-h}]_{16} \cdot 4K^+ \cdot 4pic^-$ is demonstrated. Both the bound anion and cation can control the exchange of ligand into the different layers of a synthetic G-quadruplex. This regioselective exchange process allows for functionalized G-quadruplex structures to be built.

Covalent capture of lipophilic G-quadruplex **60** with reactive groups on the periphery generates a unimolecular G-quadruplex **61**. This unimolecular G-quadruplex **61** shows exceptional stability in nonpolar and polar solvents, even without the presence of cations. Furthermore, this unimolecular G-quadruplex transports monovalent cation across phospholipid membranes. The design of transmembrane transporters is of particular interest for their potential as new ion sensors, catalysts and anti-microbial agents.

LIPOPHILIC G-QUADRUPLEXES: STRUCTURAL STUDIES, POST-ASSEMBLY
MODIFICATION, AND COVALENT CAPTURE.

by

Mark Steven Kaucher

Dissertation submitted to the Faculty of the Graduate School of the
University of Maryland, College Park in partial fulfillment
of the requirements for the degree of
Doctor of Philosophy
2006

Advisory Committee:

Professor Jeffery T. Davis, Chair
Professor Kyu Y. Choi
Professor Bryan W. Eichhorn
Professor Daniel E. Falvey,
Associate Professor Lyle Isaacs

© Copyright by

Mark Steven Kaucher

2006

DEDICATION

To Mom, Dad, Grandmom, Michael, and Kevin for all of their support over the years. Thank you.

ACKNOWLEDGEMENTS

First, I would like to thank Prof. Jeffery T. Davis for not only teaching, helping and working with me so closely over the years but also for giving me the freedom and support to investigate new strategies and problems in my research. This wouldn't be possible without him, thank you. I would also like to thank Prof. Lyle Isaacs for helpful suggestions in chemistry and my future. Moreover, his class on supramolecular chemistry was one of the most interesting and inspirational classes I have taken throughout my academic career. I would also like to thank Profs. Bryan Eichhorn, Steven Rokita, Daniel E. Falvey, Kyu Y. Choi, Phil DeShong, and Ashton Cropp for helpful discussions and suggestions.

I am also very grateful for the help of Dr. Yiu-Fai Lam and Dr. Yinde Wang for their training, help, and discussions on NMR spectroscopy. In particular, Yiu-Fai helped by working with me on to set up new experiments and teaching me new techniques. He taught me more about NMR spectroscopy than I would have ever imagined. Thank you.

I would also like to acknowledge Noel Whittaker for teaching me both electrospray and MALDI mass spectrometry. I am also grateful for Dr. Jim Fettingner for working on crystal structures.

I would also like to thank the Davis research group. I especially want to thank Dr. Frank Kotch for helping me start off my Ph.D. career and acting as a second advisor in my first year and for helping me with future decisions. Thank you. I would also like to thank fellow graduate students: Jenny Kuebler for helping me out and teaching me new techniques, Ma Ling for being so kind, Sofya Berezin for helping me with physical

chemistry questions, William Harrell for helpful discussions, and Oluyomi Okunola for helping me with general chemistry questions. I am also grateful for Dr. Paul Santacrose for guiding me through chemistry problems, teaching me new techniques, and helpful discussions. I would also like to thank undergraduates I also had the pleasure of working with: Hojun Li and Kevan Salimian for helpful discussions, Maura Iezza and Bryna Clover for help with my first paper, and Kristen Roskov and Tanya Weerakkody for synthesis work.

I would also like to thank the many international groups I also had the pleasure of working and publishing with: the Gottarelli group in Italy, the Cohen group in Israel, the Reinhoudt group in the Netherlands, and the Rivera group in Puerto Rico. In particular, I would like to thank Marilyn Garcia from the Rivera group for working with me and teaching me how to perform molecular modeling calculations on G-quadruplex crystal structures.

I would also like to thank fellow classmates and friends that made my first graduate school year fun: Mathew Harney, Albert Epshteyn, Emily Weinert, and Amy Finch. In particular, I would like to thank Steven Polansky for both helpful suggestions and for always letting me into the CD room.

I would also like to thank my closest friends (Sean Hill, Charles Catalano, Jeremy Wick, Kevin Kaucher, Sara Finley, Mike Paxson, and Melissa Matonis) for their friendship and relaxing talks. Thank you.

I am very grateful to Yma Castillo for not only being a supportive friend but also for being a more amazing girlfriend. Thank you. I love you.

Lastly, I would like to thank my family again. My parents, grandparents, and

brothers for their support. Mom and Dad for always being supportive and for always giving advice. Grandmom for all the work and help she's done for me. Kevin for being a friend and helping me out when I needed it. Mike for always giving me advice and offering his help. Thank you, I love you all!

TABLE OF CONTENTS

LIST OF TABLES	x
LIST OF FIGURES	xi
LIST OF SCHEMES.....	xxv
LIST OF EQUATIONS	xxviii
Chapter 1. The G-Quadruplex in Nanostructures and Biomaterials	1
1.1 Introduction.....	1
1.2 Thesis Organization	1
1.3 Guanine is a Building Block for Diverse Assemblies	2
1.4 Guanosine Forms Self-Assembled Cyclic Structures – G-Quartets	5
1.5 G-rich DNA and RNA Regions Form G-quadruplex Structures.....	6
1.6 Self-Assembly of Lipophilic Guanosine Analogs.	9
1.6.1 Guanosine Self-Assemble in Nonpolar Solvents.....	9
1.6.2 Enantiomeric Self-Association of Lipophilic Nucleosides.....	13
1.6.3 “Empty” G-Quartets.....	15
1.6.4 Increasing the Number of Hydrogen Bonds in a G-quartet.	18
1.6.5 The G-Quartet and Dynamic Covalent Chemistry.....	19
1.7 Biosensors and Nanostructures Based on DNA G-Quadruplex Structures.	25
1.7.1 Potassium Ion Sensors.	25
1.7.2 G-Quadruplexes as Optical Sensors for Proteins.....	31
1.7.3 G-Quadruplexes in the Electrochemical Detection of Proteins.	38
1.7.4 Biosensors for Nucleic Acids.....	41

1.7.5 The Use of G-Quadruplexes in Building Nanomachines.....	42
1.7.6 New G-Quadruplex Structures from Synthetic DNA Analogs.....	44
1.8 Summary of the G-Quadruplex as a Scaffold in Nanostructures and Biomaterials	51
Chapter 2. Pulsed Field Gradient NMR Helps Determine the Solution Structure of Lipophilic G-Quadruplexes.	52
2.1 Introduction.....	52
2.2 PFG-NMR Theory	54
2.3 Diffusion NMR Confirms Hexadecamer in Solution.	62
2.4 Evidence for Cooperativity.....	68
2.5 PFG-NMR Shows Octameric Intermediate.	70
2.6 Investigations on Different Octamer Species	77
2.7 Conclusion	85
Chapter 3. Regioselective Ligand Exchange	87
3.1 Introduction.....	87
3.2 Isotopomer Formation.....	89
3.2.1 Subunit Exchange into the Outer Layer.....	91
3.2.2 Stabilization of the Inner G-Quartet Layer by the Anion.	94
3.2.3 Stabilization of the Inner Layer G-Quartet by the Cation.....	96
3.2.4 Destabilization of the Outer G-quartet Layer by Small Molecules	100
3.3 Regioselective Exchange of Different Subunits.	103
3.3.1 Amphiphilic G-Quadruplex Formation.....	108
3.4 Conclusion	109

Chapter 4. Covalent Capture Leads To Synthetic Na⁺ Transmembrane Transporters.	110
4.1 Introduction.....	110
4.1.1 The G-quartet Motif as a Scaffold for Transmembrane Transporters.	111
4.2 Covalent Capture Strategies.....	116
4.3 Attempts to Covalently Capture a G-quartet.	118
4.4 Covalent Capture Yields a Unimolecular G-Quadruplex.	126
4.4.1 Formation of Noncovalent G-quadruplex Formation 60	129
4.4.2 Olefin Metathesis Yields Unimolecular G-Quadruplex 61	132
4.4.3 Extending the Linker Arms on the Noncovalent G-Quadruplex Does Not Produce a Unimolecular G-quadruplex.	138
4.4.4 Unimolecular G-Quadruplex 61 is More Stable than the Noncovalent G- Quadruplex 60	143
4.4.5 Unimolecular G-quadruplex 61 is a Transmembrane Na ⁺ Transporter	151
4.4.6 Unimolecular G-quadruplex Transports Li ⁺ and K ⁺ Across EYPC Liposomes.	154
4.5 Conclusion	156
 Chapter 5. Future Directions	 158
 Chapter 6. Experimental and References.	 162
6.1 General Experimental	162
6.2 Synthesis	163
6.3 ESI-MS Experiments on G 29	178
6.4 PFG-NMR Experiments.	178

6.5 Determination of DNP Anion Exchange Rates.	181
6.7 HPTS Assay.....	182
6.8 DMF-d ₇ Folding-Unfolding Experiments on Unimolecular G-quadruplex 61 . ..	183
6.9 ²³ Na NMR Experiments.....	183
References	185

LIST OF TABLES

Table 2.1. Diffusion Coefficients for G 8 Hexadecamer/Monomer System.....	67
Table 2.2. Diffusion Coefficients for G 24 Octamer/Hexadecamer System.....	75
Table 2.3. Diffusion Coefficients for G 29 Octamer/Octamer System.....	82
Table 4.1. Diffusion Coefficients for G-quadruplex 60	132
Table 4.2. Diffusion Coefficients for G-quadruplex 61	136

LIST OF FIGURES

Figure 1.1. a) G-quartet contains four hydrogen bonded guanine bases and b) ion channel embedded in a phospholipid membrane.	2
Figure 1.2. Natural nucleobases.	3
Figure 1.3. Depiction of the Watson-Crick edges and Hoogsteen edges of guanine 2	4
Figure 1.4. Self-assembled structures of guanine: a) ribbon with a dipole, b) ribbon with no dipole, and c) cyclic tetramer (G-quartet).	4
Figure 1.5. Depiction of the G-quadruplex cylinder formed by the self-assembly of 5'-GMP 6	6
Figure 1.6. Examples of nucleic acid G-quadruplexes: a) unimolecular, b) edgewise loop bimolecular, c) diagonal loop bimolecular, and d) parallel tetraplex. Gray rectangles represent G-quartets, while the lines represent the phosphate backbone.	6
Figure 1.7. Examples of binding sites that are targeted by telomerase inhibitors.	7
Figure 1.8. Schematic of the thrombin binding aptamer (TBA).	9
Figure 1.9. Lipophilic [dG 7] ₈ • K ⁺ octamer formed by extraction of K ⁺ picrate from water into CHCl ₃ . The gray wedges represent dG 7 , while the black sphere represents K ⁺	10
Figure 1.10. Crystal structure shows that the cation-templated self-assembly of 16 equivalents of G 8 gives a lipophilic G-quadruplex [G 8] ₁₆ • 3K ⁺ /Cs ⁺ • 4pic ⁻ . This G-quadruplex is prepared quantitatively by extracting salts from water with a CHCl ₃ solution of G 8	12

Figure 1.11. G 8 undergoes cation dependant enantiomeric self-association. Racemic (<i>D</i> , <i>L</i>)-G 8 self-assembles in the presence of Ba ²⁺ to give homochiral G-quadruplexes [(<i>D</i>)-G 8] ₁₆ • 2Ba ²⁺ • 4pic ⁻ and [(<i>L</i>)-G 8] ₁₆ • 2Ba ²⁺ • 4pic ⁻ . Addition of K ⁺ to G 8 gave a diastereomeric mixture of heterochiral assemblies. The green wedges represent (<i>L</i>)-G 8 , while the red wedges represent (<i>D</i>)-G 8 . The blue and gray spheres represent Ba ²⁺ and K ⁺ respectively.....	14
Figure 1.12. Conformationally constrained G 10 forms a G-quartet without presence of a templating cation.....	16
Figure 1.13. A schematic representation of [cG 11] ₂ • MX • (H ₂ O) _n that shows the anion and cation binding sites.....	17
Figure 1.14. a) An empty G-quartet formed by guanine 12 . b) A hydrogen bound network of empty G-quartets. Each G-quartet can form up to eight additional hydrogen bonds with neighboring G-quartets (arrows).....	18
Figure 1.15. A G-quartet formed from dG 13 , a modified nucleobase with an expanded Hoogsteen hydrogen bonding face. Note the additional hydrogen bonds, depicted by arrows, thought to be a reason for increased stability.....	19
Figure 1.16. The AssP disulfide product is selectively amplified in the presence of a G-quadruplex template.....	21
Figure 1.17. Oxidation of the PNA strands T _{SH} and G _{SH} provides disulfides. In the presence of K ⁺ , G _{SS} G is amplified. The structure depicted for (G _{SS} G) ₂ represents just one possible orientation of a bimolecular G-quadruplex.....	22
Figure 1.18. The stability of G-quartet hydrogel B altered the dynamic equilibrium of acylhydrazones and directed reaction of the G hydrazide 16 with aldehyde 18	24
Figure 1.19. a) Structure of G-G 20 and schematic of the reversible formation of	

polymeric G-quartet based hydrogels. Changing pH in the presence of [2.2.2]cryptand 21 modulated the sol-gel equilibrium. b) Representation of the modulation of the gel-sol status induced by the sequence of triggering agents.....	25
Figure 1.20. Chemical structure of the PSO-py and the expected G-quadruplex induced by K^+ binding. Pyrene excimer emission occurs in the presence of K^+ . Reprinted with permission from John Wiley & Sons, Inc.	27
Figure 1.21. Chemical structure of the PSO and the expected G-quadruplex induced by K^+ binding. In this case FRET occurs in the presence of K^+ . Reprinted with permission from the American Chemical Society..	28
Figure 1.22. An optical K^+ sensor based on a complex formed between G-quadruplex DNA and a conjugated cationic polymer. Reprinted with permission from John Wiley & Sons, Inc.....	29
Figure 1.23. Schematic representation of an optical K^+ sensor based on G-quadruplex-polymer interactions that lead to FRET. Reprinted with permission from the American Chemical Society.	30
Figure 1.24. A fluorescein modified DNA oligonucleotide that functions as biosensor for thrombin.....	32
Figure 1.25. A protein biosensor based on the “aptamer beacon” strategy. Thrombin shifts the DNA’s conformational equilibrium to G-quadruplex and produces an increase in fluorescence as the donor-quencher groups get farther apart, compared to the stem-loop structure. Reprinted with permission from Elsevier.	33
Figure 1.26. Structure of a) acceptor-donor TBA and b) schematic showing FRET upon binding of thrombin to TBA.	34
Figure 1.27. The Structure-Switching Signaling Aptamer. A DNA duplex	

<p>composed of three strands of DNA places a fluorophore (F) close to a quencher group (Q). Upon addition of thrombin, the QDNA piece is released, and the fluorescence increases. Reprinted with permission from John Wiley & Sons, Inc.....</p>	35
<p>Figure 1.28. a) Detection of thrombin by binding 2 different G-quadruplexes at different epitope binding sites. b) Association of the 2 strands of DNA on the thrombin surface leads to fluorescence quenching.....</p>	36
<p>Figure 1.29. Amplified detection of thrombin based on enlargement of Au nanoparticles.....</p>	37
<p>Figure 1.30. Electrochemical detection of thrombin through the coupled oxidation of glucose by glucose dehydrogenase.....</p>	38
<p>Figure 1.31. Electrochemical biosensors for the detection of thrombin a) “signal-off system” described for a 35mer oligonucleotide containing the TBA sequence and b) “signal-on” system.</p>	40
<p>Figure 1.32. Optical detection of DNA by catalytic activation of thrombin upon dissociation of an intramolecular thrombin-TBA complex.</p>	42
<p>Figure 1.33. A DNA-based nanomachine that binds and releases thrombin. Binding of DNA strand Q to TBA-protein complex release thrombin, and addition of complementary DNA strand R removes Q and shifts equilibrium back to the TBA-thrombin complex. Reprinted with permission from John Wiley & Sons, Inc.....</p>	43
<p>Figure 1.34. Structures of DNA and LNA showing a) DNA in the C2'-<i>endo</i> conformation and b) LNA locked into the C3'-<i>endo</i> conformation.</p>	45
<p>Figure 1.35. Schematic showing a) antiparallel DNA G-quadruplex and b) parallel DNA G-quadruplex. Substitution of a single DNA monomer with a LNA analog results in conformational switching between the two structures. Reprinted with permission from the American Chemical Society.</p>	46

Figure 1.36. Possible structures of hybrid 1:1 PNA ₂ -DNA ₂ quadruplexes (bold = DNA, gray =PNA) where the PNA strands are (A) diagonally opposite or (B) adjacent to each other. Reprinted with permission from the American Chemical Society.....	48
Figure 1.37. Possible G-Quadruplex structures formed by PNA. Reprinted with permission from the American Chemical Society.....	49
Figure 2.1. Translational motion of a molecule in two dimensions.....	54
Figure 2.2. Calculation of the radius of a monomer of a sphere of a specific volume.....	56
Figure 2.3. Calculation of the radius of a dimer that is twice the volume of its monomer	56
Figure 2.4. The ratio of the diffusion coefficients of a dimer to monomer.	57
Figure 2.5. a) STE-PFG pulse sequence. See text for more information. The effect of signal intensity from the PFG NMR experiment b) without and c) with diffusion. After the 90° RF pulse that magnetically rotates the spins from the z-axis to the x-y axis. After application of a linear magnetic field gradient, the spins are phase shifted depending on the strength of the gradient. Following a 180° refocusing pulse, another magnetic field gradient is applied to shift the spins back into phase.....	58
Figure 2.6. Shigemi tubes: plug, tube, and plug and tube assembled.....	61
Figure 2.7. Variable temperature ¹ H NMR spectra of [G 8] ₁₆ • 4K ⁺ • 4pic ⁻ (0.059 mM) dissolved in CD ₃ CN. Signals for monomer G 8 (red) predominate at high temperatures, whereas signals for the hexadecameric complex [G 8] ₁₆ • 4K ⁺ • 4pic ⁻ (blue) predominate at low temperatures. The picrate peak is shown in green.....	65

Figure 2.8. Stack plot of ^1H NMR spectra for a mixture of G 8 , G-quadruplex 22 and A 23 . Signals for a) A 23 H8, b) G 8 H8, and c) G-quadruplex 22 “inner” H8 with increasing gradient strength in CD_3CN at 21 °C. d) Stejskal-Tanner plot of G 8 , $[\text{G } \mathbf{8}]_{16} \cdot 4 \text{K}^+ \cdot 4 \text{pic}^- \mathbf{22}$ and A 23 in CD_3CN at 21 °C.....	67
Figure 2.9. a) Variable temperature CD spectra of $[\text{G } \mathbf{8}]_{16} \cdot 4 \text{K}^+ \cdot 4 \text{pic}^- \mathbf{22}$ in CD_3CN . b) Plot of CD absorbance at 248 nm as a function of temperature.	70
Figure 2.10. The ^1H NMR spectra of G 24 at 400 MHz.....	71
Figure 2.11. ^1H NMR spectra in CD_2Cl_2 at 21 °C of complexes formed by extraction of K(DNP) with G 24 . a) Octamer 27 , $[\text{G } \mathbf{24}]_8 \cdot \text{K}^+ \cdot \text{DNP}^-$, formed in liquid-liquid extraction; b) hexadecamer 28 , $[\text{G } \mathbf{24}]_8 \cdot \text{K}^+ \cdot (2,6\text{-DNP})^-$, formed in solid-liquid extraction; c) mixture of octamer 27 and hexadecamer 28	73
Figure 2.12. CD spectra of a) octamer 27 , $[\text{G } \mathbf{24}]_8 \cdot \text{K}^+ \cdot \text{DNP}^-$, and b) hexadecamer 28 , $[\text{G } \mathbf{24}]_8 \cdot \text{K}^+ \cdot (2,6\text{-DNP})^-$. The samples were at concentrations of 0.15 mM in G 24 in CH_2Cl_2	74
Figure 2.13. Stejskal-Tanner plot of octamer 27 and hexadecamer 28 . Diffusion coefficients for octamer 27 $[\text{G } \mathbf{24}]_8 \cdot \text{K}^+ \cdot \text{DNP}^-$ and hexadecamer 28 $[\text{G } \mathbf{24}]_8 \cdot \text{K}^+ \cdot \text{DNP}^-$ in CDCl_3 at 21 °C.....	75
Figure 2.14. Formation of octamer 27 and hexadecamer 28 starting with monomer 24	76
Figure 2.15. ^1H NMR spectra in CDCl_3 at 21 °C of complexes formed by extraction of Na picrate with G 29 . a) A species of empirical formula $[\text{G } \mathbf{29}]_{4n} \cdot n\text{Na}^+ \cdot n(\text{pic})^-$ formed by solid-liquid extraction; b) octamer $[\text{G } \mathbf{29}]_8 \cdot \text{Na}^+ \cdot (\text{pic})^- \mathbf{33}$ formed by washing solution in part a) with water. The identity of the peak with an \times is unknown.....	78

Figure 2.16. CD spectra of a) complex of formula $[G \mathbf{29}]_{4n} \cdot (n)Na^+ \cdot n(pic)^-$ and b) $[G \mathbf{29}]_8 \cdot Na^+ \cdot pic^-$ 33 . Both samples were at concentrations of 0.34 mM in G 29 in CH_2Cl_2	80
Figure 2.17. Lowering the temperature to $-4^\circ C$ allows for the sharpening of the N2H signals in $[G \mathbf{29}]_8 \cdot 2 Na^+ \cdot 2 pic^-$ 31	81
Figure 2.18. a) ESI-MS spectrum of G 29 in $CHCl_3$ after solid-liquid extraction of Na^+ -picrate. b) ESI-MS spectrum of the same solution after washing with water	83
Figure 2.19. Addition of capping anions leads to octamer 33 , while addition of noncapping anion salts leads to hexadecamer 34	85
Figure 3.1. 400 MHz 1H NMR spectrum in CD_2Cl_2 at rt of G 35-d . The asterisk indicates the C8 residual 1H signal.	90
Figure 3.2. 400 MHz 1H NMR spectra in CD_2Cl_2 at rt of nondeuterated G-quadruplex $[G \mathbf{8-h}]_{16} \cdot 2Ba^{2+} \cdot 4DNP^-$ (top) and deuterated G-quadruplex $[G \mathbf{35-d}]_{16} \cdot 2Ba^{2+} \cdot 4DNP^-$ (bottom). The asterisks indicates the C8 residual 1H signal. Signals labeled with “a” indicate “outer” layer 1H signals, while signals labeled with “b” indicate “inner” layer 1H signals	91
Figure 3.3. H8 region of 400 MHz 1H NMR spectra in CD_2Cl_2 ; a) solution of $[\mathbf{8-h}]_{16} \cdot 2Ba^{2+} \cdot 4DNP^-$ (0.39 mM) and G 35-d (6.2 mM) immediately after mixing; b) the sample in a) after 4 days at room temp; c) solution of G 8-h (6.2 mM) and $[\mathbf{35-d}]_{16} \cdot 2Ba^{2+} \cdot 4DNP^-$ (0.39 mM) immediately after mixing; (d) the sample in c) after 4 days at rt.....	92
Figure 3.4. Control experiment shows 50-50 % mixture of deuterated and nondeuterated guanosine in both the inner and outer layers. The 1H NMR spectrum shows that the 1H signal intensities of the inner and outer H8 signals, indicated by *’s, are diminished by 50 %.....	93
Figure 3.5. Integration of the H8 NMR signal for the “inner” G-quartet in the	

exchange of 16 equiv of G 35-d (6.2 mM) with a) [G 8-h] ₁₆ • 2Ba ²⁺ • 4DNP ⁻ and b) [G 35-d] ₁₆ • 2Ba ²⁺ • 4DNP ⁻ . Exchange was done at room temp in CD ₂ Cl ₂	96
Figure 3.6. NMR integration of H8 signals in exchange of 16 equiv of 1-d (6.2 mM) with a) [1-h] ₁₆ • 2Ba ²⁺ • 4DNP ⁻ and b) [1-h] ₁₆ • 4K ⁺ • 4DNP ⁻ . Reactions were done at rt in 50-50 % CD ₃ CN-CD ₂ Cl ₂ . Depictions show different cation occupancy of the G-quadruplexes.....	97
Figure 3.7. a) [G 8-h] ₁₆ • 2Ba ²⁺ • 4DNP ⁻ with 2mM cryptate(Ba ²⁺ (DNP ⁻) ₂) at various temperatures in 1:1 CD ₂ Cl ₂ -CD ₃ CN. b) [G 8-h] ₁₆ • 4K ⁺ • 4DNP ⁻ with 4 mM cryptate and 4 mM K ⁺ (DNP ⁻) at various temperatures in 1:1 CD ₂ Cl ₂ -CD ₃ CN. Asterisks signify protons related to “free” and complexed DNP anion as they coalesce.....	98
Figure 3.8. a) Tautomerization of 2-hydroxypyridine 42 . b) Weakening of the G-quartet through hydrogen bonding of guanine and hydroxypyridine 42	101
Figure 3.9. Reaction progress for the regioselective ligand exchange process with small molecule catalysts: 3.7-3.11. [G 8-h] ₁₆ • 2Ba ²⁺ • 4DNP ⁻ (0.39 mM), G 35-d (6.2 mM), and small molecule (6.2 mM) at time intervals after mixing as a function of the outer H8 signal intensity. No significant decay in the H8 outer layer was observed for these experiments.....	102
Figure 3.10. 400 MHz ¹ H NMR spectrum in CD ₂ Cl ₂ at rt of TIPS-G 45	105
Figure 3.11. 400 MHz ¹ H NMR spectrum in CD ₂ Cl ₂ at rt of a) [<i>t</i> BDMS-G 8] ₁₆ • 2Ba ²⁺ • 4DNP ⁻ and b) [TIPS-G 45] ₁₆ • 2Ba ²⁺ • 4DNP ⁻	106
Figure 3.12. 400 MHz ¹ H NMR integration of the SiCH ₃ proton signals in exchange of 16 equiv of TIPS-G 45 (6.4 mM) with [<i>t</i> BDMS-G 8] ₁₆ • 2Ba ²⁺ • 4DNP ⁻ at rt in CD ₂ Cl ₂	107
Figure 3.13. NMR integration of the SiCH ₃ proton signals in exchange of 16	

equiv of TIPS-G 45 (6.4 mM) with [<i>t</i> BDMS-G 8] ₁₆ • 2Ba ²⁺ • 4DNP ⁻ at rt in CD ₂ Cl ₂	107
Figure 4.1. a) G-quartet and b) Crystal structure of lipophilic G-quadruplex [G] ₁₆ • 4M ⁺ with its front partially stripped away for clarity. The yellow spheres correspond to the cations that align the central region of the G-quadruplex.	112
Figure 4.2. Representation of the a) Oxy-1.5 bimolecular quadruplex with bound NH ₄ ⁺ . The blue and red spheres represent outer and inner NH ₄ ⁺ respectively, while the green spheres represent solvated NH ₄ ⁺ . The gray squares represent G-quartets and the lines represent the DNA backbone. b) Solvated NH ₄ ⁺ replaces the outer NH ₄ ⁺ causing a flow mechanism of the cations through the G-quadruplexes.....	113
Figure 4.3. a) Rigid rod motif. b) Guanine dimer.....	114
Figure 4.4. Structure, dimer, and binding sites of cG 11	115
Figure 4.5. Folate derivative 49 and tetramer 50 of the folate dendrimers.....	116
Figure 4.6. Dimer of a C8 substituted guanine unit with an N2 substituted guanine unit.....	120
Figure 4.7. The ¹ H NMR spectrum of G 51 in DMSO-d ₆	121
Figure 4.8. a) ¹ H NMR spectrum of G 51 in CDCl ₃ , b) after extraction of Ba(DNP) ₂ , from water into CDCl ₃ and c) selected region of 2D NOESY spectrum of sample from b) showing NOEs between H 10 to H16a.....	123
Figure 4.9. ESI-MS of [G 51] ₈ • Ba ⁺² • 2DNP ⁻ formed by liquid-solid extraction of Ba(DNP) ₂ with G 51 in CHCl ₃	124
Figure 4.10. Selected ¹ H NMR region of G 58 showing that H16 and H15 that are trans to each other.	126

Figure 4.11. The ^1H NMR spectrum of G 59 at 400 MHz in DMSO- d_6 .	129
Figure 4.12. CD spectrum of G-quadruplex 60 (0.171 mM) in CH_2Cl_2 using a 1.0 cm path length quartz cuvette. The positive CD band centered at 280 nm is characteristic of stacked G-quartets within a chiral G-quadruplex.	130
Figure 4.13. ^1H NMR spectrum (CD_2Cl_2) of G-quadruplex 60 , $[\text{G } \mathbf{59}]_{16} \cdot 4\text{K}^+ \cdot 4\text{DNP}^-$. The designations inner and outer refer to the inner and outer layers that provide 2 sets of signals observed for this D_4 -symmetric hexadecamer.	131
Figure 4.14. Diffusion NMR data for non-covalent G-quadruplex 60 . Stejskal–Tanner plot of G-quadruplex 60 and A 23 in CD_2Cl_2 at 21.8 °C.	132
Figure 4.15. A region of the 400 ^1H NMR spectra (DMSO- d_6) with a) precursor G 59 and b) purified unimolecular G-quadruplex 61 . The arrow and dotted lines show where the H12' peak shifts and the disappearance of the H13' signals. The H12' peak at 5.71 ppm is due to a cis/trans mixture	133
Figure 4.16. ESI-MS of G-quadruplex 61 in 1:2 $\text{H}_2\text{O}-\text{CH}_3\text{CN}$ showing the triply charged ion for $[\text{G } \mathbf{61} \cdot 4\text{K}]^{+3}$ at m/z 2766.3.	134
Figure 4.17. ESI-MS of G-quadruplex 61 in 1:2 $\text{H}_2\text{O}-\text{CH}_3\text{CN}$ of unimolecular G-quadruplex 61 a) after purification by flash chromatography and b) after washing with K(DNP). This change in the ESI-MS shows the ability to exchange cations in G-quadruplex 61 from Na^+ to K^+ .	135
Figure 4.18. Diffusion NMR data for a unimolecular G-quadruplex 61 . Stejskal–Tanner plot of G 59 , G-quadruplex 61 and A 23 in hydrogen bonding disrupting solvent, DMSO- d_6 at 21.8 °C.	136
Figure 4.19. A region of the 400 MHz ^1H NMR spectra (CD_2Cl_2) of a) precursor G-quadruplex 60 and b) unimolecular G-quadruplex 61 . The spectra	

show the hydrogen bonded signals for the N1H and N2HA inner and outer sets of signals observed for the two D ₄ -symmetric hexadecamers.....	137
Figure 4.20. CD spectra of a) unimolecular G-quadruplex 61 (0.011 mM) (red line) and b) precursor G-quadruplex 60 in CH ₂ Cl ₂ using a 1.0 cm path length quartz cuvette. The positive CD band centered at 280 nm is characteristic of stacked G-quartets within a chiral G-quadruplex.....	137
Figure 4.21. The ¹ H NMR spectrum of G 66 at 400 MHz in DMSO-d ₆	140
Figure 4.22. CD spectrum of G-quadruplex 70 (0.15 mM) in CH ₂ Cl ₂ using a 1.0 cm path length quartz cuvette. The positive CD band centered at 285 nm is characteristic of stacked G-quartets within a chiral G-quadruplex.....	141
Figure 4.23. ¹ H NMR spectrum (CD ₂ Cl ₂) of G-quadruplex 70 , [G 66] ₁₆ · 4K ⁺ · 4BPh ₄ ⁻ . The designations inner and outer refer to the inner and outer layers that provide 2 sets of signals observed for this D ₄ -symmetric hexadecamer	142
Figure 4.24. A region of the 400 MHz ¹ H NMR spectra (DMSO-d ₆) of unimolecular G-quadruplex 61 a) 10 minutes and b) one week after dissolving into DMSO-d ₆ . The spectra shows what appears to be the hydrogen bonded signals for the N1H and N2HA signals (*).	143
Figure 4.25. Selected N1H region of the 400 MHz ¹ H NMR spectra (DMF-d ₇) of a) unimolecular G-quadruplex 61 at 9 °C, b) 7 °C, c) 21 °C, and d) noncovalent G-quadruplex 60 at 21 °C. The percentage of folded to unfolded structures are also shown. The ¹ H NMR spectra were generated by heating the sample up to 100 °C for 4 h, cooling down to the desired temperature, and waiting until the sample comes to equilibrium. Folded-unfolded ratios are ballpark numbers, since it takes a significant amount of time for the sample to come to completion at low temperatures.	145

Figure 4.26. Selected N1H region of the 400 MHz ¹ H NMR spectra (DMF-d ₇) of unimolecular G-quadruplex 61 at 103 °C after a) 30 min, b) 90 min, and c) 220 min	146
Figure 4.27. Selected N1H region of the 400 MHz ¹ H NMR spectra (DMF-d ₇) of unimolecular G-quadruplex 61 at a) 21 °C, b) at 21 °C with 4 equiv. [2.2.2]cryptand 21 , c) b at 10 °C, d) after annealing (100 °C) b, e) at -43 °C, and f) schematic showing a possible intermediate after the addition of [2.2.2]cryptand 21	147
Figure 4.28. Selected N1H region of the ¹ H NMR spectra (CD ₂ Cl ₂) of a) unimolecular G-quadruplex 61 and b) with 16 eq [2.2.2]cryptand 21 . Additional ²³ Na NMR spectra of c) unimolecular G-quadruplex 61 and d) with 16 eq [2.2.2]cryptand 21	149
Figure 4.29. G-quartet a) with bound M ⁺ cation and b) without cation.....	149
Figure 4.30. CD spectra of a) noncovalent G-quadruplex 60 (0.011 mM) (green line) and b) with 3 equiv. [2.2.2]cryptand 21 (red line) in CH ₂ Cl ₂ using a 1.0 cm path length quartz cuvette.....	150
Figure 4.31. CD spectra of a) unimolecular G-quadruplex 61 (0.011 mM) (green line) and b) with 160 equiv. [2.2.2]cryptand 21 (red line) in CH ₂ Cl ₂ using a 1.0 cm path length quartz cuvette.....	150
Figure 4.32. CD spectra of unimolecular G-quadruplex 61 (0.05 mM) in 10 mM sodium phosphate (pH 6.4) with a) and without b) EYPC liposomes (100 nm).....	152
Figure 4.33. Transport of Na ⁺ as determined in a pH gradient assay. EYPC liposomes (100 nm) containing HPTS dye (0.1 mM) in 100 mM NaCl, 10 mM sodium phosphate (pH 6.1) were suspended in 100 mM NaCl, 10 mM sodium phosphate (pH 6.1). The compounds, G 59 , G-quadruplex 61 or gramicidin, were added at t = 0 s as DMSO solutions to give a 1:100 ligand to lipid ratio. The addition of NaOH	

solution at $t = 40$ s established a pH gradient of about 1 pH unit. At $t = 430$ s the liposomes were destroyed with Triton-X detergent. Measurement of the fluorescence of the trianionic and tetraanionic forms of HPTS dye allowed determination of the liposomal pH.....153

Figure 4.34. A series of ^{23}Na NMR spectra 10 min after addition of a) metathesis product **61**, b) **G 59**, c) DMSO blank and d) gramicidin to a solution of EYPC liposomes (200 nm) that initially contained 100 mM LiCl, 10 mM lithium phosphate suspended in an extravesicular buffer containing 100 mM NaCl, 10 mM sodium phosphate. Transport of Na^+ across the bilayer is indicated by a ^{23}Na NMR peak at δ 0.24 ppm154

Figure 4.35. Transport of Li^+ as determined in a pH gradient assay. EYPC liposomes (100 nm) containing HPTS dye (0.1 mM) in 100 mM LiCl, 10 mM lithium phosphate (pH 6.5) were suspended in 100 mM LiCl, 10 mM lithium phosphate (pH 6.5). The compounds, **G 59**, G-quadruplex **61** or gramicidin, were added at $t = 0$ s as DMSO solutions to give a 1:100 ligand to lipid ratio. The addition of LiOH solution at $t = 40$ s established a pH gradient of about 1 pH unit. At $t = 430$ s the liposomes were destroyed with Triton-X detergent. Measurement of the fluorescence of the trianionic and tetraanionic forms of HPTS dye allowed determination of the liposomal pH.....155

Figure 4.36. Transport of K^+ as determined in a pH gradient assay. EYPC liposomes (100 nm) containing HPTS dye (0.1 mM) in 100 mM KCl, 10 mM potassium phosphate (pH 6.4) were suspended in 100 mM KCl, 10 mM potassium phosphate (pH 6.4). The compounds, **G 59**, G-quadruplex **61** or gramicidin, were added at $t = 0$ s as DMSO solutions to give a 1:100 ligand to lipid ratio. The addition of KOH solution at $t = 40$ s established a pH gradient of about 1 pH unit. At $t = 430$ s the liposomes were destroyed with Triton-X detergent. Measurement of the fluorescence of the trianionic and tetraanionic forms of HPTS dye allowed determination of the liposomal pH.....156

Figure 6.1. a) Schematic of G-quadruplex with a focus on the sugar moiety. b) Selected region of ^1H - ^1H NOESY spectrum at 400 MHz of G-quadruplex $\text{TIPS-G } \mathbf{45}]_{16} \cdot 2\text{Ba}^{2+} \cdot 4\text{DNP}^-$. The signal for inner CH_3 has NOE's to both the inner and outer H1' signals, while the outer CH_3 only has an NOE to the inner H1'. Since the CH_3 is too far to have an NOE with the intermolecular H1' signal, crystal structures show that it is close enough between layers to have an intramolecular NOE.169

Figure 6.2. Selected region of 2D COSY spectrum of sample of G-quadruplex $[\text{G } \mathbf{51}]_8 \cdot \text{Ba}^{2+} \cdot \text{DNP}^-$173

LIST OF SCHEMES

Scheme 2.1. Structures of G 8 , G-quadruplex [G 8] ₁₆ ·4 K ⁺ · 4 pic ⁻ 22 and A 23	63
Scheme 2.2. Mixing of homodimers to yield a 2:1:1 mixture of heterodimer and the two homodimers. Red spheres are Ba ²⁺ , blue spheres are Sr ²⁺ , green wedges are G 8 , and brown blocks are picrate; front picrate not shown for clarity	63
Scheme 2.3. Synthesis of G 24	70
Scheme 2.4. Formation of [G 24] ₈ · K ⁺ · DNP ⁻ 27 and [G 24] ₁₆ · 4 K ⁺ · 4 DNP ⁻ 28	71
Scheme 2.5. Self-assembly of G 29 and Na ⁺ picrate. Tetramer 30 , octamer 31 , and polymer 32 are potential structures for [G 29] _{4n} ·(n)Na ⁺ ·n(pic) ⁻	79
Scheme 3.1. Regioselective ligand exchange into G-quadruplex with isotopically labeled ligands.	88
Scheme 3.2. Synthesis of G 35-d	90
Scheme 3.3. Model of anions binding to exocyclic N2 amino protons of the inner layer. This anion-nucleobase hydrogen bond helps stabilize the inner layers of the G-quadruplex. Sugars and other anions are omitted for clarity.	95
Scheme 3.4. In more polar solvents, weaker binding anions allow for the hexadecamer to break into octamers for a) divalent cation G-quadruplexes, while b) monovalent cations stabilize the hexadecameric G-quadruplex with their “bridging” cations	100

Scheme 3.5. Regioselective exchange of TIPS-G 45 into [tBDMS-G 8] ₁₆ • 2Ba ²⁺ • 4DNP ⁻	104
Scheme 3.6. Proposed synthesis of amphiphilic G-quadruplexes through ligand exchange.	108
Scheme 4.1. Lipophilic G-quadruplex incorporated into a phospholipid bilayer in a) idealized and b) proposed conditions. Noncovalent lipophilic G-quadruplexes do not preserve their structure in the demanding conditions of phospholipid bilayers in aqueous solutions.	111
Scheme 4.3. Schematic of the covalent capture of lipophilic G-quadruplexes	118
Scheme 4.4. Design scheme for covalent capture of G 51 through formation of G-quartet 52 and cross metathesis to yield G-quartet 53 . NOEs between H16a and H10 for G-quartet 52 are shown, see text for details	119
Scheme 4.5. Synthesis of N2, C8-disubstituted G 51	121
Scheme 4.6. Stille coupling of G 56 to yield G 58 through isomerization of the allylic bond.....	125
Scheme 4.7. Schematic showing G 59 (gray wedges) extracting K ⁺ (blue spheres) to form G-quadruplex 60 . Following G-quadruplex formation, cross metathesis yields unimolecular G-quadruplex 61	127
Scheme 4.8. Synthesis of G 59	128
Scheme 4.9. Synthesis of G 66	139
Scheme 4.10. Equilibrium between structured unimolecular G-quadruplex 61 (left) and “unfolded” unimolecular G-quadruplex 61 (right)..	144

Scheme 4.11. Schematic showing removal of cation in nonpolar solvent.
Proposed structure of cation “free” unimolecular G-quadruplex in
nonpolar solvents.148

LIST OF EQUATIONS

Equation 2.1. Diffusion coefficient related to the hydrodynamic frictional coefficient.	55
Equation 2.2. Hydrodynamic frictional coefficient for a sphere.	55
Equation 2.3. Diffusion coefficient related to the radius of a sphere.	55
Equation 2.4. Ratio of two diffusion coefficients related to a sphere.	55
Equation 2.5. Volume of a sphere, where R equals the radius.	56
Equation 2.6. Intensity related to the diffusion coefficient and the gradient pulse	59
Equation 2.7. Normalized intensity as a function of the diffusion coefficient and gradient pulse.	60
Equation 3.1. Exchange rate at coalescence.	98

Chapter 1. The G-Quadruplex in Nanostructures and Biomaterials

A great deal of the material in this chapter will be published in reference 1:

- Kaucher, M. S.; Harrell Jr., W. A.; Davis, J. T. "Chapter 10: *The G-Quartet in Supramolecular Chemistry and Nanoscience*" *Quadruplex Nucleic Acids*, Neidle, S.; Balasubramanian, S. (Ed.), Royal Society of Chemistry, Cambridge, U.K., **2007**, in press.

1.1 Introduction

Molecular self-assembly is a powerful method to build noncovalent structures from smaller building blocks.²⁻⁴ For example, the bottom-up approach using self-assembly is increasingly being used to build nanotubes.^{5,6} In recent years, self-assembly has focused on the development of functional materials.⁷⁻¹¹ This thesis, "Lipophilic G-Quadruplexes: Structural Studies, Post-Assembly Modification, and Covalent Capture" describes how function, cation transport, was installed into self-assembled structures through structural studies and manipulation of noncovalent structures.

1.2 Thesis Organization

This thesis is organized into six chapters. The initial goal of this research was to develop synthetic ion channels built using G-quadruplex (stacked G-quartets) scaffolds that function in membranes (**Figure 1.1**). The design of synthetic pores, channels and transmembrane transporters has been of particular interest for their potential as new ion sensors, catalysts and anti-microbial agents.¹² **Chapter 1** discusses how the G-quartet motif has been utilized for the synthesis of new nanostructures and biomaterials.¹

Strategies to build functional materials utilizing both lipophilic and DNA G-quadruplexes are discussed. This background provides an understanding for the significance of the techniques, strategies, and successes of the research described in this thesis. The structural studies presented in **Chapter 2** gives insight into the process of self-assembly in solution. This insight helps us gain some control of the size of these lipophilic G-quadruplexes. **Chapter 3** describes the regioselective exchange of ligands into the G-quadruplex, a process that promises to yield functionalized scaffolds. **Chapter 4** discusses how synthetic ion transporters based on G-quadruplex scaffolds were built through covalently trapping these hydrogen bonded structures. **Chapter 5** describes future directions. Finally, **Chapter 6** contains the experimental protocols used for the research described in **Chapters 2-4**.

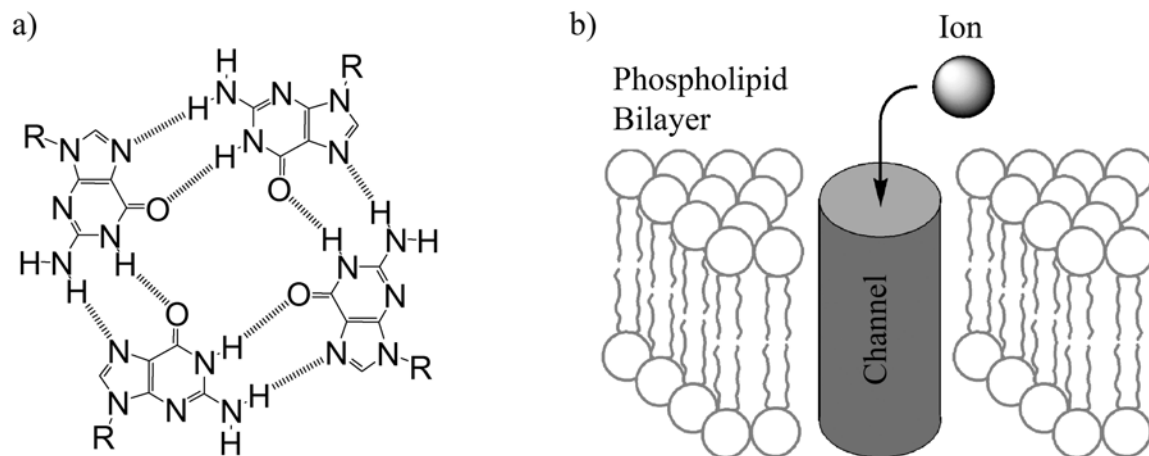


Figure 1.1. a) G-quartet contains four hydrogen bonded guanine bases and b) ion channel embedded in a phospholipid membrane.

1.3 Guanine is a Building Block for Diverse Assemblies

Nucleobases are well known for their ability to form complementary hydrogen bonds with their base pairs (**Figure 1.2**). These hydrogen bonds, on the Watson-Crick

edge, are essential in holding DNA duplexes together.¹³ Although all nucleobases can form additional hydrogen bonds through their Hoogsteen edges, guanine is well-known for its ability to self-associate.¹⁴

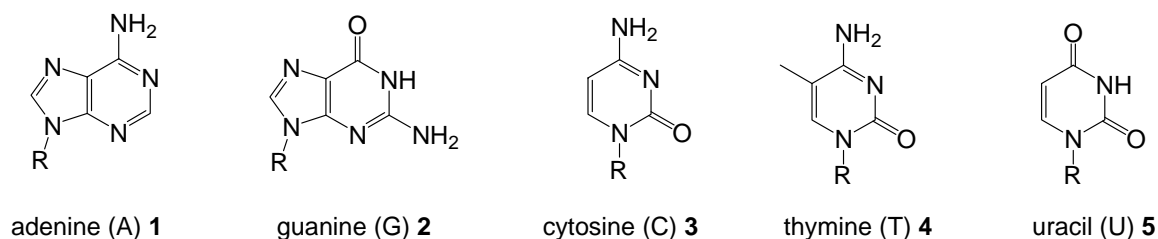


Figure 1.2. Natural nucleobases.

Guanine **2** contains both a Watson-Crick edge and a Hoogsteen edge (**Figure 1.3**).¹³ Moreover, the Watson-Crick edge has two hydrogen bond donors that can hydrogen bond with the two hydrogen bond acceptors on the Hoogsteen edge. With this series that are possible for hydrogen bonds, there are several different structures of self-associated guanine (**Figure 1.4**). Not including dimers, there are two long polymeric or ribbon structures that guanine can form.¹⁴⁻¹⁶ The first structure is a ribbon with an overall dipole (**Figure 1.4a**), while the other ribbon has no dipole (**Figure 1.4b**). Although ribbons with no dipoles are favored, ribbons with dipoles are observed particularly when R is a large group. **Figure 1.4c** shows a third self-assembled structure that guanine can form: a cyclic self-assembled structure. This cyclic structure, the G-quartet, is typically favored in the presence of cations, since cations stabilize the electrostatically negative regions of the central oxygens of the G-quartet. The sugar moiety typically associated with the guanine base also has a large impact on the structure formed by guanine derivatives.^{15,17,18}

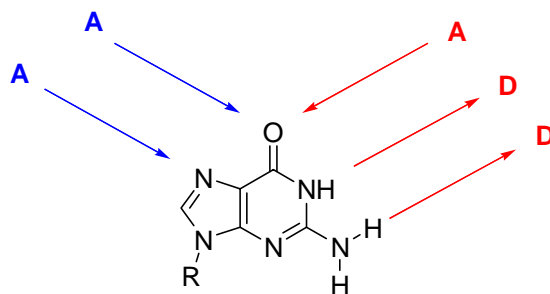


Figure 1.3. Depiction of the Watson-Crick edges and Hoogsteen edges of guanine 2.

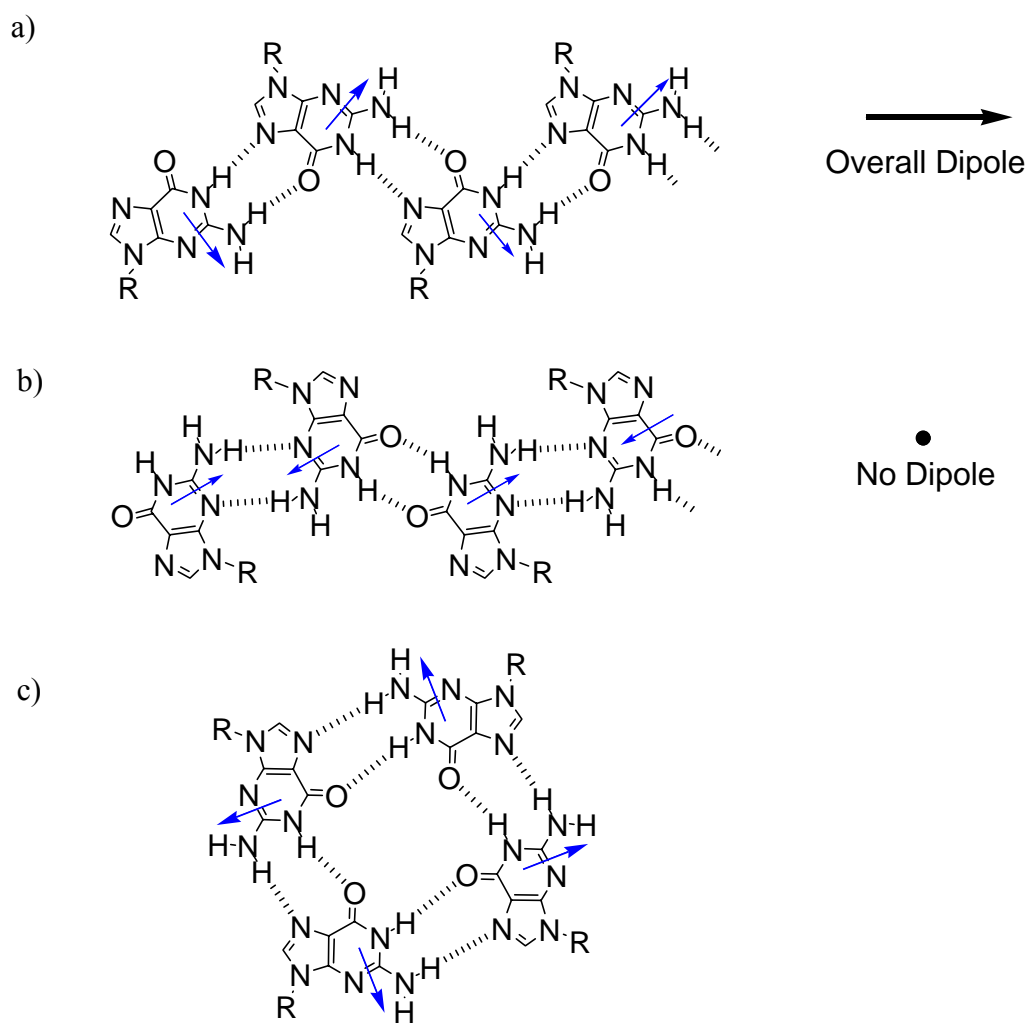


Figure 1.4. Self-assembled structures of guanine: a) ribbon with a dipole, b) ribbon with no dipole, and c) cyclic tetramer (G-quartet).

1.4 Guanosine Forms Self-Assembled Cyclic Structures – G-Quartets

The G-quartet was first identified in 1962 as the basic building block for formation of hydrogels by 5'-GMP **6**.¹⁹ Gellert and colleagues used fiber diffraction data to propose that a square planar G-quartet was formed by eight intermolecular hydrogen bonds between the Hoogsteen and Watson-Crick edges of neighboring nucleobases (**Figure 1.4c**). Shortly after, polyguanylic acid was also found to form multistranded helical coils.²⁰ It was also observed that hydrogels were not formed at basic pH. The smaller G-quartet assemblies in basic conditions could be studied by NMR spectroscopy.²¹ It was later shown that alkali metals (Na^+ and K^+) stabilized these G-quartets. Coordination to the four inward directed carbonyl oxygens by alkali metal ions enabled the G-quartets to be stacked into G-quadruplexes. Pinnavaia and colleagues found that 5'-GMP **6** forms diastereomeric $\text{G}_8\text{-K}^+$ octamers by sandwiching two G-quartets with eight inward directed carbonyl oxygens coordinated to a central cation.²² More recently, Wu and colleagues used a combination of data from diffusion NMR and dynamic light scattering measurements to determine the size of nanostructures formed by sodium 5'-GMP **6** at pH 8 (**Figure 1.5**).²³ Wu's group identified two major species in solution: stacked 5'-GMP monomers and stacked G-quartets. For 5'-GMP concentrations in the 18-34 wt % range, the structures had an average length between 8 and 30 nm, corresponding to a cylinder composed of 24-87 stacked G-quartets. The impressive length of G-quadruplexes formed from 5'-GMP **6** in water underscores the highly cooperative participation of hydrogen bond, ion-dipole, and π - π stacking interactions inherent to these G-quartet based assemblies.

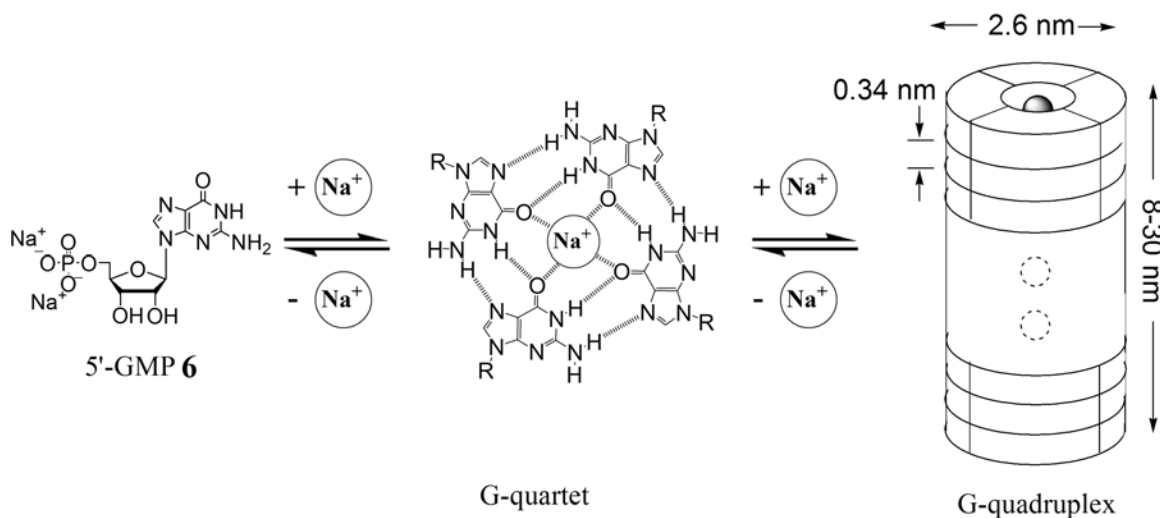


Figure 1.5. Depiction of the G-quadruplex cylinder formed by the self-assembly of 5'-GMP **6**.²³

1.5 G-rich DNA and RNA Regions Form G-quadruplex Structures

Both DNA and RNA have been found to fold into G-quadruplex structures. These tertiary structures of the folded DNA and RNA molecules can be either unimolecular, bimolecular, or a tetraplex (**Figure 1.6**).²⁴⁻²⁷ The biological importance of these DNA and RNA G-quadruplex structures have come under increased attention, in particular with regard to telomeric DNA and nucleic acid aptamers.²⁴⁻²⁷

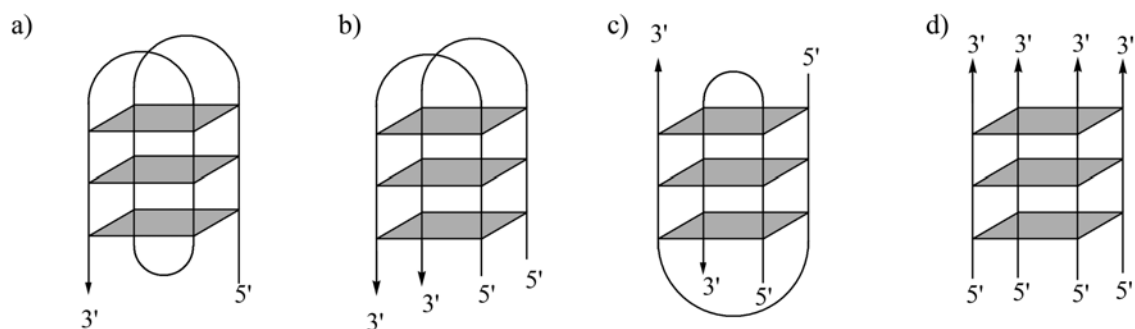


Figure 1.6. Examples of nucleic acid G-quadruplexes: a) unimolecular, b) edgewise loop bimolecular, c) diagonal loop bimolecular, and d) parallel tetraplex. Gray rectangles represent G-quartets, while the lines represent the phosphate backbone.

Telomeric DNA is a G-rich region at the end of DNA strands. In healthy cells, telomeric DNA slowly decays, which eventually leads to cell death.^{24,28-32} In tumorous cells, telomeric DNA is extended through the action of the telomerase enzyme, thus allowing the tumorous cell life to be prolonged.³³ Telomeres are single-stranded DNA substrates for telomerase enzymes.²⁴⁻²⁷ Since these G-rich ends of DNA can form G-quadruplexes and stop telomerase from extending the DNA, G-quadruplex stabilizing molecules are potentially valuable anticancer drugs.³⁴⁻⁴¹ These telomerase inhibitors recognize the face, edge, loop, or groove of the G-quadruplex (**Figure 1.7**).³⁴⁻⁴¹

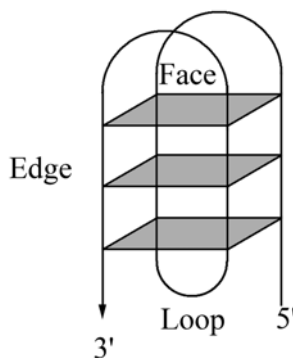


Figure 1.7. Examples of binding sites that are targeted by telomerase inhibitors.

Furthermore DNA and RNA aptamers are nucleic acid species that fold into tertiary structures that can bind to specific targets such as small molecules.⁴² One of the more studied G-rich aptamers is the thrombin binding aptamer. The thrombin binding aptamer (TBA) is a 15-residue DNA oligonucleotide with the sequence d(5'-GGTTGGTGTGGTTGG-3') that binds with high affinity and selectivity to the protease thrombin.⁴³ Nanomolar concentrations of this DNA aptamer can inhibit formation of the fibrin clots that result from thrombin activation. Shortly after its discovery, the groups of

Bolton and Feigon used NMR spectroscopy to determine TBA's solution structure in the presence of K^+ .^{44,45} The single-stranded d (5'-GGTTGGTGTGGTTGG-3') can form a unimolecular G-quadruplex that is shaped like a chair, with two stacked G-quartets connected by two TT loops and a central 3-base TGT loop (**Figure 1.8**). Potassium cation is essential for the templation and stabilization of the chair-type G-quadruplex by TBA, and both solution NMR spectroscopy and mass spectrometry have shown that the TBA G-quadruplex has a pronounced selectivity for coordination of K^+ over Na^+ .^{45,46} An x-ray crystal structure of a thrombin-TBA complex confirmed TBA's chair-like structure and suggested that this G-quadruplex DNA bound to the fibrinogen exosite, an anion binding location distinct from the protease's active site.⁴⁷ Later experiments have shown that thrombin has 2 distinct binding epitopes that recognize different G-quadruplex ligands.⁴⁸ By using thrombin mutants, competitive binding assays and chemical cross-linking, Tasset and colleagues confirmed that the 15-mer TBA binds to the fibrinogen exosite, whereas another 29-mer oligonucleotide, one that folds into a different G-quadruplex topology, binds tightly to thrombin's heparin-binding exosite. A number of thrombin biosensors have been developed based on the simultaneous use of these 2 distinct G-quadruplex recognition sites. Although the TBA aptamer originally gained notoriety for its potential as a therapeutic anti-thrombolytic agent, this oligonucleotide has also been important in the supramolecular chemistry of G-quadruplexes. As described in more detailed below, the TBA sequence has served as the primary model for the development of a range of sensors and nanomachines.

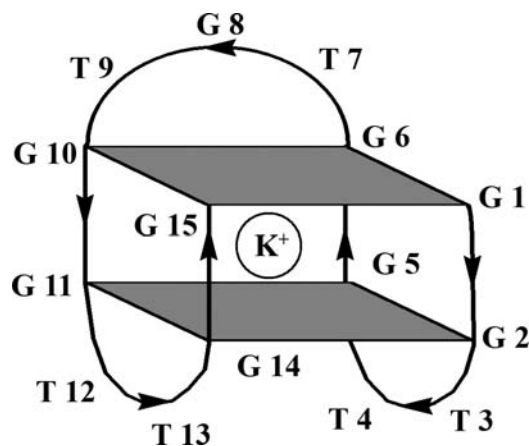


Figure 1.8. Schematic of the thrombin binding aptamer (TBA).

1.6 Self-Assembly of Lipophilic Guanosine Analogs.

1.6.1 Guanosine Self-Assemble in Nonpolar Solvents

In 1990, Guschlbauer suggested that water was an indispensable solvent for guanosine self-assembly and that self-assembly in nonpolar solvents would give rise to poorly organized structures.¹⁵ Due to the poor solubility of guanosine, it was not until the ribose hydroxyl groups were modified with protecting groups that it was recognized that lipophilic guanosine nucleosides could self-associate into discrete assemblies in organic solvents. Five years after Guschlbauer's review, Gottarelli and his colleagues reported the first guanosine assembly in nonpolar solvents. This lipophilic guanosine (3', 5'-didecanoyl-2'-dG **7**) extracted K^+ picrate from water into chlorinated organic solvents to give a discrete and highly stable $[dG \mathbf{7}]_8 \cdot K^+$ octamer.⁴⁹ A G-quartet stacked polymer, $[dG \mathbf{7}]_n \cdot nK^+$, formed in hydrocarbon solvents gave hexagonal packed liquid crystals. Similar to the situation in water, the K^+ cation was absolutely essential for templation and stability of the G-quartets (**Figure 1.9**).

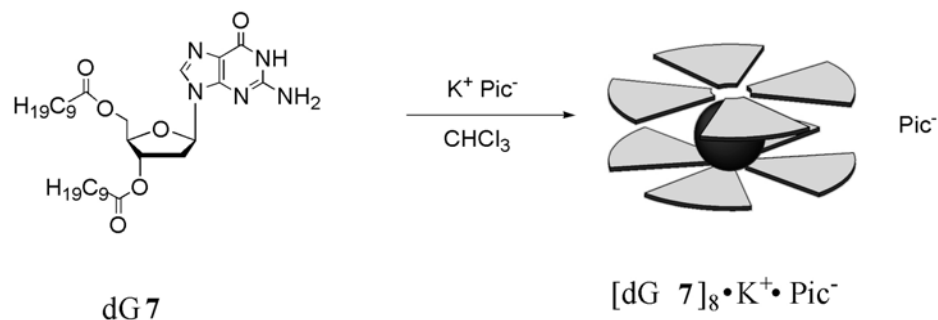


Figure 1.9. Lipophilic $[\text{dG 7}]_8 \cdot \text{K}^+$ octamer formed by extraction of K^+ picrate from water into CHCl_3 . The gray wedges represent dG 7, while the black sphere represents K^+ .⁴⁹

It was also observed that hydrogen bonded ribbons were formed by dG 7 in the absence of K^+ .⁵⁰ Through changing either the sugar substituents or the solvent, Gottarelli et. al. modulated the specific hydrogen-bonding pattern (obtaining either a ribbon structure with dipole or no dipole shown in **Figure 1.4a** and **b**). These ordered ribbons were shown to have some potential applications in the molecular electronics field. In particular, Gottarelli and colleagues made an organic semiconductor using dG 7. Asymmetric I - V curves, characteristic of molecular rectifiers, were attributed to the dipole that is inherent to the supramolecular structure of ribbon A (**Figure 1.4a**).⁵¹

As mentioned previously, hydrogen-bonded G ribbons can be converted to stacked cyclic G-quartets through the addition of a templating cation. The Davis and Gottarelli groups collaborated to solve the NMR structure of $[\text{dG 7}]_8 \cdot \text{KI}$ in CDCl_3 .⁵² Interestingly, this discrete octamer $[\text{dG 7}]_8 \cdot \text{KI}$ existed as a single supramolecular diastereomer with K^+ sandwiched between an all-*anti* G-quartet and an all-*syn* G-quartet. Shortly after, Fettinger and coworkers solved a x-ray crystal structure to definitively prove that larger lipophilic G-quadruplexes are formed in high diastereoselectivity, even

from nonpolar organic solvents.⁵³ The lipophilic G-quadruplex, $[G \mathbf{8}]_{16} \cdot 3K^+ \cdot Cs^+ \cdot 4pic^-$, is a complex composed of 24 total components: four stacked G-quartets, four cations and four anions. The monomeric guanosine, 5'-silyl-2',3'-isopropylidene G **8**, extracted K^+ picrate from water into CH_2Cl_2 to form lipophilic G-quadruplexes (**Figure 1.10**). This G-quadruplex is constructed of a pair of head-to-tail $[G \mathbf{8}]_8$ octamers. Each octamer uses 8 carbonyl oxygens to coordinate sandwiched K^+ ions. A third K^+ ion holds the two $[G \mathbf{8}]_8$ octamers together and a solvated Cs^+ ion caps the structure. The solvated capping cation is loosely bound to the G-quadruplex. The 4 hydrogen bonded G-quartets within $[G \mathbf{8}]_{16} \cdot 3K^+ \cdot Cs^+ \cdot 4pic^-$ all show π -stacking separations of 3.3-3.4 Å. Furthermore, the four picrate anions hydrogen bond to the exposed N2 amino groups and extend from the two central G-quartets to form an anionic belt wrapped around the G-quadruplex periphery. Clearly, this G-quadruplex showed function by extracting alkali metals from water into organic solvents.

It was noted early on that this G-quadruplex structure resembled an ion channel with its cations aligned within the central cavity and a lipophilic exterior. These stable lipophilic G-quadruplex structures, held together by numerous non-covalent interactions, can be used either as biomimetic models for DNA G-quadruplex structures or for the development of functional supramolecular systems, including synthetic ion channels.¹⁴

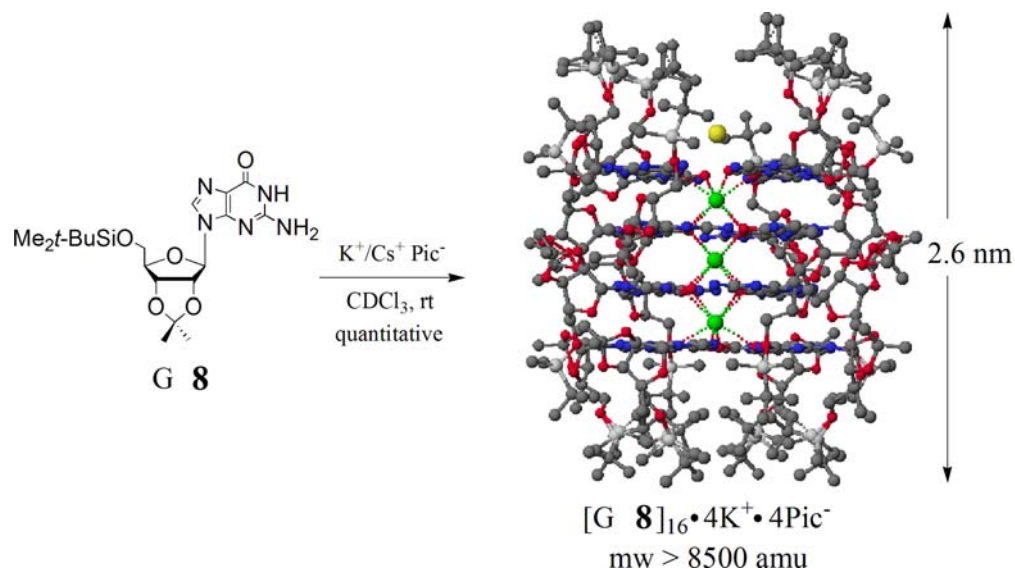


Figure 1.10. Crystal structure shows that the cation-templated self-assembly of 16 equivalents of **G 8** gives a lipophilic G-quadruplex $[\text{G } \mathbf{8}]_{16} \cdot 3\text{K}^+/\text{Cs}^+ \cdot 4\text{pic}^-$. This G-quadruplex is prepared quantitatively by extracting salts from water with a CHCl_3 solution of **G 8**.⁵³

Using solid state NMR spectroscopy, Wu and colleagues used ^{23}Na and ^{39}K NMR to identify these specific channel cations.^{54,55} This solid-state NMR work was essential, since these lipophilic G-quadruplexes could then be reliably used as a model for the 5'-GMP G-quadruplex. The 5'-GMP G-quadruplex's G-quartet-bound and phosphate-bound cations were subsequently identified. This model is likewise useful for identifying cations in DNA G-quadruplexes.

Moreover, G-quadruplexes containing divalent cations such as Pb^{2+} , Ba^{2+} or Sr^{2+} are both thermodynamically and kinetically more stable than are the corresponding G-quadruplex assemblies that contain monovalent Na^+ or K^+ .⁵⁶ This enhancement in stability in the presence of the divalent cations over monovalent cations is most likely due to the stronger ion-dipole interactions between the bound cations and the coordinating carbonyl oxygens. The cooperative enhancement of the strength of the G-quartet's

hydrogen bonds from the bound divalent cations may also further stabilize these G-quadruplexes. It was also observed that not only the cations, but the anions stabilize these lipophilic G-quadruplex.^{57,58} **Chapter 3** takes advantage of these stabilizing forces by cation and anion in achieving the post-assembly modification of these non-covalent structures.

1.6.2 Enantiomeric Self-Association of Lipophilic Nucleosides.

The bound cation can also influence the supramolecular stereochemistry of the noncovalent structure. A series of diastereomers can be formed by the optically active **8**. For **G 8**, the cation's identity (Ba^{2+} vs. K^+) has a significant influence on the level of diastereoselectivity in the self-association process.⁵⁹ G-quadruplexes formed with monovalent cations, K^+ , and a racemic mixture of (*D*, *L*)-**G 8** are a mixture of heterochiral diastereomers, as determined by ^1H NMR spectroscopy. However, divalent Ba^{2+} when mixed with (*D*, *L*)-**G (8)** gave homochiral G-quadruplexes (**Figure 1.11**). The almost complete enantiomeric self-recognition from this cation-dependent diastereoselectivity was suggested to be caused by the enhanced enthalpy inherent to the divalent cation-oxygen interaction that might help overcome the unfavorable entropy associated with enantiomeric self-sorting.

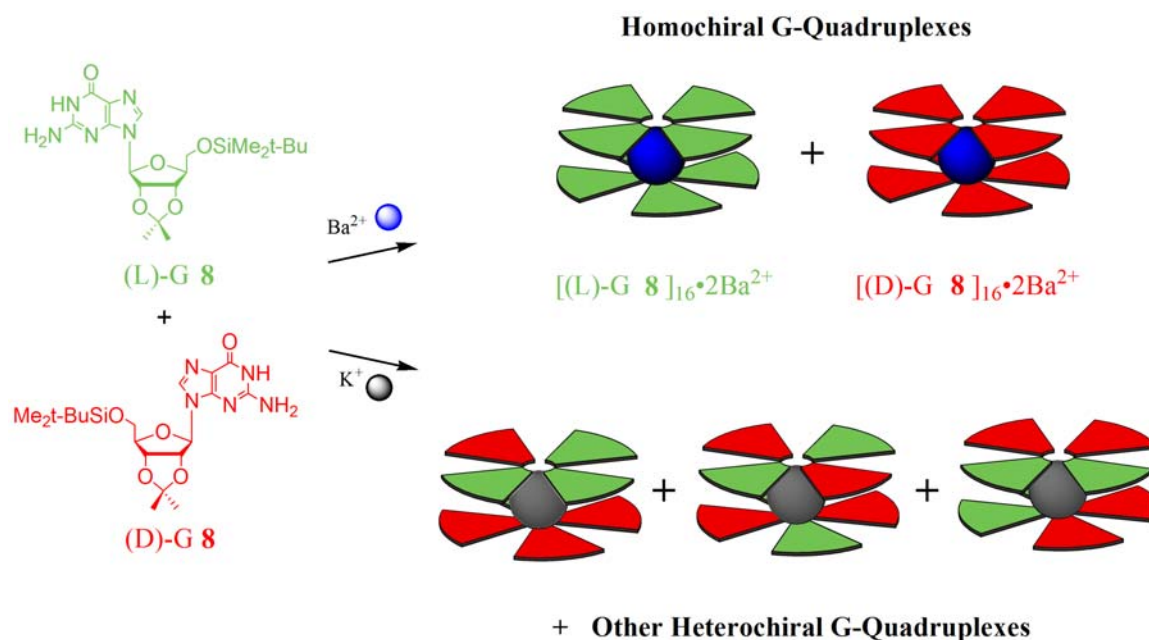
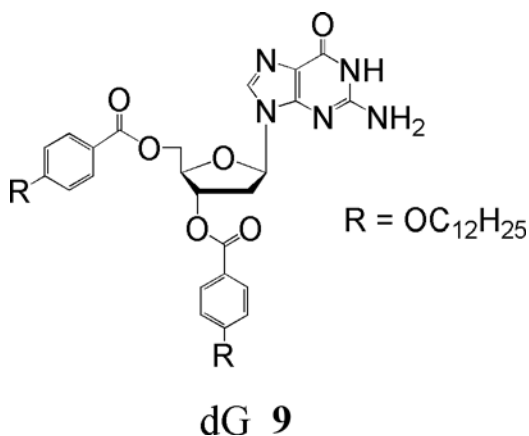


Figure 1.11. G **8** undergoes cation dependant enantiomeric self-association. Racemic (*D*, *L*)-G **8** self-assembles in the presence of Ba^{2+} to give homochiral G-quadruplexes $[(D)\text{-G } \mathbf{8}]_{16} \cdot 2\text{Ba}^{2+} \cdot 4\text{pic}^-$ and $[(L)\text{-G } \mathbf{8}]_{16} \cdot 2\text{Ba}^{2+} \cdot 4\text{pic}^-$. Addition of K^+ to G **8** gave a diastereomeric mixture of heterochiral assemblies.⁵⁹ The green wedges represent (*L*)-G **8**, while the red wedges represent (*D*)-G **8**. The blue and gray spheres represent Ba^{2+} and K^+ respectively.

Since the anion binding groove of the G-quadruplex is chiral, these lipophilic G-quadruplexes might be useful as chiral resolving agents or as enantioselective catalysts. Gottarelli and colleagues reported that G-quartet structures formed from dG **9** are modestly enantioselective in their ability to extract chiral anions from water into organic solvents. Specifically, dG **9** was shown to extract K^+ N-dinitrophenyl- (*L*)-tryptophan salt from water into CDCl_3 with a 3:1 enantioselectivity over the (*D*)-Trp enantiomer. This modest enantioselectivity suggests that there must be significant interactions between anions and the chiral G-quadruplex.⁶⁰



1.6.3 “Empty” G-Quartets.

Although cations are usually essential for the templation of G-quartets, there have been examples of G-quartets formed in the absence of cations. Generally, guanosine analogs form hydrogen-bonded dimers or ribbons. Sessler and colleagues solved a crystal structure of G **10** that revealed an “empty” G-quartet. G **10** was shown to self-assemble into a G-quartet even without the assistance of a templating cation.⁶¹ Attachment of sterically bulky groups, a dimethylaniline unit, to the C8 position of the guanine ring gave a conformationally constrained nucleoside that prefers to adopt a *syn* glycosidic bond conformer in both the solid state and solution. This *syn* conformation prevents the nucleoside from any hydrogen-bonded ribbon formation and thus favors formation of the macrocyclic G-quartet (**Figure 1.12**). This study showed how control over the monomer can have profound impacts in the self-assembly of guanosine analogs.

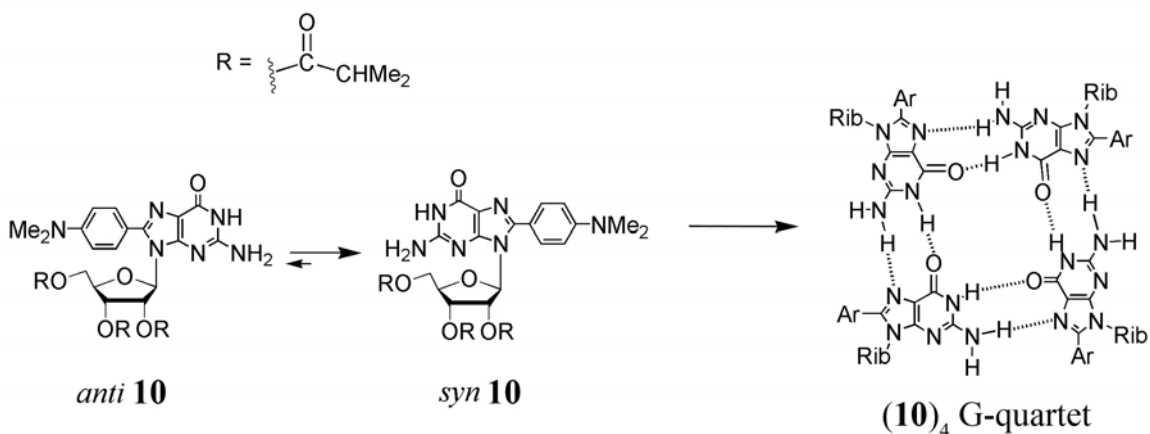


Figure 1.12. Conformationally constrained G **10** forms a G-quartet without presence of a templating cation.⁶¹

Shortly after, Kotch and colleagues showed that a calixarene-guanosine analog forms a hydrogen-bonded dimer $(cG \mathbf{11})_2 \cdot (\text{H}_2\text{O})_n$ in wet CDCl_3 , with water presumably taking the cation's place within the center G-quartet cavity (**Figure 1.13**).⁶² In dry CDCl_3 , poorly aggregated structures were observed. This finding was consistent with a prediction, made by Gellert and colleagues in 1962 that an “empty” G-quartet might contain a cavity that could bind water molecules.¹⁹

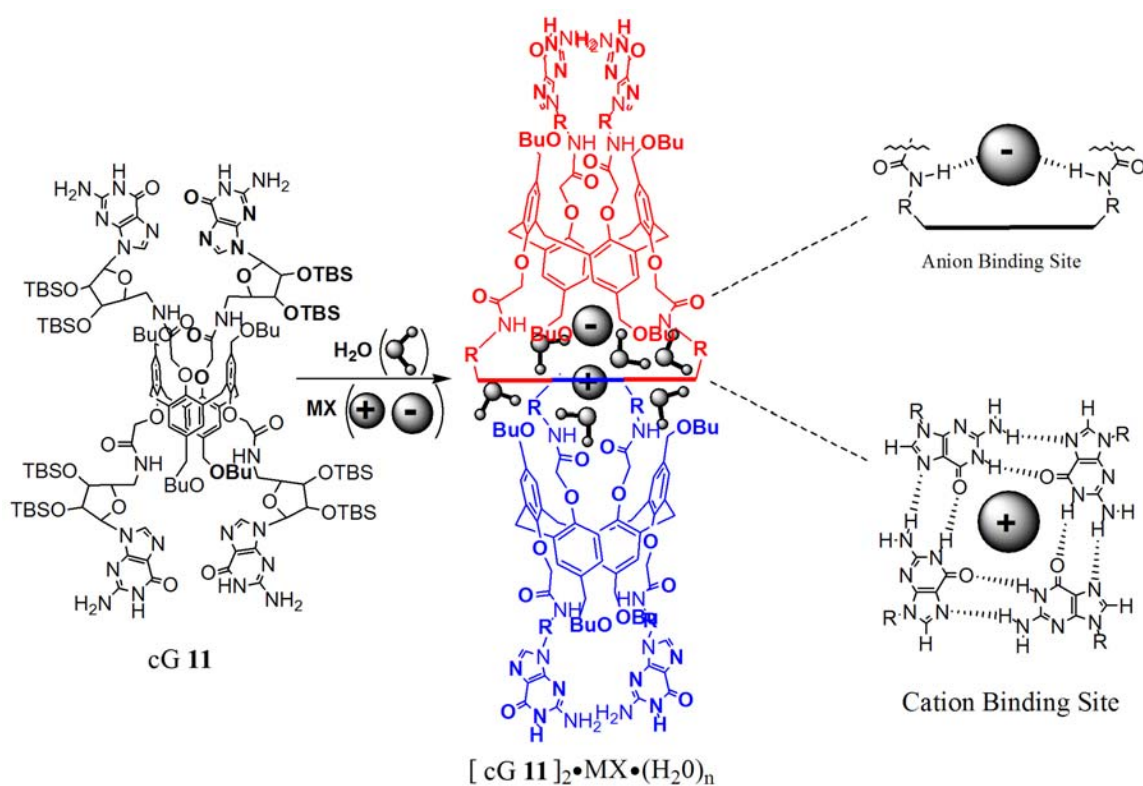


Figure 1.13. A schematic representation of $[\text{cG } 11]_2 \cdot \text{MX} \cdot (\text{H}_2\text{O})_n$ that shows the anion and cation binding sites.⁶²

More recently, Besenbacher and colleagues showed that guanine **12** can form a kinetically stable “empty” G-quartet on a gold surface (**Figure 1.14**).⁶³ Using AFM they found that the empty G-quartet was not the thermodynamic minimum, as annealing the deposited G-quartet network led to rearrangement into a hydrogen-bonded ribbon. In this case, the available N9-H and the neighboring N3 positions of guanine **12** seem crucial for stabilizing the network of connected G-quartets. The Besenbacher paper is the first demonstration that guanine itself forms cyclic quartets, as other G-quartets have always involved N9-substituted G nucleobases.

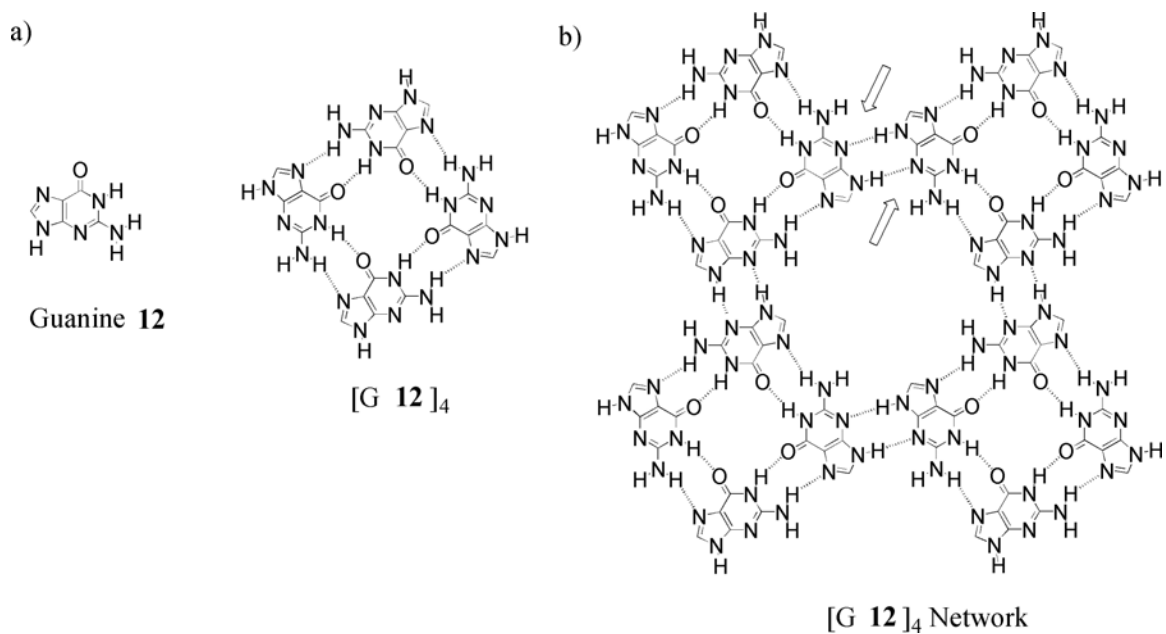


Figure 1.14. a) An empty G-quartet formed by guanine **12**. b) A hydrogen bond network of empty G-quartets. Each G-quartet can form up to eight additional hydrogen bonds with neighboring G-quartets (arrows).⁶³

1.6.4 Increasing the Number of Hydrogen Bonds in a G-quartet.

Recently, Rivera and coworkers reported another way to stabilize G-quartet units by using 8-aryl-dG analogs such as dG **13**.⁶⁴ By adding a hydrogen bond acceptor to the C8 position, an additional hydrogen bond was forced between the exocyclic N2 amino hydrogen and the carbonyl of the hydrogen bond acceptor (**Figure 1.15**).

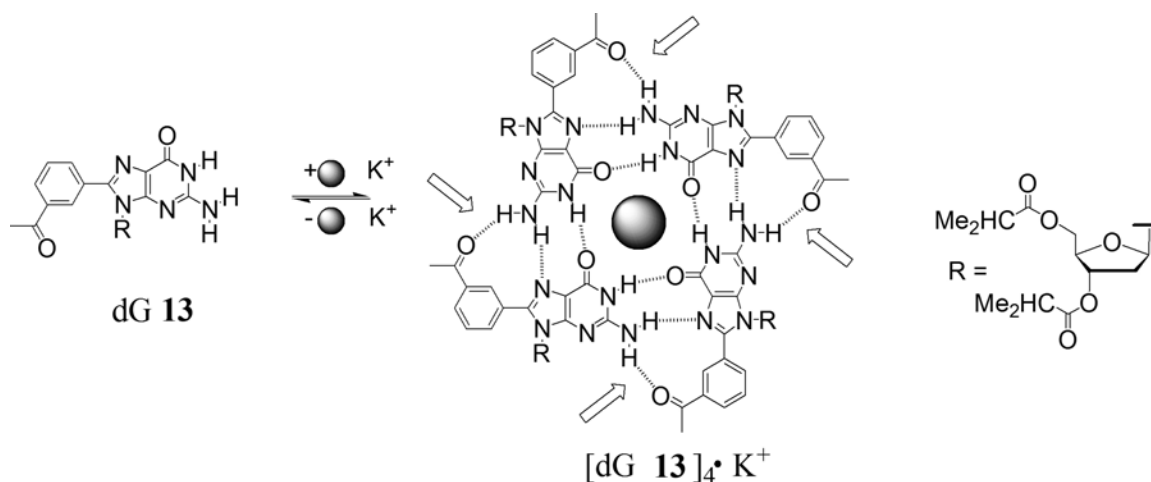


Figure 1.15. A G-quartet formed from **dG 13**, a modified nucleobase with an expanded Hoogsteen hydrogen bonding face. Note the additional hydrogen bonds, depicted by arrows, thought to be a reason for increased stability.⁶⁴

The G-quadruplex $[\text{dG } \mathbf{13}]_{16} \cdot 3\text{K}^+$ showed an increased stability when compared with assemblies from the unsubstituted G derivatives as proven by variable temperature and dilution NMR experiments. Rivera proposed that the stability of the 8-aryl-dG analog **13** was due to a combination of factors. Again, the C8 substitution forces the derivative into the *syn* conformation, therefore precluding formation of hydrogen bonded ribbon structures. Additionally, the four additional aromatic rings attached to C8 provide larger surface for π - π interactions between the stacked G-quartets. And lastly, the C8 substituent in **dG 13** enables four additional hydrogen bonds per G-quartet, as depicted by the arrows in **Figure 1.15**.

1.6.5 The G-Quartet and Dynamic Covalent Chemistry.

Dynamic covalent chemistry (DCC) is now a major synthesis strategy in supramolecular chemistry, enabling amplification of select compounds from a dynamic

combinatorial library (DCL) of equilibrating compounds.^{65,66} In this approach, building blocks that form reversible covalent bonds are used to build a DCL. Stabilization of a library member upon addition of a template results in a new equilibrium. The end result, in accord with Le Chatelier's principle, is amplification of stabilized products in the mixture.

This DCC strategy has been used to produce new ligands that bind to G-quadruplexes. Previous studies have shown that i) acridone ligands (A) stack on the terminal tetrad of a G-quadruplex and that ii) certain peptides (P) interact with the grooves formed by the DNA backbone of the tetraplex.⁶⁷⁻⁷⁰ Balasubramanian and colleagues used a disulfide exchange reaction, carried out in the presence of glutathione disulfide and a G-quadruplex template, to identify new G-quadruplex interactive ligands that combine both the acridone and peptide recognition motifs.⁷¹ Disulfide exchange under aqueous conditions is popular for DCC applications, as the reaction is relatively rapid at pH > 7 but not under acidic conditions (pH < 5). Thus, disulfide exchange can be carried out under reversible conditions at moderate pH but then the reaction can be acid quenched to determine product composition. Using the deoxyoligonucleotide 5'-biotin(GTTAGG)₅, that contains the human telomeric sequence as a template, Balasubramanian's team demonstrated that there was a 400 % increase in the formation of the heterodimeric disulfide AssP, a compound containing both the acridone (from A **14**) and peptide (from P **15**) domains, when compared to control experiments carried out in the absence of a G-quadruplex (**Figure 1.16**). In addition, the authors made the surprising discovery that the peptide dimer PssP was formed in 5-fold greater amount in the presence of the G-quadruplex template. Quantitative binding studies using surface

plasmon resonance showed that the complexes formed by these new ligands and the human telomere G-quadruplex have dissociation constants of $K_d = 30$ and $22.5 \mu\text{M}$ for AssP and PssP, values that are far lower than the dissociation constant for the AssA-DNA complex ($K_d > 2.5 \text{ mM}$). This same research group also used disulfide exchange to identify pyrrole-amide dimers formed with modest amplification in the presence of a G-quadruplex template.⁷² These two studies established that DCC could provide new G-quadruplex ligands, a potentially important endeavor in the search for effective telomerase inhibitors.

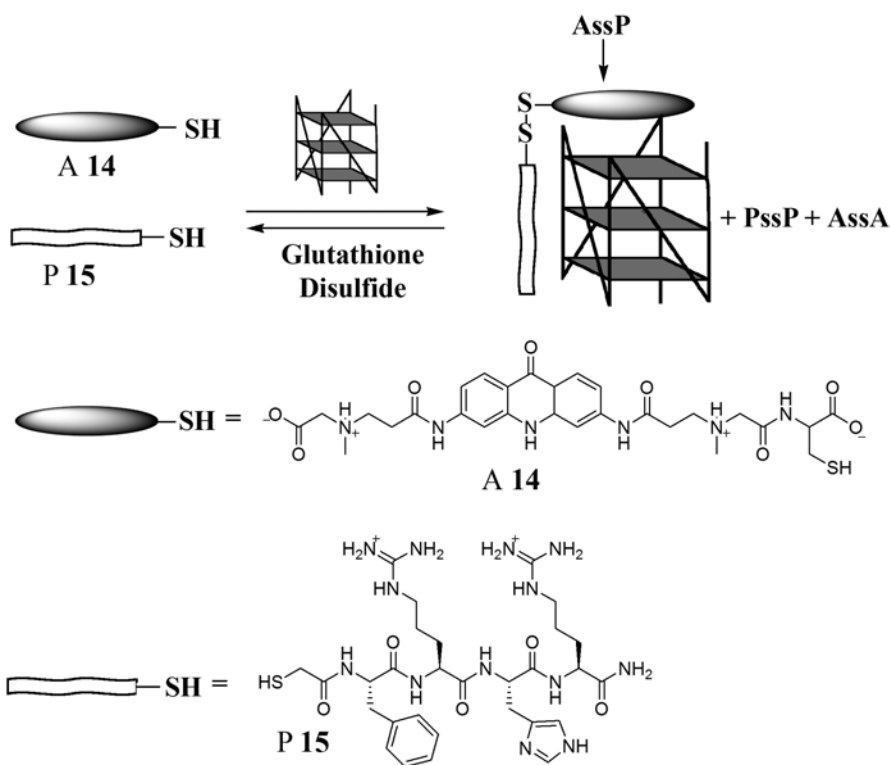


Figure 1.16. The AssP disulfide product is selectively amplified in the presence of a G-quadruplex template.⁷¹

In addition to the discovery of new ligands that interact with tetraplex structures, the DCC concept has also been used by the Balasubramanian and Lehn groups to form new G-quadruplex structures, each with its own unique properties.⁷³⁻⁷⁵ Thus,

Balasubramanian and colleagues reported that a G-rich PNA, modified to allow for covalent bond formation between strands, underwent “self-templation” to form a bimolecular G-quadruplex.⁷⁴ In this study, they showed that formation of a non-covalent PNA G-quadruplex preceded covalent bond formation. The authors first demonstrated that an equimolar mixture of PNA-peptide strands, namely Lys-TGGG-GlyGlyCys-SH (G_S) and Lys-TTTT-GlyGlyCys-SH (T_S) gave a 1:2:1 statistical mixture of the 3 possible disulfides $G_{SS}G$, $G_{SS}T$ and $T_{SS}T$ when oxidized with sodium perborate (**Figure 1.17**). In contrast, the slower air oxidation of a mixture of the same 2 PNA strands gave a 2:1:2 ratio of $G_{SS}G$, $G_{SS}T$ and $T_{SS}T$ indicating that $G_{SS}G$ was somehow stabilized under these oxidation conditions. Mass spectrometry and UV melting experiments indicated that the $G_{SS}G$ dimer formed a bimolecular G-quadruplex ($G_{SS}G$)₂, presumably a bimolecular hairpin structure wherein the Gly-Cys-Cys-Gly tetrapeptide forms the loop regions. Other measurements indicated that the G_S PNA strands were preorganized into a G-quadruplex prior to formation of the disulfide bond that gave the $G_{SS}G$ product. Significantly, formation of the $G_{SS}G$ disulfide bond depended on the cation template, being most effective with K^+ , the cation that best stabilizes a G-quadruplex.

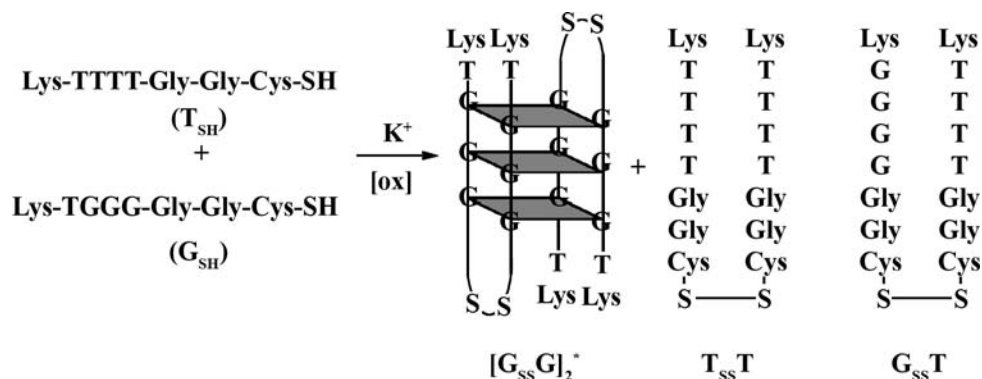


Figure 1.17. Oxidation of the PNA strands T_{SH} and G_{SH} provides disulfides. In the presence of K^+ , $G_{SS}G$ is amplified. The structure depicted for ($G_{SS}G$)₂ represents just one possible orientation of a bimolecular G-quadruplex.⁷⁴

Lehn and Sreenivasachary have recently described a G-quartet based system wherein component selection from a DCL is driven by the product's physical properties.⁷³ They first showed that guanosine hydrazide **16** formed viscous, thermally reversible gels at moderate pH in the presence of Na⁺ and K⁺. These gels arose from the stacking and crosslinking of cation stabilized G-quartets. The 5'-hydrazide group in G-quartet gels formed by G **16** was then reacted with various aldehydes to form acylhydrazone bonds, allowing the authors to study the effects of sidechain modification on gel properties. While addition of some aldehydes destroyed the hydrogels, other aldehydes (including **17**) formed acylhydrazone gels that were even stronger than the parent gel from hydrazide G **16**. These findings prompted the authors to explore whether the stability of the gel phase might drive component selection in a DCL (**Figure 1.18**). A dynamic mixture composed of 4 acylhydrazones, from reaction of aldehydes **17** and **18** with hydrazides G **16** and serine **19**, was generated under conditions where the 5'-acylhydrazones could equilibrate by undergoing reversible bond cleavage and reformation. The resulting product distribution, measured by ¹H NMR, was sensitive to temperature. At 80 °C, well above the gel transition temperature, the solution distribution of products was statistical, indicating that the 4 acylhydrazones (A-D) were of similar stability. Between 25-55 °C acylhydrazone B, in its gel-state, and C in solution were significantly favored over acylhydrazones A and D. In this case, self-assembly of hydrazide G **16** was driven by selection of the components that gave the most stable hydrogels. The stability of G-quartet hydrogel B altered the dynamic equilibrium of acylhydrazones and directed reaction of the hydrazide G **16** with aldehyde **18**. Lehn explained that “...(t)he process amounts to gelation-driven self-organization with

component selection and amplification...based on G-quartet formation and reversible covalent connections.” This DCC approach may well have broad applications in medicinal chemistry and material science.

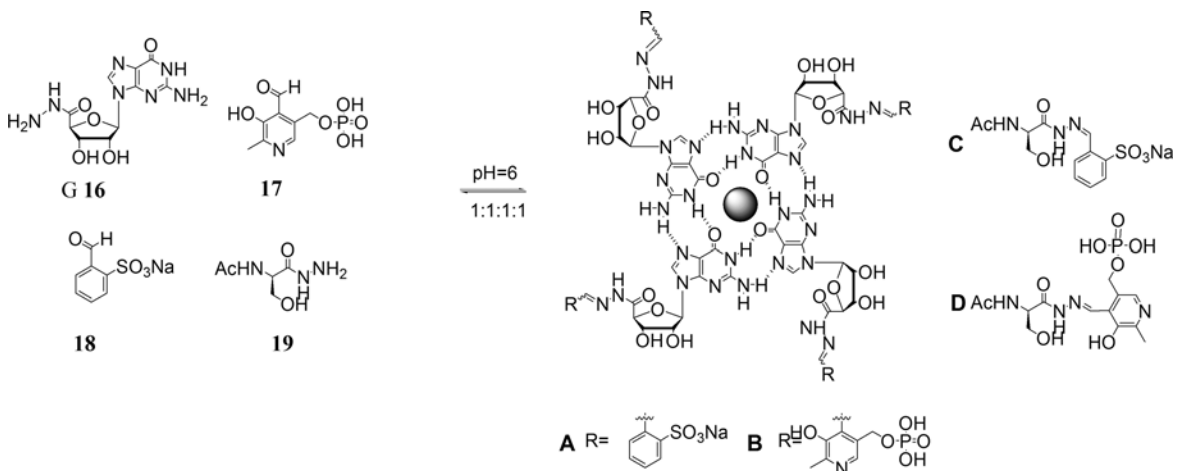


Figure 1.18. The stability of G-quartet hydrogel **B** altered the dynamic equilibrium of acylhydrazones and directed reaction of the G hydrazide **16** with aldehyde **18**.⁷³

Ghossoub and Lehn have recently described another dynamic sol-gel interconversion process, in this case triggered by the reversible binding and release of K⁺ by a G-quartet hydrogel.⁷⁵ Supramolecular hydrogels formed by the ditopic monomer G-G **20** were readily converted to soluble (G-G)_n polymers upon addition of [2.2.2]-cryptand **21**, an ionophore able to extract the stabilizing K⁺ from the G-quartet hydrogel. The gel state could be regenerated upon expelling K⁺ from the [K⁺ 2.2.2]-cryptate complex by protonating the [2.2.2]cryptand's bridgehead nitrogen atoms to give [2H⁺ 2.2.2] **21**. In this way, gel-sol interconversion was effected over multiple cycles by simply controlling the equilibrium of the bound K⁺ between the G-quartet and the [2.2.2]cryptand, a ligand whose cation binding properties can be modulated by the solution pH (**Figure 1.19**).

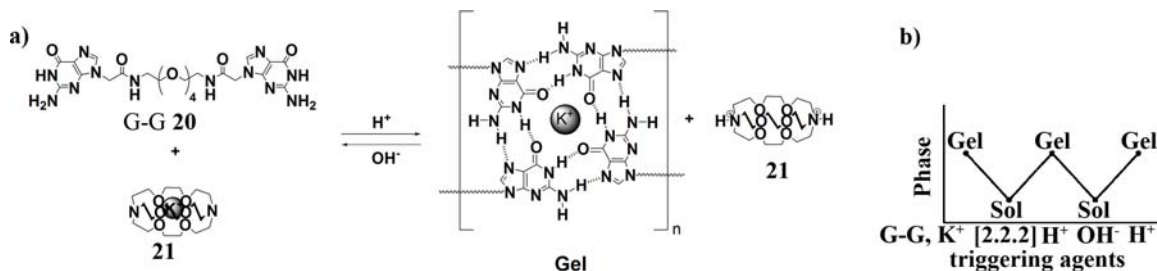


Figure 1.19. a) Structure of G-G **20** and schematic of the reversible formation of polymeric G-quartet based hydrogels. Changing pH in the presence of [2.2.2]cryptand **21** modulated the sol-gel equilibrium. b) Representation of the modulation of the gel-sol status induced by the sequence of triggering agents.⁷⁵

1.7 Biosensors and Nanostructures Based on DNA G-Quadruplex Structures.

1.7.1 Potassium Ion Sensors.

As described earlier, TBA, a 15-mer oligonucleotide, folds into stable G-quadruplexes under well-defined conditions. TBA has been exploited to develop optical and electronic sensors, for analytes ranging from K^+ ion to proteins to nucleic acids based on this facet. The use of the TBA sequence as the basis for a biosensor is nicely demonstrated in a recent study by Takenaka's group.⁷⁶ They used a modified TBA as a fluorescent indicator for detecting K^+ in water. Attachment of pyrene groups to the 5' and 3'-ends of the DNA gave a probe coined "PSO-py" for potassium sensing oligonucleotide-pyrene. This PSO-py is a promising sensor for the real-time detection of K^+ in biological and environmental samples. One challenge in developing an optical K^+ sensor is achieving selectivity in the presence of high Na^+ concentrations. Another challenge is to obtain a fast response that allows for real-time monitoring of the cation. PSO-py used the excimer formation from π -stacked pyrenes to signal K^+ binding. In the absence of K^+ , PSO-py is primarily unfolded and provides little excimer emission. In the

presence of K^+ , the 5' and 3' ends of the folded DNA stack pyrenes in a face-to-face geometry to give a new excimer band (**Figure 1.20**). Importantly, the presence of other cations gave little interference as only K^+ binds with high-affinity to the TBA G-quadruplex. The fluorescence spectrum of PSO-py in the absence of K^+ showed a weak monomer emission at 390 nm. Addition of K^+ gave a strong excimer band at 480 nm, accompanied by quenching of monomer emission. Changes in excimer fluorescence indicated that the K^+ and Na^+ complexes of PSO-py had dissociation constants (K_d) of 7.33 and 272 mM, respectively. This K^+/Na^+ selectivity coefficient of 37 for PSO-py is higher than for many other previous K^+ sensors. Independent CD measurements of PSO-py, in the presence and absence of K^+ , confirmed that the excimer fluorescence corresponded to a structural shift from a random coil to a chair-like G-quadruplex. The dynamics of the fluorescence response for the PSO-py/ K^+ system also showed a short response time (within seconds) upon variation in ion concentration. Moreover, this dynamic excimer fluorescence was both reversible and reproducible. The PSO-py oligonucleotide, well suited for real-time monitoring of K^+ in water, is representative of a range of bioprobes that have been rationally designed by using knowledge of G-quadruplex structure and properties.

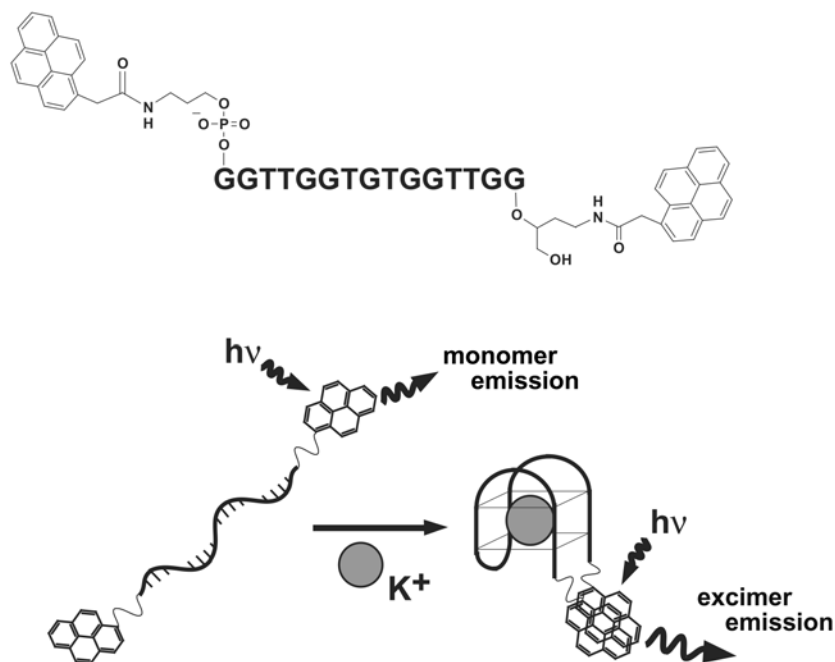


Figure 1.20. Chemical structure of the PSO-py and the expected G-quadruplex induced by K^+ binding. Pyrene excimer emission occurs in the presence of K^+ . Reprinted with permission from John Wiley & Sons, Inc.⁷⁶

The PSO-py oligonucleotide, which uses excimer emission as an optical signal, is actually a second-generation sensor. Takenaka's prototype, described in 2002, was a modified DNA oligonucleotide that underwent efficient fluorescence resonance energy transfer (FRET) upon folding into an intramolecular G-quadruplex.⁷⁷ This original PSO with the sequence d (5'-GGGTTAGGGTTAGGGTTAGGG-3') had a 6-carboxyfluorescein donor group attached to its 5'-end and a rhodamine acceptor linked to the 3'-terminus. When folded into a G-quadruplex, the 2 chromophores are located close enough together to undergo efficient energy transfer (**Figure 1.21**). Importantly, G-quadruplex formation by this PSO, as measured by FRET, was again highly selective for K^+ over Na^+ .

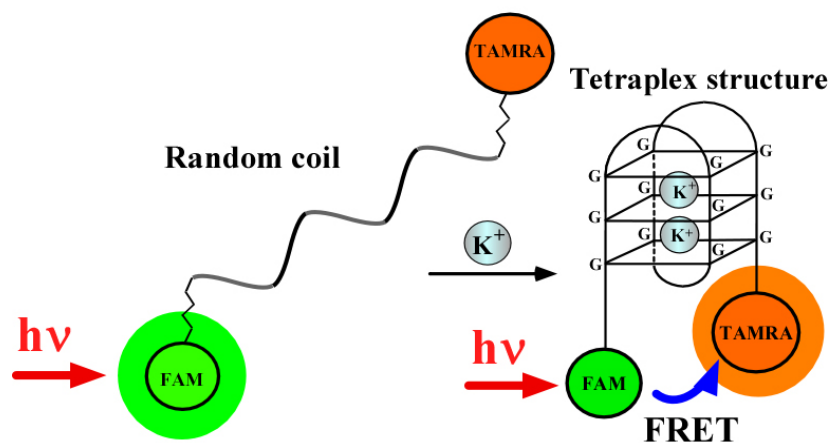
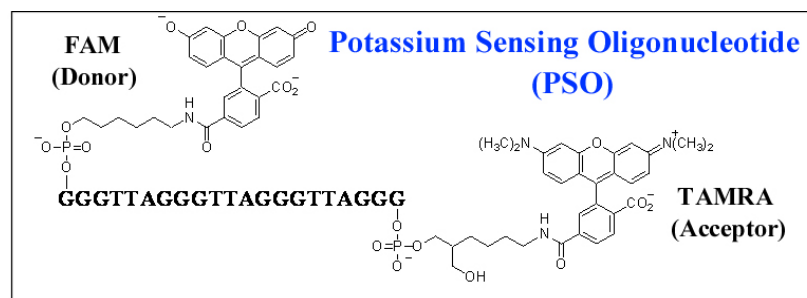


Figure 1.21. Chemical structure of the PSO and the expected G-quadruplex induced by K^+ binding. In this case FRET occurs in the presence of K^+ . Reprinted with permission from the American Chemical Society.⁷⁷

Ho and Leclerc described another interesting method for the optical detection of K^+ , based on formation of colored complexes between a cationic polythiophene and negatively charged DNA (**Figure 1.22**).^{78,79} Because of changes in the conformation of its conjugated backbone, this flexible polymer senses different DNA topologies. Ho and Leclerc showed that this polythiophene distinguishes the single-stranded and G-quadruplex forms of TBA, enabling the polymer to be used as a selective probe for K^+ , since that specific ion is required for folding TBA. This simple “staining” method for detection of the TBA G-quadruplex (or for any species that templates or stabilizes G-quadruplex structure) has the obvious advantage that it does not require chemical labeling

of the DNA. Ho and Leclerc have also shown that their method is useful for the selective and sensitive (femtomolar range) measurement of the thrombin protein and for the highly enantioselective detection of L-adenosine.⁷⁸ Leclerc's biosensor strategy should also be ideal for identification of small molecules that bind to the G-quadruplex, thus providing a new method for screening potential anti-telomerase drugs.

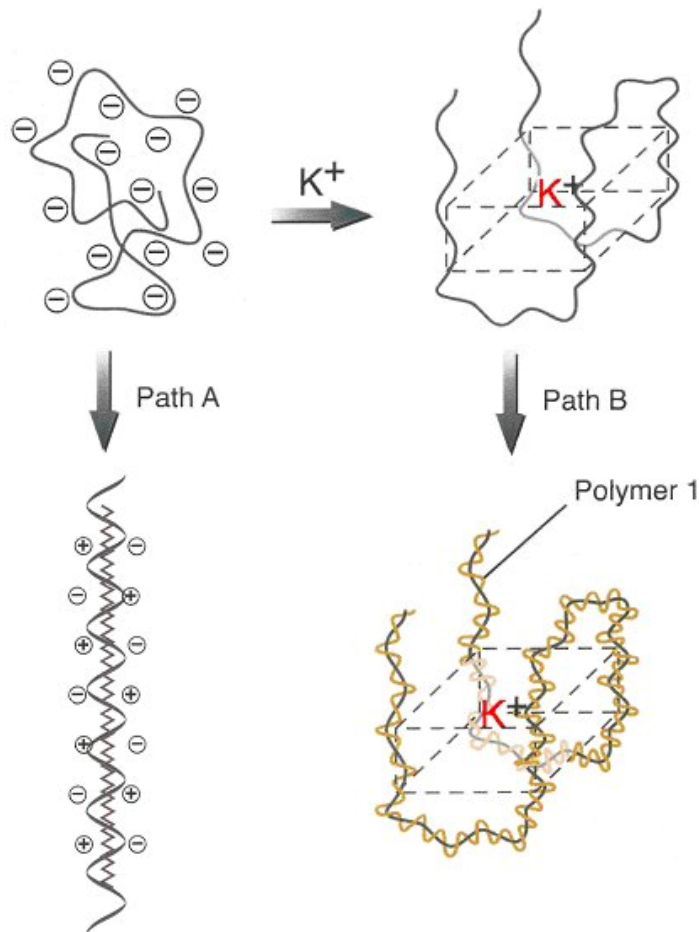


Figure 1.22. An optical K^+ sensor based on a complex formed between G-quadruplex DNA and a conjugated cationic polymer. Reprinted with permission from John Wiley & Sons, Inc.⁷⁸

Wang and co-workers recently developed a related polymer-based assay for K^+ detection that benefits from the sensitivity that is available from the FRET process. In

their case, energy transfer was observed from a cationic conjugated polymer to a TBA oligonucleotide labeled at its 5'-end with a fluorescein acceptor. Notably, they observed a significant increase in emission at 518 nm for the polymer-labeled TBA complex only when in the presence of relatively low concentrations of K^+ . The magnitude of the FRET signal, which has a $1/r^6$ dependence on the distance between donor and acceptor, was attributed to the stronger electrostatic interactions that hold the cationic polymer closer to the compact and charge-dense G-quadruplex form of the TBA (**Figure 1.23**). In this way, K^+ ion was readily detected in water at low concentrations, even when other monovalent and divalent cations were present in excess.⁸⁰

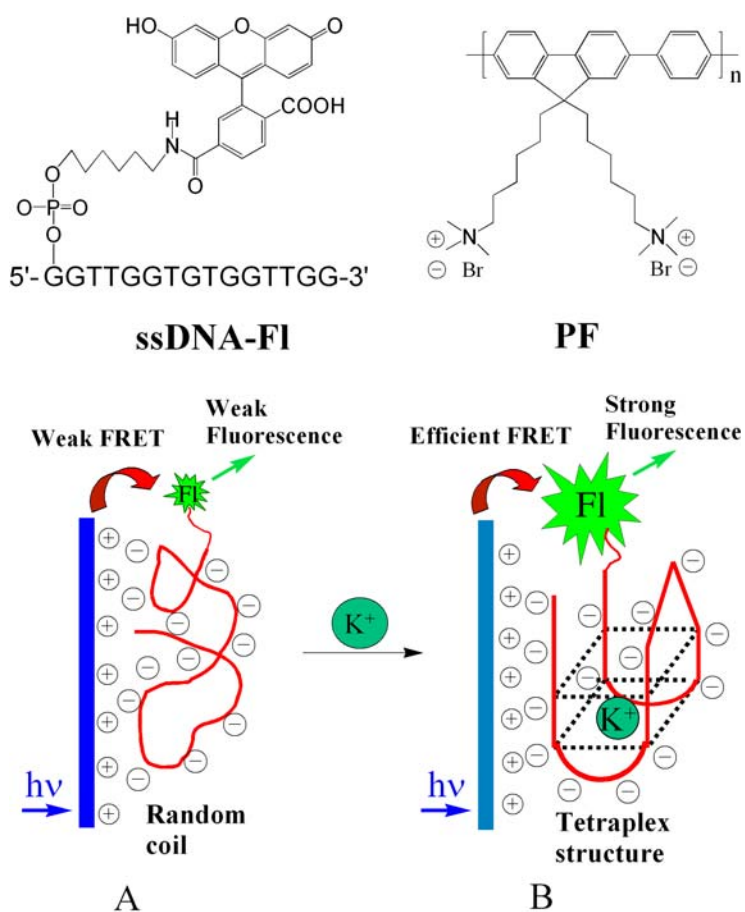


Figure 1.23. Schematic representation of an optical K^+ sensor based on G-quadruplex-polymer interactions that lead to FRET. Reprinted with permission from the American Chemical Society.⁸⁰

1.7.2 G-Quadruplexes as Optical Sensors for Proteins.

In 1998, Hieftje and colleagues described the first example of a protein sensor formed by the TBA sequence.⁸¹ They prepared a DNA conjugate that had the TBA labeled at its 5'-end with fluorescein and modified at its 3'-end by an amino siloxane linker, enabling covalent attachment of the oligonucleotide to a glass surface (**Figure 1.24**). Once the modified DNA had been tethered to glass they used evanescent-wave-induced detection of fluorescence anisotropy to detect the specific binding of thrombin in solution to the immobilized TBA ligand. The resulting protein-DNA complex, being much larger than the DNA probe showed a significant change in its rotational diffusion rate, as detected by the change in fluorescence anisotropy. The change in fluorescence anisotropy was specific to both the TBA and the protein analyte. Thus, scrambled DNA sequences that don't form G-quadruplexes did not show any enhanced fluorescence anisotropy. Likewise, serine proteases other than thrombin did not bind to the fluorescein-labeled TBA. This TBA biosensor was sensitive and rapid, as it could detect as little as 0.7 amol of thrombin over a dynamic range of 3 orders of magnitude (from nanomolar to micromolar) in less than 10 minutes.

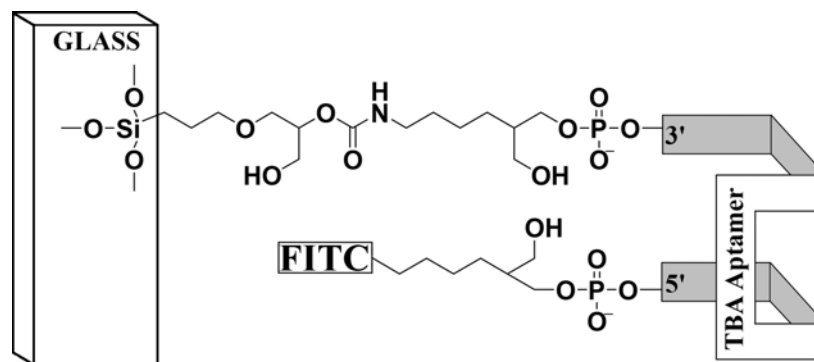


Figure 1.24. A fluorescein modified DNA oligonucleotide that functions as biosensor for thrombin.⁸¹

Lee and Walt used a related strategy to build a thrombin biosensor by covalent attachment of the TBA sequence to silica microspheres.⁸² They then used a fiber optic device to detect the binding of fluorescein-labeled thrombin to these glass beads. They also developed a more practical assay that involved the competitive binding and displacement of fluorescein-labeled thrombin by unlabeled protein. Despite the need for specialized equipment this paper described an assay for thrombin in solution that was highly selective, rapid and reproducible.

In 2001 Stanton and colleagues described the use of “aptamer beacons” for the direct detection of thrombin binding.⁸³ They chemically synthesized an oligonucleotide that contained the TBA sequence embedded within a longer DNA strand that was designed to form a stem-loop structure in the absence of thrombin. This DNA oligonucleotide contained a fluorescein chromophore at its 5'-end and a quencher group at its 3'-end. Thus, when the oligonucleotide was in its stem-loop conformation the 5'-fluorescein was quenched by the nearby 3'-DABCYL unit. Addition of thrombin shifted the DNA's conformational equilibrium from the stem-loop structure to a folded G-quadruplex, causing an increase in the chromophore-quencher distance and a

fluorescence enhancement (**Figure 1.25**). The authors stressed that this method for thrombin detection could, in principle, be applied to other nucleic acid aptamers by simply embedding the protein binding sequence within an unproductive stem-loop structure that contained juxtaposed fluorescent label and quencher. Binding of the target protein should shift the conformational equilibrium and stabilize the aptamer's structure, resulting in fluorescence enhancement as the fluorophore-quencher separation changes. They envisioned using this strategy to make biosensors for proteomics applications using high-throughput, automated selection techniques.

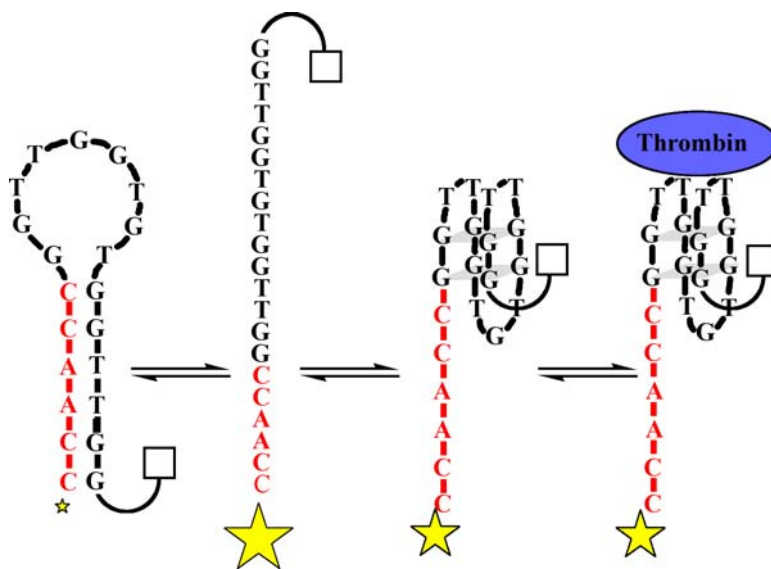


Figure 1.25. A protein biosensor based on the “aptamer beacon” strategy. Thrombin shifts the DNA’s conformational equilibrium to G-quadruplex and produces an increase in fluorescence as the donor-quencher groups get farther apart, compared to the stem-loop structure. Reprinted with permission from Elsevier.⁸³

Tan and colleagues also used the aptamer beacon strategy to develop real time sensing of thrombin.^{84,85} In addition to using fluorescence quenching, they also used both FRET and excimer strategies that allowed for significant fluorescence enhancement upon formation of a DNA-thrombin complex. Their aptamer beacon design involved labeling

the 5'-end of a 15-mer with an energy acceptor, 6-FAM, and the 3'-end with a coumarin group as an energy donor. (**Figure 1.26**) This modified 15-mer tended to favor a random coil conformation in low salt and the absence of thrombin, whereas the equilibrium was shifted to the folded TBA G-quadruplex in the presence of thrombin. This conformational change resulted in a significant enhancement in the fluorescence signal for 6-FAM as the chromophores came closer together in the folded state. These assays were highly sensitive giving a detection limit of 112 ± 9 pM for thrombin.

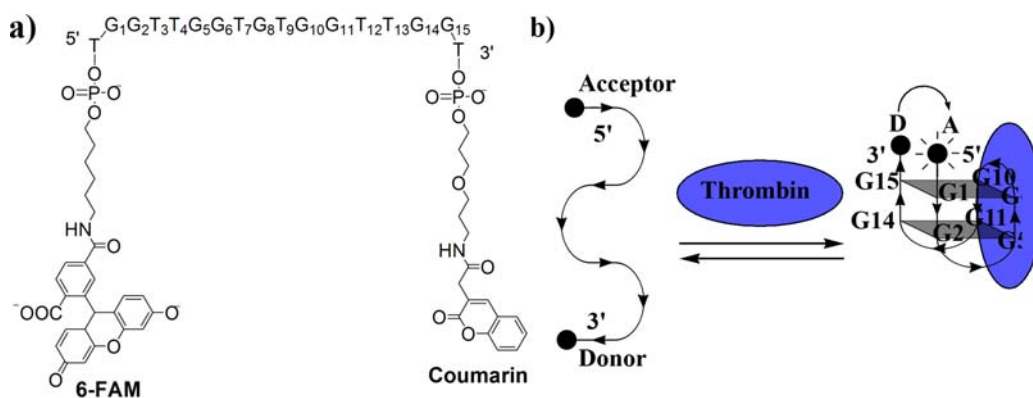


Figure 1.26. Structure of a) acceptor-donor TBA and b) schematic showing FRET upon binding of thrombin to TBA.⁸⁴

In 2003, Nutiu and Li described a strategy for the preparation of fluorescent sensors based on their use of so-called “Structure-Switching Signaling Aptamers”.^{86,87} These DNA aptamers work by undergoing a major structural change from duplex DNA to a DNA-target complex. The starting duplex is formed between a DNA strand that contains the aptamer sequence and 2 shorter oligonucleotides; one of the shorter oligonucleotides contains a fluorophore and the other short strand contains a quencher. In the absence of the thrombin target the aptamer strand binds to the short oligonucleotide

containing the quencher, bringing it into proximity to the fluorophore and causing maximum quenching. Upon addition of the thrombin protein, the aptamer sequence releases the short oligonucleotide containing the bound quencher, resulting in a strong fluorescence enhancement. (Figure 1.27)

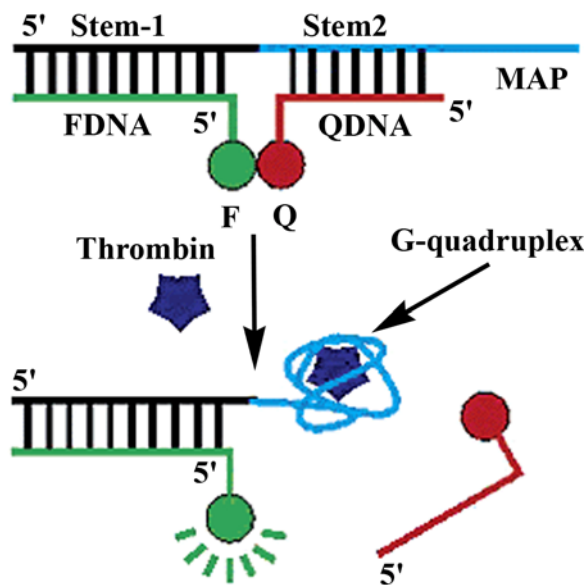


Figure 1.27. The Structure-Switching Signaling Aptamer. A DNA duplex composed of three strands of DNA places a fluorophore (F) close to a quencher group (Q). Upon addition of thrombin, the QDNA piece is released, and the fluorescence increases. Reprinted with permission from John Wiley & Sons, Inc.⁸⁷

In 2005, Heyduk and Heyduk took advantage of the fact that thrombin has 2 different DNA binding epitopes to facilitate the simultaneous co-association of 2 different aptamers.⁸⁸ Each aptamer was outfitted with a flexible linker region and a DNA sequence that would allow DNA duplex formation and enable simultaneous FRET enhancement. In the absence of the thrombin analyte the 2 DNA strands don't associate because the complementary binding region is too short. However, when both sequences are bound to thrombin the increased entropy favors duplex formation and subsequent FRET enhancement (Figure 1.28).

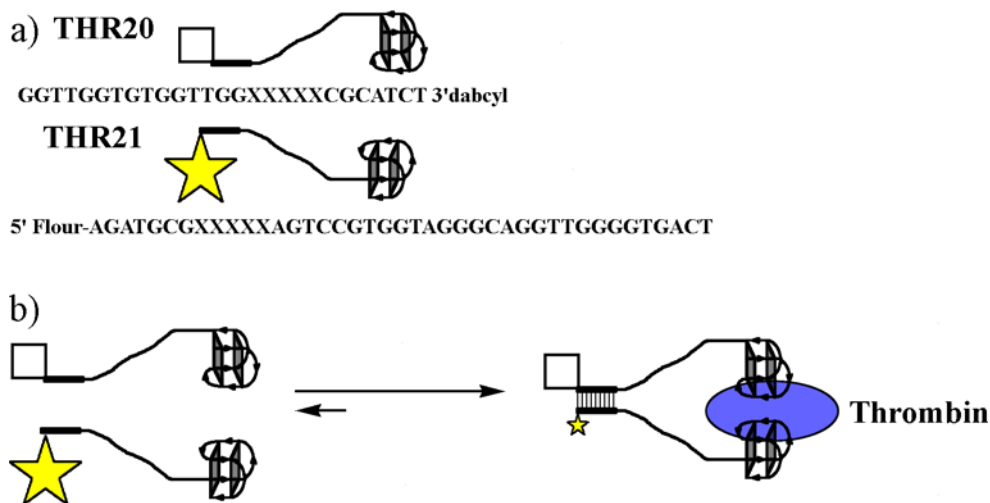


Figure 1.28. a) Detection of thrombin by binding 2 different G-quadruplexes at different epitope binding sites. b) Association of the 2 strands of DNA on the thrombin surface leads to fluorescence quenching.⁸⁸

Willner and colleagues used thrombin's 2 binding epitopes to design an ingenious method for the optical detection of thrombin.⁸⁹ Willner's group used gold nanoparticles functionalized with thiolated aptamers to enable the amplified detection of thrombin both in solution and on glass surfaces (**Figure 1.29**).^{90,91} Reaction of the functionalized Au nanoparticles with thrombin in solution led to significant aggregation, since thrombin's two binding epitopes enabled crosslinking of the Au nanoparticles. Addition of thrombin led to a significant decrease in the plasmon absorbance for the Au nanoparticles. The isolated precipitates were resuspended in solution containing a CTAB surfactant and then used to seed nanoparticle growth using HAuCl₄ and NADH. This catalytic growth of the nanoparticles was monitored by the gold's increased plasmon absorbance at 530 nm. Furthermore, the enlarged nanoparticles showed a red-shifted absorbance at 650 nm that was proposed to originate from a coupled plasmon exciton due

to contacts between enlarged Au nanoparticles. These solution protocols for Au nanoparticle growth were also adapted to enable the optical sensing of thrombin on glass. A TBA oligonucleotide containing a siloxane unit was covalently attached to a glass surface and thrombin was bound to the resulting monolayer. The Au nanoparticles containing the thiolated TBA were then allowed to bind to thrombin through the second epitope site. Catalytic growth of the bound Au nanoparticles was then carried out in the presence of HAuCl_4 , CTAB, and NADH. Both absorbance spectra and QCM measurements confirmed that the thrombin could be detected in a concentration dependant fashion. SEM images also showed that the Au nanoparticles came in contact with each other, entirely consistent with the presence of the interparticle absorbance band at 650 nm.

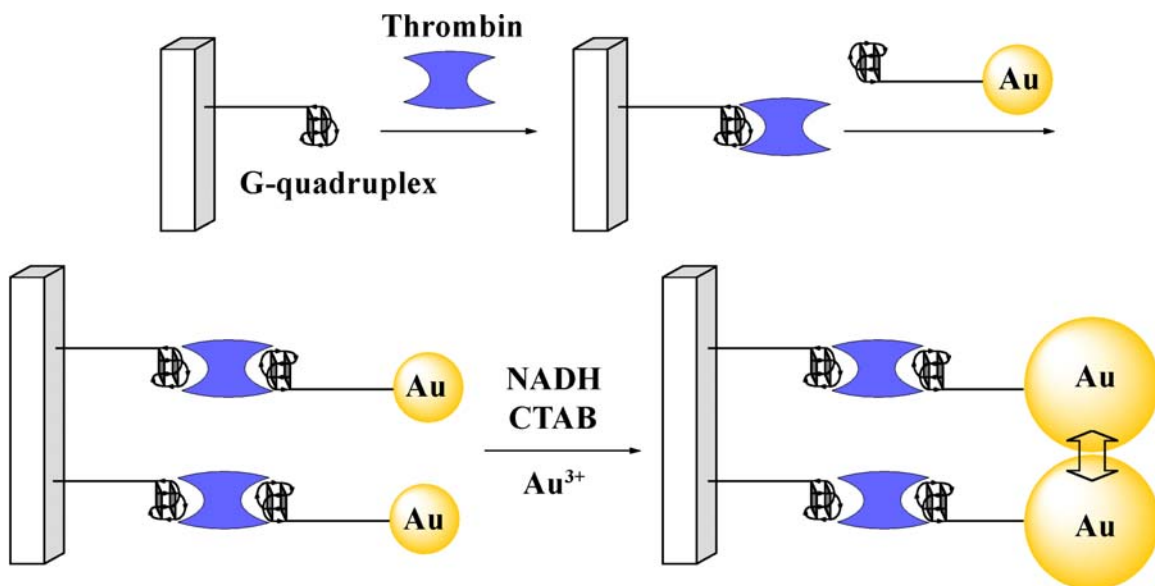


Figure 1.29. Amplified detection of thrombin based on enlargement of Au nanoparticles.⁸⁹

1.7.3 G-Quadruplexes in the Electrochemical Detection of Proteins.

In the past few years a new direction in TBA-based biosensors has been the development of methods for the electrochemical detection of thrombin. Some of the reported advantages of these electrochemical biosensors are their potential to provide high sensitivity, fast response times, low costs, easy fabrication, and the possibility for miniaturization. Ikebukoru and colleagues were the first to report on a TBA based electrochemical sensor.⁹² Like others, they took advantage of thrombin's two separate binding sites. Fabrication of the device involved immobilizing a thiolated TBA sequence onto a gold electrode. A second oligonucleotide that can fold into a G-quadruplex structure was covalently modified at its 3'-end with the enzyme glucose dehydrogenase (GDH). Addition of thrombin to this solution resulted in formation of a sandwich structure wherein the GDH was brought close to the gold electrode. Oxidation of glucose by the immobilized GDH enzyme resulted in a measurable electrical current (**Figure 1.30**). No current was detected in the absence of thrombin, demonstrating that the GDH needs to be close to the Au electrode. Using this electrochemical detection device, thrombin at concentrations as low as 1 μM could be detected.

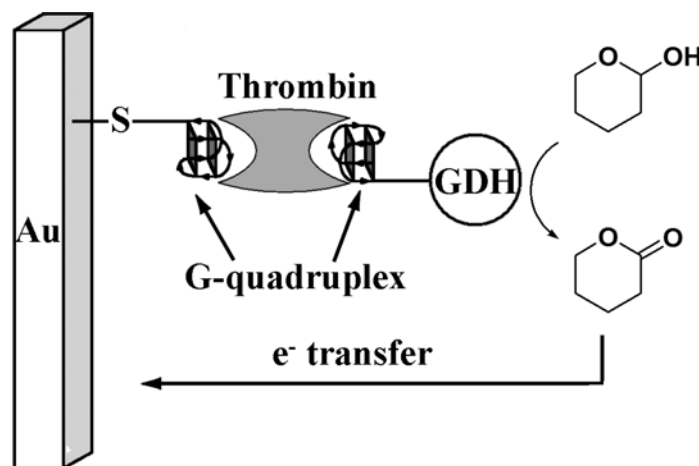


Figure 1.30. Electrochemical detection of thrombin through the coupled oxidation of glucose by glucose dehydrogenase.⁹²

In the last year a flurry of papers from the groups of Hianik, Plaxco, Lee and O'Sullivan have appeared describing a variety of approaches for the electrochemical detection of thrombin.⁹³⁻⁹⁷ Plaxco and colleagues used a 5'-thiolated DNA oligonucleotide containing both the TBA sequence and an electrochemically active group (methylene blue) attached to the 3'-end of the DNA.⁹⁴ This modified DNA oligonucleotide was attached via its thiol tether to the gold electrode. In the absence of thrombin the DNA adopts a conformation such that the electroactive methylene blue label can bind to the gold surface and enable electron transfer with the electrode. However, binding of thrombin by the folded TBA sequence results in a conformational change that turns off electron transfer between the 3'-methylene blue label and the gold electrode. Presumably the aptamer's conformational change significantly increases the electron-tunneling distance between the electrode and the electroactive label. This particular sensor, used to measure thrombin in blood serum, demonstrated excellent dynamic range of 10-700 nM and outstanding sensitivity, such that thrombin at 10-100 nM concentrations could be measured from blood plasma (**Figure 1.31a**).

Radi and O'Sullivan recently described a similar approach wherein they attached a thiolated TBA sequence containing a redox-active ferrocene group to a gold electrode.⁹⁷ A bifunctional 15-base TBA derivative with a ferrocene group and a thiol at its respective 5' and 3' termini was prepared. After anchoring this electroactive aptamer to a gold electrode the rest of the gold surface was coated with 2-mercaptoethanol to form a mixed monolayer. Cyclic voltammetry (CV), differential pulse voltammetry (DPV), and electrochemical impedance spectroscopy (EIS) were used to characterize this DNA-

modified electrode. The modified electrode gave a voltammetric signal due to the redox reaction of the TBA's ferrocene group. The increase in signal intensity upon binding thrombin to the TBA sensor was attributed to a conformational transition from random coil to the folded G-quadruplex (**Figure 1.31b**). In this “signal-on” system, which contrasts to Plaxco’s “signal-off” system,⁹⁴ the authors noted an increased electrochemical signal upon binding thrombin. They suggested that the short length of their DNA tether resulted in a conformational change that brings the ferrocene label closer to the electrode surface and increases electron transfer. This “signal-on” electrochemical biosensor was used for the detection of thrombin without the need for any special reagents. The sensor had nanomolar detection limit for its target and showed little interference from nonspecific proteins. The aptasensor could be easily regenerated and reused 25 times without any loss in detection sensitivity.⁹⁵

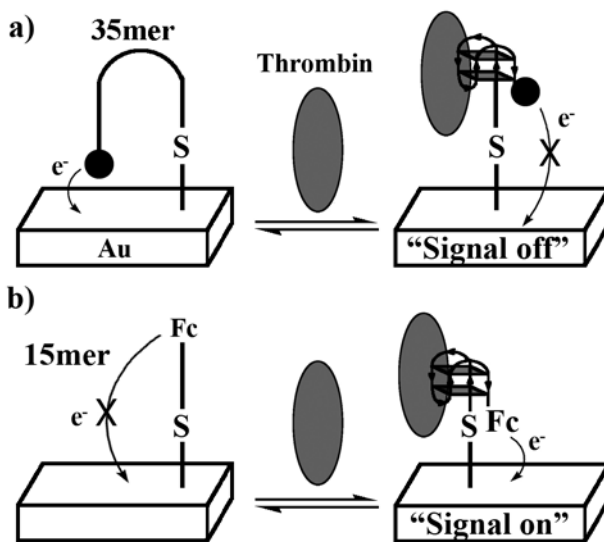


Figure 1.31. Electrochemical biosensors for the detection of thrombin a) “signal-off system” described for a 35mer oligonucleotide containing the TBA sequence and b) “signal-on” system.^{94,97}

1.7.4 Biosensors for Nucleic Acids.

DNA can also be optically detected using TBA-thrombin interactions.⁹⁸⁻¹⁰⁰ Fan and colleagues used an electrochemical version of the “molecular beacon” approach to detect DNA hybridization by measuring the electrochemical signal that accompanied a conformational change in the sensor.¹⁰⁰ Their strategy involved attaching a ferrocene tag to a thiolated TBA sequence within a stem-loop DNA structure, followed by subsequent attachment of the labeled DNA to a gold electrode. Hybridization of this sensor with a complementary DNA sequence then triggered a conformational change in this surface-confined TBA sensor, which led to a corresponding change in the electron tunneling distance between the Au electrode and the ferrocene label. Using cyclic voltammetry, target DNA concentrations as low as 10 pM could be measured using this sensor.

In an elegant approach toward DNA detection, Willner and colleagues introduced the use of “catalytic beacons”.^{98,99} Their method is illustrated in **Figure 1.32**. The thrombin protein was covalently modified with an oligonucleotide containing the TBA sequence.⁹⁹ In the absence of a complementary DNA strand the appended TBA sequence folds into a G-quadruplex and blocks the enzyme’s active site. Addition of a complementary DNA strand unfolds the G-quadruplex, resulting in substrate access to the thrombin’s active site. Hydrolysis of a fluorophore labeled peptide then results in a readily detectable optical signal.

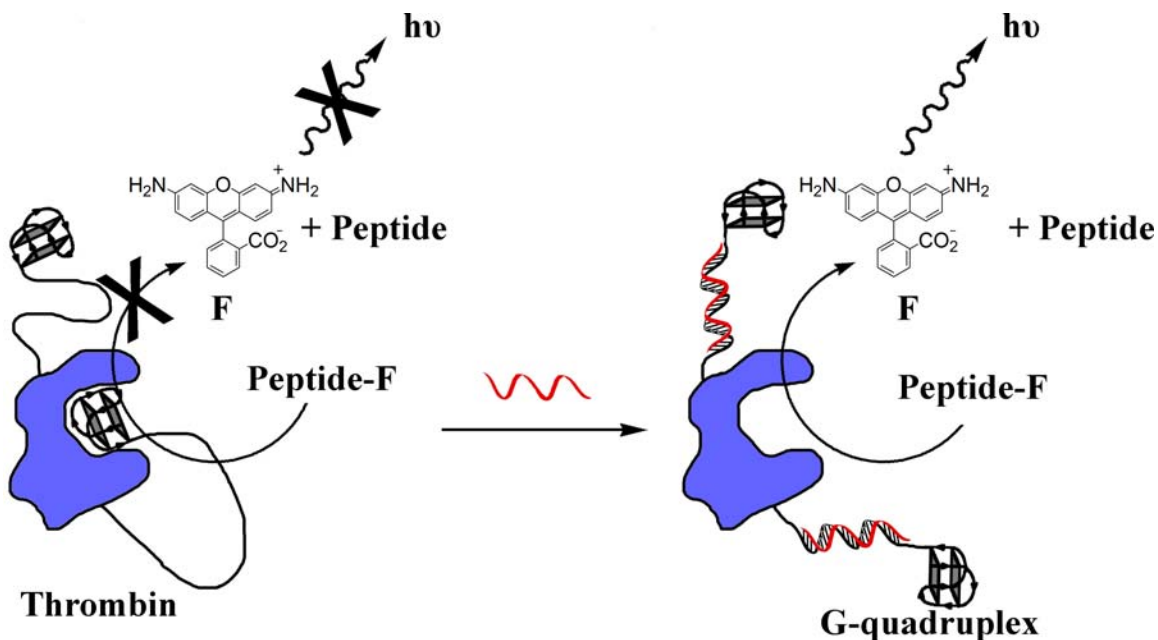


Figure 1.32. Optical detection of DNA by catalytic activation of thrombin upon dissociation of an intramolecular thrombin-TBA complex.⁹⁹

1.7.5 The Use of G-Quadruplexes in Building Nanomachines.

The TBA sequence has also been used as the basis for single molecule systems that have been coined “nanomachines” or nanomotors.¹⁰¹⁻¹⁰³ Li and Tan first demonstrated that conformational switching of a DNA oligonucleotide between its duplex and its folded G-quadruplex forms resulted in a flexing motion.¹⁰¹ They used FRET to follow this shrinking and expansion motion in real time. In a similar fashion, Alberti and Mergny reported that the conformational equilibrium between DNA duplex and quadruplex defines a nanomolecular machine.¹⁰² Thus, the conformational states of a 21-mer DNA oligonucleotide, modified with 5'-fluorescein donor and 3'-rhodamine acceptor groups, could be readily detected by using FRET techniques. Switching between the folded unimolecular G-quadruplex and a duplex conformation caused a 5-6 nm

displacement along the length of the oligonucleotide. This nanomachine could be cycled between its closed G-quadruplex state and open duplex state by sequential addition of other DNA strands, a so-called "C-fuel" and a "G-fuel". The "C-fuel" unfolded the unimolecular G-quadruplex to generate a duplex, while the "G-fuel" strand was used to liberate the labeled 21-mer so that it could refold into a G-quadruplex structure.

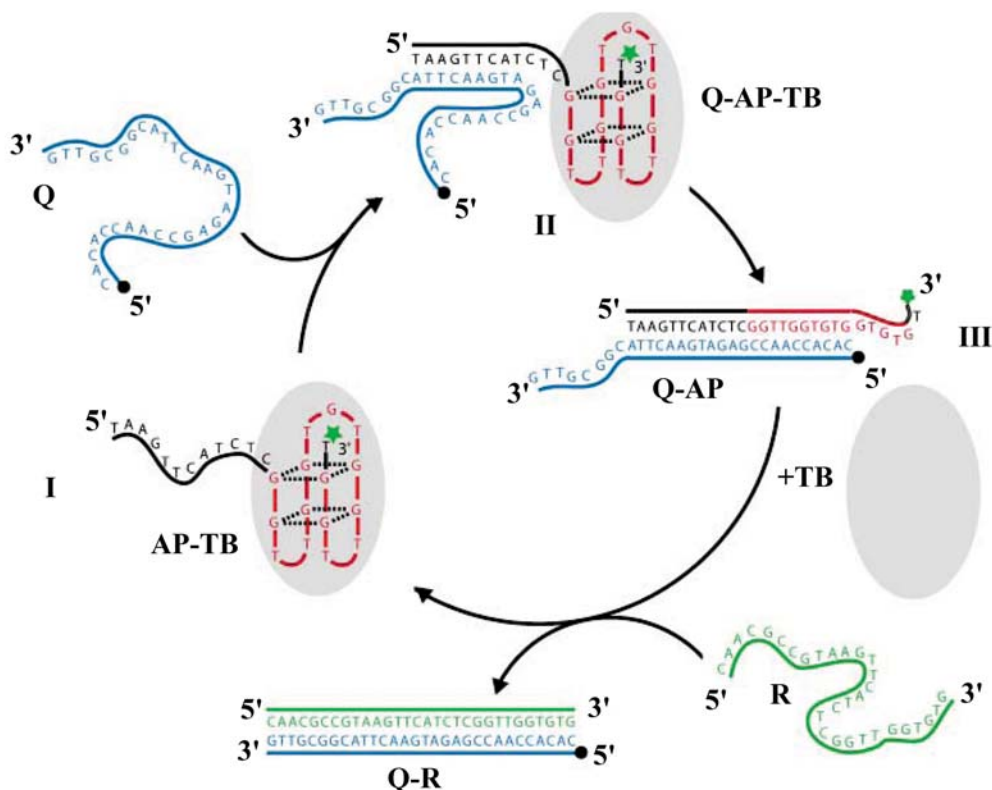


Figure 1.33. A DNA-based nanomachine that binds and releases thrombin. Binding of DNA strand Q to TBA-protein complex release thrombin, and addition of complementary DNA strand R removes Q and shifts equilibrium back to the TBA-thrombin complex. Reprinted with permission from John Wiley & Sons, Inc.¹⁰³

Simmel and coworkers recently described a nanomachine that can bind and release thrombin as it undergoes conformational switching (**Figure 1.33**).¹⁰³ In this DNA-

based machine, the TBA sequence was fused to another DNA sequence that can partially bind another DNA sequence (Q). Upon addition of the Q DNA to the TBA-thrombin complex, the G-quadruplex region unfolds and releases the bound thrombin protein. Addition of another DNA strand (R) that is complementary to Q, frees up the TBA sequence and allows it to refold. Thus, this nanomachine represents a new way to control the reversible binding of thrombin in solution.

1.7.6 New G-Quadruplex Structures from Synthetic DNA Analogs.

Polymers other than canonical DNA and RNA oligonucleotides can also form G-quadruplexes. The ability to alter the polymer backbone may result in G-quadruplexes with a variety of potential applications in supramolecular chemistry, biotechnology and nanotechnology. In addition, studies on nucleic acid analogs may lead to insights into the structural factors that control fundamental issues about the thermodynamics and kinetics of the G-quadruplex motif in the parent DNA and RNA nucleic acids.

For example, locked nucleic acids (LNA) have conformationally constrained ribose units that are fixed in a C3'-endo conformation by a methylene bridge between the 2'-O and 4'-C atoms (**Figure 1.34**).^{104,105} This RNA-like C3'-endo sugar pucker reduces backbone flexibility and helps drive the attached nucleobase to adopt an *anti* conformation about the glycosidic bond. Dominick and Jarstfer recently showed that replacement of individual dG residues with LNA nucleotides in the Oxy28 telomeric sequence d (G₄T₄G₄T₄G₄T₄G₄) dramatically alter the topology of the resulting G-quadruplex.¹⁰⁶ Oligonucleotides with four G-rich tracts can adopt either parallel or antiparallel intramolecular G-quadruplexes. For example, the human telomeric sequence

d (AGGG(TTAGGG)₃) forms a unimolecular propeller structure whose phosphate backbone sections are all parallel to one another. On the other hand, the Oxy28 sequence forms an antiparallel crossover basket, with the G residues alternating in a syn-anti-syn-anti fashion along the individual G4 tracts. Because 3'-endo nucleotides prefer to adopt an anti glycosidic bond, the authors postulated that incorporation of LNA residues into Oxy28 might drive the formation of a parallel G-quadruplex.

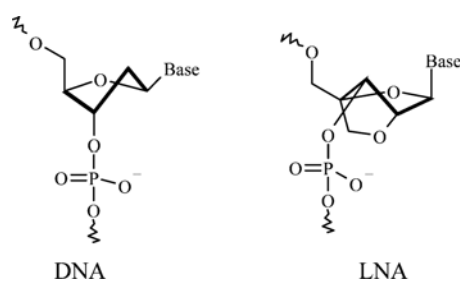


Figure 1.34. Structures of DNA and LNA showing a) DNA in the C2'-*endo* conformation and b) LNA locked into the C3'-*endo* conformation.^{104,105}

Dominick and Jarstfer inserted LNA into specific positions of the Oxy28 sequence and used CD spectroscopy to determine both the folding topology and thermodynamic stability of a family of modified oligonucleotides.¹⁰⁶ In all cases, substitution of an LNA residue led to G-quadruplexes that were destabilized relative to the parent Oxy28 sequence. However, in some cases, even single nucleotide changes shifted the G-quadruplex from an antiparallel to a parallel propeller structure in the presence of K⁺ (**Figure 1.35**). This remarkable finding drives home the point that even single internal modifications within the oligonucleotide backbone can dramatically influence the structure of the resulting G-quadruplex.

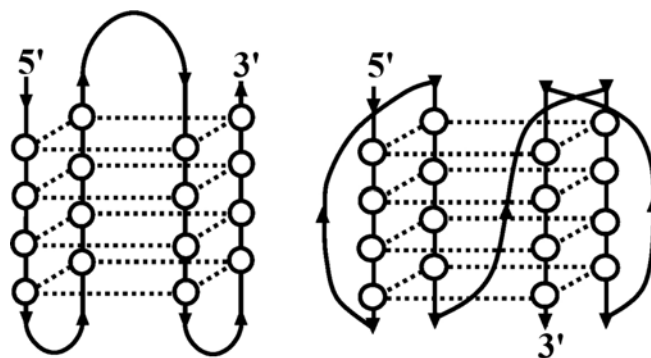


Figure 1.35. Schematic showing a) antiparallel DNA G-quadruplex and b) parallel DNA G-quadruplex. Substitution of a single DNA monomer with a LNA analog results in conformational switching between the two structures. Reprinted with permission from the American Chemical Society.¹⁰⁶

In another informative study, Mayol and colleagues demonstrated the significant impact that LNA can have on both the thermodynamics and kinetics of G-quadruplex folding.¹⁰⁷ They used ¹H NMR and CD measurements to characterize a well-defined G-quadruplex [tgggt]₄ with three stacked G-quartets. Like the analogous d[TGGGT]₄, this LNA G-quadruplex formed a symmetric structure with all 4 strands parallel to one another. The LNA G-quadruplex [tgggt]₄ was more stable, with a higher melting temperature, than the corresponding DNA and RNA quadruplexes. Importantly, these CD melting and annealing measurements also revealed that the LNA strands had a much faster association rate than do DNA and RNA at micromolar concentrations. Mayol's study indicates that the significant preorganization of the LNA backbone, coupled with the stabilization of *anti*-glycosidic bonds, provides an entropy gain that leads to faster kinetics for G-quadruplex formation.¹⁰⁸

Peptide nucleic acids (PNA), nucleobase oligomers wherein the anionic phosphate backbone is replaced by neutral N-(2-aminoethyl) glycine linkages, also form a variety

of G-quadruplex structures. Both DNA and RNA G-quadruplexes can be invaded by a homologous PNA strand to give hybrid PNA₂-DNA₂ G-quadruplexes.^{109,110} Armitage and colleagues showed that the PNA H-G₄T₄G₄-Lys-NH₂ hybridizes with its homologous DNA d (G₄T₄G₄) to give a G-quadruplex consisting of 2 strands of DNA and 2 strands of PNA. FRET measurements using labeled polymers indicated that strands were organized such that the 2 DNA strands are parallel with each other and the 5' ends of the DNA point in the same direction as the N-termini of the PNA strands (**Figure 1.36**). Of the 2 possible structures envisioned for such a PNA₂-DNA₂ hybrid Armitage favored the “alternating” structure (A) over the “adjacent” structure (B) for two reasons: electrostatic repulsion would be minimized by separating the 2 anionic DNA strands and FRET experiments indicated that the donor and acceptor were closer to one another when both the PNA and DNA strands were labeled. Armitage also made some important observations about G-quadruplex kinetics in comparing the CD melting profiles for this hybrid PNA₂-DNA₂ G-quadruplex with that for the hairpin dimer formed by the homologous DNA. The DNA hairpin dimer showed significant hysteresis upon cooling, indicating that the rate of association of 2 strands to make the hairpin dimer is relatively slow. In contrast, the hybrid PNA₂-DNA₂ showed little hysteresis in the melting and annealing process, indicating that the kinetics for strand association are much faster for the 4-stranded PNA G-quadruplex. Armitage suggested that this faster hybridization kinetics was due to the lack of negative charges along the PNA backbone and, possibly, due to electrostatic attraction of the PNA's positively charged N-terminus with the anionic DNA. Armitage concluded his paper by noting that, in principle, PNA₄ G-quadruplexes should be possible.

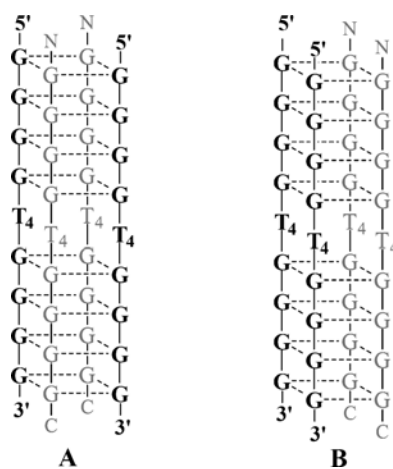


Figure 1.36. Possible structures of hybrid 1:1 PNA₂-DNA₂ quadruplexes (bold = DNA, gray =PNA) where the PNA strands are (A) diagonally opposite or (B) adjacent to each other. Reprinted with permission from the American Chemical Society.¹¹⁰

Shortly after Armitage's paper on hybrid PNA₂-DNA₂ G-quadruplexes, Balasubramanian and colleagues reported formation of intermolecular G-quadruplexes composed solely of 4 PNA strands.¹¹¹ Based on the combined ESI-MS, UV and CD data they identified a 4-stranded PNA quadruplex (Lys-TG₃-NH₂)₄ that aligned in an antiparallel fashion. This PNA sequence, which contains only 1 chiral center at its terminal Lys residue, exhibited an induced CD spectrum characteristic for stacked G-quartet chromophores, with a negative CD band at 270 nm and a positive band at 288 nm. UV melting experiments revealed that this particular PNA G-quadruplex was not nearly as stable, nor as cooperative in its formation, as the corresponding DNA quadruplex (TG₃)₄. Subsequent to Balasubramanian's report, Armitage and colleagues showed that another PNA sequence also form intermolecular G-quadruplexes. Thus, depending on the conditions, the PNA (H-G₄T₄G₄-Lys-NH₂) forms either a 4-stranded quadruplex or a two-stranded hairpin dimer (**Figure 1.37**).¹¹² Unlike the (Lys-TG₃-NH₂)₄ G-quadruplex

studied by Balasubramanian, this $(\text{H-G}_4\text{T}_4\text{G}_4\text{-Lys-NH}_2)_4$ PNA quadruplex was stabilized by the presence of Na^+ and K^+ . Since their backbones are neutral, Armitage noted that a PNA G-quadruplex might be an excellent candidate for transporting cations across cell membranes.

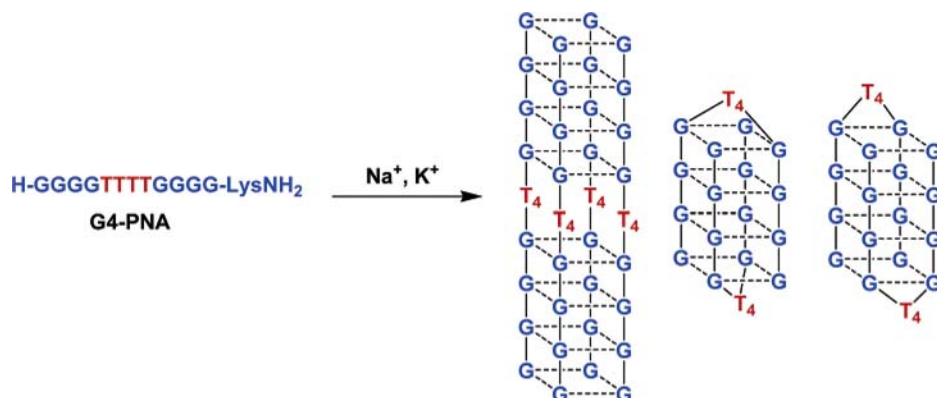


Figure 1.37. Possible G-Quadruplex structures formed by PNA. Reprinted with permission from the American Chemical Society.¹¹²

Most recently, Giancola and colleagues reported on the thermodynamic and kinetic properties of G-quadruplexes formed from chimeras 5'-tGGGT-3' and 5'-TGGG-3'-t, sequences that contain a single PNA residue at the ends of a DNA sequence.¹¹³ Using CD spectroscopy and calorimetry, they found that these chimeric PNA-DNA quadruplexes were thermodynamically more stable than the corresponding DNA G-quadruplex. Furthermore, the kinetics of quadruplex formation, as measured by melting and annealing experiments, indicated a reaction order of 4.0 in strand concentration. Both chimeric G-quadruplexes assembled more slowly than the corresponding DNA, as the rate constants at 20 °C were $(3.0 \pm 0.2 \times 10^7)$ for $[\text{5'-TGGGGT-3'}]_4$ and $(2.1 \pm 0.2 \times 10^7)$ for the chimeras. Giancola et al. also identified a kinetically stable intermediate, suggested to be a dimer during the process of G-quadruplex formation. Their data agreed

with a mechanism for G-quadruplex formation, first put forth by Wyatt for DNA,¹¹⁴ wherein single and double strand species are in an equilibrium favoring single strand, and the step going from dimer to quadruplex is rate limiting. Such a mechanism is consistent with the 4th-order dependence of the association rate on single-strand concentration, but does not require the unlikely event of a four-body collision. Studies on such nucleic acid analogs, showing that incorporation of a single PNA residue into a DNA strand can influence biophysical properties, may well help guide the design of new biopolymer conjugates with improved molecular recognition properties.

Finally, it is important to recognize that folded oligonucleotides can also be functional. For example, Sen's group has described a series of DNA oligonucleotide aptamers that are catalysts.¹¹⁵⁻¹²⁰ Aptamers, selected with a transition state analog N-methylmesoporphyrin, catalyzed the Cu²⁺ and Zn²⁺ metallation of porphyrins.¹¹⁵ This catalytic DNA, which requires K⁺ for its activity, may either bind the porphyrins by external stacking or by intercalation between G-quartets. Li and Sen concluded that these DNA chelataes used substrate binding energy to distort the porphyrin's planar conformation, making the porphyrin more basic and easier to metallate.¹¹⁶ They suggested that the G-quartet is sufficiently rigid to enable this substrate distortion. Sen's group also identified G-quadruplex DNA aptamers with peroxidase activity.^{118,119} Their DNA-hemin complexes had enhanced peroxidase activity, when compared to the heme cofactor alone. Again, they concluded that the folded DNA activates the bound heme and enhances peroxidase activity.¹¹⁹ Willner's group used this hemin binding aptamer as the basis for the clever development of a DNA sensor.⁹⁸

Most recently Sen and Cinnapen used *in vitro* selection to discover a DNA

aptamer that can catalyze the photoreactivation of thymine-thymine cyclobutane dimers in DNA.¹²⁰ Thus, a 42-mer nucleotide repaired a thymine-thymine dimer substrate with 305 nm light, showing an efficiency that rivaled that of the native photolyase enzyme. A G-quadruplex unit, formed by specific guanine bases within this 42-mer deoxyribozyme, was proposed to function as a light-harvesting antenna, with photoreactivation of the thymine-thymine dimer proceeding via electron donation from an excited guanine base within the G-quadruplex. These studies by Sen underscore the potential for using G-quadruplexes to function as catalysts.

1.8 Summary of the G-Quadruplex as a Scaffold in Nanostructures and Biomaterials

This chapter has described some of the supramolecular structures that have been built using guanine self-assembly. These synthetic G-quartet systems, in addition to providing models for understanding assembly in DNA and RNA, also have potential impact on sensor development, materials science, and nanoscience. Both the lipophilic G-quadruplexes, synthetic, and natural G-quadruplexes can be useful motifs to build new structures and biomaterials. The use of guanine self-assembly to form self-assembled ionophores, dynamic liquid crystals, hydrogels, noncovalent polymers, nanomachines, biosensors, therapeutic aptamer and catalysts highlight the many functions that can arise from G-quadruplexes. An additional function that can arise from G-quadruplexes, synthetic ion channels, is highlighted in Chapter 4 of this thesis.

Chapter 2. Pulsed Field Gradient NMR Helps Determine the Solution Structure of Lipophilic G-Quadruplexes.

The majority of this chapter has been published in reference 121:

- Kaucher, M. S.; Lam, Y. F.; Pieraccini, S.; Gottarelli, G.; Davis, J. T. "Using diffusion NMR to characterize guanosine self-association: Insights into structure and mechanism." *Chem.-Eur. J.* **2004**, *11*, 164-173.

2.1 Introduction.

The initial goal of the research in this chapter was to characterize the structures of different noncovalent structures built through guanosine self-assembly. Characterization of supramolecular structures is often difficult and a continuous challenge in the field. Even with the advancement of nanoscale synthesis of functional material that has had a large degree of success in supramolecular chemistry,^{3,4,122} solid-state structures through crystallization of these structures is often difficult or not possible. Furthermore, packing forces may give solid-state structures that are not well-populated or present in solution. Mass spectrometry,¹²³ analytical ultracentrifugation,¹²⁴⁻¹²⁶ dynamic light scattering,¹²⁷ gel permeation chromatography, and vapor pressure osmometry have been used to determine sizes of supramolecular complexes. Unfortunately, these techniques don't provide the atomic resolution offered by NMR spectroscopy. On the other hand, standard NMR techniques are excellent at determining molecular composition, but defining the sizes of high-symmetry complexes can be difficult or not possible.

Pulsed field gradient (PFG) NMR, a method for measuring diffusion rates, provides information about the sizes of molecules in solution.¹²⁸⁻¹³² PFG-NMR, used to study self-association of natural products,¹³³⁻¹³⁵ peptides,^{136,137} and proteins,¹³⁸⁻¹⁴² is also

an emerging technique in supramolecular chemistry. Diffusion NMR has been used to define the aggregation state of ion pairs and other organometallic assemblies,^{65,143-146} as well as determine the sizes of dendrimers, supramolecular polymers and nanoparticles.¹⁴⁷⁻¹⁵⁰ Further detail on these experiments will be discussed in this chapter.

The Cohen group have been pioneers in utilizing diffusion NMR in combinatorial and supramolecular chemistry.¹⁵¹ Cohen and colleagues used diffusion NMR in host-guest chemistry, with detailed studies of macrocyclic complexes.¹⁵¹⁻¹⁵⁵ Recently, this technique has been used to investigate issues of structure and mechanism in molecular self-assembly. Hydrogen-bonded rosettes, calixarene-nucleoside conjugates and stacked bisphenylenes have been sized using diffusion NMR.^{62,156,157} Solvation's key role in stabilizing resorcinarene capsules has been revealed through this technique.¹⁵⁸⁻¹⁶⁰ In addition to structural characterization, diffusion NMR can also provide insight into dynamic processes that occur during self-assembly.¹⁶¹⁻¹⁶⁴

The following sections describe how this PFG-NMR technique was utilized to characterize lipophilic guanosine derivatives.^{14,121} As previously mentioned, guanosine derivatives organize in the presence of alkali and alkaline earth cations to give hydrogen bonded G-quartets (**Scheme 2.1**).^{15,19,21,22} These G-quartets undergo further association by stacking into columns known as G-quadruplexes. The number of stacked G-quartets is often difficult to deduce from NMR and CD in the solution state. A better understanding of assembly-disassembly pathways, including identification of stable intermediates, is critical for learning how to construct and manipulate these synthetic G-quadruplexes. Below, three examples where the use of diffusion NMR to characterize structure also helps illuminate factors that control guanosine self-assembly are described.¹²¹

2.2 PFG-NMR Theory

PFG NMR spectroscopy is a powerful technique for measuring diffusion coefficients in solution. Translational diffusion is the thermally random movement of molecules. The net distance traveled from where the molecule starts to where it ends is measured, the path the molecule travels is irrelevant. **Figure 2.1** shows a molecule diffusing in two dimensions. Many variables can affect molecular diffusion such as the molecule's hydrodynamic properties, temperature, concentration, chemical exchange, reactions, restricted motion, and solvent viscosity.¹²⁸

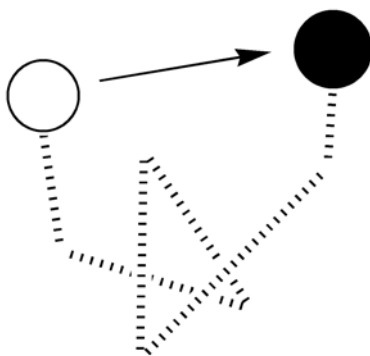


Figure 2.1. Translational motion of a molecule in two dimensions.

From the Stokes-Einstein equation and equations for the hydrodynamic frictional coefficients, the diffusion coefficient can be estimated from the size of the molecule. The Stokes-Einstein equation relates the diffusion coefficient to the hydrodynamic frictional coefficient, which is a function of the shape and size of the molecule (**Equation 2.1**), where k is the Boltzmann constant and T is the temperature in Kelvin. Using the hydrodynamic frictional coefficient for a sphere (**Equation 2.2**), the diffusion coefficient of a sphere is a function of the radius (**Equation 2.3**), where η is the solvent viscosity and R is the radius of the sphere. In this simplified approach, if two different diffusion

coefficients of different spheres were measured in the same environment, the ratio of these diffusion coefficients would be inversely related to the radii of the spheres (**Equation 2.4**).¹⁶⁵

$$D = \frac{k \cdot T}{f}$$

Equation 2.1. Diffusion coefficient related to the hydrodynamic frictional coefficient.

$$f = 6 \cdot \pi \cdot \eta \cdot R$$

Equation 2.2. Hydrodynamic frictional coefficient for a sphere.

$$D = \frac{k \cdot T}{6 \cdot \pi \cdot \eta \cdot R}$$

Equation 2.3. Diffusion coefficient related to the radius of a sphere.

$$\frac{D_a}{D_b} = \frac{\left(\frac{k \cdot T}{6 \cdot \pi \cdot \eta \cdot R_a} \right)}{\left(\frac{k \cdot T}{6 \cdot \pi \cdot \eta \cdot R_b} \right)} = \frac{R_b}{R_a}$$

Equation 2.4. Ratio of two diffusion coefficients related to a sphere.

Since the radius of a sphere is a function of its volume, the hydrodynamic radius can be estimated from a given volume (**Equation 2.5**). For shapes and geometries other than spheres, there are other equations for the hydrodynamic frictional coefficient. These equations and subsequent theories are well developed and mathematically derived.^{166,167}

Using **Equation 2.5**, the relationship of a monomer to a dimer can be calculated by assuming that the dimer is a sphere of twice the volume. Relating the volume (v) to the radius of a monomer is calculated in **Figure 2.2**. Similarly, calculating the radius of a dimer that is twice the volume of a monomer is shown in **Figure 2.3**. Using these two radii, the ratio of diffusion coefficient of a dimer to the diffusion coefficient of a monomer should be equal to 0.794 (**Figure 2.4**).

$$v = \frac{4}{3} \cdot \pi \cdot R^3$$

Equation 2.5. Volume of a sphere, where R equals the radius.

$$v = \frac{4}{3} \cdot \pi \cdot (R_{\text{monomer}})^3 \qquad R_{\text{monomer}} = \sqrt[3]{\frac{v}{\frac{4}{3} \cdot \pi}}$$

Figure 2.2. Calculation of the radius of a monomer of a sphere of a specific volume.

$$2 \cdot v = \frac{4}{3} \cdot \pi \cdot (R_{\text{dimer}})^3 \qquad R_{\text{dimer}} = \sqrt[3]{\frac{2 \cdot v}{\frac{4}{3} \cdot \pi}} = \sqrt[3]{2} \cdot \sqrt[3]{\frac{v}{\frac{4}{3} \cdot \pi}}$$

Figure 2.3. Calculation of the radius of a dimer that is twice the volume of its monomer.

$$\frac{D_{\text{dim}}}{D_{\text{mon}}} = \frac{R_{\text{mon}}}{R_{\text{dim}}} = \frac{\sqrt[3]{\frac{x}{\frac{4}{3} \cdot \pi}}}{\sqrt[3]{2} \cdot \sqrt[3]{\frac{x}{\frac{4}{3} \cdot \pi}}} = \frac{1}{\sqrt[3]{2}} = 0.794$$

Figure 2.4. The ratio of the diffusion coefficients of a dimer to monomer.

The hydrodynamic radius is a function of both the size of the molecule and its solvation sphere(s). The solvation spheres observed are time averaged spheres.¹⁶⁸ In aqueous medium, the hydration spheres are complex and often difficult to predict accurately.¹⁶⁹⁻¹⁷¹ This is typically true for hydrogen bonding solvents, where solvent-solute interactions are strong. Fortunately, the solvation spheres in organic solvents are less of a problem due to the apolar nature of the solvents.

As mentioned before, there are several techniques for measuring diffusion coefficients but PFG-NMR has advantages of requiring low concentrations and being noninvasive.¹²⁸ PFG-NMR utilizes a gradient field to measure the diffusion coefficients of molecules in an NMR tube. When a magnetic gradient field is applied to a sample, a magnetic field is generated in the z-axis of the NMR tube (**Figure 2.5a**). This magnetic gradient field is linear, so molecules on the bottom of the NMR tube feel the effects stronger than do the molecules at the top of the NMR tube.¹⁵¹ The magnetic gradient field phase shifts the peaks in the NMR spectrum to a different frequency due to them being in different environments of the gradient field. This first magnetic gradient field pulse dephases the NMR spectrum by making it nonhomogenous. After a period of time (Δ), a second magnetic gradient field is applied in the opposite direction, which should

rephase the system if the molecules are not diffusing (**Figure 2.5a**).¹⁶⁵ Under the correct conditions, the molecules should diffuse to another position in the NMR tube over time Δ (**Figure 2.5c**). When the molecules diffuse to a different position in the NMR tube, they will be in a different environment, and consequently the rephasing will not yield a coherent signal. This scrambling of signals leads to the diminishing of peak intensities in the NMR spectrum, which can be plotted as a function of the diffusion coefficient.¹⁷²

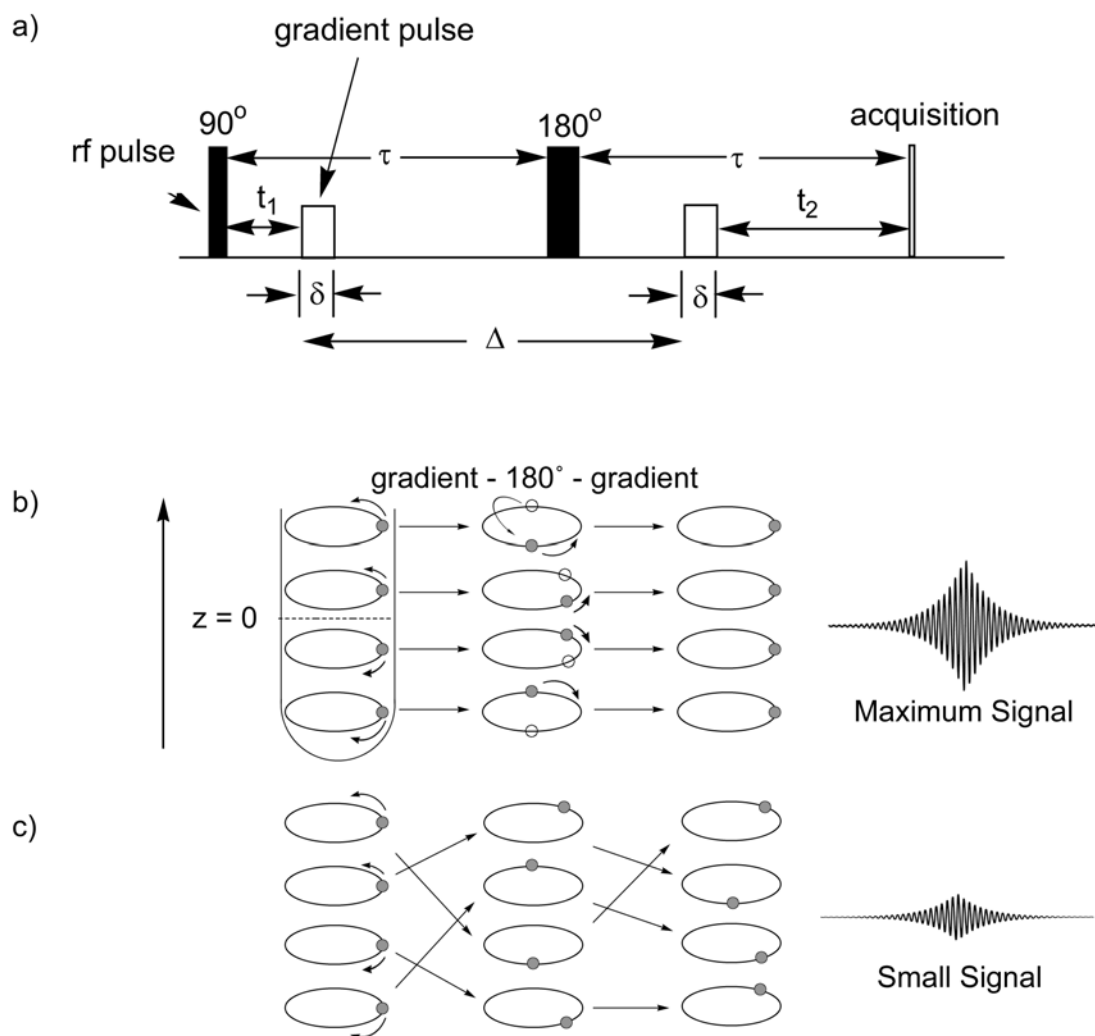


Figure 2.5. a) STE-PFG pulse sequence.¹⁶⁵ See text for more information. The effect of signal intensity from the PFG NMR experiment b) without and c) with diffusion. The 90° rf pulse magnetically rotates the spins from the z-axis to the x-y axis. After application of a linear magnetic field gradient, the spins are phase shifted depending on the strength of the gradient. Following a 180° refocusing pulse, another magnetic field gradient is applied to shift the spins back into phase.¹³⁰

The stimulated echo (STE) PFG sequence is shown in **Figure 2.5a**.¹⁶⁵ This sequence has the standard $90^\circ - \tau - 180^\circ - \tau$ -acquire pulse sequence with the two gradient pulses inserted. The first 90° pulse causes the nuclei to align on the y-axis, after which a gradient is applied for specific duration (δ) and gradient strength (g). This gradient has the effect of dephasing the spectrum as previously mentioned. After time τ , a 180° pulse is delivered to refocus the net nuclear magnetic moment. After this refocusing pulse, another gradient is delivered in the opposite direction to rephase the spectrum. Finally, after another time period of τ , the spectrum is acquired. Following this sequence, the dephasing of the spectrum can be affected by the gradient strength (g), gradient duration (δ), and the mixing time (Δ) between the two opposite gradients.¹⁶⁵

The NMR signal intensity is also a function of the diffusion coefficient as seen in **Equation 2.6**, where γ is the gyromagnetic ratio of the nucleus being studied. In theory, only two NMR spectra are needed to yield the diffusion coefficient, which would be an NMR spectrum without a gradient pulse and an NMR spectrum at a certain g , δ , and Δ . Stejskal-Tanner plots of the normalized signal intensity ($\ln(I/I_0)$) as a function of the gradient (**Equation 2.7**) are often used to calculate the diffusion coefficient from the slope of the line. Furthermore, this plot is used to evaluate if there is any exchange or other species overlapping with the signal. If there is one species, there is a single ordered exponential decay observed, while two different sized species would yield a second ordered exponential decay and so forth. In the standard pulse sequence, once the δ and Δ are optimized, these values are kept constant, while the gradient strength is varied. In theory and in practice, changing one of these variables, while keeping the other two constant, produces the same results.^{173,174}

$$I = I_0 \cdot e^{-\left[(-D) \cdot (2 \cdot \pi \cdot \gamma \cdot g \cdot \delta)^2 \cdot \left(\Delta - \frac{\delta}{3}\right)\right]}$$

Equation 2.6. Intensity related to the diffusion coefficient and the gradient pulse.

$$\ln\left(\frac{I}{I_0}\right) = -D \cdot (2 \cdot \pi \cdot \gamma \cdot g \cdot \delta)^2 \cdot \left(\Delta - \frac{\delta}{3}\right)$$

Equation 2.7. Normalized intensity as a function of the diffusion coefficient and gradient pulse.

PFG-NMR is diverse in that a number of nuclei may be used to measure the diffusion coefficient. Nuclei such as ^1H , ^{13}C , ^{15}N , ^{31}P , and ^{19}F have been used to measure diffusion coefficients.^{138,175} These nuclei are chosen depending on their resolution, abundance, and relaxation times, which affect the time and accuracy of the PFG-NMR experiment.

In PFG-NMR experiments, the diffusion coefficient is calculated from well resolved peaks to ensure accurate measurement of diffusion coefficients. Furthermore, the area, as opposed to the peak intensity, is used to give more accurate measurement of diffusion coefficients. In terms of hardware setup, certain steps are needed to ensure accurate measurements of diffusion coefficients. First, the stability of the NMR spectrometer is critical. Vibrations may create fluctuations in the NMR, which can cause the diffusion coefficients to be unstable. Also, spinning causes similar disturbances, creating inaccurate measurements of the diffusion coefficient. Temperature control over the system is critical, since temperature plays a key role in the measurement of diffusion

coefficients. The flow rate of nitrogen to cool the sample must be done at an optimal flow rate to cool the sample sufficiently, while not causing the sample to fluctuate. Along the same lines, convection currents caused by large volumes of solvent cause fluctuations in the sample. To limit these currents, Shigemi tubes are used to keep the solvent height of the NMR tube to 1 cm (**Figure 2.6**).¹⁷⁶⁻¹⁷⁸ Furthermore, the sample height is kept at 1 cm so that it is in the radio frequency of the coils and so that the z-axis is linear to the volume occupied by the sample.¹⁷⁹ At this height, the sample will respond linearly to the power applied.¹⁷⁹ In addition, when comparing two samples, it is critical to keep the temperature and concentrations the same. The use of an internal standard in these experiments helps ensure that these conditions are identical. It is imperative that the gradient hardware and probe are calibrated for these experiments. Typically, nuclei that have a reasonable relaxation time are used for practical reasons concerning the length of the experiment.

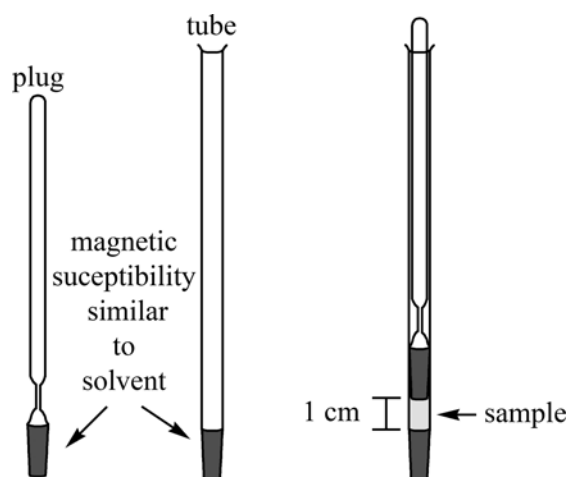
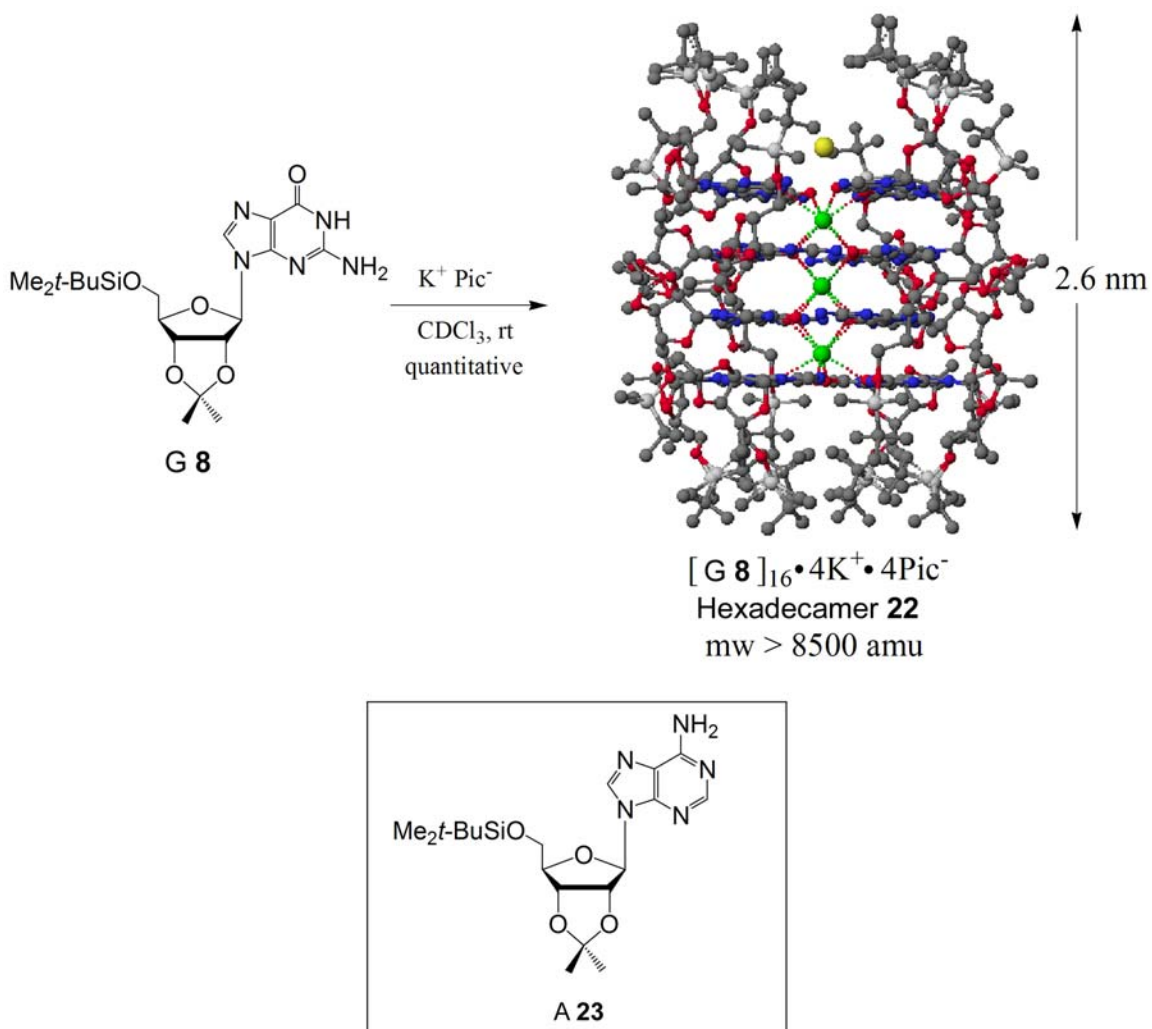


Figure 2.6. Shigemi tubes: plug, tube, and plug and tube assembled.

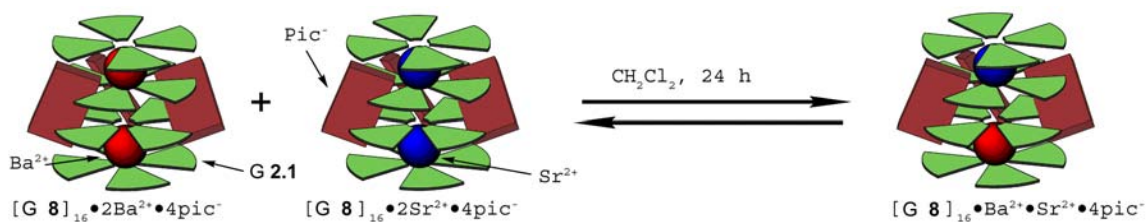
The following diffusion experiments were carried out with a Bruker DRX-500 spectrometer, using the STE Pulse Gradient sequence in FT mode.¹⁸⁰ To improve homogeneity, a “13 interval pulse sequence” was used with two pairs of bipolar gradients.^{139,181} This pulse sequence is similar in theory and principles as the ST-pulse sequence explained earlier. All samples for the diffusion measurements were prepared in Shigemi tubes and the temperature was actively controlled at 21.0 ± 0.1 °C. Diffusion coefficients were derived using integration of the desired peaks to a single exponential decay, using the “Simfit (Bruker XWINNMR v3.1)” software.

2.3 Diffusion NMR Confirms Hexadecamer in Solution.

Previous studies by former group member Scott Forman and Dr. James Fettinger showed X-ray crystallography evidence that 5'-TBDMS-2',3'-isopropylidene G **8** forms an ordered pseudo D_4 -symmetric hexadecamer composed of four stacked G-quartets (**Scheme 2.1**).⁵³ This G-quadruplex **22**, with empirical formula $[G \mathbf{8}]_{16} \cdot 4 K^+ \cdot 4 pic^-$, is stabilized by four co-axial cations and by four picrate anions. The anions use hydrogen bonds to clamp together the “inner” two G-quartets. Similar solid-state structures for $[G \mathbf{8}]_{16} \cdot 2 M^{2+} \cdot 4 pic^-$ were obtained with the divalent cations Ba^{2+} and Sr^{2+} .^{59,182} Electrospray mass spectrometry of these complexes showed significant amounts of $[G \mathbf{8}]_{16} \cdot 2 M^{2+}$ in the gas phase. Furthermore, NMR mixing experiments in CD_2Cl_2 suggested that the G-quadruplex was a hexadecamer through indirect solution state evidence monitored by 1H NMR spectrometry, where homodimers $[G \mathbf{8}]_{16} \cdot 2Ba^{2+} \cdot 4Pic^-$ and $[G \mathbf{8}]_{16} \cdot 2Sr^{2+} \cdot 4Pic^-$ formed a statistical mixture of the homodimers and heterodimer $[G \mathbf{8}]_{16} \cdot Ba^{2+} \cdot Sr^{2+} \cdot 4Pic^-$ (**Scheme 2.2**).⁵⁸ My goal was to get stronger evidence that the G-quadruplex is a hexadecamer in solution.



Scheme 2.1. Structures of **G 8**, G-quadruplex $[\text{G } \mathbf{8}]_{16} \cdot 4 \text{K}^+ \cdot 4 \text{pic}^-$ **22** and **A 23**.



Scheme 2.2. Mixing of homodimers to yield a 2:1:1 mixture of heterodimer and the two homodimers. Red spheres are Ba^{2+} , blue spheres are Sr^{2+} , green wedges are **G 8**, and brown blocks are picrate; front picrate not shown for clarity.⁵⁸

Because of the extensive characterization in the solid, gas, and solution phases, it was reasoned that G **8** and its K⁺ G-quadruplex **22** would provide an excellent test for using diffusion NMR to characterize guanosine self-association in solution. The goal was to determine whether the hexadecamer [G **8**]₁₆·4 K⁺·4 pic⁻ could be reliably identified in an equilibrium mixture that also contained “monomeric” G **8**.⁵⁵ Such identification is essential for understanding the factors that control the thermodynamics and kinetics of guanosine self-assembly.

The G-quadruplex **22** shows only aggregated complex in its ¹H NMR spectrum when it is dissolved in nonpolar solvents such as CD₂Cl₂ ($\epsilon_r = 9.1$), while it shows what resembles monomer in polar solvents such as DMSO-d₆ ($\epsilon_r = 45.0$). In intermediate polarity solvents such as CD₃CN ($\epsilon_r = 38.8$), the ¹H NMR spectrum of the dissolved G-quadruplex appears to be an equilibrium mixture of aggregated complex and monomer G **8**. This equilibrium in CD₃CN can be shifted to the “monomeric” guanosine G **8** or aggregated G-quadruplex **22** by varying the temperature (**Figure 2.7**). When crystalline [G **8**]₁₆·4 K⁺·4 pic⁻ **22** is dissolved in CD₃CN at rt, three sets of ¹H NMR signals are observed (**Figure 2.9**). These separate signals, in slow exchange on the NMR chemical shift time-scale, were distinguished using 2D COSY and NOESY experiments.⁵³ One set of the NMR signals was assigned to “monomeric” G **8**, with the understanding that these signals also contained time-averaged contributions from higher oligomers (mostly dimers) that are in fast exchange with monomer.¹⁸³⁻¹⁸⁵ The other two sets of ¹H NMR signals, always present in a 1:1 ratio, arise from the distinct “outer” and “inner” G-quartets that make up the pseudo D₄-symmetric [G **8**]₁₆ hexadecamer **22**.

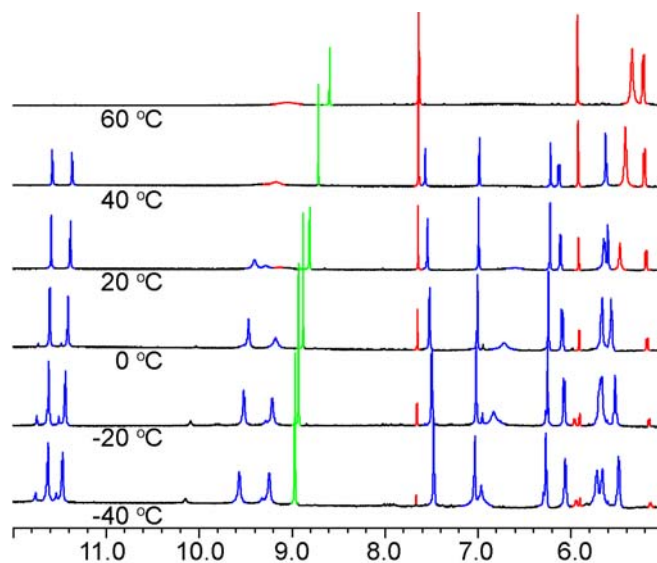


Figure 2.7. Variable temperature ^1H NMR spectra of $[\text{G } \mathbf{8}]_{16} \cdot 4\text{K}^+ \cdot 4\text{pic}^-$ (0.059 mM) dissolved in CD_3CN . Signals for monomer **G 8** (red) predominate at high temperatures, whereas signals for the hexadecameric complex $[\text{G } \mathbf{8}]_{16} \cdot 4\text{K}^+ \cdot 4\text{pic}^-$ (blue) predominate at low temperatures. The picrate peak is shown in green.

Since these two species are well resolved by ^1H NMR, PFG-NMR can be used on the same sample to obtain diffusion coefficients for the “monomeric” **G 8** and its complex with K^+Pic^- . Diffusion NMR studies were done at 21 °C using a solution prepared by dissolving crystalline $[\text{G } \mathbf{8}]_{16} \cdot 4\text{K}^+ \cdot 4\text{pic}^-$ in CD_3CN (0.059 mM). These conditions provide an equilibrium mixture of 94 % monomer **G 8** and 6 % G-quadruplex **22** as determined by NMR spectroscopy. The lipophilic adenosine **A 23** was used as an internal standard (6 eq) to size the two guanosine species. Adenosine **23** is of similar size as **G 8** but is not known to self-associate in CD_3CN or interact noticeably with either **G 8** or G-quadruplex **22** under these conditions.

An approximate $D_{16\text{mer}}/D_{\text{monomer}}$ ratio from available crystal structure data was calculated from the crystal structures of the respective structures. The molecular volume for $[\text{G } \mathbf{8}]_{16} \cdot 4\text{K}^+ \cdot 4\text{pic}^-$ is $12,140 \text{ \AA}^3$ and the molecular volume for **G 8** is estimated to be

586 Å³. The molecular volume for [G **8**]₁₆•4 K⁺•4 pic⁻ was taken from its crystal structure.⁵³ While the crystal structure of monomeric G **8** has not been elucidated, the crystal structure of an isomer, 5'-TBDMS-2',3'-isopropylidene isoguanosine, has been solved.¹⁸⁶ The molecular volume for this isomeric isoG was used as an estimate for the molecular volume of G **8**. Assuming that both compounds are spherical, these volumes provide average hydrodynamic radii of 14.26 Å for [G **8**]₁₆•4 K⁺•4 pic⁻ and 5.19 Å for G **8**, values that predict a theoretical $D_{16\text{ mer}}/D_{\text{G } 8}$ ratio of 0.36.¹⁸⁷

The influence of increasing magnetic field gradient strength (g) on the intensity of aromatic signals for the sample containing G **8**, A **23** and G-quadruplex **22** is shown in **Figure 2.8a-c**. The corresponding Stejskal-Tanner plots obtained from average values for eight separate diffusion NMR measurements are shown in **Figure 2.8d**. Analysis of H8 peak intensities gave diffusion coefficients of $D_s = 13.60 \pm 0.30 \times 10^{-10} \text{ m}^2 \text{ s}^{-1}$ for A **23** (δ 8.21 ppm) and $D_s = 12.00 \pm 0.20 \times 10^{-10} \text{ m}^2 \text{ s}^{-1}$ for G **8** (**Table 2.1**). The G-quadruplex **22** (δ 6.99 ppm for H8 of the “inner” G-quartet) has a much slower diffusion coefficient in CD₃CN ($D_s = 4.70 \pm 0.10 \times 10^{-10} \text{ m}^2 \text{ s}^{-1}$) than A **23** or G **8**. The experimental ratio of diffusion coefficients for G-quadruplex **22** and A **23** ($D_s(\text{G } 22)/D_s(\text{A } 23) = 0.35$) agree well with the theoretical $D_{16\text{ mer}}/D_{\text{monomer}}$ ratio of 0.36, indicating that hexadecamer [G **8**]₁₆•4 K⁺•4 pic⁻ is indeed the structure observed by NMR spectroscopy.

Table 2.1. Diffusion Coefficients for G **8** Hexadecamer/Monomer System.^[a]

	$D_s(\text{G } \mathbf{8})$	$D_s(\mathbf{22})$	$D_s(\text{A } \mathbf{23})$	Ratio	Ratio	Ratio
	($10^{-10} \text{ m}^2/\text{s}$)	($10^{-10} \text{ m}^2/\text{s}$)	($10^{-10} \text{ m}^2/\text{s}$)	$\frac{D_s(\mathbf{22})}{D_s(\mathbf{8})}$	$\frac{D_s(\mathbf{22})}{D_s(\mathbf{23})}$	$\frac{D_s(\mathbf{8})}{D_s(\mathbf{23})}$
$\text{CD}_3\text{CN}^{[\text{b}]}$	12.30 ± 0.20	4.85 ± 0.10		0.39		
$\text{CD}_3\text{CN}^{[\text{c}]}$	12.00 ± 0.20	4.70 ± 0.10	13.60 ± 0.30	0.39	0.35	0.88
$\text{DMSO-d}_6^{[\text{d}]}$	1.90 ± 0.03		1.98 ± 0.03			

[a] The diffusion coefficients reported in **Table 2.1** are the mean \pm standard deviation of 8 separate measurements at 21°C. [b] $[\text{G } \mathbf{8}]_{16} \cdot 4\text{K}^+ \cdot 4\text{Pic}^- \mathbf{22}$ dissolved in CD_3CN . [c] $[\text{G } \mathbf{8}]_{16} \cdot 4\text{K}^+ \cdot 4\text{Pic}^- \mathbf{22}$ and A **23** dissolved in CD_3CN . [d] G **8** and A **23** dissolved in DMSO-d_6 .

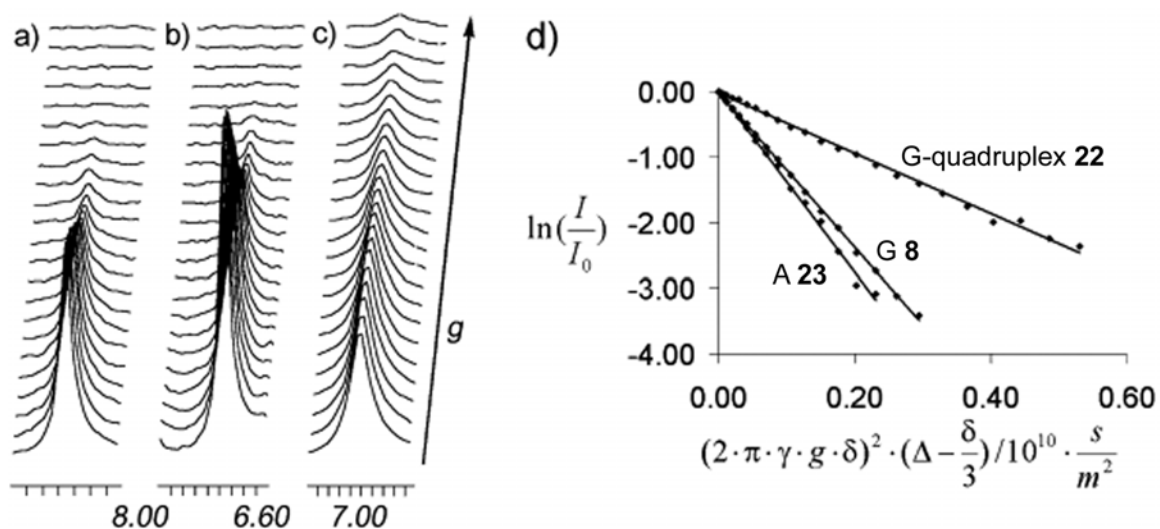


Figure 2.8. Stack plot of ¹H NMR spectra for a mixture of G **8**, G-quadruplex **22** and A **23**. Signals for a) A **23** H8, b) G **8** H8, and c) G-quadruplex **22** “inner” H8 with increasing gradient strength in CD_3CN at 21 °C. d) Stejskal-Tanner plot of G **8**, $[\text{G } \mathbf{8}]_{16} \cdot 4\text{K}^+ \cdot 4\text{pic}^- \mathbf{22}$ and A **23** in CD_3CN at 21 °C.

The slower diffusion of G **8**, relative to A **23**, is likely due to significant dimerization of G **8** in CD_3CN .¹⁸³⁻¹⁸⁵ To test this hypothesis, diffusion NMR experiments were conducted on G **8**/A **23** mixtures in DMSO-d_6 , a solvent that completely denatures

G-quadruplex **22**. Indeed, G **8** and A **23** have much closer diffusion coefficients in DMSO-d₆ (D_s (G **8**)/ D_s (A **23**) = 0.96) than in CD₃CN (D_s (G **8**)/ D_s (A **23**) = 0.88), consistent with significant inhibition of G-G dimerization by DMSO-d₆ (**Table 2,1**). The observation that the D_s (G **8**)/ D_s (A **23**) ratio was not uniform in DMSO-d₆ is not surprising given that guanosine can form hydrogen-bonded dimers even in this competitive solvent.¹⁸⁸ Another possible explanation for the decrease in D_s values for G **8**, relative to A **23**, would be chemical exchange of “free” G **8** with the G₁₆ hexadecamer **22** during the course of the diffusion NMR experiment. However, 2D-EXSY experiments in CD₃CN at room temperature using a mixing time of $t_m = 99.8$ ms (the same value as the gradient separation time, Δ , in the diffusion NMR experiments) showed no cross-peaks indicative of such monomer-hexadecamer exchange under these conditions.

However, closer inspection of these diffusion coefficients revealed that not all the signals on the G₁₆ hexadecamer are equal. The guanosine peaks for the outer layers showed slightly faster diffusion coefficients than the peaks for inner G-quartet layers, indicating that there might be slow exchange occurring that is not observed in the 2D-EXSY experiment. The monomer would be more likely to exchange into the outer layers because the inner layers are more robust due to stabilization from the chelating picrate anions (see Chapter 3 for more details).

2.4 Evidence for Cooperativity

Characterization of the hexadecamer [G **8**]₁₆ · 4 K⁺ · 4 pic⁻ by diffusion NMR confirms an important feature of the cation-templated self-association of G **8**. Namely, hexadecamer **22** is part of an equilibrium with “monomeric” G **8**, and its formation is

likely to occur via a cooperative nucleation-elongation mechanism.^{189,190} Other than signals for “monomeric” G **8** and hexadecamer **22**, no NMR evidence for any other kinetically stable intermediates in CD₃CN solution are observed. Additionally, the monomer/hexadecamer ratio in CD₃CN varies significantly with temperature (**Figure 2.9**). At -40 °C, only NMR signals for hexadecamer **22** are observed. As the temperature increases, more G **8** is formed by dissociation from the G-quadruplex. At 60 °C, only G **8** is present. Stronger evidence for a cooperative equilibrium was obtained from CD spectroscopy. G-quadruplex **22**, with its stacked G-quartets, has a characteristic CD absorbance centered at 248 nm.^{53,191} **Figure 2.10** shows temperature dependent CD data for a solution of [G **8**]₁₆-4 K⁺-4 pic⁻ in CD₃CN. The sigmoidal melting curve (with $T_m = 25$ °C) is characteristic of a cooperative equilibrium. Specifically, Scatchard and Hill plots have been applied to measure cooperativity in self-assembly,^{192,193} although they are applicable only to particular cases where monovalent ligands bind to multivalent receptors.¹⁹⁴ In this case, the self-assembly of multivalent ligands (guanosine units) interact with not only multivalent receptors (cations) but themselves. While more experiments are needed to confirm the nucleation-elongation mechanism,^{189,190} and the presence of positive cooperativity,¹⁹⁵ the NMR and CD data clearly indicate that growth of the [G **8**]₁₆ hexadecamer is coupled to the K⁺ templated formation of G-quartets.¹⁹⁶

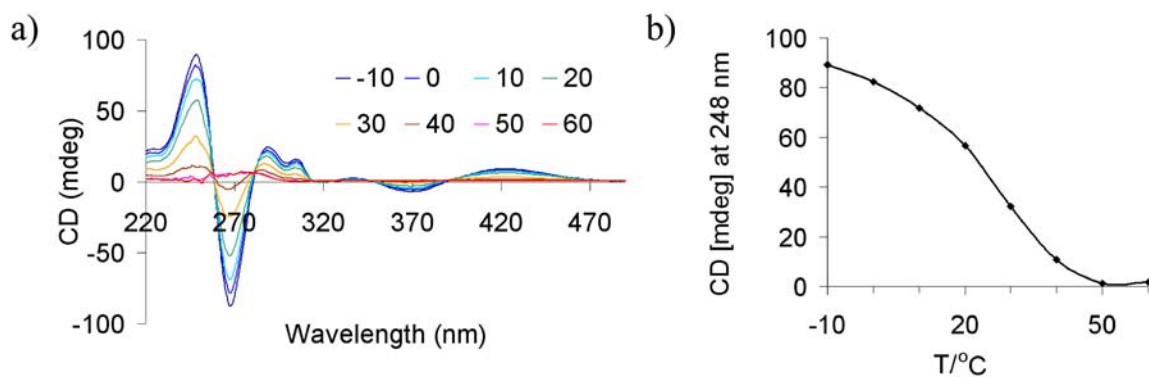
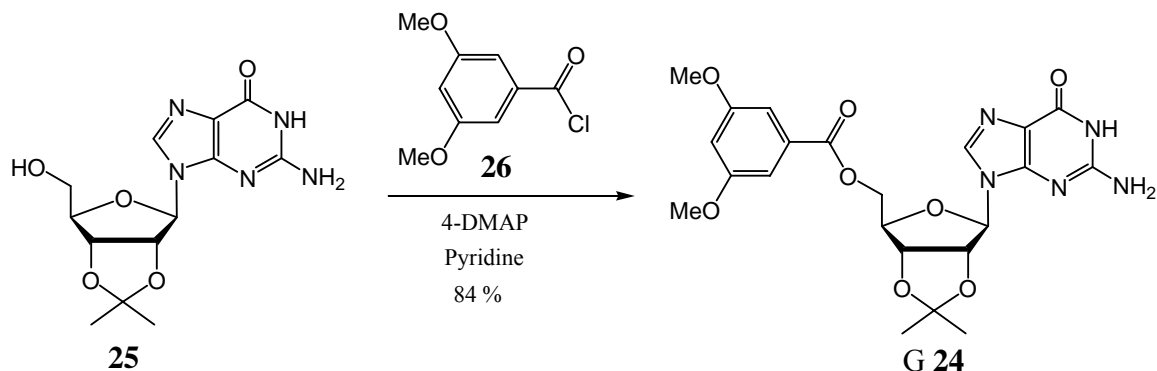


Figure 2.9. a) Variable temperature CD spectra of $[G \mathbf{8}]_{16} \cdot 4 K^+ \cdot 4 pic^- \mathbf{22}$ in CD_3CN . b) Plot of CD absorbance at 248 nm as a function of temperature.

2.5 PFG-NMR Shows Octameric Intermediate.

Although no intermediates were detected in the pathway from monomer to hexadecamer with silyl protected G **8** units, different derivatives do show the formation of kinetically stable intermediate. Guanosine **24**, 5'-(3,5-bis(methoxy)benzoyl)-2',3'-isopropylidene-guanosine, was synthesized through the acylation of commercially available 2',3'-isopropylidene-guanosine with 3,5-dimethoxybenzoic acid chloride in pyridine (Scheme 2.3). The 1H NMR in $DMSO-d_6$ is shown in Figure 2.10.



Scheme 2.3. Synthesis of G **24**.

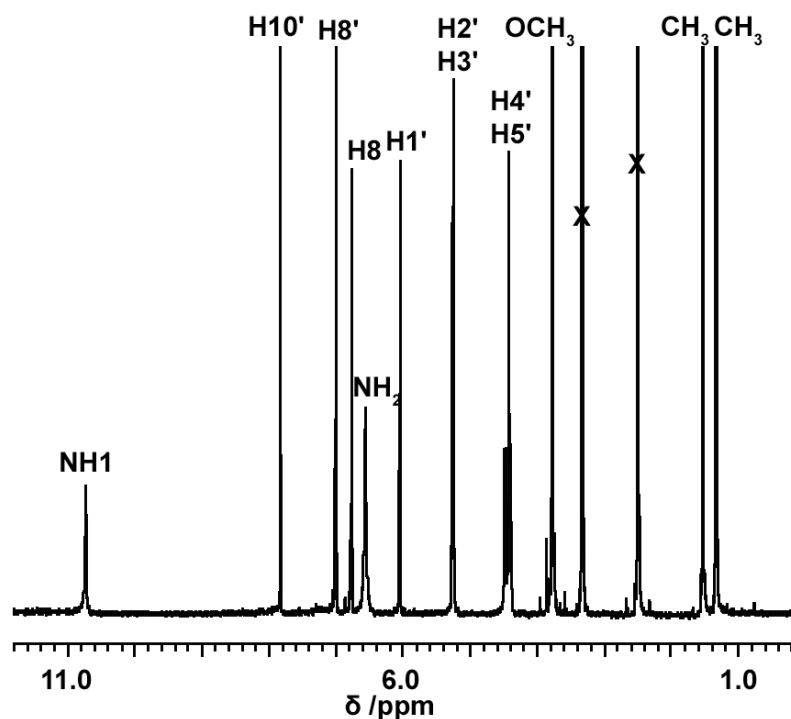
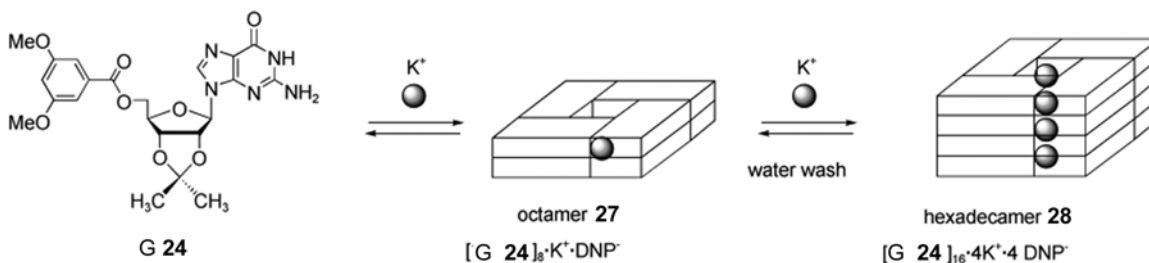


Figure 2.10. The 400 MHz ^1H NMR spectra of **G 24** in DMSO-d_6 at rt.

Upon addition of K^+ , **G 24** forms octamer **27** as an intermediate structure. Upon further addition of K^+ , hexadecamer **28** is formed. This first intermediate, a $\text{G}_8\text{-K}^+$ octamer, was readily distinguished from the larger G_{16} hexadecamer through PFG-NMR. The ratio of the octamer-hexadecamer equilibrium is a function of the K^+ cation concentration in solution (**Scheme 2.4**).



Scheme 2.4. Formation of $[\text{G } 24]_8 \cdot \text{K}^+ \cdot \text{DNP}^-$ **27** and $[\text{G } 24]_{16} \cdot 4\text{K}^+ \cdot 4\text{DNP}^-$ **28**.

The ^1H NMR spectra indicate that G **24** can form different structures in non-polar solvents CD_2Cl_2 and CDCl_3 as a function of the K^+ concentration and experimental conditions (**Figure 2.11**). Liquid-liquid extraction of K^+DNP^- (DNP: 2,6-dinitrophenolate) (1.2 equiv) from water with G **24** (10 mM) in CD_2Cl_2 provided a single set of ^1H NMR signals and a G **24**/DNP ratio of 8:1, consistent with formation of a C_4 -symmetric octamer **27** (**Figure 2.11a**). This was later to be determined as octamer **27** by PFG-NMR. Under different conditions, a new complex was generated when G **24** was used for solid-liquid extractions of K^+DNP^- (**Figure 2.11b**). In solid-liquid extractions, the two sets of ^1H NMR signals in a 1:1 ratio, the 4:1 G **24**/DNP ratio, and the appearance of signals for the hydrogen-bonded N2 amino protons between δ 9.5-9.8 ppm suggested formation of a pseudo D_4 -symmetric hexadecamer **28** with empirical formula $[\text{G } \mathbf{24}]_{16} \cdot 4 \text{K}^+ \cdot 4 \text{DNP}^-$. Since the different complexes, octamer **27** and hexadecamer **28**, exchange slowly on the NMR chemical shift timescale in CD_2Cl_2 (**Figure 2.11c**), diffusion NMR was used on this sample to compare the relative sizes of the two species.

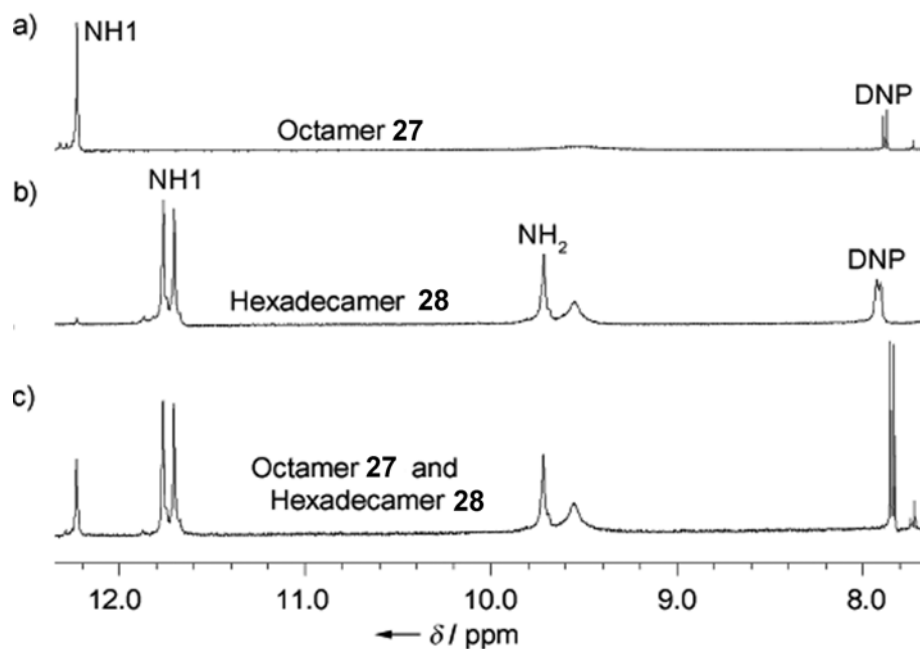


Figure 2.11. ¹H NMR spectra in CD₂Cl₂ at 21 °C of complexes formed by extraction of K(DNP) with G 24. a) Octamer 27, [G 24]₈ • K⁺ • DNP⁻, formed in liquid-liquid extraction; b) hexadecamer 28, [G 24]₁₆ • 4K⁺ • 4(2,6-DNP)⁻, formed in solid-liquid extraction; c) mixture of octamer 27 and hexadecamer 28.

Figure 2.12, shows the CD spectra of octamer 27 and hexadecamer 28 in CH₂Cl₂ at rt. Although both CD spectra have positive to negative Cotton bands centered around 280, the relative intensities of these peaks are different. The hexadecamer has a much larger negative CD band around 300 nm. Moreover, the octamer has an extra positive CD band at 320 nm. While these bands may be useful in identifying more detailed structural features,¹⁹¹ the CD spectra are unassigned and are often difficult to predict.

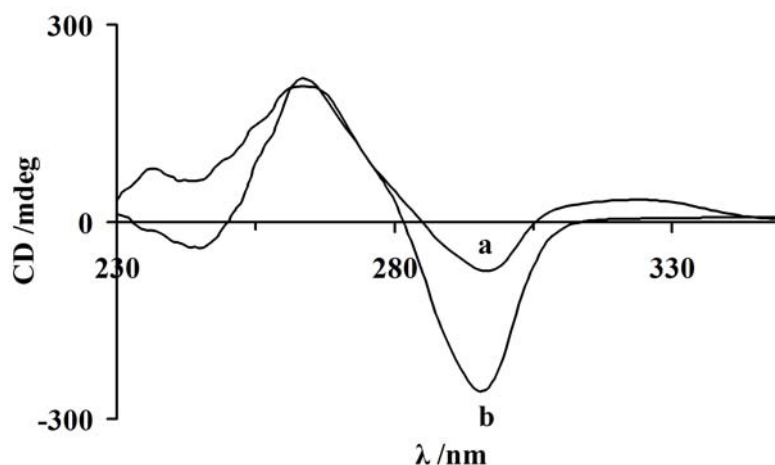


Figure 2.12. CD spectra of a) octamer **27**, $[\text{G } 24]_8 \cdot \text{K}^+ \cdot \text{DNP}^-$, and b) hexadecamer **28**, $[\text{G } 24]_{16} \cdot 4\text{K}^+ \cdot 4(2,6\text{-DNP})^-$. The samples were at concentrations of 0.15 mM in **G 24** in CH_2Cl_2 .

The Stejskal-Tanner plots from the diffusion NMR experiments in CDCl_3 are shown in **Figure 2.13**. These plots show that there is no exchange between the two species during the mixing times of the PFG-NMR experiment, since they both have single exponential decays. Analysis of amide NH peaks at δ 11.74 ppm and at δ 12.28 ppm provided diffusion coefficients of $D_s = 2.45 \pm 0.02 \times 10^{-10} \text{ m}^2 \text{ s}^{-1}$ for the species with two sets of signals (**Figure 2.11b**) and $D_s = 3.13 \pm 0.02 \times 10^{-10} \text{ m}^2 \text{ s}^{-1}$ for the species with the single set of signals (**Figure 2.11a**) shown in **Table 2.2**. This experimental ratio of 0.78 agrees well with the theoretical $D_{16 \text{ mer}}/D_{8 \text{ mer}}$ ratio of 0.79 and supports the proposal that the complex formed by liquid-liquid extraction is octamer **27** with formula $[\text{G } 24]_8 \cdot \text{K}^+ \cdot \text{DNP}^-$, whereas the species formed in the solid-liquid extraction is hexadecamer **28**, $[\text{G } 24]_{16} \cdot 4 \text{K}^+ \cdot 4 \text{DNP}^-$.

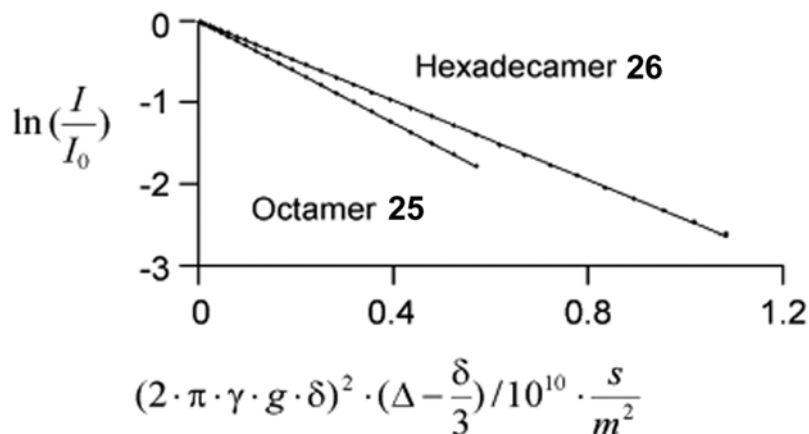


Figure 2.13. Stejskal-Tanner plot of octamer **27** and hexadecamer **28**. Diffusion coefficients for octamer **27** $[\text{G } \mathbf{24}]_8 \cdot \text{K}^+ \cdot \text{DNP}^-$ and hexadecamer **28** $[\text{G } \mathbf{24}]_{16} \cdot 4\text{K}^+ \cdot 4\text{DNP}^-$ in CDCl_3 at 21 °C.

Table 2.2. Diffusion Coefficients for G **24** Octamer/Hexadecamer System.^[a]

	$D_s(\text{G } \mathbf{27})$ ($10^{-10} \text{ m}^2/\text{s}$)	$D_s(\mathbf{28})$ ($10^{-10} \text{ m}^2/\text{s}$)	Ratio $\frac{D_s(\mathbf{28})}{D_s(\mathbf{27})}$
CD_2Cl_2	3.13 ± 0.02	2.45 ± 0.02	0.78

[a] The diffusion coefficients reported in **Table 2.2** are the mean \pm standard deviation of 8 separate measurements at 21°C

These results and characterization from PFG-NMR studies allowed for some insights into the cation-templated self-assembly of G **24** in CD_2Cl_2 . First, the C_4 -symmetric G_8 -octamer **27** is an intermediate in formation of the pseudo D_4 -symmetric G_{16} -hexadecamer **28**. Second, the K^+ concentration controls this octamer-hexadecamer equilibrium (**Figure 2.14**). Under solid-liquid extraction conditions used to generate $[\text{G } \mathbf{24}]_{16} \cdot 4 \text{K}^+ \cdot 4 \text{DNP}^-$ **28**, sufficient K^+ cation is brought into solution to link together two $[\text{G } \mathbf{24}]_8 \cdot \text{K}^+$ octamers (**Scheme 2.3**). However, this bridging K^+ cation must be held less tightly by

hexadecamer **28** than are the cations stabilizing the C_4 -symmetric $[G \mathbf{24}]_8 \cdot K^+$ octamers. This conclusion was supported by an experiment wherein washing a CD_2Cl_2 solution of hexadecamer **28** with water resulted in complete formation of octamer $[G \mathbf{24}]_8 \cdot K^+ \cdot DNP^-$ **27**. Likewise, addition of solid K^+DNP^- to a CD_2Cl_2 solution of octamer **27** gave quantitative conversion to hexadecamer **28**. The hexadecamer can be built or disassembled through washing to give a unit that is half its size and be built back by adding more cation. This is similar to the gel “off” – “on” experiments by Lehn in which cations were removed to make gels and added to change the gels back to liquids (see **Figure 1.19**).⁷³ This K^+ -dependent switching of the equilibrium between octamer **27** and hexadecamer **28** is also similar to NMR solution studies on the human telomere sequence $d(T_2AG_3)$, a G-rich DNA that forms a G-quadruplex monomer at 50 mM K^+ cation concentration and a dimer of co-axial G-quadruplexes at 300 mM K^+ cation concentration.¹⁹⁷

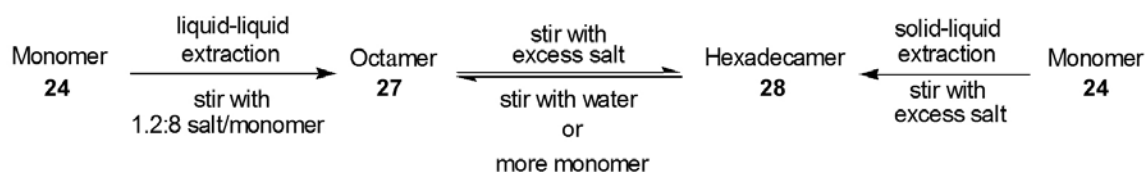
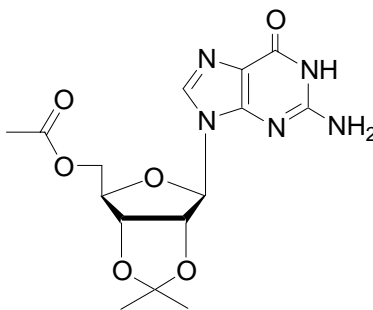


Figure 2.14. Formation of octamer **27** and hexadecamer **28** starting with monomer **24**.

This octamer intermediate **27** is seen primarily in nonpolar solvents. In more polar solvents, such as CD_3CN , only hexadecamer and monomer are observed. Furthermore, different cations or anions affect the stability of this intermediate. The octamer is generally not seen in Na^+ complexes as well as complexes with non-chelating anions such as BPh_4^- .

2.6 Investigations on Different Octamer Species

Previous work by Silvia Pieraccini from the Gottarelli group in Bologna concluded that 5'-O-acetyl-2',3'-O-isopropylidene-guanosine (**29**) formed a tetramer in the presence of saturated Na(picrate) in CDCl₃, and formed an octamer after washing with water based on ¹H NMR spectroscopy.¹⁹⁸ Speculatively, the size of this intermediate was assumed to be a tetramer or polymeric species, so diffusion NMR was utilized to discriminate between different possible structures with identical component ratios.



G **29**

Solid-liquid extraction of Na⁺ picrate into CDCl₃ by 5'-O-acetyl-2',3'-O-isopropylidene G **29** gave a complex with a single set of NMR signals and a G **29**/picrate molar ratio of 4:1 (**Figure 2.15a**). Since one Na⁺ cation is extracted for each picrate anion, this data indicates formation of a complex with an empirical formula of [G **29**]_{4n}⁺ (n)Na⁺ • n(pic)⁻. As depicted in **Scheme 2.5**, the structures that are consistent with this formula are an isolated C₄-symmetric G-quartet, [G **29**]₄•Na⁺•pic⁻ **30**, a pseudo-D₄-symmetric octamer with two bound Na⁺ cations, [G **29**]₈ • 2 Na⁺ • 2 pic⁻ **31**, and polymer, ([G **29**]₄ • Na⁺ • pic⁻)_n **32**. In theory, the doubly charged octamer [G **29**]₈ • 2 Na⁺ • 2 pic⁻ **31** might be expected to give two sets of NMR signals, but if the “capping” Na⁺ ion is in

fast exchange then only a single set of ^1H NMR signals would be observed. Additionally, depending on how the G-quartets are stacked, the symmetry of the octamer can be broken. The first two possible structures, a single Na^+ -filled G-quartet and a doubly charged octamer, have been previously identified in the gas phase.¹⁹⁹⁻²⁰¹ Neither a doubly charged octamer or a singly charged G-quartet has been reported in solution to date. However, polymeric stacked G-quartets of 87 stacked G-quartets were recently reported by the Wu group.²⁰²

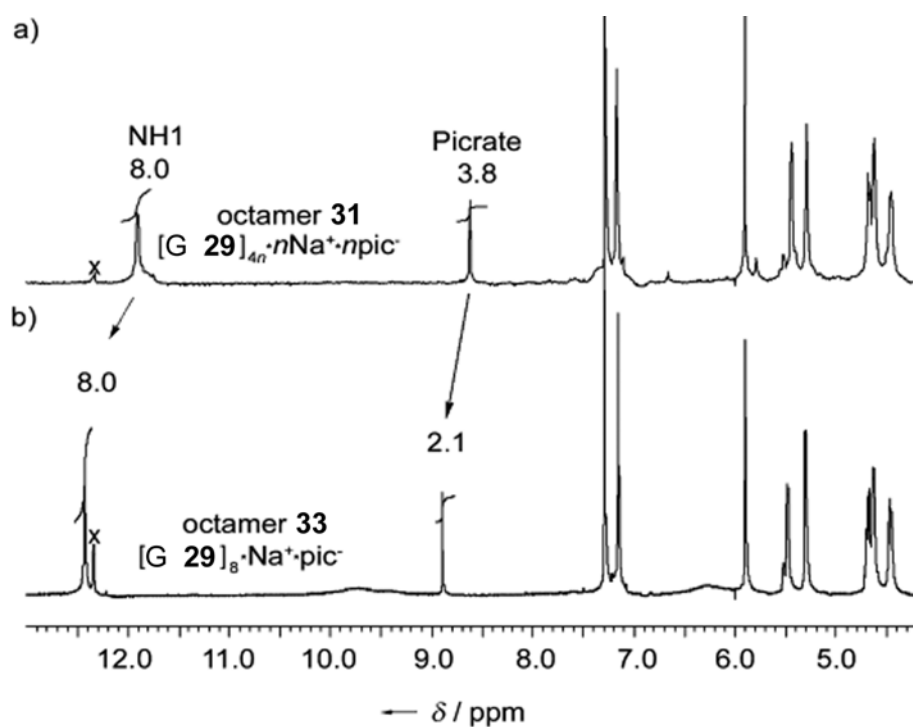


Figure 2.15. ^1H NMR spectra in CDCl_3 at 21°C of complexes formed by extraction of Na picrate with G **29**. a) A species of empirical formula $[\text{G } \mathbf{29}]_{4n} \cdot n\text{Na}^+ \cdot n(\text{pic})^-$ formed by solid-liquid extraction; b) octamer $[\text{G } \mathbf{29}]_8 \cdot \text{Na}^+ \cdot (\text{pic})^-$ **33** formed by washing solution in part a) with water. The identity of the peak with an \times is unknown.

chromophore, is diagnostic of an assembly with at least two chiral G-quartets rotated with respect to one another.¹⁹¹ While this data rules out the isolated G-quartet $[G\ 29]_4 \cdot Na^+ \cdot pic^-$ **30** as a structural possibility for $[G\ 29]_{4n} \cdot (n)Na^+ \cdot n(pic)^-$, the octamer $[G\ 29]_8 \cdot 2 Na^+ \cdot 2 pic^-$ **31** and polymeric $([G\ 29]_4 \cdot Na^+ \cdot pic^-)_n$ **32** can not be distinguished by CD spectroscopy. Again, diffusion NMR proved to be valuable in distinguishing between these structures.

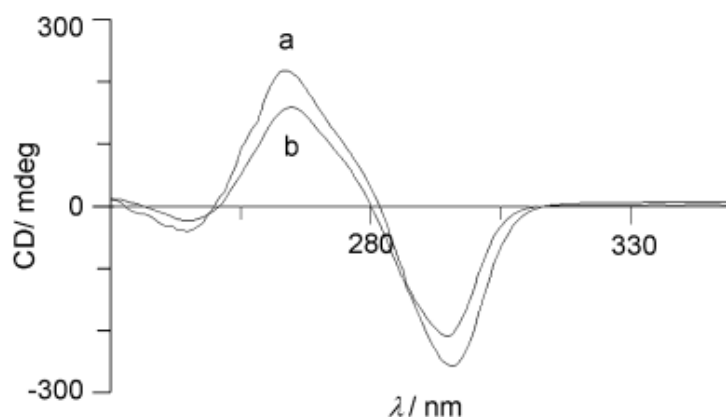


Figure 2.16. CD spectra of a) complex of formula $[G\ 29]_{4n} \cdot (n)Na^+ \cdot n(pic)^-$ and b) $[G\ 29]_8 \cdot Na^+ \cdot pic^-$ **33**. Both samples were at concentrations of 0.34 mM in $G\ 29$ in CH_2Cl_2 .

Although $[G\ 29]_8 \cdot Na^+ \cdot pic^-$ **33** showed two distinct broad N2 amino proton signals for the hydrogen bonding and exocyclic N2H protons at δ 9.8 and δ 6.3 ppm respectively, $[G\ 29]_8 \cdot 2 Na^+ \cdot 2 pic^-$ **31** showed no signals for these protons (presumably because they are coalesced due to being in fast exchange). Lowering the temperature to -4 °C allowed for the N2 amino proton signals to be observed and assigned (**Figure 2.17**).

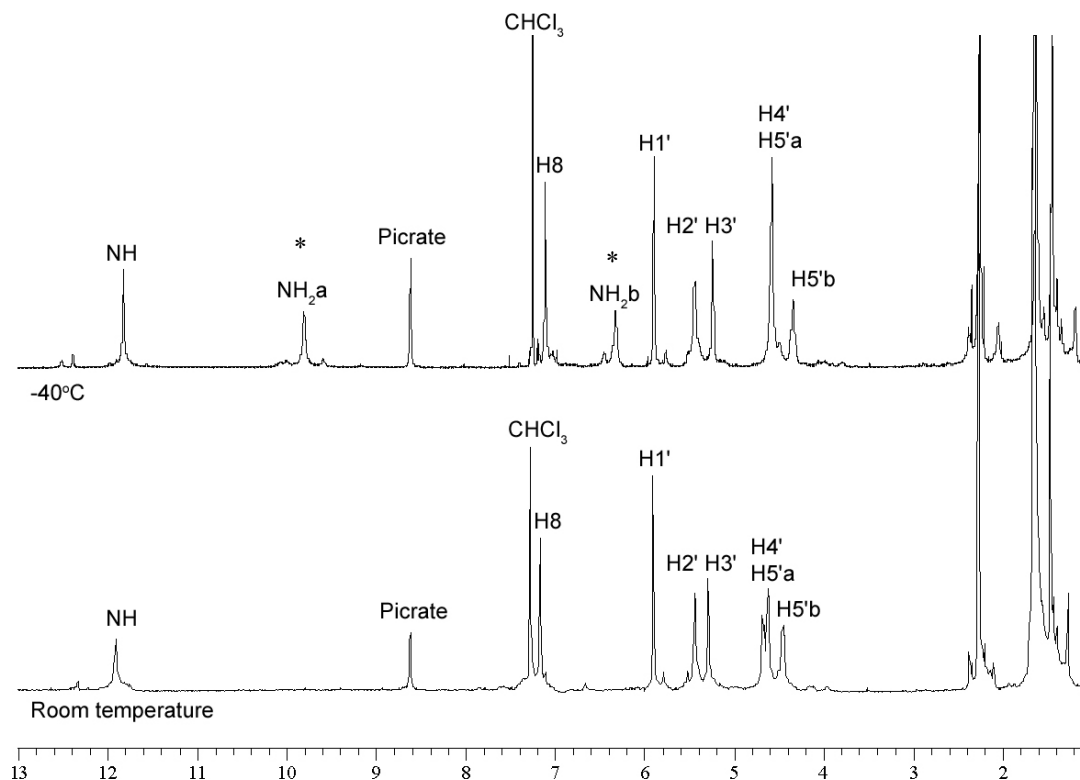


Figure 2.17. Lowering the temperature to $-4\text{ }^{\circ}\text{C}$ allows for the sharpening of the N2H signals in $[\text{G } 29]_8 \cdot 2 \text{Na}^+ \cdot 2 \text{pic}^-$ **31**. These N2H signals are indicated by asterisks.

Since octamer $[\text{G } 29]_8 \cdot \text{Na}^+ \cdot \text{pic}^-$ **33** and the $[\text{G } 29]_{4n} \cdot (n)\text{Na}^+ \cdot n(\text{pic})^-$ complex are in fast chemical shift exchange in CD_2Cl_2 , individual diffusion coefficients for the two different complexes can not be determined from the same NMR experiment (unlike **G 29** where the two species were in slow exchange). Instead, **A 23** was used as an internal standard in separate diffusion NMR experiments, with solvent, temperature and concentration held constant. The Stejskal-Tanner plots revealed $D_{\text{exptl}}/D_{\text{A } 23}$ values of 0.49 for the octamer $[\text{G } 29]_8 \cdot \text{Na}^+ \cdot \text{pic}^-$ **33** and 0.47 for the $[\text{G } 29]_{4n} \cdot (n)\text{Na}^+ \cdot n(\text{pic})^-$ complex (**Table 2.3**). These plots revealed that both were single exponential decays, so there was only one species for each signal. Both of these experimental diffusion coefficients agree well with the theoretical $D_{8 \text{ mer}}/D_{\text{monomer}}$ value of 0.50, indicating that

the self-assembled species generated by solid-liquid extraction of Na⁺ picrate with G **29** must be an octamer bound to two equivalents of Na⁺ picrate, namely [G **29**]₈ • 2 Na⁺ • 2 pic⁻ **31**.

Table 2.3. Diffusion Coefficients for G **29** Octamer/Octamer System.^[a]

	$D_s(\text{G } \mathbf{29})$ (10 ⁻¹⁰ m ² /s)	$D_s(\text{anion})$ (10 ⁻¹⁰ m ² /s)	$D_s(\text{A } \mathbf{23})$ (10 ⁻¹⁰ m ² /s)	Ratio $\frac{D_s(\mathbf{29})}{D_s(\mathbf{23})}$	Ratio $\frac{D_s(\text{anion})}{D_s(\mathbf{23})}$
33	4.06 ± 0.10	5.88 ± 0.05 Pic ⁻	8.62 ± 0.08	0.47	0.68
31	4.19 ± 0.05	6.54 ± 0.04 Pic ⁻	8.60 ± 0.08	0.49	0.76
34	3.30 ± 0.07	8.72 ± 0.10 BPh ₄ ⁻	8.62 ± 0.08	0.38	1.01

[a] The diffusion coefficients reported in **Table 2.3** are the mean ± standard deviation of 8 separate measurements at 21 °C.

The diffusion NMR results were supported by electrospray mass spectrometry (ESI-MS) of samples sprayed from solutions of CDCl₃ and analyzed by Silvia Pieraccini at the University of Bologna. Thus, samples generated by the solid-liquid extraction of sodium picrate with G **29** gave the doubly charged octamer ([G **29**]₈ • 2 Na)²⁺ (*m/z* 1484) as the strongest signal in the mass spectrum. A much smaller peak for ([G **29**]₁₆ • 3 Na)³⁺ (*m/z* 1972) was sometimes observed at low cone voltages. (40 eV). In contrast, liquid-liquid extraction of sodium picrate with G **29** led to formation of the singly charged ion ([G **29**]₈ • Na)⁺ (*m/z* 2945) as the major species (**Figure 2.18**).^{200,201}

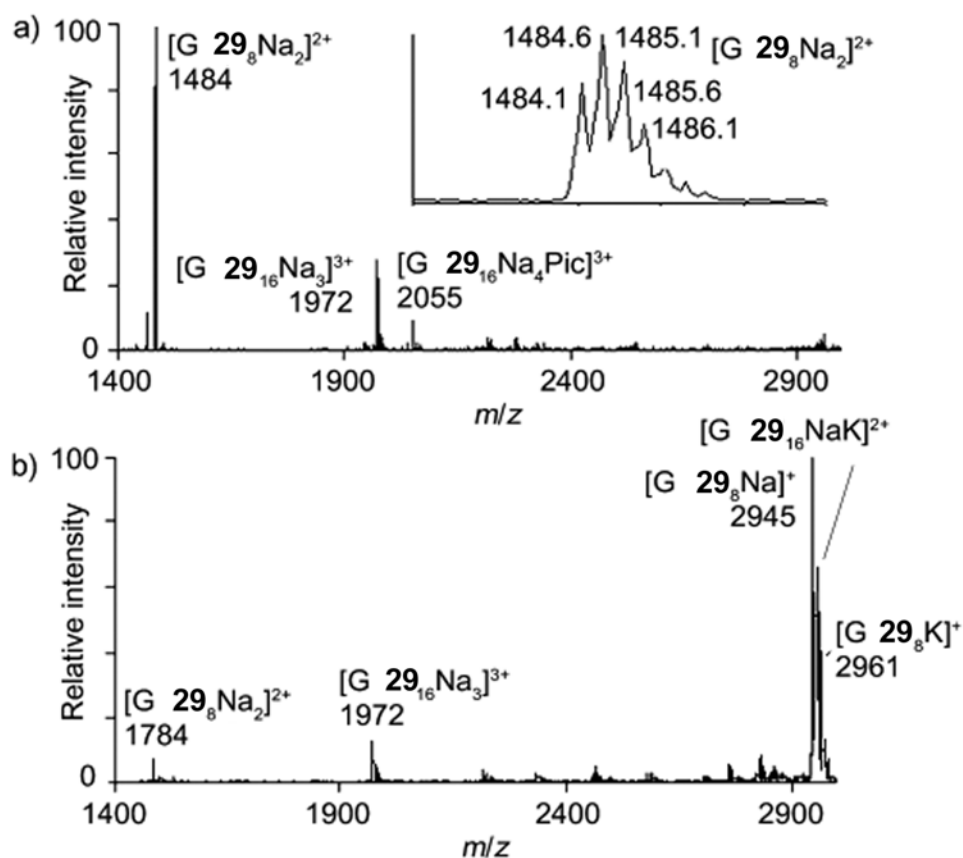


Figure 2.18. a) ESI-MS spectrum of G **29** in CHCl_3 after solid-liquid extraction of Na^+ -picrate. b) ESI-MS spectrum of the same solution after washing with water.

As depicted in **Figure 2.19**, the octamer $[\text{G } \mathbf{29}]_8 \cdot 2 \text{Na}^+ \cdot 2 \text{pic}^-$ **31** is stable under the solid-liquid conditions because the coordination sphere of the “capping” Na^+ in **31** is completed by a picrate anion, thus inhibiting growth of structures such as hexadecamer $[\text{G } \mathbf{29}]_{16} \cdot 4 \text{Na}^+ \cdot 4 \text{pic}^-$ under these conditions. The picrate anion is well known to function as a bidentate ligand for metal cations in crown ethers, serving to inhibit formation of sandwich complexes.^{203,204} This proposal is supported by the observation that picrate's NMR signal is shifted far upfield ($\Delta\delta = 0.29$ ppm) in $[\text{G } \mathbf{29}]_8 \cdot 2 \text{Na}^+ \cdot 2 \text{pic}^-$ **31**, relative to octamer $[\text{G } \mathbf{29}]_8 \cdot \text{Na}^+ \cdot \text{pic}^-$ **33**, presumably due to shielding of the bound picrate anion by the nearby G-quartet (**Figure 2.15**). Similar upfield shifts of the picrate

NMR signal, caused by anion- π interactions, have been noted in crown ether chemistry. The “capping” and “free” picrate anions appear to be in a time averaged fast exchange, so the diffusion coefficient of the picrate should be intermediate between the values for the “capping” picrate anion and the picrate anion on $[\text{G } \mathbf{29}]_8 \cdot \text{Na}^+ \cdot \text{pic}^- \mathbf{33}$. Furthermore, the calculated diffusion coefficient for this “capping” picrate in $[\text{G } \mathbf{29}]_8 \cdot 2 \text{Na}^+ \cdot 2 \text{pic}^- \mathbf{31}$ ($D_s = 5.88 \pm 0.05 \times 10^{-10} \text{ m}^2 \text{ s}^{-1}$) is much lower than picrate's diffusion coefficient in $[\text{G } \mathbf{29}]_8 \cdot \text{Na}^+ \cdot \text{pic}^- \mathbf{33}$ ($D_s = 6.54 \pm 0.04 \times 10^{-10} \text{ m}^2 \text{ s}^{-1}$), also consistent with intimate coordination of this “capping” anion with the guanosine octamer. Because of the fast exchange of the two picrate anions in $[\text{G } \mathbf{29}]_8 \cdot 2 \text{Na}^+ \cdot 2 \text{pic}^- \mathbf{31}$, the observed diffusion coefficient represents an average value. In estimating the diffusion coefficient for the “capping” picrate in $\mathbf{31}$ the other anion is assumed to have the diffusion coefficient of the picrate in $[\text{G } \mathbf{29}]_8 \cdot \text{Na}^+ \cdot \text{pic}^- \mathbf{33}$.

To test the hypothesis that a “capping” picrate anion stabilizes the octamer $[\text{G } \mathbf{29}]_8 \cdot 2 \text{Na}^+ \cdot 2 \text{pic}^- \mathbf{31}$, similar solid-liquid extractions were conducted in CD_2Cl_2 with NaPh_4B , a salt containing the poorly coordinating tetraphenylborate anion (**Figure 2.19**). Indeed, the NMR signal pattern (2 sets of signals in a 1:1 ratio) and integration (a $\text{G } \mathbf{29}:\text{Ph}_4\text{B}$ ratio of 4:1) were consistent with formation of hexadecamer $[\text{G } \mathbf{29}]_{16} \cdot 4 \text{Na}^+ \cdot 4 \text{Ph}_4\text{B}^- \mathbf{34}$. The diffusion coefficient for this complex $\mathbf{34}$ ($D_s = 3.30 \pm 0.07 \times 10^{-10} \text{ m}^2 \text{ s}^{-1}$), with **A 23** as an internal standard, was also consistent with generation of a hexadecamer ($D_{16 \text{ mer}}/D_{\text{monomer}} = 0.38$, see **Table 2.3**). Additionally, the diffusion coefficient of the anion, BPh_4^- , had a much faster diffusion coefficient than the picrate anions ($D_s = 8.72 \pm 0.10 \times 10^{-10} \text{ m}^2 \text{ s}^{-1}$). These experiments indicate that the counter-anion can dramatically influence the course of guanosine self-assembly.^{58,60,182}

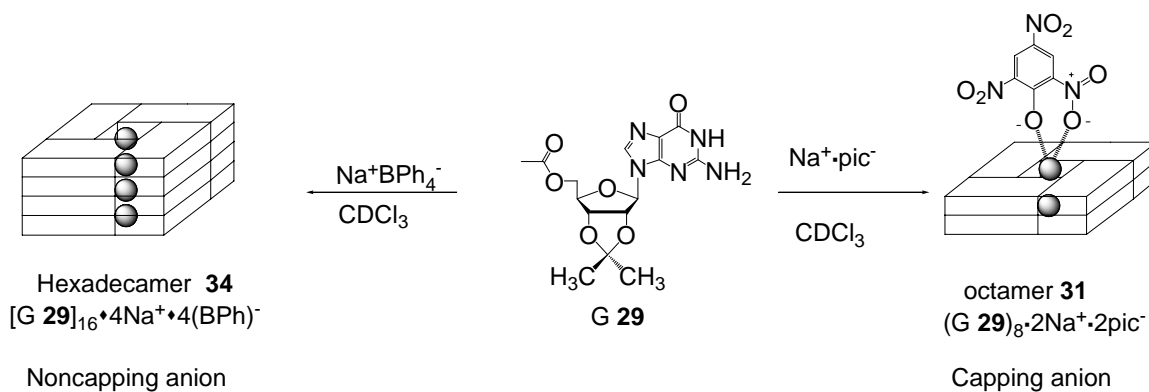


Figure 2.19. Addition of capping anions leads to octamer **31**, while addition of noncapping anion salts leads to hexadecamer **34**.

2.7 Conclusion

Utilizing PFG-NMR, the solution size structure of several lipophilic G-quadruplexes and their intermediates were characterized. These experiments led to important insights into the self-assembly of lipophilic G-quadruplexes. More specifically, the solution-state structure of the $[G \text{ 8}]_{16} \cdot 4 K^+ \cdot 4 pic^-$, G-quadruplex **22**, was determined to be a hexadecamer, which is useful knowledge for controlling post-modification of the self-assembled structure (see Chapter 3). It is important to know the size of the structure since it allows us to be sure that the hexadecamer has discrete inner and outer G-quartet layers that may vary in their accessibility for manipulation. Additionally, knowing that the G-quadruplex **22** is a hexadecamer provides information that it is roughly the size of known ion channels that span phospholipid membranes.²⁰⁵ These experiments unequivocally characterize the solution size of these lipophilic G-quadruplexes. Furthermore, the self-assembly process of G **8** into G-quadruplex **22** was determined to be a two-state mechanism with no visible NMR intermediates in CD_3CN .

Although both the “free” monomer and hexadecamer are observed at room temperature under the right conditions, shifting of this equilibrium is observed upon changes in temperature and concentration. This shifting of the equilibrium along with the knowledge that is a cooperative two-state equilibrium process also allows us to rationally manipulate the G-quadruplex.

Altering the ligand structure from G **8** to G **24** and the solvent from CD₃CN to CD₂Cl₂ allowed us to identify a discrete octameric intermediate in G-quadruplex formation. Again, the size of this octamer intermediate was confirmed from a series of diffusion NMR experiments.

Furthermore, diffusion NMR was used to distinguish between possible structures of identical sub-unit stoichiometry. The identity of the [G **29**]₈ • 2 Na⁺ • 2 pic⁻ **31** doubly charged octamer identity gave insights into how discrete intermediates can be stabilized by the “capping” anion. Self-assembly of G **29** was shown to be dependant on the anion, cation, and solvent and was confirmed by ESI-MS.

This diffusion NMR technique enabled us to better understand the self-assembly processes of G analogs, especially regarding the roles of cation, anion and solvent. The knowledge and insight gained from these experiments allowed for further manipulation of the pre-assembled G-quadruplex.

Chapter 3. Regioselective Ligand Exchange.

The majority of this chapter has been published in reference 206:

- Davis, J. T.; Kaucher, M. S.; Kotch, F. W.; Iezzi, M. A.; Clover, B. C.; Mullaugh, K. M. "Kinetic control in noncovalent synthesis: Regioselective ligand exchange into a hydrogen bonded assembly." *Org. Lett.* **2004**, 6, 4265-4268.

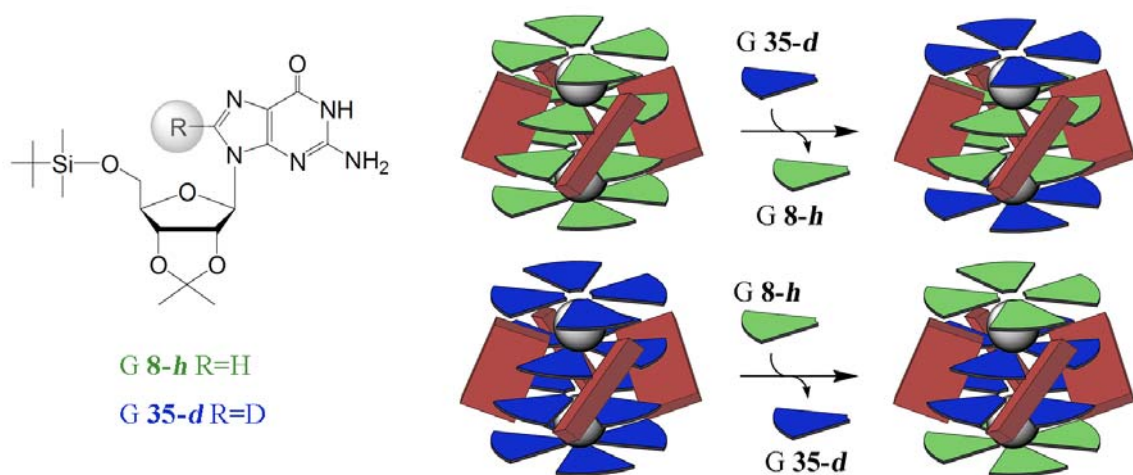
Some of the experimental work described in this chapter was performed by Maura A. Iezza and Bryna C. Clover, both undergraduates, working under my supervision.

3.1 Introduction

The initial goal of the research in this chapter was to construct amphiphilic G-quadruplexes. G-quadruplexes were functionalized through a regioselective exchange process described in this chapter.²⁰⁶ Highly functionalized G-quadruplexes may be critical for gaining function for uses as nanotubes and wires,^{6,207-215} gelators,⁷³ biosensors,^{79,80,83} or synthetic ion channels.²¹⁶⁻²¹⁸ Amphiphilic G-quadruplexes, which contained hydrophilic groups on the exterior and hydrophobic groups on the interior, might help align G-quadruplexes in phospholipid bilayers, allowing these G-quadruplexes to be potentially useful as synthetic ion channels.

Kinetically controlled covalent synthesis has been one of the great successes of the last 50 years in natural product synthesis. Covalent synthesis has yielded complex molecules with functional diversity and stereochemistry that can be achieved through kinetically controlled reactions. Until recently, there has not been the same level of success in non-covalent synthesis.^{3,4,219-230} Since self-assembly relies on the spontaneous formation of molecular assemblies, multiple structures are often obtained with similar energy levels. Even though this is valuable for building structures with diversity,

creating discrete structures is often difficult.²³¹ Crystal engineering, equilibrium shifting and the use of molecular chaperones have been some of the methods that have accomplished building non-covalent structures with defined composition and stereochemistry.²³²⁻²³⁷ Similarly, post-modification of non-covalent structures can lead to discrete structures that are kinetically stable.²³⁸⁻²⁴¹ There have been very few examples of kinetically stable hydrogen bonded systems. Coordination and mechanically locked systems have been typically used to kinetically stabilize noncovalent systems since they rely on much stronger bonds than hydrogen bonds.²⁴²⁻²⁴⁷ The regioselective ligand exchange that is reported in this chapter provides a method to create kinetically stable hydrogen-bonded structures. Formation of the noncovalent structures followed by subunit exchange into more labile regions of the noncovalent structure allows for the possibility of noncovalent structure to be formed that are highly diverse and functionalized.²⁴⁸ As a proof of concept, regioselective exchange of isotopically labeled ligands (G **8-h** and G **35-d**), where G **35-d** is a guanosine derivative deuterated at the C8 position, was first demonstrated (**Scheme 3.1**).

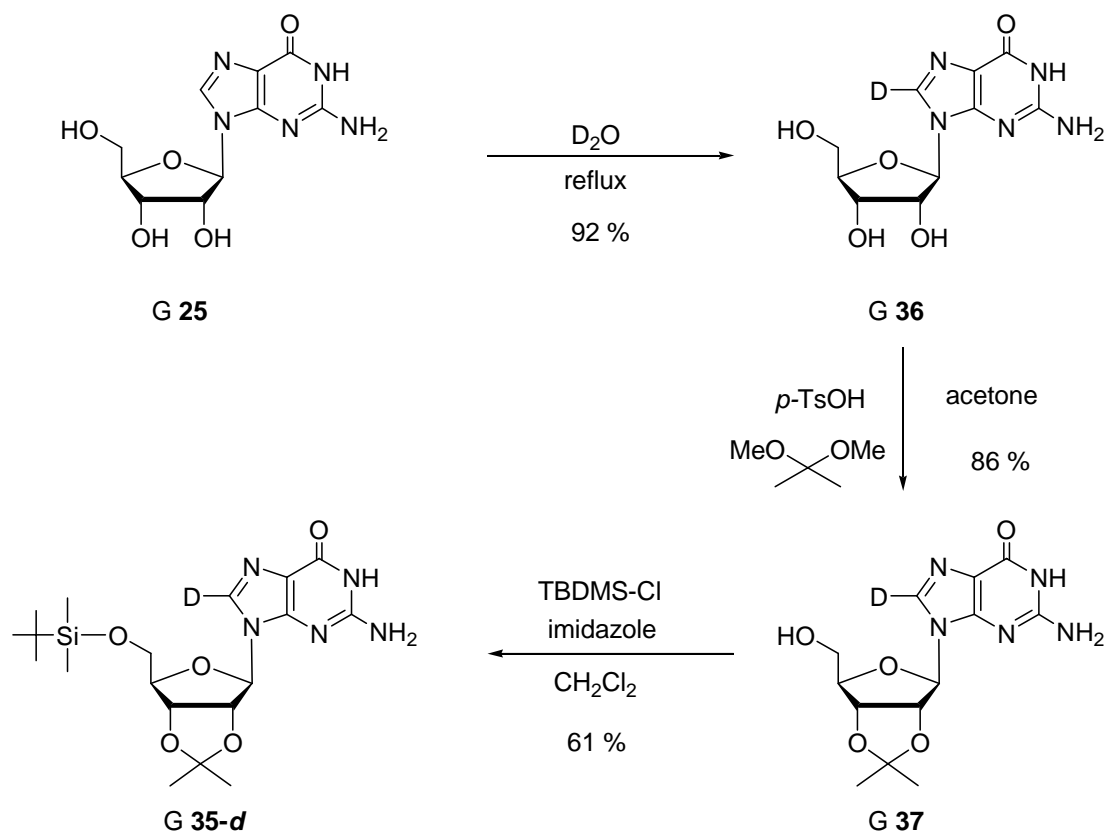


Scheme 3.1. Regioselective ligand exchange into G-quadruplex with isotopically labeled ligands.

3.2 Isotopomer Formation.

In **Scheme 3.1**, the spheres represent cations and the blocks represent anions. The green and blue wedges represent nondeuterated H8 **8-h** and deuterated $^2\text{H}8$ **35-d** guanosine respectively. In this section, the regioselective pseudo self-exchange of G **35-d** with G **8-h** subunits in the G-quadruplex is described. Since both the cation and anion can control the stability of the G-quadruplex, both ions show influences on this regioselective exchange process of isotopically labeled subunits. This demonstration of the regioselective exchange process produces some of the largest non-covalent isotopomers yet reported. Additionally, this process demonstrates control over post-assembly modification that can be applied in general to non-covalent synthesis.

Deuterated G **35-d**, 2',3'-O-isopropylidene-5'-*t*-butyldimethylsilyl-8-*d*-guanosine, was synthesized through H8/D8 exchange by refluxing G **3.2** in D_2O (**Scheme 3.2**).²⁴⁹ This exchange was followed by routine modification of the ribose in G **3.3** to give G **3.1-d**. The ^1H NMR spectra of G **35-d** was similar to G **8-h** except for the diminished H8 signal intensity. The ^1H NMR spectrum shown in **Figure 3.1** indicated less than 2 % of any residual ^1H intensity at the H8 position. Formation of the 98 % deuterated G-quadruplex $[\text{G } \mathbf{35-d}]_{16} \cdot 2\text{Ba}^{2+} \cdot 4\text{DNP}^-$ was achieved in a similar manner to that of the unlabeled G-quadruplex $[\text{G } \mathbf{8-h}]_{16} \cdot 2\text{Ba}^{2+} \cdot 4\text{DNP}^-$ (**Figure 3.2**). The NMR spectra of these two G-quadruplexes are identical except for the diminished H8 signals intensities in the deuterated G-quadruplex. The G-quadruplex ^1H NMR spectra were assigned by a series of COSY, NOESY, HMBC, and HSQC 2D NMR experiments, similar to those previously reported by the Davis group.^{56,58}



Scheme 3.2. Synthesis of **G 35-d**.

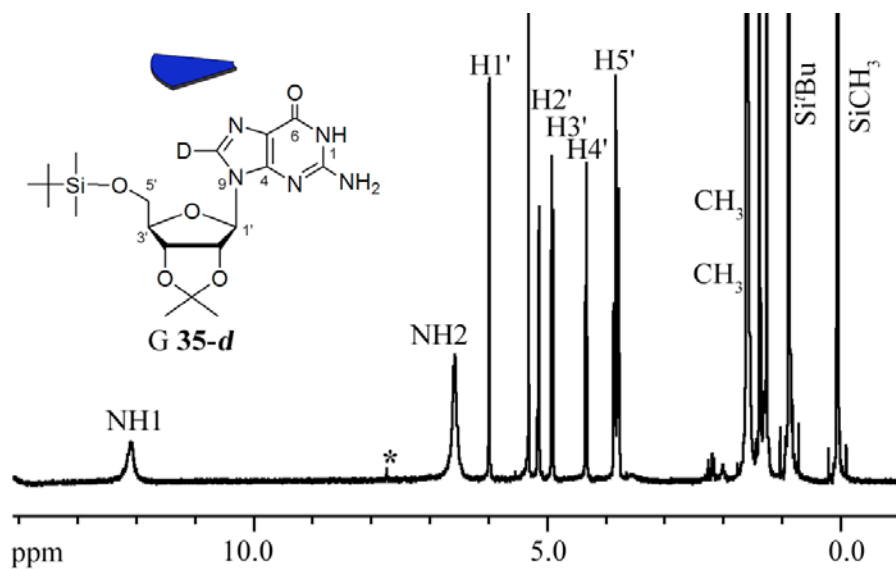


Figure 3.1. 400 MHz ^1H NMR spectrum of **G 35-d** in CD_2Cl_2 at rt. The asterisk indicates the C8 residual ^1H signal.

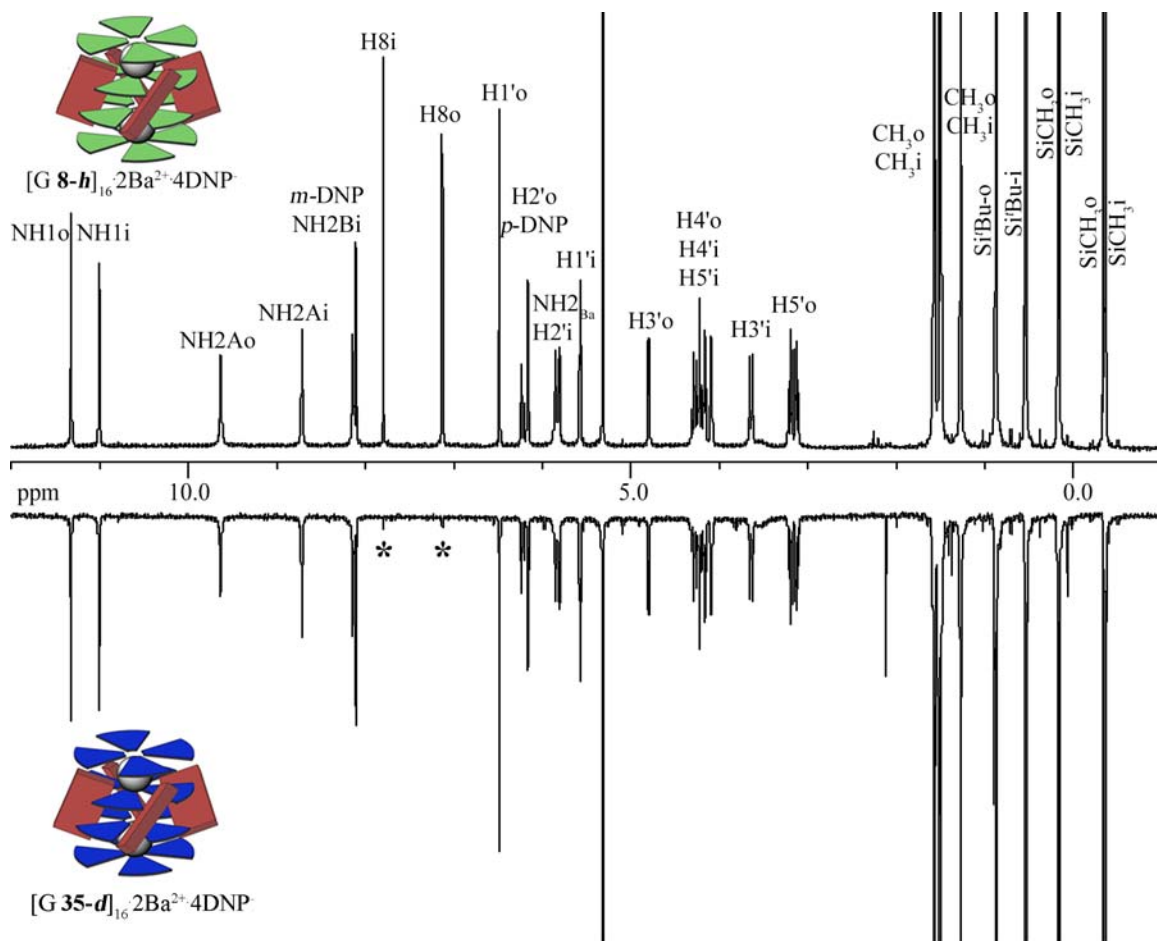


Figure 3.2. 400 MHz ¹H NMR spectra in CD₂Cl₂ at rt of nondeuterated G-quadruplex [G 8-h]₁₆ • 2Ba²⁺ • 4DNP⁻ (top) and deuterated G-quadruplex [G 35-d]₁₆ • 2Ba²⁺ • 4DNP⁻ (bottom). The asterisks indicates the C8 residual ¹H signal. Signals labeled with “a” indicate “outer” layer ¹H signals, while signals labeled with “b” indicate “inner” layer ¹H signals.

3.2.1 Subunit Exchange into the Outer Layer.

Figure 3.3a shows the ¹H NMR spectrum immediately after mixing [G 8-h]₁₆ • 2Ba²⁺ • 4DNP⁻ with G 35-d in CD₂Cl₂. Since the C8 position of G 35-d is deuterated, only the protons of the G-quadruplex are visible in the ¹H NMR spectrum. **Figure 3.3b** shows the ¹H NMR spectrum after 4 days of mixing. While the peak intensity for the H8

outer G-quartet layer diminishes, the “free” G **8-h** H8 peak increases with no noticeable changes in the peak intensity of the inner G-quartet layer. The “free” guanosine is defined as unassembled ligand, where it may be a mixture of oligomers, dimers, and mainly monomer in nonpolar solvents.¹⁸³⁻¹⁸⁵

Conversely, **Figure 3.3c** shows the ¹H NMR spectrum immediately after mixing of [G **35-d**]₁₆ • 2Ba²⁺ • 4DNP⁻ with G **8-h** in CD₂Cl₂. Since the C8 positions of [G **35-d**]₁₆ • 2Ba²⁺ • 4DNP⁻ are deuterated, only the protons of the G **8-h** are visible in the ¹H NMR spectrum. **Figure 3.3d** shows the ¹H NMR spectrum after 4 days of mixing. This spectrum shows that only the peak intensity of the “outer” G-quartet layer increases, indicating that the ligand exchange process is regioselective for the outer G-quadruplex layers of [G **3.1**]₁₆ • 2Ba²⁺ • 4DNP⁻ under these conditions.

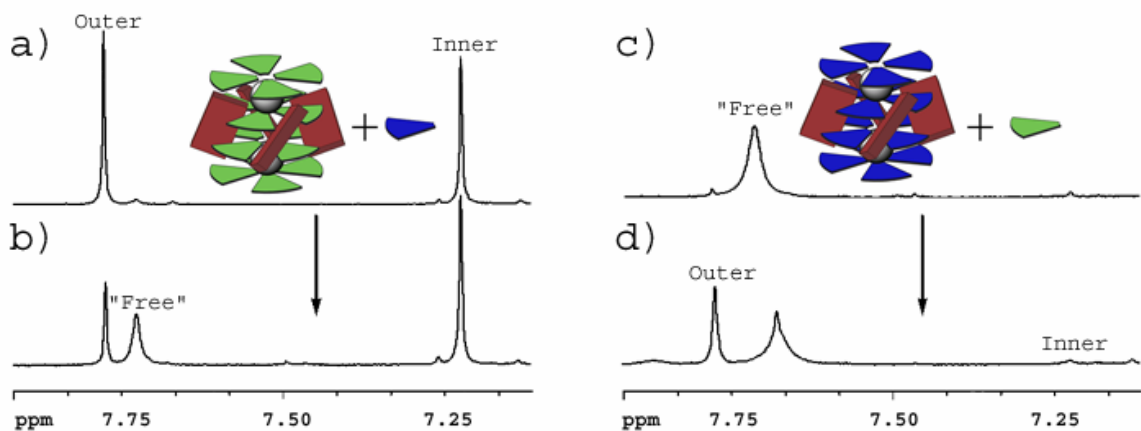


Figure 3.3. H8 region of 400 MHz ¹H NMR spectra in CD₂Cl₂; a) solution of [**8-h**]₁₆ • 2Ba²⁺ • 4DNP⁻ (0.39 mM) and G **35-d** (6.2 mM) immediately after mixing; b) the sample in a) after 4 days at room temp; c) solution of G **8-h** (6.2 mM) and [**35-d**]₁₆ • 2Ba²⁺ • 4DNP⁻ (0.39 mM) immediately after mixing; (d) the sample in c) after 4 days at rt.

Control experiments were run where a 50-50 % mixture of deuterated and non-

deuterated ligands were mixed with K^+Pic^- , leading to the formation of a G-quadruplex with a 50-50 % mixture of deuterated ligand in both the outer and inner layers. The 50-50 % mixture of deuterated and nondeuterated guanosine in both layers clearly shows that this self-assembly process is under thermodynamic control since there is no driving force for the labeled or unlabeled ligands to segregate into a specific layer (**Figure 3.4**).

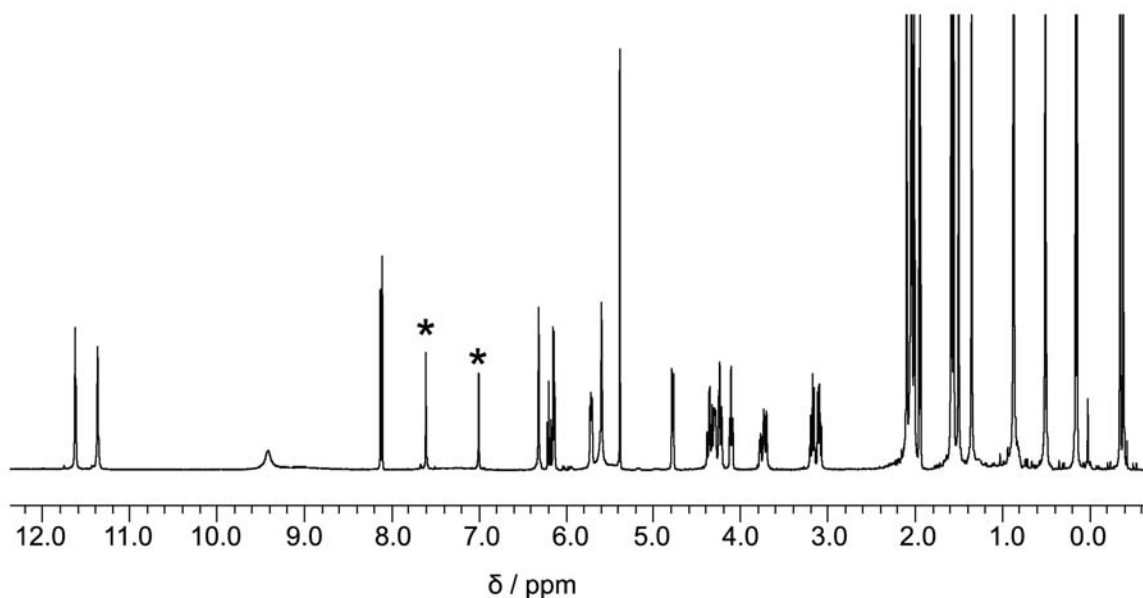


Figure 3.4. Control experiment shows 50-50 % mixture of deuterated G **35-d** and nondeuterated guanosine G **8-h** in both the inner and outer layers of the hexadecameric G-quadruplex formed by extraction of $Ba^{2+}DNP^-$. The 1H NMR spectrum shows that the 1H signal intensities of the inner and outer H8 signals, indicated by *'s, are diminished by 50 %.

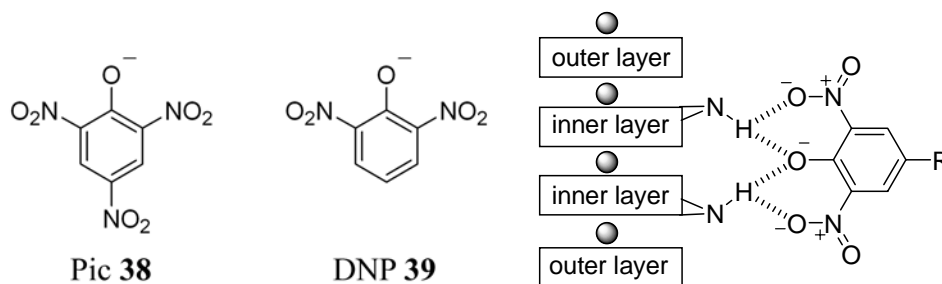
In theory, isotopomers could be made through exchange of G **35-d** with $[G \text{ 8-h}]_{16} \cdot 2Ba^{2+} \cdot 4DNP^-$ quadruplex or by exchange of G **8-h** with $[G \text{ 35-d}]_{16} \cdot 2Ba^{2+} \cdot 4DNP^-$ quadruplex to give its isomer in CD_2Cl_2 . An incorporation of G **8-h** (95 %) was observed for the regioselective exchange process with $[G \text{ 8-h}]_{16} \cdot 2Ba^{2+} \cdot 4DNP^-$ when 160

equivalents of the exchanging ligand was used. The statistical distribution of this exchange process should be 95 % since 160 labeled units are exchanged into the outer layer of the G-quadruplex, which contains 8 unlabeled units in the outer layer

$$\left(\frac{160}{160 + 8} = 0.95 \right).$$

3.2.2 Stabilization of the Inner G-Quartet Layer by the Anion.

DNA G-quadruplexes can be stabilized through the binding of small molecules. As mentioned before, this area is of particular importance for telomerase inhibitors. Similar to telomerase inhibitors, the anion of lipophilic G-quadruplex can affect the stability of the self-assembled structure. Crystal structures and NMR spectroscopy studies have shown that the lipophilic G-quadruplex is stabilized by the bound anion.^{53,58} The anion, picrate **38**, hydrogen bonds to the G-quadruplex surface. More specifically, this nucleobase-anion hydrogen bond is formed between the exocyclic N2 amino protons of the G-quadruplex inner layer and the oxygens of the nitro groups and phenolate oxygen of the anion (**Scheme 3.3**). This additional stability of the inner layers over the outer layers of the G-quadruplex can be exploited since ligands in the outer layers should be more labile towards exchange. The hexadecameric G-quadruplex can be seen as a dimer of octamers, where the two octamers are held together by anions. The stability of these inner layers can be controlled by the basicity of the anion. Picric acid **38** (Pic) has a pK_a of 0.38, while 2,6-dinitrophenol **39** (DNP) has a pK_a of 3.96.^{58,250} On this notion, the DNP anion was reasoned to stabilize the inner layer more than the picrate anion since DNP is a stronger base.



Scheme 3.3. Model of anions binding to exocyclic N2 amino protons of the inner layer. This anion-nucleobase hydrogen bond helps stabilize the inner layers of the G-quadruplex. Sugars and other anions are omitted for clarity.

Figure 3.5a shows how the strongly bound DNP anion **39** in $([G \text{ 8-}h]_{16} \cdot 2Ba^{2+} \cdot 4DNP^-)$ stabilizes the G-quadruplex, such that only ligands within the “outer” G-quartet layer are exchanged with G **35-d**, while the “inner” G-quartet remains unchanged. The graphs in **Figure 3.5** show how the H8 signal intensity changes over time for the “free,” “inner,” and “outer” ligands. Conversely, **Figure 3.5b** shows how the relatively weaker bound Pic anion **38** in $([G \text{ 8-}h]_{16} \cdot 2Ba^{2+} \cdot 4Pic^-)$ doesn’t stabilize the G-quadruplex as both the “outer” and “inner” G-quartet layers decrease in signal intensity. With strongly binding anions, regioselective ligand exchange into the outer G-quartet layer was accomplished. However, weakly binding anions (Pic⁻) or noncoordinating ions (such as BPh₄⁻) do not stabilize the G-quadruplex’s inner layers enough to allow for regioselective subunit exchange. This study demonstrates the importance of the anion in stabilizing the inner G-quartet layers so that the regioselective ligand exchange process of G **35-d** into the outer G-quartet layers is maintained. Additionally, the anion has similarities to telomerase inhibitors that stabilize G-quadruplexes through binding to the exposed G-quartet edges.³⁴⁻⁴¹

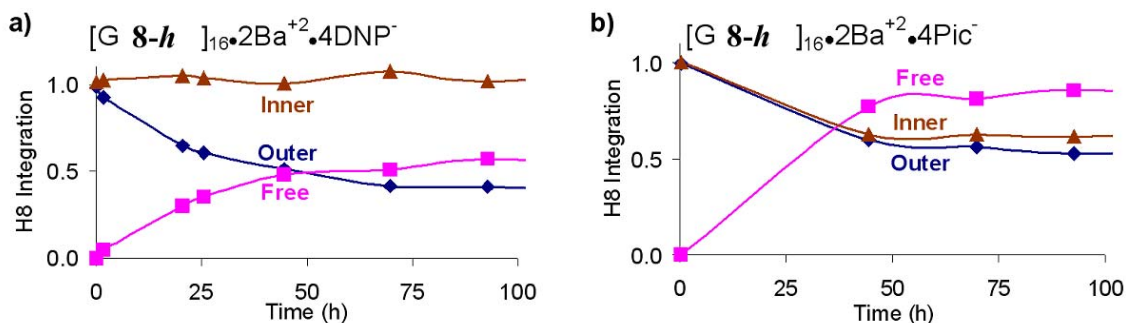


Figure 3.5. Integration of the H8 NMR signal for the “inner” G-quartet in the exchange of 16 equiv of G **35-d** (6.2 mM) with a) $[G \mathbf{8-h}]_{16} \cdot 2Ba^{2+} \cdot 4DNP^{-}$ and b) $[G \mathbf{8-h}]_{16} \cdot 2Ba^{2+} \cdot 4Pic^{-}$. Exchange was done at room temp in CD_2Cl_2 .

3.2.3 Stabilization of the Inner Layer G-Quartet by the Cation.

The cation is essential for the stabilization of DNA G-quadruplexes.²² The trend for DNA G-quadruplexes to bind monovalent cations was found to be $K^{+} > Rb^{+} > Na^{+} \gg Li^{+}, Cs^{+}$.²⁵¹⁻²⁵⁴ Furthermore, these G-quadruplexes are more stable with divalent cations, such as Ba^{2+} , Ca^{2+} , Pb^{2+} , and Sr^{2+} , than with monovalent cations.^{46,255-260} This is not surprising since higher charged species have stronger ion-dipole interactions.

Likewise, the lipophilic G-quadruplex ($[G \mathbf{8-h}]_{16} \cdot 2Ba^{2+} \cdot 4DNP^{-}$) is cation dependent and shows similar cation selectivity as its DNA counterpart.^{56,59,182,261-263} Since specific cations should stabilize the G-quadruplex better, the regioselective ligand exchange process should also be affected by the cation that is present in the G-quadruplex ($[G \mathbf{8-h}]_{16} \cdot nM^{n+} \cdot 4DNP^{-}$). As mentioned before, divalent cations stabilize G-quadruplexes better than monovalent cations. Although divalent cations stabilize the G-quadruplex ($[G \mathbf{8-h}]_{16} \cdot 2Ba^{2+} \cdot 4DNP^{-}$) more than monovalent cations ($[G \mathbf{8-h}]_{16} \cdot 4K^{+} \cdot 4DNP^{-}$), regioselective exchange of isotopically labeled ligands into the outer layers is only regioselective with monovalent cations in polar solvents.

When using a more polar 50-50 % CD₃CN-CD₂Cl₂ solvent system, the anions do not coordinate nearly as well to the G-quadruplex as they do in nonpolar solvents such as CH₂Cl₂. So in more polar solvents, such as 50-50 % CD₃CN-CD₂Cl₂, the anions are not hydrogen bonded to the G-quadruplex and do not have an effect on the regioselective ligand exchange process. Additionally, the ligand exchange reaction is much faster in hydrogen-bond disrupting solvent since it weakens the hydrogen-bonds of the G-quadruplex. **Figure 3.6a** shows the exchange of G **35-d** with the divalent barium complex ([G **8-h**]₁₆ • 2Ba²⁺ • 4DNP⁻), where both the “outer” and “inner” layers decrease at similar rates. In contrast, the exchange process of G **35-d** with the monovalent potassium complex ([G **8-h**]₁₆ • 4K⁺ • 4DNP⁻) shows the “outer” layer decreasing at a much faster rate than the “inner” layer (**Figure 3.6b**).

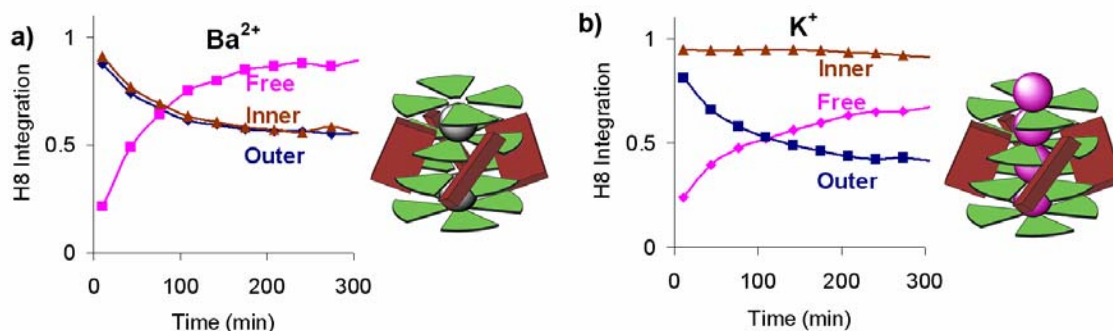


Figure 3.6. NMR integration of H8 signals in exchange of 16 equiv of G **35-d** (6.2 mM) with a) [G **8-h**]₁₆ • 2Ba²⁺ • 4DNP⁻ and b) [G **8-h**]₁₆ • 4K⁺ • 4DNP⁻. Reactions were done at rt in 50-50 % CD₃CN-CD₂Cl₂. Depictions show different cation occupancy of the G-quadruplexes.

To rule out the possibility that the anion governed the regioselectivity of the ligand exchange process, ¹H VT-NMR was used to calculate the exchange rates of the “free” anion and “bound” anion through **Equation 3.1**.

$$\text{rate} = 2\pi\Delta\nu$$

Equation 3.1. Exchange rate at coalescence

In order to calculate the exchange of the DNP anion for these systems, an equal amount of free DNP was added to the $(G\ 8-h)_{16}$ G-quadruplex. To help solvate the DNP salts, [2.2.2]cryptand **21**, was added to sequester the excess M^{n+} . The stack plots shown in **Figure 3.7** show both the monovalent and divalent G-quadruplexes contain DNP anions that are in fast exchange with “free” DNP anions. The signals of the DNP anions coalesced at -52°C for the Ba^{2+} G-quadruplex ($[G\ 8-h]_{16} \cdot 2\text{Ba}^{2+} \cdot 4\text{DNP}^-$) (**Figure 3.7a**), while the signals coalesced at -8°C for the K^+ G-quadruplex ($[G\ 8-h]_{16} \cdot 4\text{K}^+ \cdot 4\text{DNP}^-$) (**Figure 3.7b**).

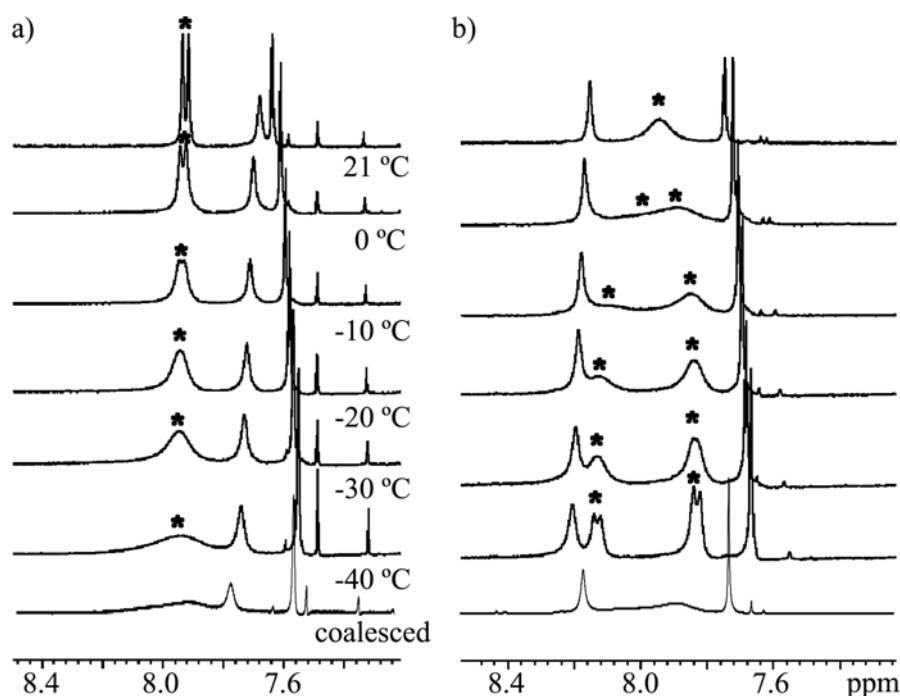
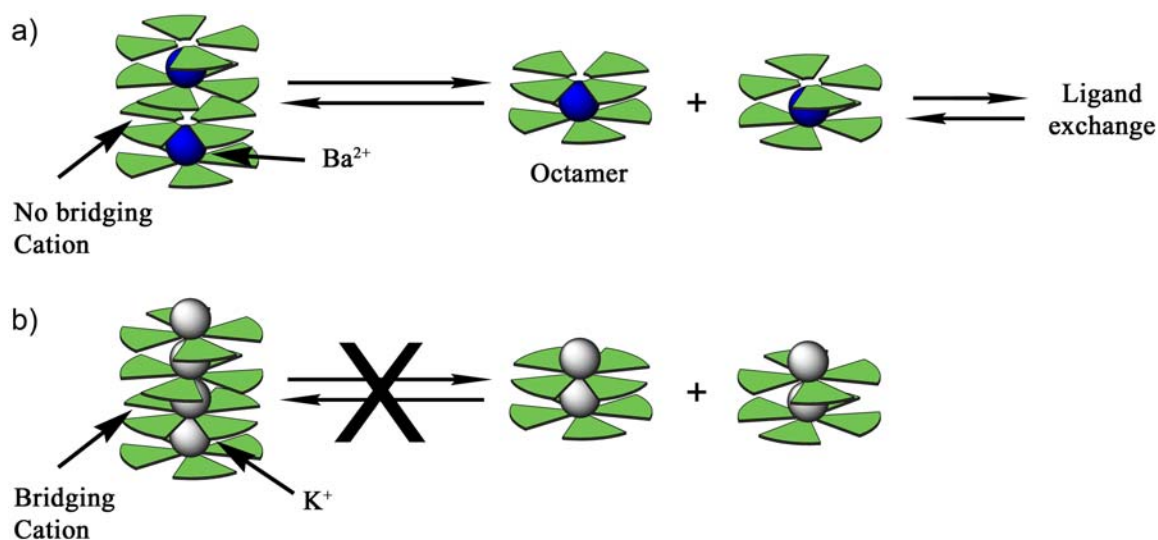


Figure 3.7. a) $[G\ 8-h]_{16} \cdot 2\text{Ba}^{2+} \cdot 4\text{DNP}^-$ with 2mM cryptate and 2mM $\text{Ba}^{2+}(\text{DNP}^-)_2$ at various temperatures in 1:1 $\text{CD}_2\text{Cl}_2\text{-CD}_3\text{CN}$. b) $[G\ 8-h]_{16} \cdot 4\text{K}^+ \cdot 4\text{DNP}^-$ with 4mM cryptate and 4 mM $\text{K}^+(\text{DNP}^-)$ at various temperatures in 1:1 $\text{CD}_2\text{Cl}_2\text{-CD}_3\text{CN}$. Asterisks signify protons related to “free” and complexed DNP anion as they coalesce.

The coalescence points for the DNP anion signals of the respective Ba^{2+} or K^+ G-quadruplexes were used to calculate the exchange rates. These exchange rates were calculated to be 588 s^{-1} and 687 s^{-1} for the “free” and “bound” DNP anions of the Ba^{2+} or K^+ G-quadruplexes, respectively. These exchange rates equate to free energies of activation for the anions of the Ba^{2+} and K^+ G-quadruplexes of $\Delta G^\ddagger = 12.0 \text{ kcal/mol}$ and 10.0 kcal/mol , respectively. The exchange rates show that the Ba^{2+} G-quadruplex binds the DNP⁻ anion tighter than does the K^+ G-quadruplex. These results rule out the possibility that the ligand exchange process with the Ba^{2+} G-quadruplex was not regioselective because it wasn't binding its anions as strongly as the K^+ G-quadruplex.

These results suggest that even when the anions are stripped from the G-quadruplex, monovalent cations stabilize the hexadecamer through their bridging cation between the two octamers and doesn't allow for the hexadecamer to fall apart. (**Scheme 3.4**). G-quadruplexes with divalent cations have no bridging cation to stabilize the hexadecamer once the anions fall off, so they break into octamers. Ligand exchange into the “inner” or “outer” layers is not regioselective in these octamers since they do not contain discrete inner and outer regions. These results demonstrate the importance of monovalent cations in stabilizing the hexadecameric G-quadruplex from breaking apart into octamers in more polar solvents.



Scheme 3.4. In more polar solvents, weaker binding anions allow for the hexadecamer to break into octamers for a) divalent cation G-quadruplexes, while b) monovalent cations stabilize the hexadecameric G-quadruplex with their “bridging” cations.

3.2.4 Destabilization of the Outer G-quartet Layer by Small Molecules

Destabilizing the outer G-quartet layer allows for faster exchange into the outer G-quartet layer. Small molecules were shown to have a profound impact on the half-life of the regioselective ligand exchange process. Since the G-quadruplex might be weakened through additional hydrogen-bonding molecules, small molecules with complementary hydrogen bond edges may impact the regioselective subunit exchange process of these G-quadruplexes. A series of compounds **40-44** were tested for their influence on the ligand exchange process: acetic acid **40**, 2-aminopyridine **41**, 2-hydroxypyridine **42**, formamide **43**, and 5'-*t*-butyldimethyl-2',3'-O-isopropylidene-uridine **44**. Additionally, a higher amount of guanosine may be enough to autocatalyze the regioselective exchange process since it can form additional hydrogen bonds.²⁶⁴⁻²⁶⁷ It was hypothesized that rate accelerations can be achieved through weakening the G-

quartet hydrogen-bonds through hydrogen bonding with its exocyclic N2 hydrogen and N3 nitrogen (**Figure 3.8**).

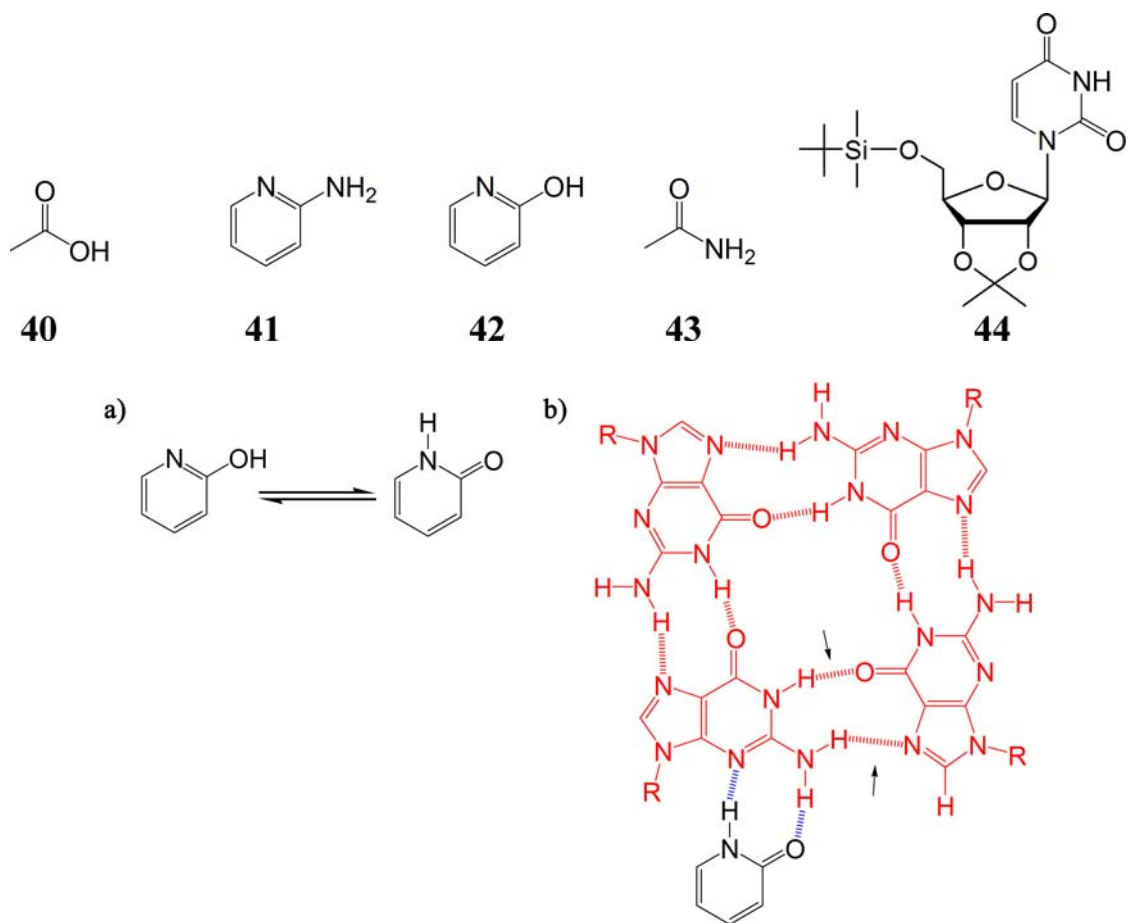


Figure 3.8. a) Tautomerization of 2-hydroxypyridine **42**. b) Weakening of the G-quartet through hydrogen bonding of guanine and hydroxypyridine **42**.

The experiments were conducted by mixing $[\mathbf{8-h}]_{16} \cdot 2\text{Ba}^{2+} \cdot 4\text{DNP}^-$ (0.39 mM), G **1-d** (6.2 mM), and small molecule (6.2 mM) and taking ^1H NMR spectra at different time intervals. Of the molecules tested, 2-hydroxypyridine **42** had a profound impact on the time it took for ligand exchange process to be completed, allowing for completion of the reaction in 40 h instead of over 200 h for the regioselective exchange of G **35-d** into the $[\text{G } \mathbf{8-h}]_{16} \cdot 2\text{Ba}^{2+} \cdot 4\text{DNP}^-$ complex in CDCl_3 (**Figure 3.9**). In general, molecules

with amide functionalities appeared to have an impact on the half-life of the reaction. Thus, uridine **44** and formamide **40**, also showed marked decreases in the half-life of the exchange process, while amidine functionalities, 2-aminopyridine **41**, showed no change in the reaction time. Acetic acid **40** led to decomposition of the G-quadruplex. The protic nature of acetic acid resulted in protonation of the guanosine's N2 and N7 amines, thereby disrupting the hydrogen-bonded G-quadruplex.²⁶⁸

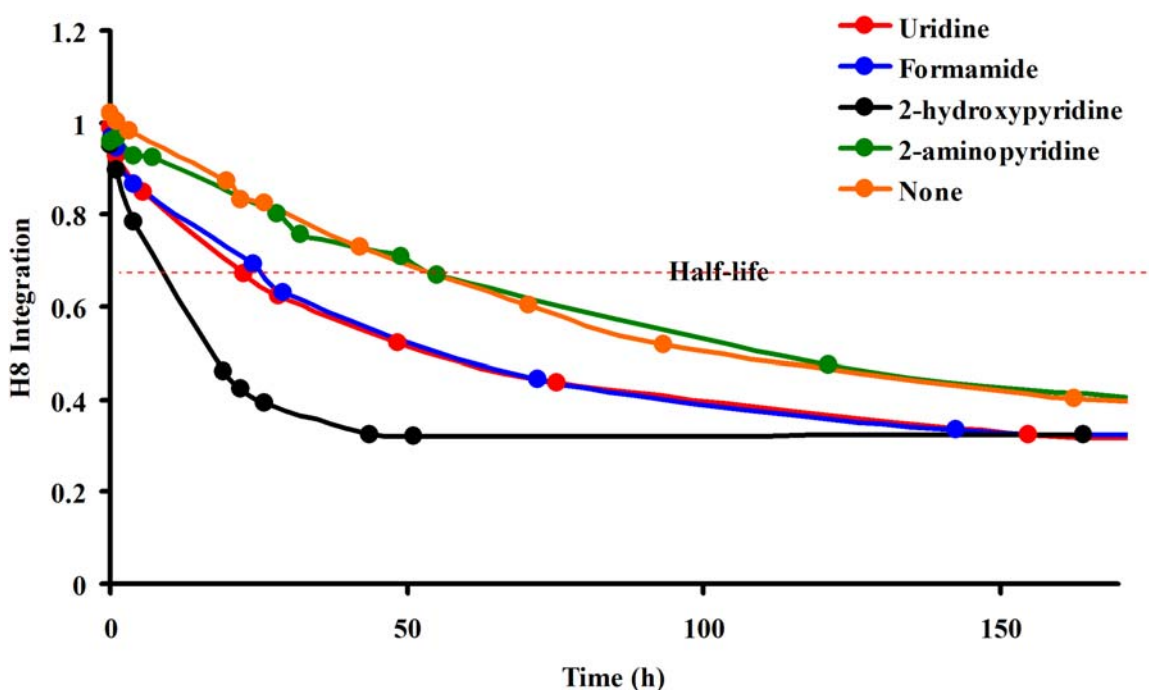


Figure 3.9. Reaction progress for the regioselective ligand exchange process with small molecule catalysts: **41-44**. [$G\ 8-h$]₁₆ • 2Ba²⁺ • 4DNP⁻ (0.39 mM), G **35-d** (6.2 mM), and small molecule (6.2 mM) at time intervals after mixing as a function of the outer H8 signal intensity. No significant decay in the H8 outer layer was observed for these experiments.

Half-lives of these exchange reactions were determined by the time it took the outer H8 signal intensity to reach 0.67, since the reaction was complete at an outer H8 signal intensity of 0.33. The outer H8 signal intensity was complete at 0.33 since 16 G

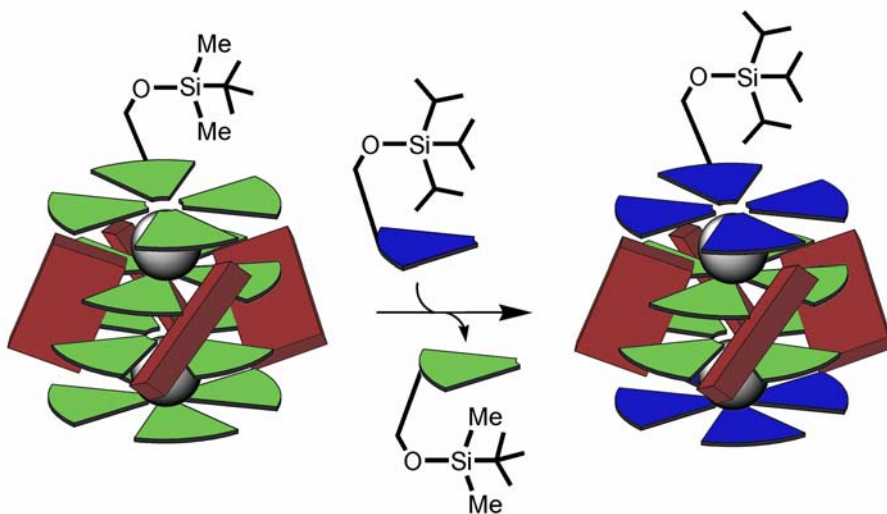
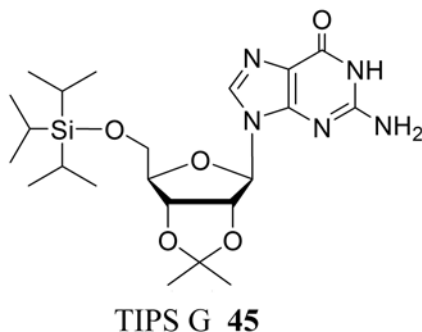
35-d were used to exchange into the outer layer that contains 8 G **8-h**. The calculated half-life of regioselective pseudo-exchange of G **35-d** into $[G \text{ 8-h}]_{16} \cdot 2Ba^{2+} \cdot 4DNP^-$ was 55 h. The half-life using 2-hydroxypyridine **42** was reduced to 9 h. This marked rate increase is most likely due to the complementary hydrogen bonding sites of the amide to the exposed hydrogen bonding sites of the guanosine in the G-quartet. Formamide **43** and uridine **44** had half-lives of 25 and 23 hours respectively. This catalyzed reaction showed no appreciable loss in regioselectivity (less than 5 %) with the exception of formamide (11 %). Addition of these compounds shows no noticeable 1H NMR peak shifts of the complex or monomer indicating that no new structures were formed.

These results indicate that the amide functionality weakens the hydrogen-bonding of the G-quadruplex's outer layers, allowing for an increase in the subunit exchange rate. Additionally, acidic protons may lead to loss in regioselectivity or decomposition of the G-quadruplex. Furthermore, these results show that the addition of uridine may weaken hydrogen bonds of the G-quartets through binding to the exposed face of the G-quartet, although there is evidence that nucleobases form additional hydrogen bonds to the G-quartet exposed face that stabilize RNA G-quadruplexes.²⁶⁹

3.3 Regioselective Exchange of Different Subunits.

After demonstrating the regioselective exchange of isotopically labeled subunits exchange of diverse subunits was performed (**Scheme 3.5**). A sterically bulkier substrate, 2',3'-O-isopropylidene-5'-triisopropylsilyl-guanosine (TIPS-G **45**), was used in this exchange process. The TIPS protecting group is widely used because it is bulkier than the TBS protecting group with a cone angle of 160° vs. 139° for TBS.²⁷⁰ Additionally, it

was hypothesized that the isopropyl groups on TIPS might interdigitate with each other, stabilizing the structure similar to that seen for leucine zipper proteins.²⁷¹



Scheme 3.5. Regioselective exchange of TIPS-G **45** into $[t\text{BDMS-G } \mathbf{8}]_{16} \cdot 2\text{Ba}^{2+} \cdot 4\text{DNP}^-$.

TIPS-G **3.9** was synthesized via routine modification of the ribose with triisopropylsilylchloride and gave a similar ^1H NMR as $t\text{BDMS-G } \mathbf{8}$ (**Figure 3.10**). Additionally, the formation of the TIPS G-quadruplex $[\text{TIPS-G } \mathbf{3.9}]_{16} \cdot 2\text{Ba}^{2+} \cdot 4\text{DNP}^-$ was achieved in a similar manner to that of the TBDMS G-quadruplex $[t\text{BDMS-G } \mathbf{8}]_{16} \cdot 2\text{Ba}^{2+} \cdot 4\text{DNP}^-$. The ^1H NMR spectra between $[t\text{BDMS-G } \mathbf{8}]_{16} \cdot 2\text{Ba}^{2+} \cdot 4\text{DNP}^-$ and $[t\text{BDMS-G } \mathbf{8}]_{16} \cdot 2\text{Ba}^{2+} \cdot 4\text{DNP}^-$ were essentially identical with the exception of the silyl

region (**Figure 3.11**). The G-quadruplex, $[t\text{BDMS-G } \mathbf{8}]_{16} \cdot 2\text{Ba}^{2+} \cdot 4\text{DNP}^-$, also showed slight upfield shifts of the inner H2'i and outer exocyclic N2H_{A0} protons and a downfield shift for the inner H3'i proton. Additionally, the inner H5'o protons were resolved in the TIPS-G **45** G-quadruplex indicating small structural changes in the inner G-quartet layers. The G-quadruplex ¹H NMR spectra were assigned by a series of COSY, NOESY, HMBC, and HSQC 2D NMR experiments, similar to those previously reported by the Davis group.^{56,58}

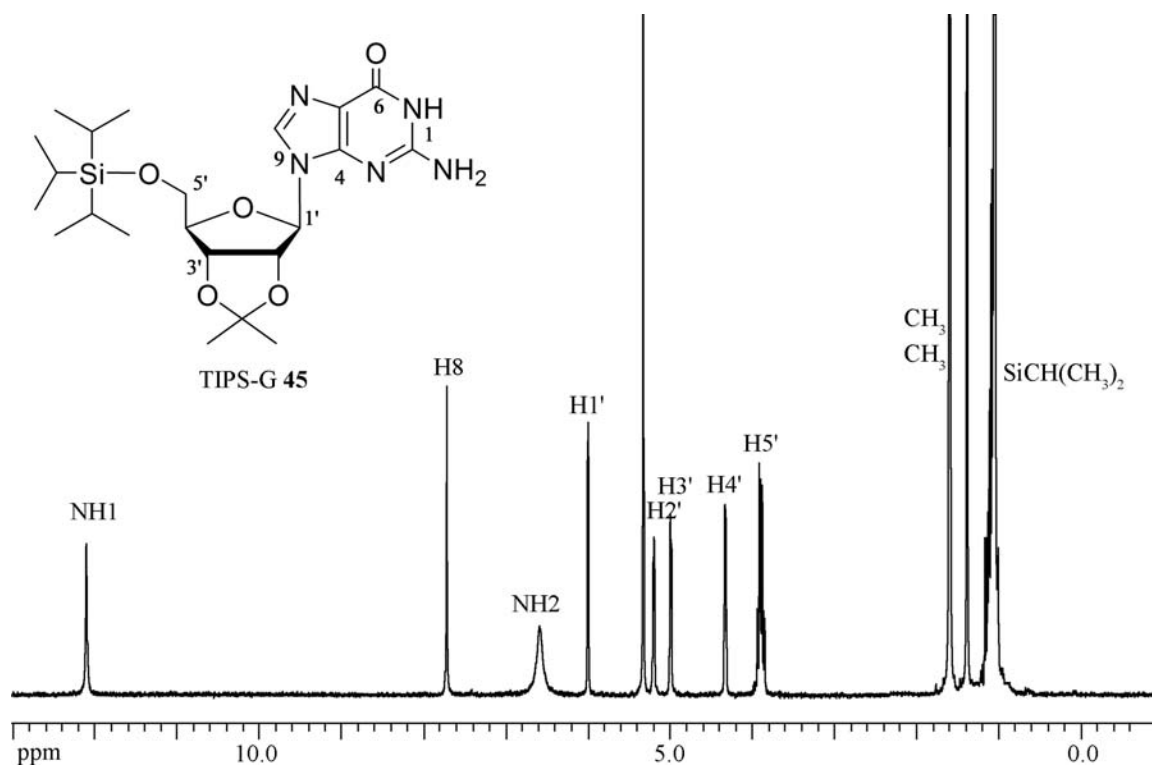


Figure 3.10. 400 MHz ¹H NMR spectrum of TIPS-G **45** in CD₂Cl₂ at rt.

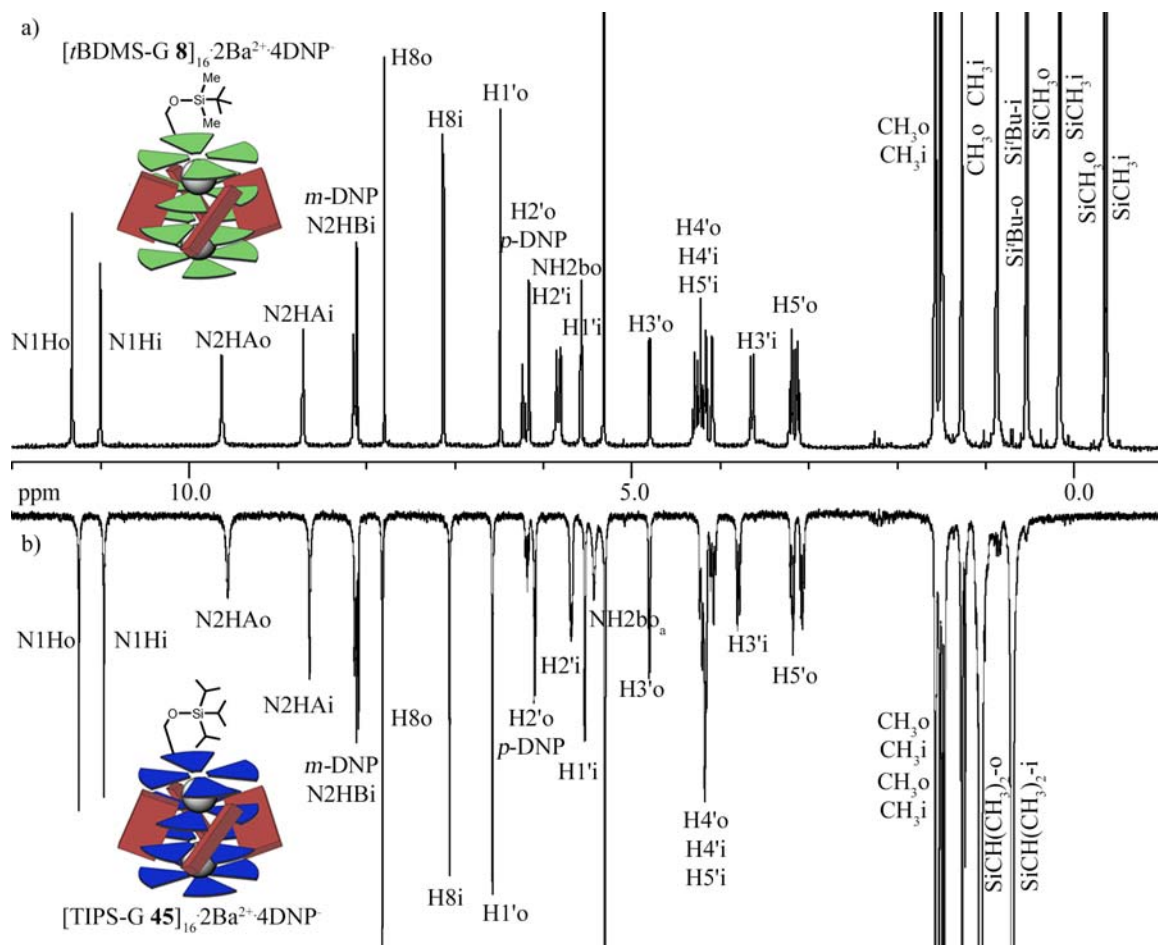


Figure 3.11. 400 MHz ^1H NMR spectrum in CD_2Cl_2 at rt of a) $[\text{tBDMS-G } \mathbf{8}]_{16} \cdot 2\text{Ba}^{2+} \cdot 4\text{DNP}^-$ and b) $[\text{TIPS-G } \mathbf{45}]_{16} \cdot 2\text{Ba}^{2+} \cdot 4\text{DNP}^-$.

The regioselective exchange of 16 equiv. of TIPS-G **45** into $[\text{tBDMS-G } \mathbf{8}]_{16} \cdot 2\text{Ba}^{2+} \cdot 4\text{DNP}^-$ in CD_2Cl_2 proved to behave similarly to the isotopically labeled experiments with incorporation only into the outer layer. The reaction progress was measured by tracking the integration of the SiCH_3 protons of *t*BDMS-G **8** (**Figure 3.12**). The reaction appeared to be complete in 12 h with about 80 % incorporation of TIPS-G **45** into the outer layer (**Figure 3.13**). This is a much higher ratio than the statistical ratio of 67 % incorporation indicating a preference for TIPS-G **45** to be on the outer layer of the mixed G-quadruplex over *t*BDMS-G **8**.

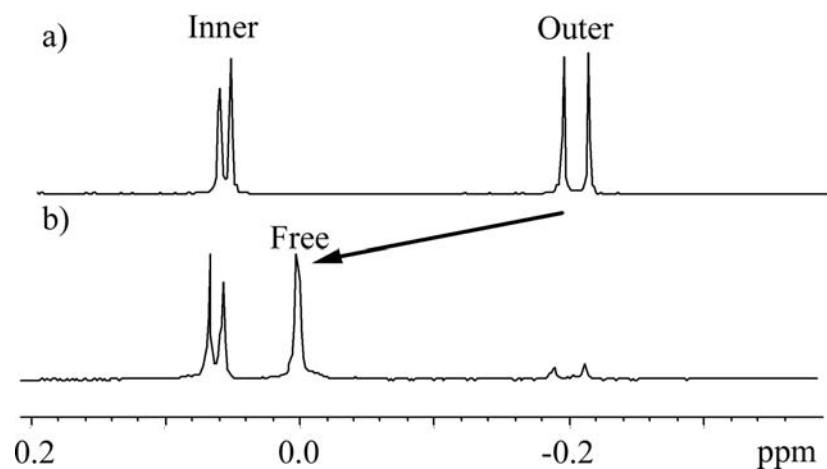


Figure 3.12. 400 MHz ¹H NMR integration of the SiCH₃ proton signals in exchange of 16 equiv of TIPS-G **45** (6.4 mM) with [*t*BDMS-G **8**]₁₆ • 2Ba²⁺ • 4DNP⁻ at rt in CD₂Cl₂.

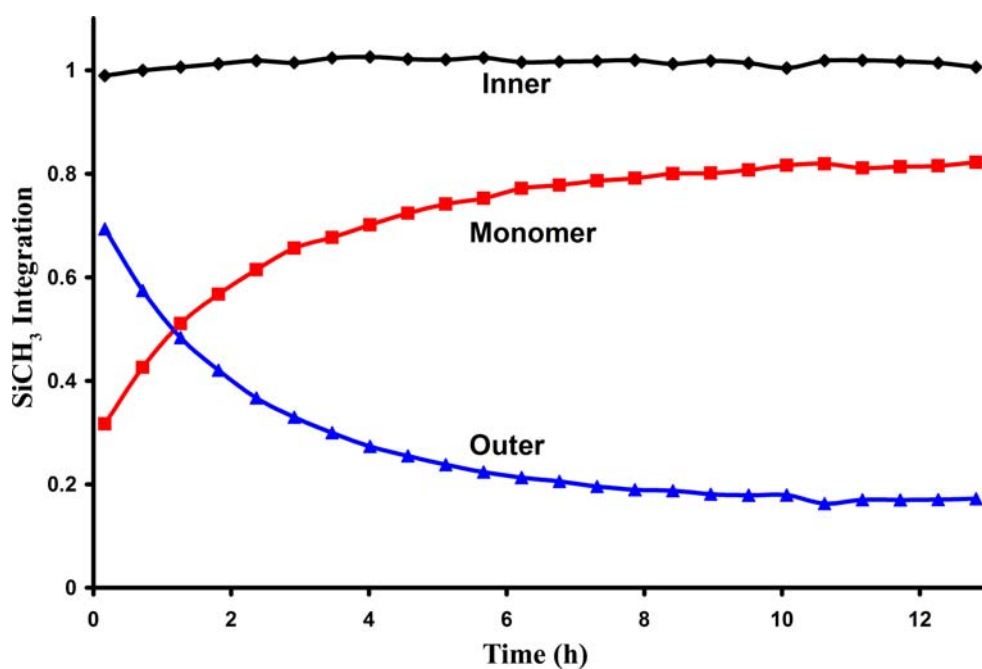


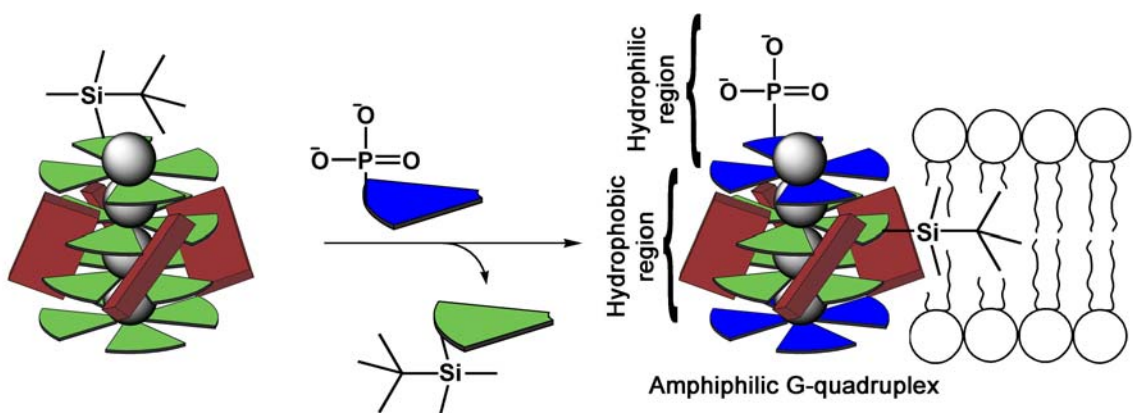
Figure 3.13. NMR integration of the SiCH₃ proton signals in exchange of 16 equiv of TIPS-G **45** (6.4 mM) with [*t*BDMS-G **8**]₁₆ • 2Ba²⁺ • 4DNP⁻ at rt in CD₂Cl₂.

Control experiments where 50-50 % *t*BDMS-G **8** to TIPS-G **45** were stirred with Ba(DNP)₂ in CD₂Cl₂ led to results where the *t*BDMS-G **8** was primarily in the inner

layer, while TIPS-G **45** was primarily in the outer layer. Indeed, the ratio of inner to outer layers for *t*BDMS-G **8** was 67 % inner and 33 % outer layer.²⁷²

3.3.1 Amphiphilic G-Quadruplex Formation

Amphiphilic G-quadruplexes are of great interest because they would help align and embed these structures inside of phospholipid membranes. This alignment of the G-quadruplex would help facilitate an ion flow across the phospholipid membrane. Unfortunately, the manipulation of G-quadruplexes to form amphiphilic G-quadruplexes such as that shown in **Scheme 3.6** were unsuccessful. Failures to exchange in hydrophilic ligands, such as 5'-GMP or guanosine, into the outer layers were coupled by the poor solubility of these ligands, destruction of the G-quadruplex and formation of nonordered structures. Additionally, little or no regioselective ligand exchange was observed under various solvent conditions.



Scheme 3.6. Proposed synthesis of amphiphilic G-quadruplexes through ligand exchange.

3.4 Conclusion

In conclusion, these studies show that regioselective ligand exchange can be controlled by both the cation and anion that help stabilize the noncovalent structure. By kinetically stabilizing the assembly via stronger ion-ligand interactions, certain regions of this hydrogen-bonded assembly are made resistant to the subsequent subunit exchange reaction. From a synthetic perspective, these experiments demonstrate that noncovalent interactions can be used to stabilize specific regions of large assemblies, allowing for subsequent substitution reactions at other locations to be precisely controlled. This proof of principle was demonstrated using isotopically labeled subunits. More specifically, G-quadruplexes with monovalent cations and strong binding anions allow for optimal regioselectivity in this exchange process. This process can be catalyzed by the addition of small molecules that can bind to the outer edge of the G-quadruplex. However, regioselectively incorporating diverse functionality into these hydrogen bonded structures depends on the stability of individual subunits to form stable noncovalent structures. If the G-quadruplex that is formed from its ligands is unstable, the ligand exchange process occurs into both the inner and outer layers indiscriminately. With optimal choice of ligands, subunit exchange can be accomplished in these systems. However, none of these G-quadruplex structures were stable inside of phospholipid membranes, leading to the assumption that a covalent unimolecular G-quadruplex was essential to remain intact inside of phospholipid membranes.

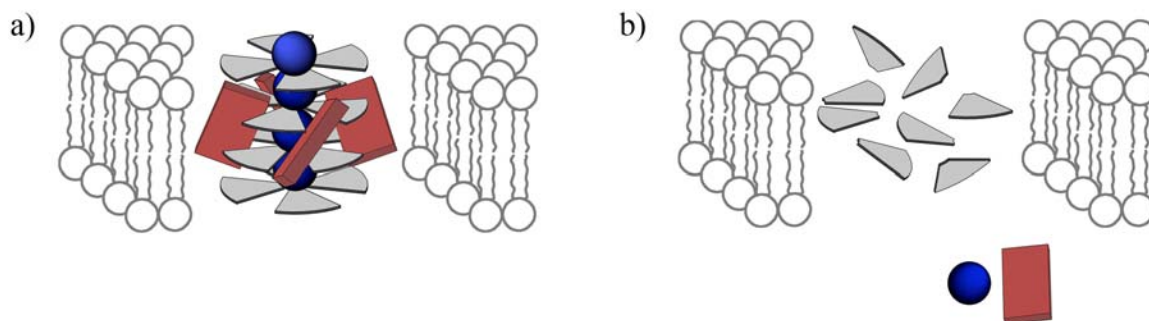
Chapter 4. Covalent Capture Leads To Synthetic Na⁺ Transmembrane Transporters.

The majority of this chapter has been published in references 273 and 274:

- Kaucher, M. S.; Harrell, W. A.; Davis, J. T. "A Unimolecular G-quadruplex that Functions as a Synthetic Transmembrane Na⁺ Transporter." *J. Am. Chem. Soc.* **2006**, *128*, 38-39.
- Kaucher, M. S.; Davis, J. T. "N2, C8-Disubstituted Guanosine Derivatives Can Form G-Quartets" *Tett. Lett.*, **2006**, *47*, 6381-6384.

4.1 Introduction

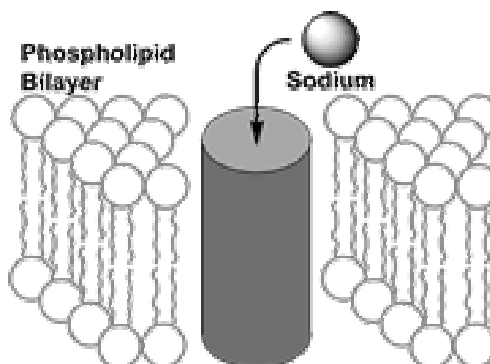
The initial goal of the research in this chapter was to prepare synthetic cation channels through the covalent capture of lipophilic G-quadruplexes. Despite the thermodynamic stability of non-covalent lipophilic G-quadruplexes ($[G\ \mathbf{8}]_{16} \cdot 4K^+ \cdot 4Pic^-$), individual guanosine subunits are in dynamic equilibrium between "monomer" and hexadecamer when lipophilic G-quadruplexes are dissolved in solution.¹²¹ Furthermore, attempts to incorporate non-covalent lipophilic G-quadruplexes ($[G\ \mathbf{8}]_{16} \cdot 4K^+ \cdot 4Pic^-$) into phospholipid membranes showed little promise, since the G-quadruplex presumably falls apart into monomers under these polar solvent conditions (**Scheme 4.1**). To circumvent problems posed by such kinetic instability, post modification of the preassembled G-quadruplex through covalent bonds was employed. It was reasoned that such post-assembly modification might provide a unimolecular G-quadruplex that would be kinetically stable and functional within hydrophobic phospholipid membranes.



Scheme 4.1. Lipophilic G-quadruplex incorporated into a phospholipid bilayer in a) idealized and b) proposed conditions. Noncovalent lipophilic G-quadruplexes do not preserve their structure in the demanding conditions of phospholipid bilayers in aqueous solutions.

4.1.1 The G-quartet Motif as a Scaffold for Transmembrane Transporters.

We,^{53,268} and others,^{111,112,275} have proposed that the G-quartet may well serve as a scaffold for building synthetic transmembrane ion channels (**Scheme 4.2**). Synthetic ion channels are open pores where inorganic compounds can move across the membrane, while synthetic pores are defined as pores where organic compounds can move across the membrane.¹² Furthermore, carriers are defined as compounds that can ferry other molecules across the transmembrane,²⁷⁶ so these carriers are constantly moving across the transmembrane unlike pores and channels, which are stationary. The design of synthetic pores, channels and transmembrane transporters has been of particular interest because they may provide new ion sensors, catalysts and anti-microbial agents.¹²



Scheme 4.2. Schematic of a sodium ion channel embedded in a phospholipid bilayer.

The G-quartet has been proposed as a scaffold for building synthetic ion channels because it is cyclic in nature, and cations can bind to the central cavity (**Figure 4.1a**). Additionally, G-quartets stack to form channel like structures, where the cations align in the middle of the tubular structure (**Figure 4.1b**).⁵³ This structure is reminiscent of the crystal structure of the potassium channel from *Streptomyces lividans* solved by the MacKinnon group.²⁷⁷

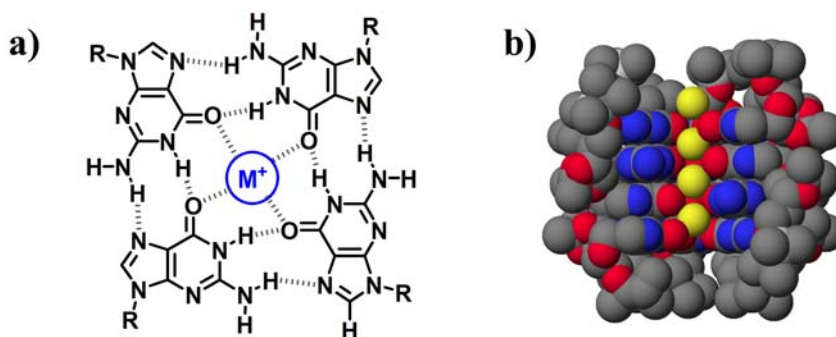


Figure 4.1. a) G-quartet and b) Crystal structure of lipophilic G-quadruplex $[G]_{16} \cdot 4K^+$ with its front partially stripped away for clarity.⁵³ The yellow spheres correspond to the cations that align the central region of the G-quadruplex.

Additionally, work done in the Feigon group showed that cations flow through DNA G-quadruplexes.²⁵² Feigon studied the DNA Oxy-1.5 bimolecular quadruplex complexed with ¹⁵N labeled NH₄⁺, using ¹⁵N heteronuclear NMR spectroscopy. These experiments identified three bound NH₄⁺ in the G-quadruplex: two symmetric NH₄⁺ in the outer binding sites and one central NH₄⁺ (**Figure 4.2**). Additionally, it was shown that these NH₄⁺ cations flowed through the central axis. The outer NH₄⁺ in **Figure 4.2** was in exchange with bulk NH₄⁺ and the central NH₄⁺, while the central NH₄⁺ was in exchange with only the outer NH₄⁺.

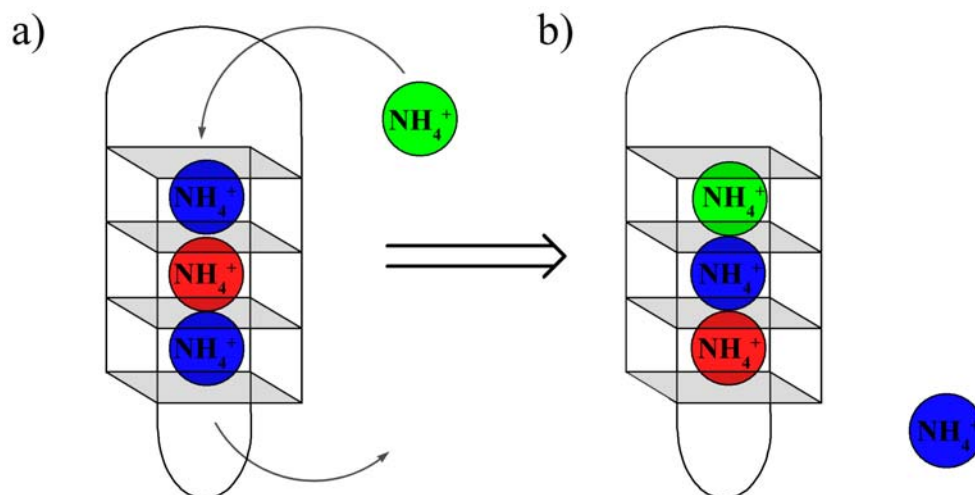


Figure 4.2. Representation of the a) Oxy-1.5 bimolecular quadruplex with bound NH_4^+ . The blue and red spheres represent outer and inner NH_4^+ respectively, while the green spheres represent solvated NH_4^+ . The gray squares represent G-quartets and the lines represent the DNA backbone. b) Solvated NH_4^+ replaces the outer NH_4^+ causing a flow mechanism of the cations through the G-quadruplexes.²⁵²

Matile and coworkers attempted to build synthetic ion channels based on the guanine base.²⁷⁵ This was the first attempt to utilize the G-quartet structure as a synthetic ion channel. Initial attempts focused on attaching guanine onto rigid rod structures (Figure 4.3a). The Matile group had previously shown that rigid rod structures **46** with appended peptides showed the ability to act as channels and pores.^{216,278} Matile proposed that rigid rod structures with appended guanine units would self-assemble in phospholipid membranes and transport cations. The control guanine dimers, **G 47**, showed poor solubility even with the attachment of long alkyl chains to the N2 position (**G 48**) (Figure 4.3b). The solubility was independent on the alkyl chain, and the solubility of these guanine dimers were roughly 500-times lower than that of the lipophilic guanosine monomers. The assumption was that the ribose unit is critical to form soluble lipophilic G-quartets.²⁷⁵

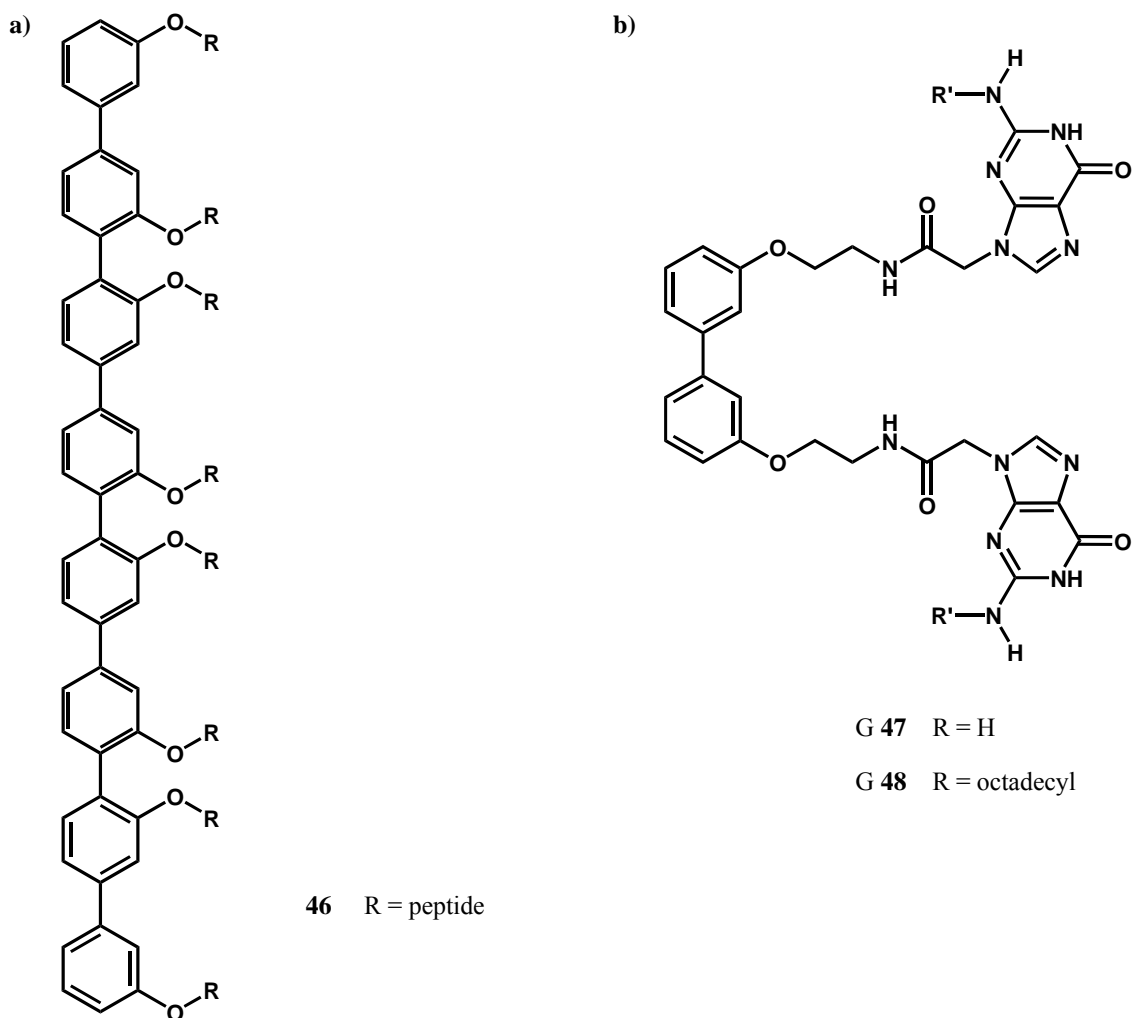


Figure 4.3. a) Rigid rod motif. b) Guanine dimer.²⁷⁵

Initial attempts to utilize G-quartets as a motif to build synthetic ion channels by the Davis group utilized a calixarene scaffold as a covalent linker to form G-quartets (**Figure 4.4**).⁶² This scaffold, a 1,3-*alternative-calix*[4]arene, was hypothesized to hold four guanosine units, two in each direction, to form nanotubular structures.²⁶⁸ Substituted 1,3-*alternative-calix*[4]arenes were previously shown to transport ions across membranes.²⁷⁹ The cG **11** derivative formed both dimeric structures⁶² and nanotubes²⁶⁸ through the formation of G-quartets depending on the conditions. This dimeric structure was comprised of distinct anion and cation binding sites. While more experiments are

needed to prove if this structure indeed transports cations, the lengthy synthesis, 12 overall steps, of cG **11** remains a daunting task for this compound ever to be used as a scaffold to construct derivatives to function as synthetic ion channels.^{62,268}

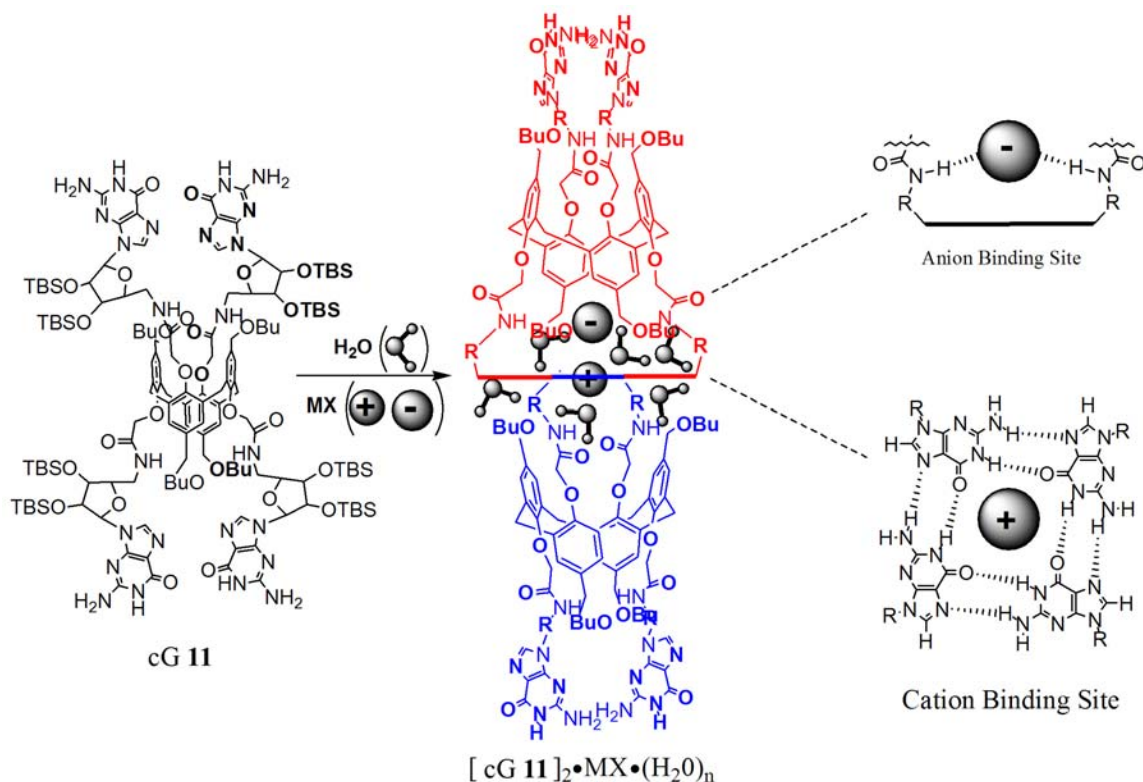


Figure 4.4. Structure, dimer, and binding sites of cG **11**.⁶²

More recently, after the publishing of the findings in this chapter, the Matile and Kato groups reported a synthetic ion channel formed by the self-association of lipophilic folate dendrimers (**Figure 4.5**).²⁸⁰ Folic acid, similar in structure to the guanine base, forms folic acid tetramers that resemble G-quartets. This report showed that the hydrogen-bonded rosette structures, $(\mathbf{49})_4$, could function as K^+ channels in planar bilayers.^{279,281-286} Although self-assembly in membranes has recently been reported,²⁸⁷ there have been very few other examples of hydrogen bonded assemblies that form stable structures in bilayer membranes.

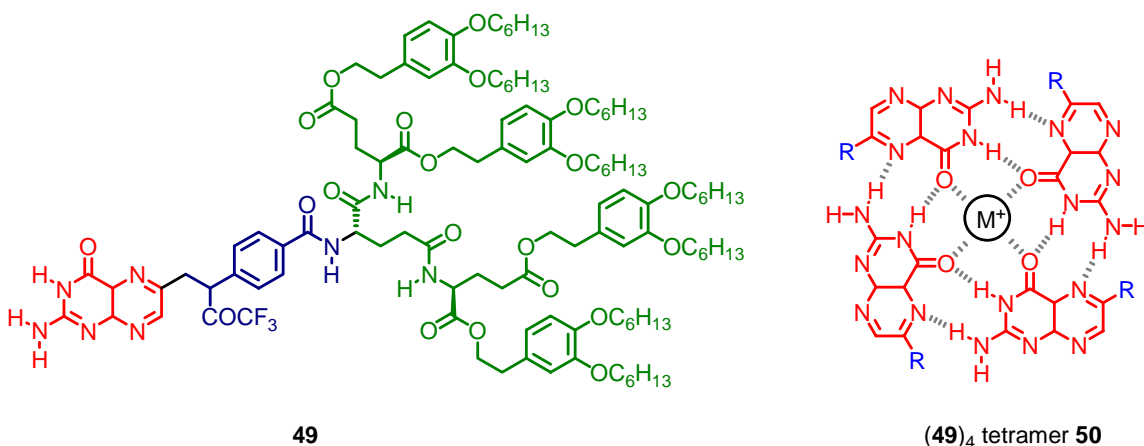


Figure 4.5. Folate derivative **49** and tetramer **50** of the folate dendrimers.

Finally, the Armitage and Balasubramanian groups have been independently working on lipophilic guanosine structures with covalent backbones. Both groups are exploiting peptide nucleic acids (PNA) as nonpolar backbones. These backbones, unlike DNA backbones, are uncharged and nonpolar. Work is ongoing in these groups to produce PNA G-quadruplex structures that might function as synthetic ion channels.^{111,112}

4.2 Covalent Capture Strategies.

As mentioned before, post-assembly modification through covalent capture of hydrogen-bonded assemblies was proposed to help stabilize the G-quadruplex in phospholipid bilayers. Covalent capture strategies have been successfully applied to various hydrogen bonded assemblies. This strategy is analogous to templated synthesis,^{288,289} such as the formation of crown ethers.²⁹⁰

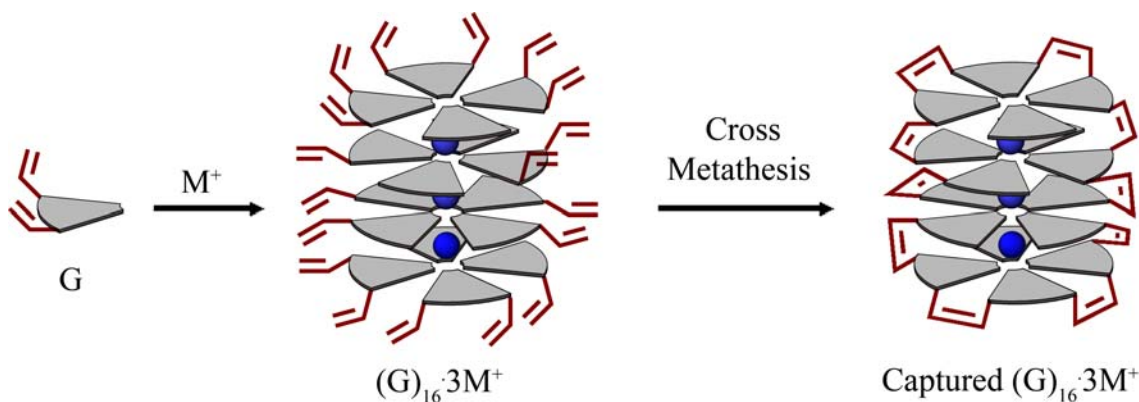
Ghadiri coined the term “covalent capture” to describe the post-modification of self-assembled structures so as to covalently lock the systems. Ghadiri showed that

functionalized cyclic peptides formed nanotubes and dimers.^{291,292} Self-assembly of these cyclic peptides, followed by covalent capture by either olefin metathesis or disulfide bond formation trapped this assembly to give a single, stable structure.^{238,293} The Reinhoudt group also employed this technique for the capture of hydrogen bonded assemblies comprised of three calixarene units held together by 144 hydrogen bonds.²⁹⁴ A 123 membered macrocycle was formed through ring closing metathesis (RCM).²⁹⁵

This covalent capture technique has also been the general strategy to synthesize catenanes and rotaxanes.^{296,297} Catenanes, interlocked rings, would almost statistically never occur without this technique.²⁹⁸ Similarly, rotaxanes, dumbbells interlocked with rings, are also synthesized using this technique.²⁹⁹

4.2.1 Covalent Capture of Self-Assembled G-quadruplexes.

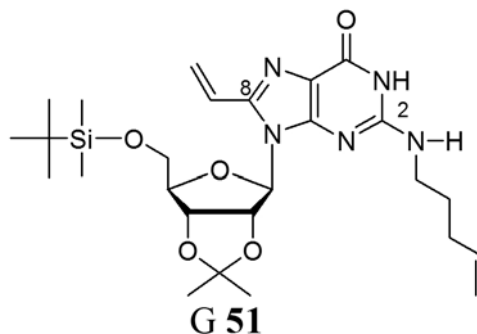
The general strategy for the covalent capture of self-assembled G-quadruplexes is shown in **Scheme 4.3**. Guanosine with appended olefin units, or other reactive groups, could be used to preassemble the G-quadruplex through the addition of M^+ . This G-quadruplex precursor could then be captured through olefin metathesis.



Scheme 4.3. Schematic of the covalent capture of lipophilic G-quadruplexes.

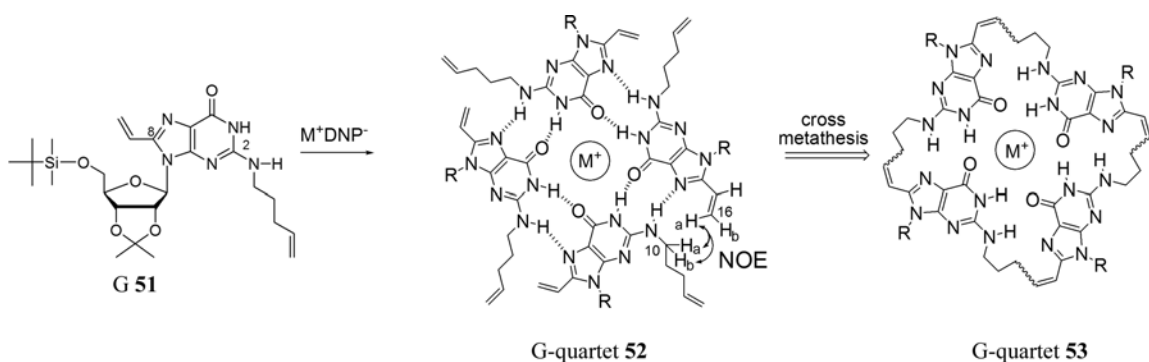
4.3 Attempts to Covalently Capture a G-quartet.

Modification of the guanine building block has typically been on the sugar unit or on the nucleobase's N9 position.²⁷³ Recent studies have described G-quadruplexes made from G derivatives substituted at their N2 or C8 positions.^{61,64,300-303} In some cases, the N2 or C8 substituents stabilized the G-quadruplex relative to the unmodified derivative.^{64,301,302} As outlined in **Scheme 4.3**, it was reasoned that modification at both N2 and C8 (**G 51**) would lead to a G-quartet that might then be cross-linked to give a “covalent” macrocycle.^{238,295,304}



As outlined in **Scheme 4.4**, the aim was to use olefin metathesis to cross-link N2, C8-disubstituted G units within an individual G-quartet **52**. A “covalent” G-quartet such as **53** should be stable and functional in water. The cation binding properties of a

“covalent” G-quartet such as **53** could be different relative to its hydrogen-bonded precursor G **51**. In this section, two key steps are described in achieving the goal of preparing a “covalent” G-quartet **53**; 1) synthesis of N2, C8-disubstituted G **51** and 2) cation-templated formation of an assembly, $[G \text{ 51}]_8 \cdot Ba^{+2} \cdot 2DNP^-$ containing hydrogen bonded G-quartets. This is the first example, to the author’s knowledge, of a G-quartet functionalized at both its N2 and C8 positions. It should also be noted that Wu and colleagues reported the first lipophilic G-quadruplex formation of N2 substituted guanosine during the publication of this work.³⁰⁵



Scheme 4.4. Design scheme for covalent capture of G **51** through formation of G-quartet **52** and cross metathesis to yield G-quartet **53**. NOEs between H16a and H10 for G-quartet **52** are shown, see text for details.

Crystal structures of the G **51** derivative, 2',3'-O-isopropylidene-5'-*t*-butyldimethylsilyl-guanosine, showed that the C8 and N2 protons are 3.76 Å apart. Molecular models using showed that a five alkyl carbon chain would give a good fit with the crystal structure (**Figure 4.6**). Molecular modeling was performed via HyperChem 7.5 for Windows, from Hypercube, Inc., with the Amber 99 force field.

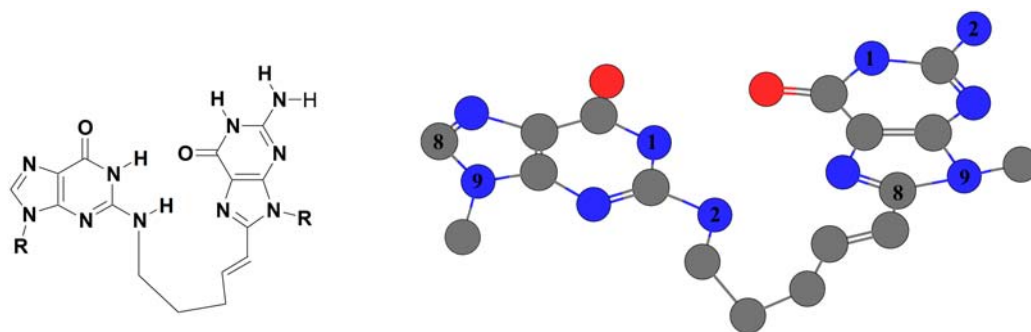
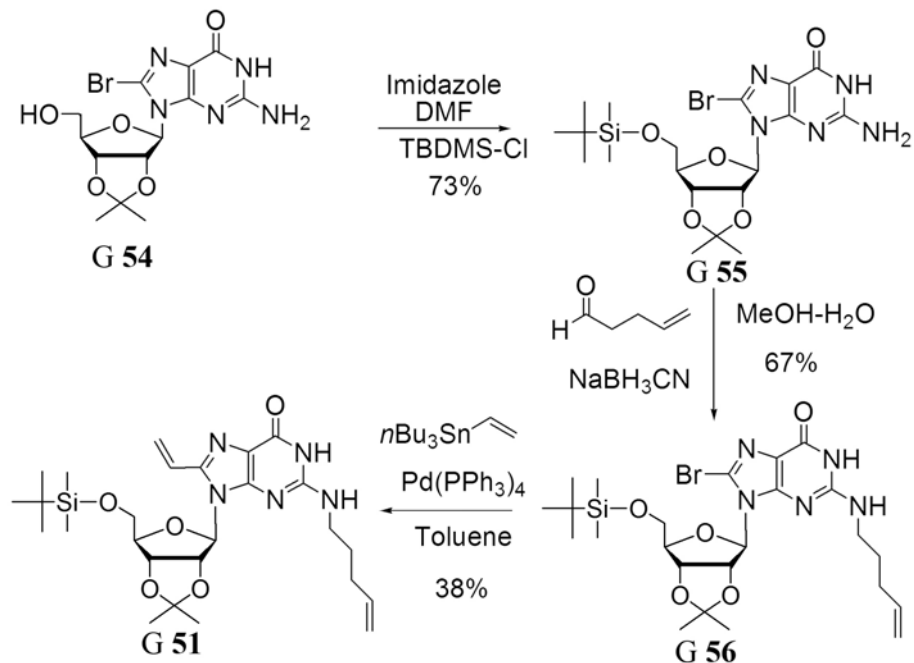


Figure 4.6. Dimer of a C8 substituted guanine unit with an N2 substituted guanine unit.

The necessary precursor **G 51** was synthesized in 4 steps from 8-bromo-2',3'-isopropylidene **G 54** (**Scheme 4.5**).³⁰⁶ The 5'-OH of **G 54** was first protected with a *t*-BDMS group (**G 4.10**). Reductive amination of 4-pentenal with the N2 amine of **G 55** gave **G 56**, and introduced the first alkene unit into the nucleobase.³⁰⁷ The second alkene group was added to the C8 position via Stille coupling; cross-coupling of **G 56** with vinyl-tri-*n*-butyltin afforded the target compound **G 51**.⁶¹ The ¹H NMR spectrum was similar to its nondialkenyl analogue (2',3'-O-isopropylidene-5'-*t*-butyldimethylsilyl-guanosine), with the addition of the alkene chains on the N2 and C8 positions (**Figure 4.7**).



Scheme 4.5. Synthesis of N₂, C₈-disubstituted G **51**.

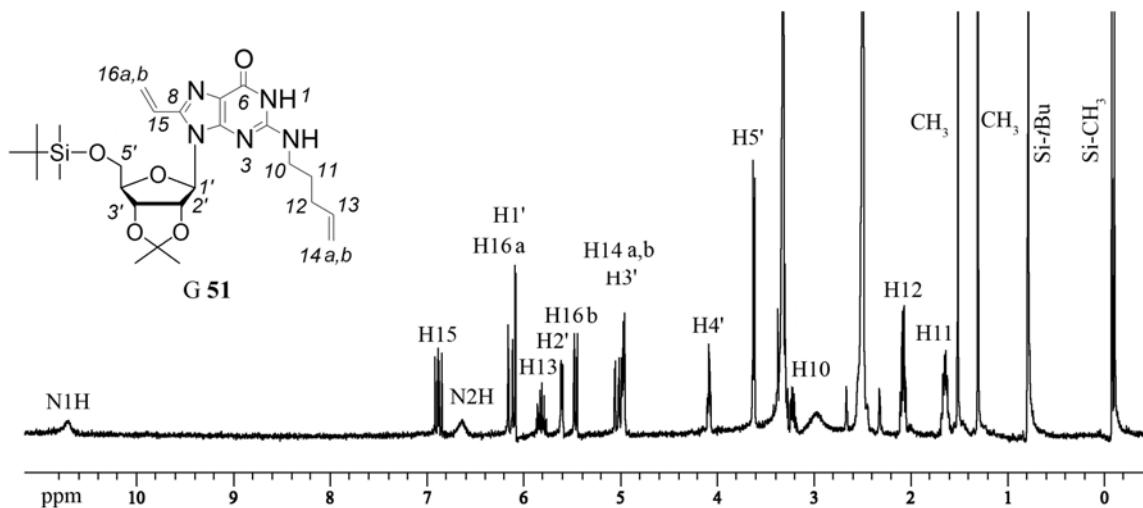


Figure 4.7. The ¹H NMR spectrum of G **51** in DMSO-d₆.

Next, G **51** was shown to form stable G-quartets. The N₂, C₈-disubstituted G **51** extracted Ba(DNP)₂ and K(DNP) salts from water into CDCl₃, as determined by NMR, ESI-MS and UV-vis data. Integration of ¹H NMR signals indicated formation of an octamer with formula [G **51**]₈ • Ba⁺² • 2DNP.^{52,308,309} NMR spectra also showed that the

N2 amino proton in $[G \mathbf{51}]_8 \cdot Ba^{+2} \cdot 2DNP^-$ moved far downfield relative to uncomplexed $G \mathbf{51}$ ($\Delta\delta = 3.40$ ppm), consistent with its involvement in a hydrogen bond (**Figure 4.8b**). Stronger support for a G-quartet came from NOEs between the C10 hydrogens and the C16a olefinic hydrogen (**Figure 4.8c**). These C10-C16a NOEs are a firm indication of a G-quartet since the C10 substituent (on the N2 sidechain) and C16 (attached to C8) are too far apart for intramolecular NOEs. These NOEs can only arise from intermolecular interactions; models show that H10 and H16 are within 3-5 Å in a G-quartet. NOEs between N2H and a C16 hydrogen were also consistent with G-quartet formation by $G \mathbf{51}$.⁶⁰

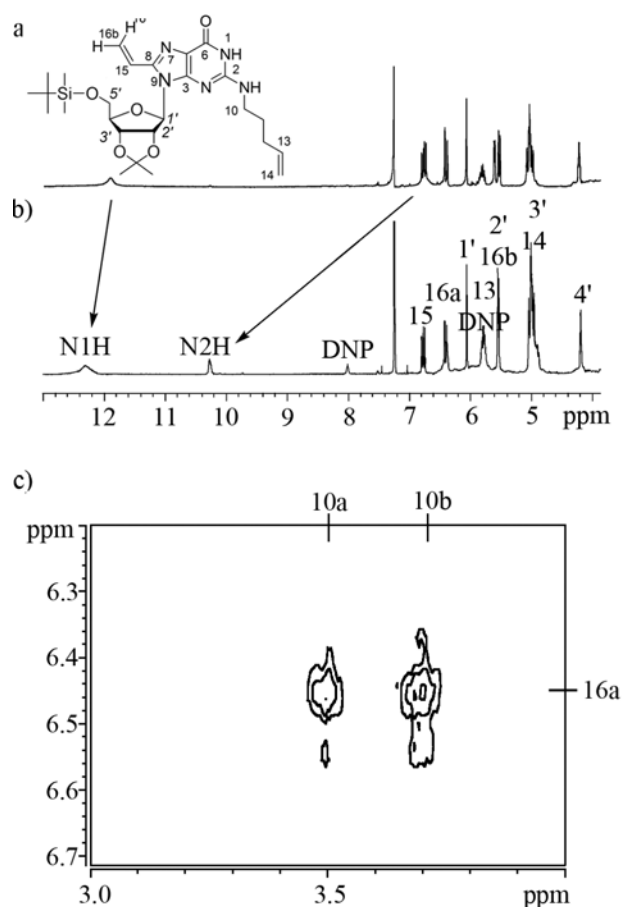


Figure 4.8. a) 1H NMR spectrum of $G \mathbf{51}$ in $CDCl_3$, b) after extraction of $Ba(DNP)_2$ from water into $CDCl_3$ and c) selected region of 2D NOESY spectrum of sample from b) showing NOEs between H 10 to H16a.

The size of the complex formed by G **51** and Ba⁺² was assessed by diffusion NMR.¹⁵¹ Pulse field gradient (PFG) experiments revealed that the complex generated by salt extraction with G **51** had a diffusion coefficient (D_s) of 6.36×10^{-10} m²/s, a value much lower than that for the internal standard, monomeric 5'-*t*-BDMS-2', 3'-isopropylidene adenosine A **23** ($D_s = 13.3 \times 10^{-10}$ m²/s). The ratio of these 2 diffusion coefficients confirmed formation of octamer [G **51**]₈ • Ba⁺².¹²¹ Mass spectrometric analysis of the complex showed a major peak ($m/z = 2195.6$) for [(G **51**)₈ • Ba]⁺² (**Figure 4.9**). The signal for [(G **51**)₄ • Na]⁺ ($m/z = 2149.2$) is likely due to cation exchange during sample preparation and analysis. In marked contrast, ESI-MS analysis of uncomplexed G **51** showed only peaks for the molecular ion [G **51** + H]⁺ and for a dimer [(G **51**)₂ + H]⁺. The NMR and MS data all indicate that the N2, C8 disubstituted G **51** can form stable G-quartets in the presence of a cation template.

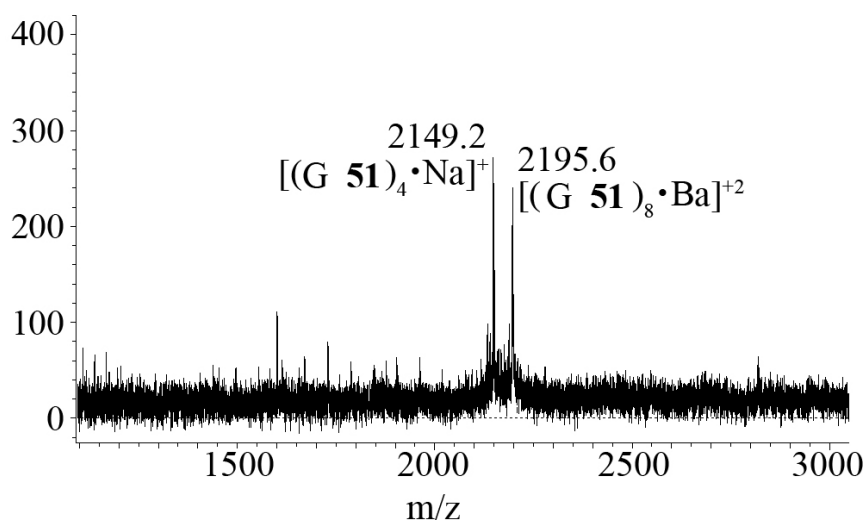
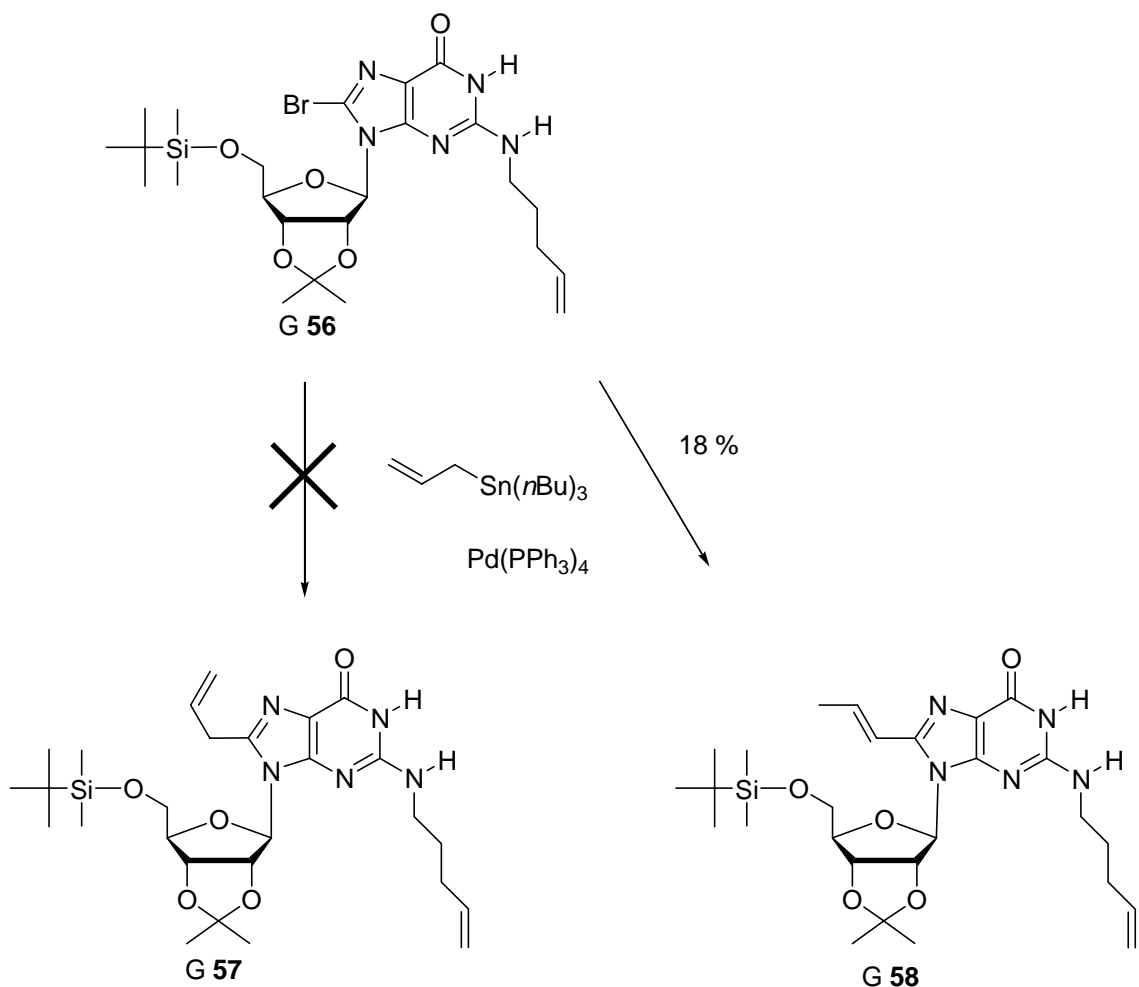


Figure 4.9. ESI-MS of [G **51**]₈ • Ba⁺² • 2DNP⁻ formed by liquid-solid extraction of Ba(DNP)₂ with G **51** in CHCl₃.

Having demonstrated formation of octamer $[(G \mathbf{51})_8 \cdot Ba]^{+2}$ attention was focused on covalently linking neighbors within an individual G-quartet. Attempts to effect olefin cross metathesis on $[(G \mathbf{51})_8 \cdot Ba]^{+2}$, using either Grubb's 1st or 2nd generation catalysts, have so far been unsuccessful.³¹⁰ This lack of cross metathesis for $[(G \mathbf{51})_8 \cdot Ba]^{+2}$ may be due to a) an improper relative orientation for the N2 and C8 alkene groups within G-quartet 3 or b) the fact that the C8 vinyl group on the purine may be too electron deficient.³¹¹ Another issue that should be considered, even when metathesis conditions are defined for this system, is that these G_8 octamers are formed by π -stacked quartets, which creates the potential to generate cross-links between G-quartet layers. Such cross-links would preclude the goal to generate an isolated covalently linked G-quartet.

In attempting to alleviate the problem of the electron deficiency of the C8 vinyl group, G **57** was chosen as a target by extending the olefin on the C8 position of the guanosine. It was reasoned that this allyl-G **57** would alleviate some of these geometric and electronic problems. The procedure for the attempted synthesis of G **57** was similar to the procedure of G **51** with the exception of using allyltributyltin in the Stille coupling. Unfortunately, the only product observed was the *trans*-alkene G **58**, while no G **57** was observed (**Scheme 4.6**).



Scheme 4.6. Stille coupling of G **56** to yield G **58** through isomerization of the allylic bond.

The ^1H NMR clearly showed the formation of G **58** through this method. The presence of the CH_3 group, as well as only two olefinic protons was clear evidence of the isomerization of the C8 allylic group. Furthermore, the ^3J coupling constant of the H15/H16 proton indicated that the double bond was *trans* (**Figure 4.10**). This isomerization is most likely due to the formation of the extended conjugated system. Similar to G **51**, G **58** formed G-quartets but did not undergo olefin metathesis.

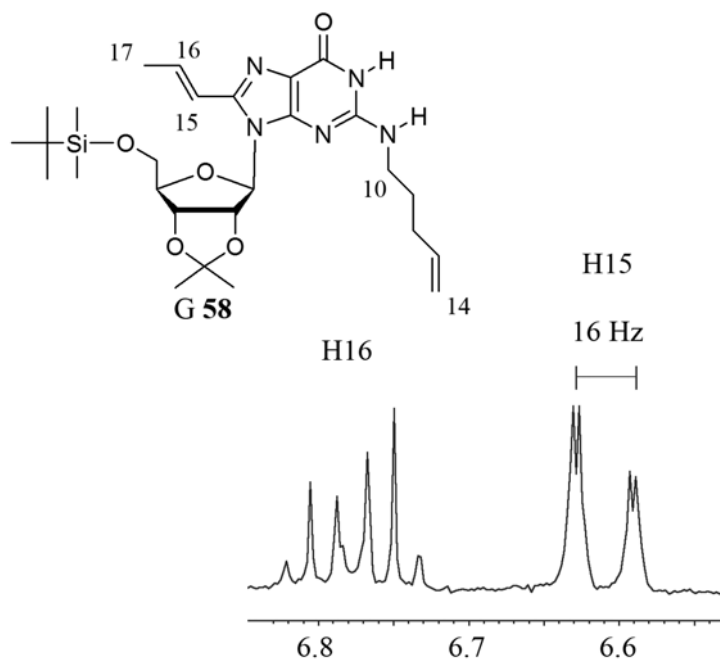


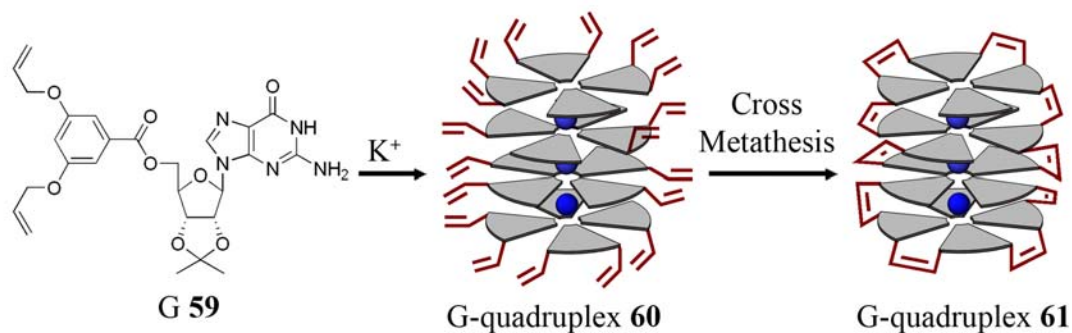
Figure 4.10. Selected ^1H NMR region of **G 58** showing that H16 and H15 that are trans to each other.

In conclusion, a synthetic route to prepare G analogs substituted at both N2 and C8 positions is reported. Importantly, the N2, C8 disubstituted **G 51** forms stable G-quartets in the presence of templating cations. The next challenge will be to identify G analogs and crosslinking strategy (olefin metathesis, disulfide or hydrazone bonds) that will enable covalent capture of an individual G-quartet.

4.4 Covalent Capture Yields a Unimolecular G-Quadruplex.

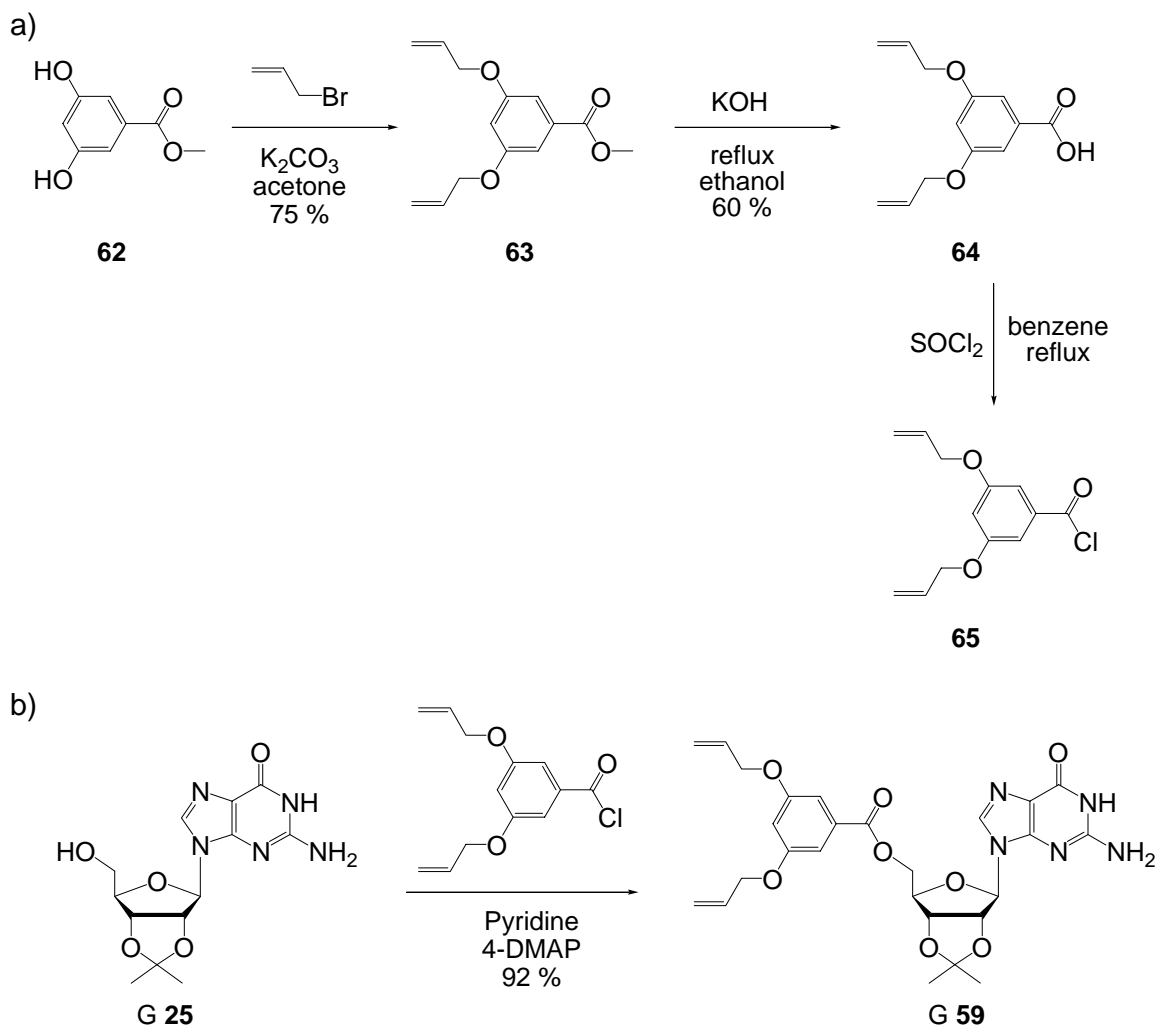
Covalent capture of the lipophilic G-quadruplex was ultimately successful with alkene groups located on the periphery of the G-quadruplex (**Scheme 4.7**).²⁷⁴ This strategy utilized 5'-(3,5-bis(allyloxy)benzoyl)-2',3'-isopropylidene **G 59** to build lipophilic G-quadruplexes. After preassembling G-quadruplex **60**, cross metathesis formed unimolecular G-quadruplex **61**. **G 59** was outfitted with two meta-substituted

allyl ethers, with the notion that such a pattern would allow for olefin metathesis both within an individual G-quartet and between layers. Also, the 3,5-diallyl ethers would be unlikely to undergo intramolecular cyclization to give a strained cyclophane.



Scheme 4.7. Schematic showing G **59** (gray wedges) extracting K^+ (blue spheres) to form G-quadruplex **60**. Following G-quadruplex formation, cross metathesis yields unimolecular G-quadruplex **61**.

The precursor, 5'-(3,5-bis(allyloxy)benzoyl)-2',3'-isopropylidene G **59** was prepared in two steps from guanosine (**Scheme 4.8b**). The acid chloride, **4.20**, was synthesized in three steps from the corresponding methyl-3,5-dihydroxy benzoate **4.17**. Alkylation, followed by hydrolysis of the ester bond gave the corresponding acid **4.19**.³¹² Refluxing the benzoic acid **4.19** with thionyl chloride yielded the desired acid chloride **4.20** (**Scheme 4.8a**). Routine isopropylidene protection, followed by acylation with 3,5-diallyloxybenzoic acid chloride (**4.20**) yielded G **59** (**Figure 4.11**).



Scheme 4.8. Synthesis of G 59.

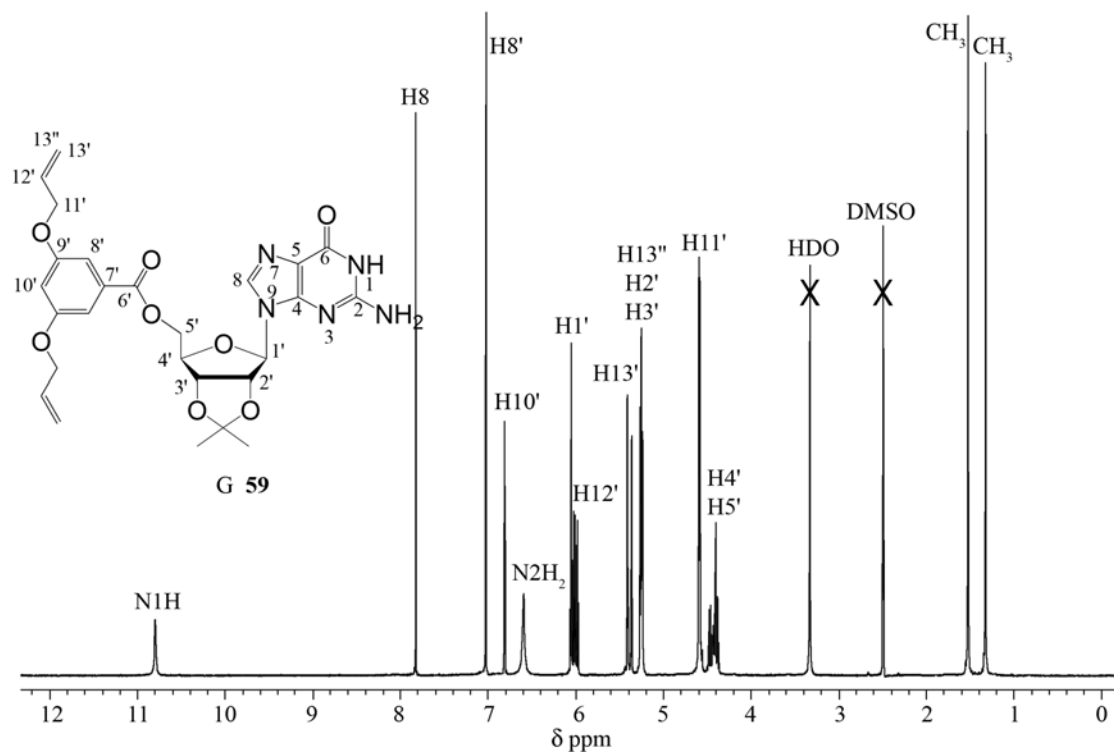


Figure 4.11. The ^1H NMR spectrum of G **59** at 400 MHz in DMSO- d_6 .

4.4.1 Formation of Noncovalent G-quadruplex Formation **60**

Solid-liquid extraction of potassium 2,6-dinitrophenolate (K^+DNP^-) by G **59** in CH_2Cl_2 gave quantitative formation of the G-quadruplex **60** as determined by CD and NMR spectroscopy. G-quadruplex **60** had the characteristic positive CD band, centered at 280 nm, for a structure with stacked G-quartets (**Figure 4.12**).^{53,191} No CD band was observed without the presence of M^+ .

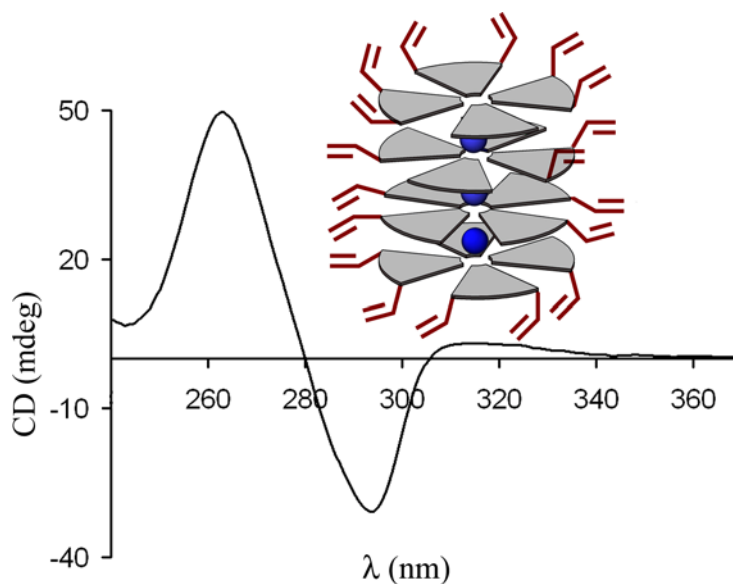


Figure 4.12. CD spectrum of G-quadruplex **60** (0.171 mM) in CH_2Cl_2 using a 1.0 cm path length quartz cuvette. The positive CD band centered at 280 nm is characteristic of stacked G-quartets within a chiral G-quadruplex.¹⁹¹

The two sets of ^1H NMR signals in a 1:1 ratio, the 4:1 ratio of NMR signals for G **59** and DNP^- anion, and signals for hydrogen-bonded N1 amide protons (δ 11.83 and 11.70) and N2 amino protons (δ 9.72 and 9.56) were characteristic of a D_4 -symmetric hexadecamer **2** of formula $[\text{G } \mathbf{59}]_{16} \cdot 4\text{K}^+ \cdot 4\text{DNP}^-$ (**Figure 4.13**).

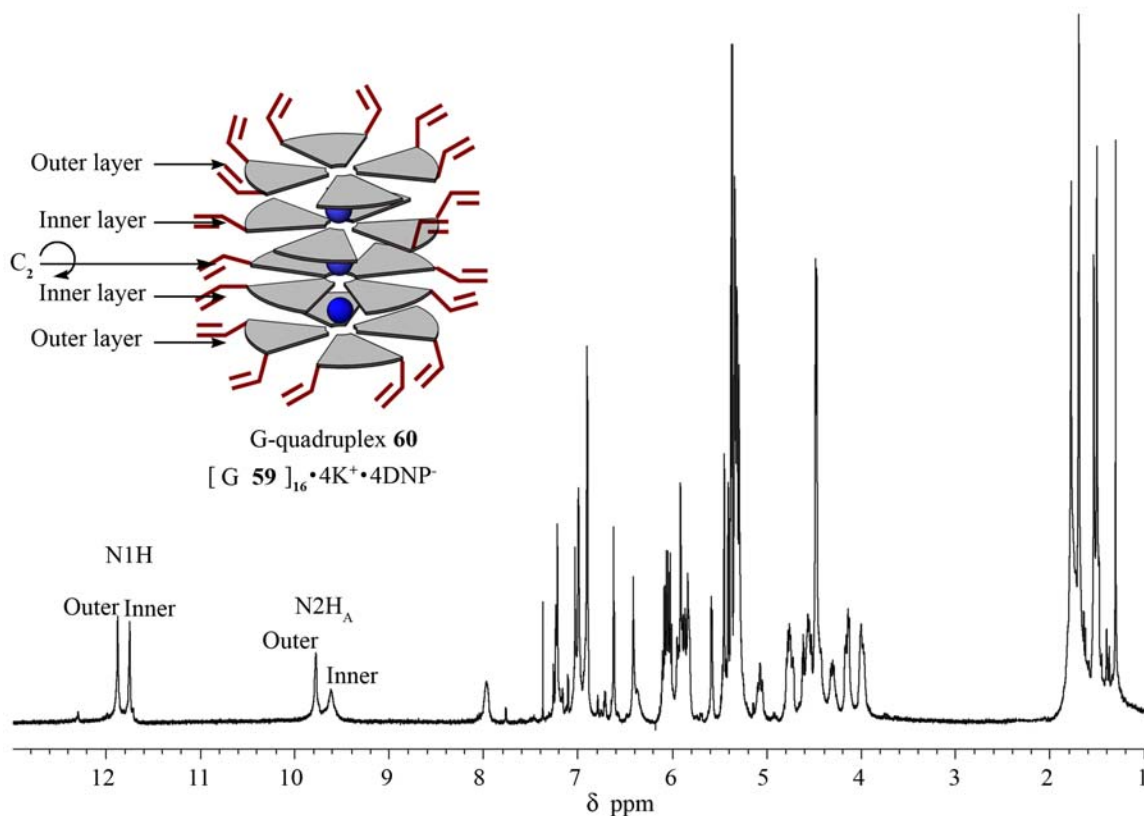


Figure 4.13. ^1H NMR spectrum (CD_2Cl_2) of G-quadruplex **60**, $[\text{G } 59]_{16} \cdot 4\text{K}^+ \cdot 4\text{DNP}^-$. The designations inner and outer refer to the inner and outer layers that provide 2 sets of signals observed for this D_4 -symmetric hexadecamer.

Pulsed-field gradient NMR experiments in CD_2Cl_2 confirmed that the non-covalent G-quadruplex **60** was indeed a hexadecameric G-quadruplex.^{121,151} The $[\text{G}]_{16}$ G-quadruplex, **60**, was much larger than the adenosine standard A **23**. The diffusion coefficients (Table 4.1) showed that G-quadruplex **60** moved much slower than A **23**. Thus, the ratio of the experimental diffusion coefficients ($D_s(\text{A } 23)/D_s[\text{G}]_{16} \text{ 60}$) = 0.33 was close to the value expected for a hexadecamer (0.35). Stejskal–Tanner plots of G-quadruplex **60** and A **23** showed that the decays were single exponential, indicating that there was no measurable exchange in the diffusion measurement (Figure 4.14).

Table 4.1. Diffusion Coefficients for G-quadruplex **60**.^[a]

	$D_s(\mathbf{60})$ (10^{-10} m ² /s)	$D_s(\mathbf{A\ 23})$ (10^{-10} m ² /s)	Ratio $\frac{D_s(\mathbf{60})}{D_s(\mathbf{23})}$
CD ₂ Cl ₂	5.57 ± 0.05	16.8 ± 0.2	0.33

[a] The diffusion coefficients reported in **Table 4.1** are the mean ± standard deviation of 4 separate measurements at 21 °C.

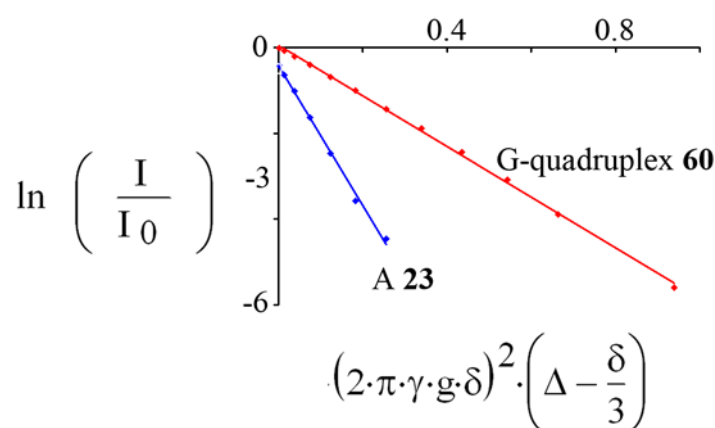


Figure 4.14. Diffusion NMR data for non-covalent G-quadruplex **60**. Stejskal–Tanner plot of G-quadruplex **60** and **A 23** in CD₂Cl₂ at 21.8 °C.¹²¹

4.4.2 Olefin Metathesis Yields Unimolecular G-Quadruplex **61**

Olefin metathesis of the self-assembled G-quadruplex **60** (8 mM), using Grubb's second-generation catalyst, (H₂IMes)(PCy₃)(Cl₂)Ru=CHPh (10 mol % per alkene unit),³¹⁰ was complete within 48 hours in CH₂Cl₂ at 35 °C. Metathesis was monitored by tracking the disappearance of the ¹H NMR signals for the terminal olefins in G-quadruplex **60** and the appearance of new signals for the secondary olefins (cis/trans mix) within the metathesis product **61** (**Figure 4.15**). The crude product showed small amounts of insoluble precipitate while the ¹H NMR showed complete loss of the H13' signal. After

silica gel purification, the unimolecular G-quadruplex was obtained in 57 % yield. Importantly, no olefin metathesis was observed when “monomeric” G **59** (130 mM) was treated with Grubb’s catalyst under similar conditions.

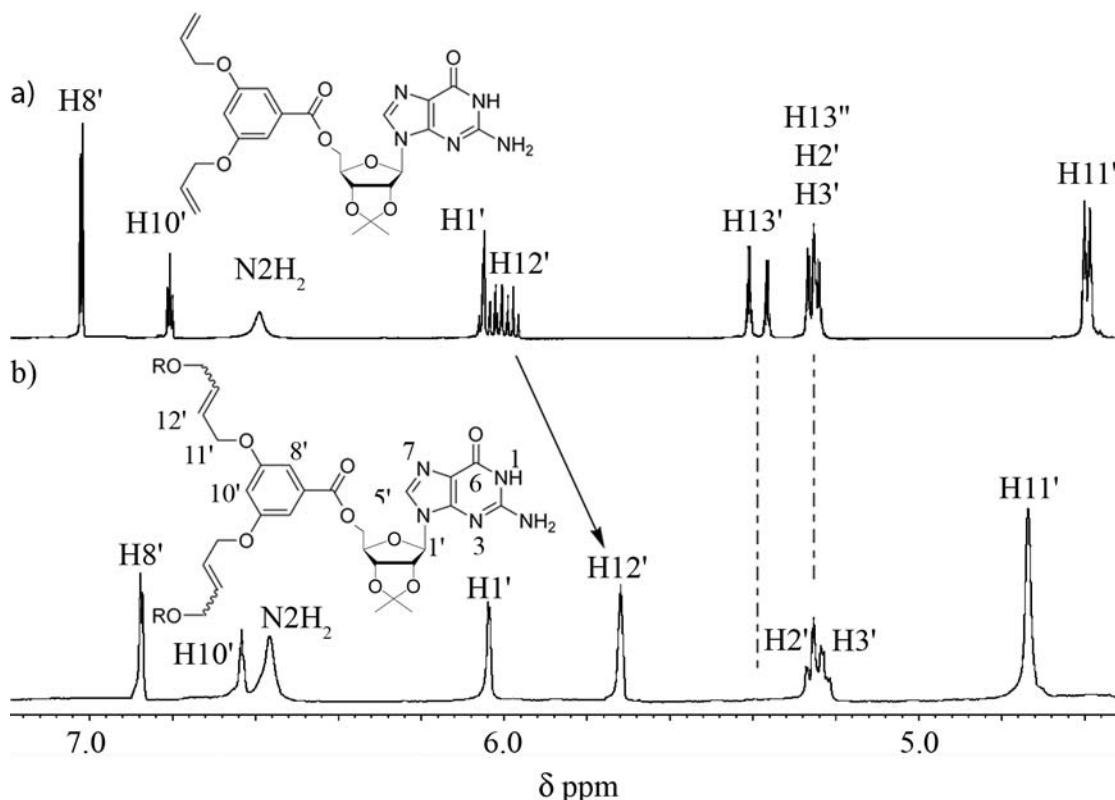


Figure 4.15. A region of the 400 ^1H NMR spectra (DMSO- d_6) with a) precursor G **59** and b) purified unimolecular G-quadruplex **61**. The arrow and dotted lines show where the H12' peak shifts and the disappearance of the H13' signals. The H12' peak at 5.71 ppm is due to a cis/trans mixture.

The structure of the metathesis product **61** was confirmed using mass spectrometry, diffusion NMR and CD spectroscopy. ESI-MS showed a parent peak at $m/z = 2766.3$ consistent for a triply charged species of formula $\text{C}_{384}\text{H}_{400}\text{N}_{80}\text{O}_{128} \cdot 3\text{K}^+$ and molecular weight of 8299 amu (**Figure 4.16**). This parent peak, $[(\text{G } \mathbf{59})_{16} \cdot 3\text{K}]^{+3}$, is the captured hexadecameric G-quadruplex with its anions and one cation stripped away. It is worth noting the labile “capping” cation is often not present in MS experiments with

the G-quadruplexes studied by the Davis group. Similarly, the anions were not shown to bind tightly to the precursor **60** or the unimolecular G-quadruplex **61**, which was confirmed in these studies. Additionally, the polar nature of the solvent in this experiment (1:2 H₂O-CH₃CN) typically destroys noncovalent G-quadruplexes. Noncovalent G-quadruplex **60**, under identical conditions, shows only peaks for [G + H]⁺ and its dimer [G₂ + H]⁺.

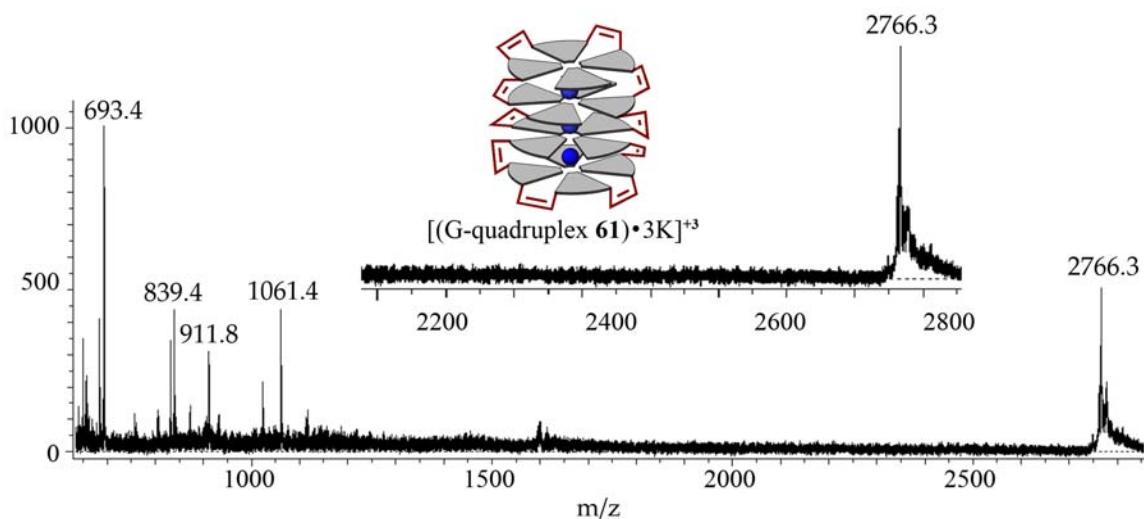


Figure 4.16. ESI-MS of G-quadruplex **61** in 1:2 H₂O-CH₃CN showing the triply charged ion for [G **61** • 4K]⁺³ at m/z 2766.3.

Other ESI-MS experiments also showed that **61** readily underwent Na⁺/K⁺ cation exchange, providing the first hint that this unimolecular G-quadruplex could mediate ion exchange. **Figure 4.17** shows how washing with a solution of K⁺ yields a [G **61**].3K⁺ G-quadruplex, while washing again with a solution of Na⁺ switches the structure back to the [G **61**].3Na⁺ G-quadruplex.

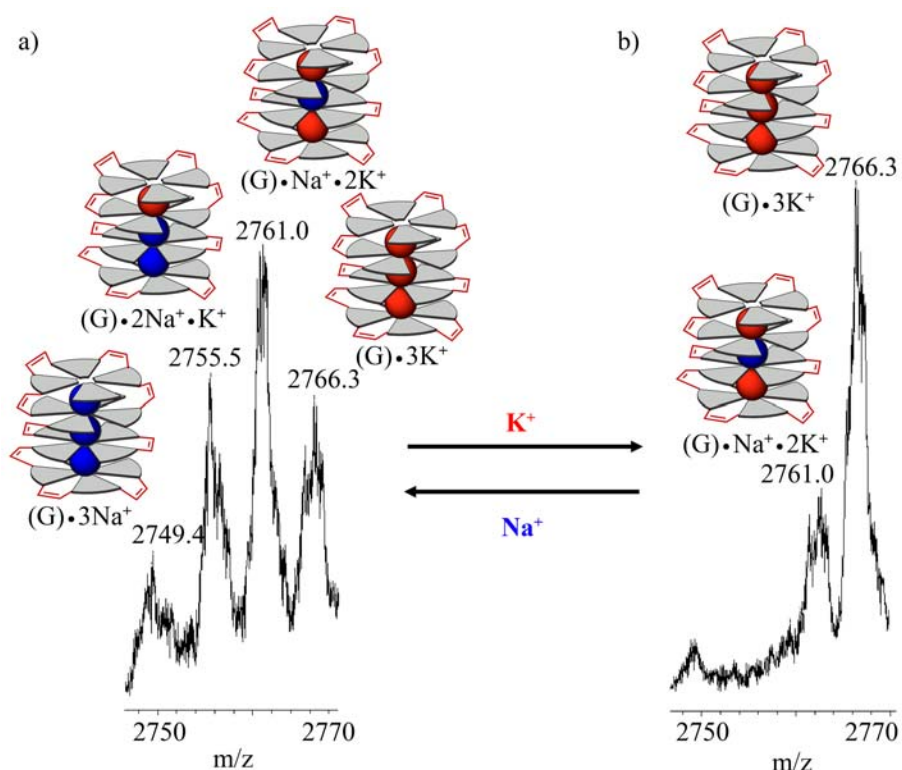


Figure 4.17. ESI-MS of unimolecular G-quadruplex **61** in 1:2 H₂O-CH₃CN a) after purification by flash chromatography and b) after washing with K(DNP). This change in the ESI-MS shows the ability to exchange cations in G-quadruplex **61** from Na⁺ to K⁺.

Pulsed-field gradient NMR experiments in the competitive solvent DMSO-d₆ confirmed that metathesis product [G]₁₆ **61** was much larger than both the precursor G **59** and adenosine standard A **23**. Thus, the ratio of the experimental diffusion coefficients ($D_s(\text{A } \mathbf{23})/D_s[\text{G}]_{16} \mathbf{61}$) = 0.40 was close to the value expected for a hexadecamer (0.37) (Table 4.2).¹²¹ Stejskal–Tanner plots of G-quadruplex **61** and A **23** showed that the decays were single exponential, indicating that there was no measurable exchange in the diffusion measurement (Figure 4.18).

Table 4.2. Diffusion Coefficients for G-quadruplex **61**.^[a]

	$D_s(\mathbf{61})$ (10^{-11} m ² /s)	$D_s(\mathbf{A\ 23})$ (10^{-11} m ² /s)	Ratio $\frac{D_s(\mathbf{61})}{D_s(\mathbf{23})}$
DMSO-d ₆	1.49 ± 0.02	3.73 ± 0.01	0.40

[a] The diffusion coefficients reported in **Table 4.2** are the mean ± standard deviation of 4 separate measurements at 21 °C.

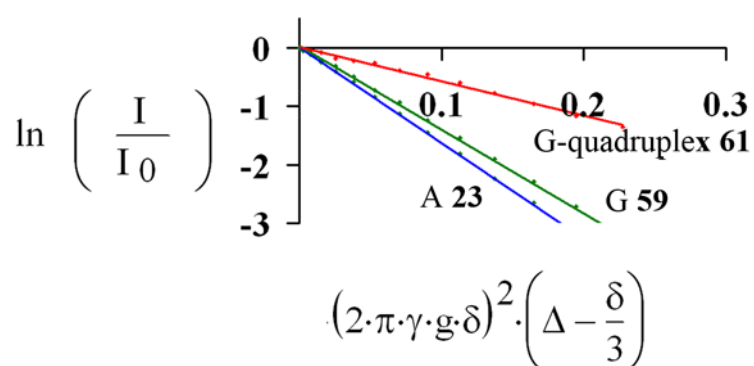


Figure 4.18. Diffusion NMR data for a unimolecular G-quadruplex **61**. Stejskal–Tanner plot of G **59**, G-quadruplex **61** and A **23** in hydrogen bonding disrupting solvent, DMSO-d₆ at 21.8 °C.¹²¹

Finally, the metathesis product [G]₁₆ **61** gave characteristic ¹H NMR signals (2 NH amide signals at δ 11.76 and 11.64), that were similar but somewhat broader than that of the unmetathesized precursor G **60** (**Figure 4.19**). The CD spectra of unimolecular G-quadruplex **61** and precursor G-quadruplex **60** in CD₂Cl₂ for a lipophilic G-quadruplex are shown in **Figure 4.19**. The CD spectrum of unimolecular G-quadruplex **61** (λ_{max} = 260 nm) is characteristic for G-quadruplex formation and is similar to that of its precursor G-quadruplex **60**.

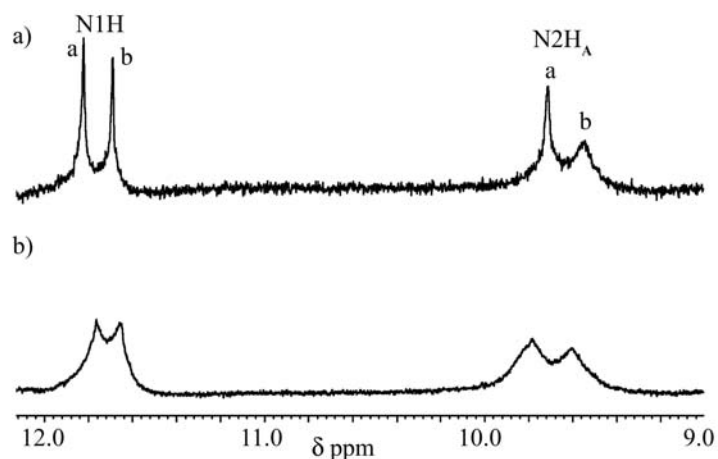


Figure 4.19. A region of the 400 MHz ^1H NMR spectra (CD_2Cl_2) of a) precursor G-quadruplex **60** and b) unimolecular G-quadruplex **61**. The spectra show the hydrogen bonded signals for the N1H and N2HA inner and outer sets of signals observed for the two D_4 -symmetric hexadecamers.

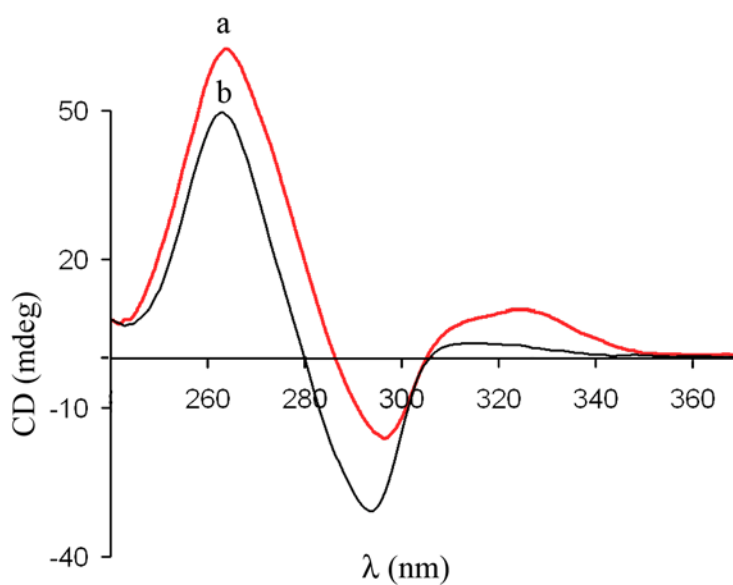
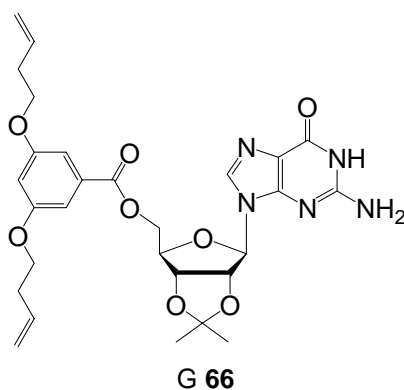


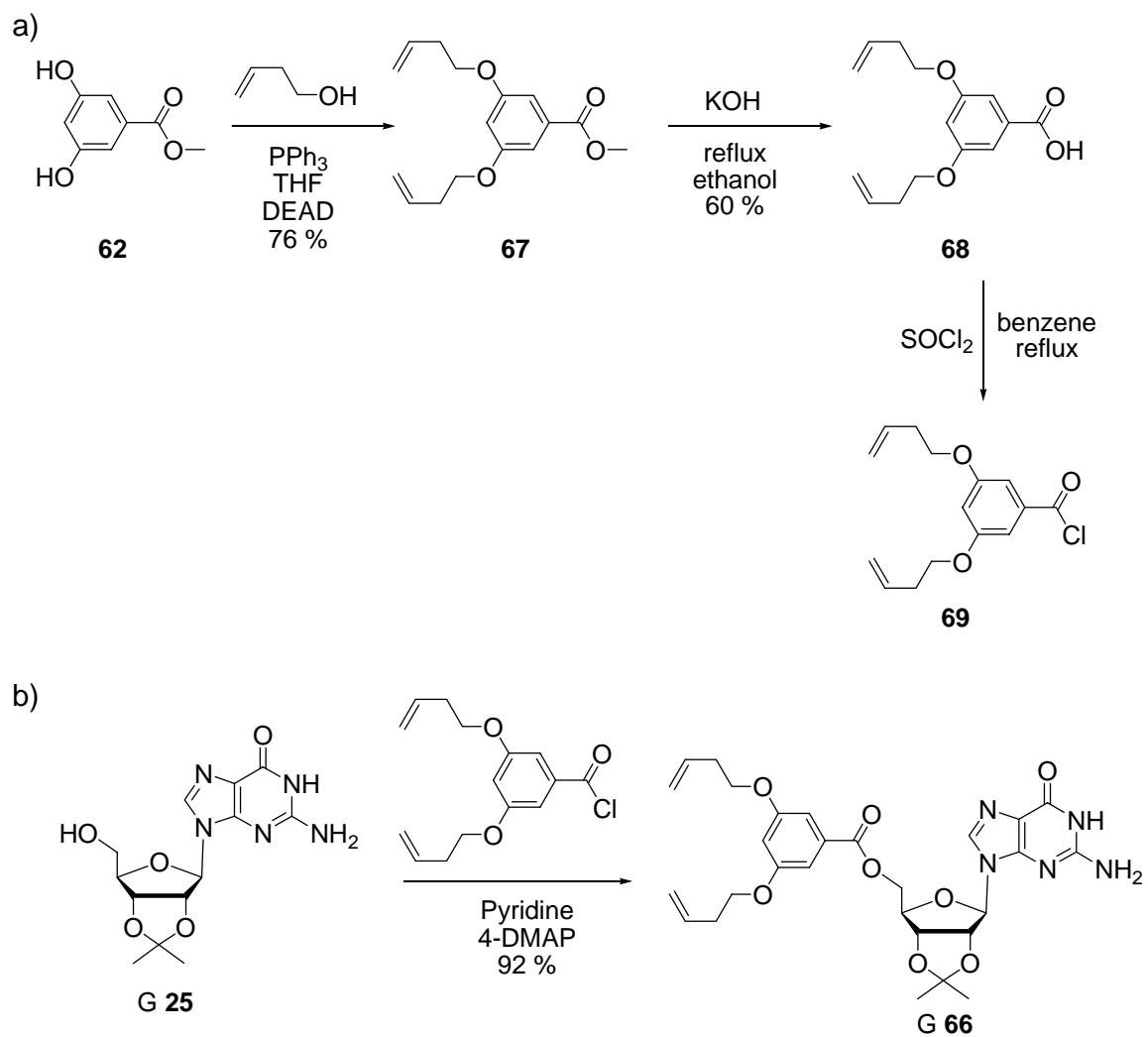
Figure 4.20. CD spectra of a) unimolecular G-quadruplex **61** (0.011 mM) and b) precursor G-quadruplex **60** in CH_2Cl_2 using a 1.0 cm path length quartz cuvette. The positive CD band centered at 280 nm is characteristic of stacked G-quartets within a chiral G-quadruplex.¹⁹¹

4.4.3 Extending the Linker Arms on the Noncovalent G-Quadruplex Does Not Produce a Unimolecular G-quadruplex.

Dialkenyl guanosine, 5'-(3,5-bis(but-3-enyloxy)benzoyl)-2',3'-isopropylidene G **66**, was also investigated for the covalent capture of its corresponding G-quadruplex. Such a unimolecular G-quadruplex with its two extra methylene bridges may a) have different selectivity than G **59**, b) have more “breathing” room to allow for larger cations to flow through the G-quadruplex and c) have different stability properties.



The derivative, 5'-(3,5-bis(but-3-enyloxy)benzoyl)-2',3'-isopropylidene G **66** was prepared in two steps from guanosine (**Scheme 4.8b**). The acid chloride, **69**, was synthesized in three steps from the corresponding methyl-3,5-dihydroxy benzoate **62**. Alkylation under Mitsunobu etherification conditions, followed by hydrolysis of the ester bond gave the corresponding acid **68** as previously reported.³¹³ It should be noted that the synthesis of the acid **68** was completed by Tanya Weerakkody, an undergraduate, under my supervision. Refluxing the benzoic acid **68** with thionyl chloride yielded the desired acid chloride **69** (**Scheme 4.8a**). Routine isopropylidene protection, followed by acylation with 3,5-diallyloxybenzoic acid chloride (**69**) yielded G **66** (**Figure 4.21**).



Scheme 4.9. Synthesis of G **66**.

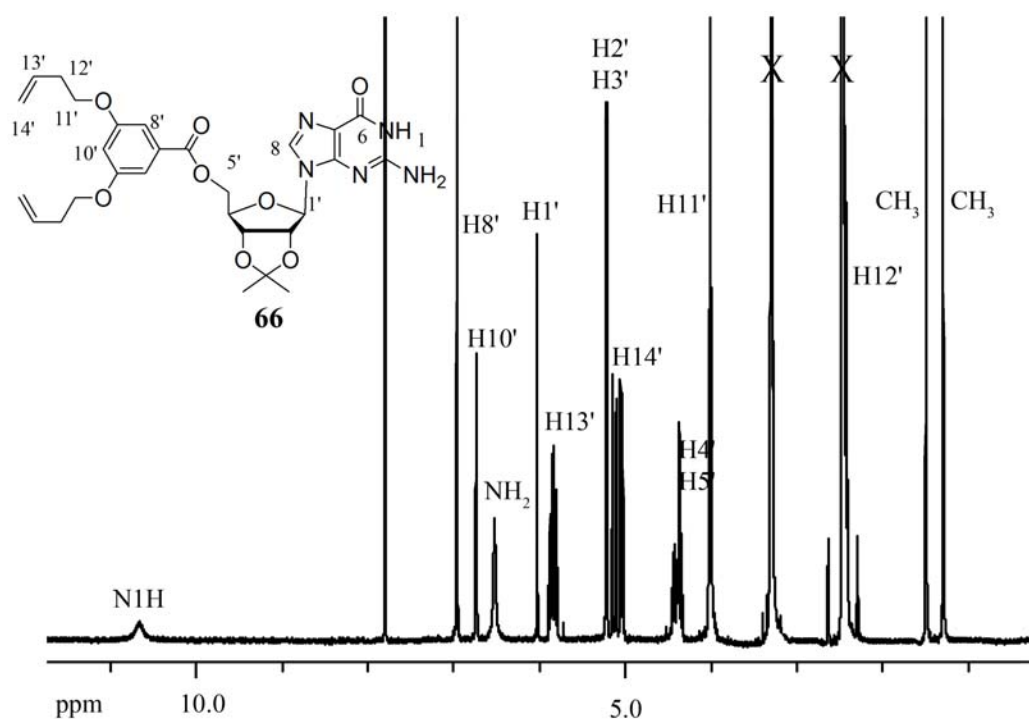


Figure 4.21. The ^1H NMR spectrum of G **66** at 400 MHz in DMSO-d_6 .

Solid-liquid extraction of potassium tetraphenylborate (K^+BPh_4^-) by G **66** in CH_2Cl_2 gave quantitative formation of the G-quadruplex **70** as determined by CD and NMR spectroscopy. G-quadruplex **70** had the characteristic negative to positive CD band, centered at 285 nm, for a structure with stacked G-quartets (**Figure 4.22**).^{53,191} No CD band was observed without the presence of M^+ . This CD spectrum of G-quadruplex **70** was notably different than the CD spectrum of allyloxy G-quadruplex **60**, with the negative band more intense than the positive band.

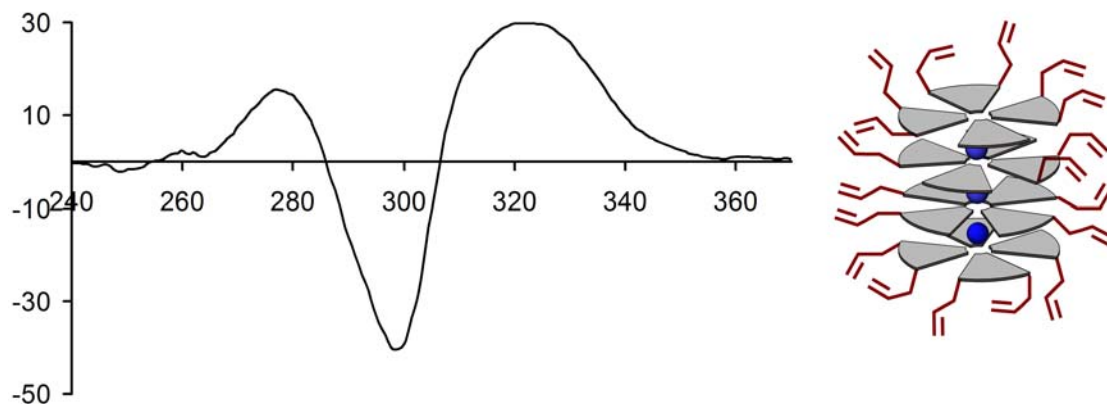


Figure 4.22. CD spectrum of G-quadruplex **70** (0.15 mM) in CH_2Cl_2 using a 1.0 cm path length quartz cuvette. The positive CD band centered at 285 nm is characteristic of stacked G-quartets within a chiral G-quadruplex.¹⁹¹

Formation of the hexadecameric G-quadruplex was also confirmed by ^1H NMR spectroscopy. The two sets of ^1H NMR signals in a 1:1 ratio, the 4:1 ratio (3.8:1) of NMR signals for G **66** and BPh_4^- anion, and signals for hydrogen-bonded N1 amide protons (δ 11.75 and 11.72) and N2 amino protons (δ 10.14 and 9.90) were characteristic of a D_4 -symmetric hexadecamer **70** of formula $[\text{G } \mathbf{66}]_{16} \cdot 4\text{K}^+ \cdot \text{BPh}_4^-$ (**Figure 4.23**). Unlike the allyloxy G-quadruplex **60**, the N1 proton signals for inner and outer layers, although resolved, were only 0.03 ppm apart for the longer-arm G-quadruplex **70**. Additionally, the N2 hydrogen bonding protons for the inner and outer layers were much further downfield ($\Delta\delta = 0.4$ ppm) in the longer-arm G-quadruplex **70** than the allyloxy G-quadruplex **60**. It should be noted that solid-liquid extractions with K^+DNP^- led to a mixture of octamer and hexadecamer, although the hexadecamer G-quadruplex ^1H NMR appeared to be identical, with the exception of the anion signals, to G-quadruplex **70**.

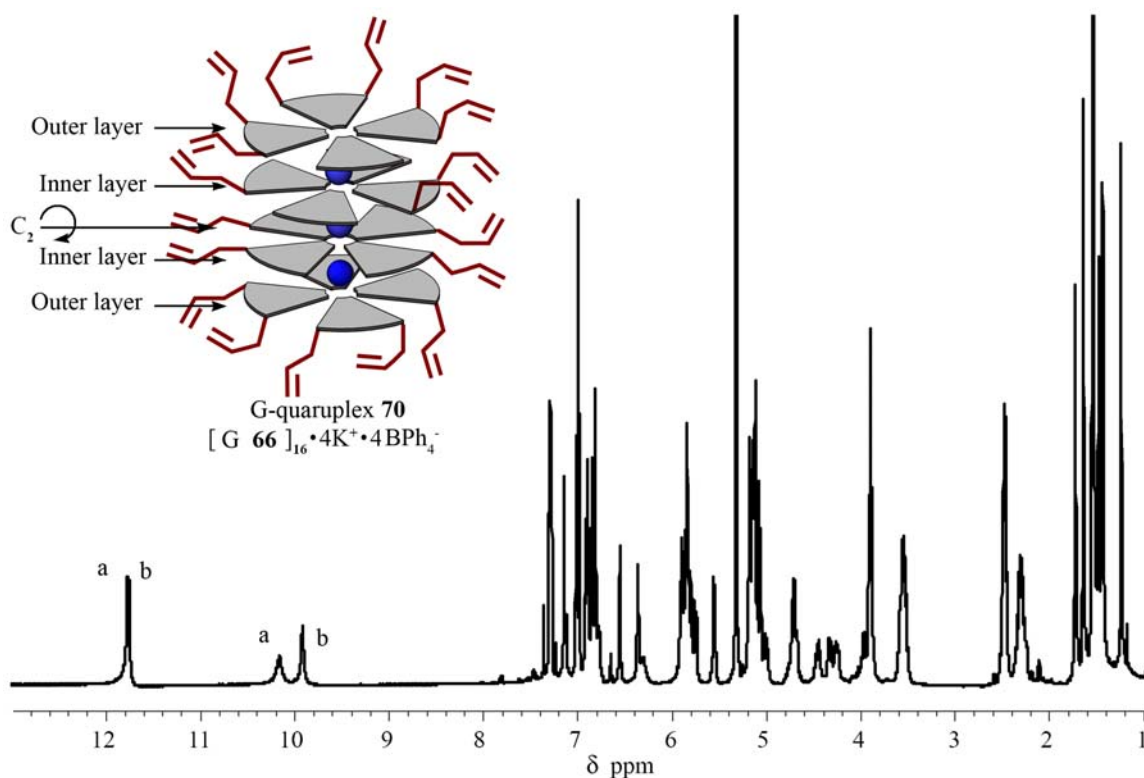


Figure 4.23. ^1H NMR spectrum (CD_2Cl_2) of G-quadruplex **70**, $[\text{G } 66]_{16} \cdot 4\text{K}^+ \cdot 4\text{BPh}_4^-$. The designations a and b refer to the inner and outer layers that provide 2 sets of signals observed for this D_4 -symmetric hexadecamer.

Unfortunately, olefin metathesis of the self-assembled G-quadruplex **70** (8 mM), using Grubb's second-generation catalyst, $(\text{H}_2\text{IMes})(\text{PCy}_3)(\text{Cl}_2)\text{Ru}=\text{CHPh}$ (10 mol % per alkene unit),³¹⁰ produced only a black solid (polymer) in CH_2Cl_2 at 35 ° C. This black solid was not soluble in DMSO-d_6 or other solvents tested, while the reaction solution only showed catalyst. The longer arms in G-quadruplex **70** must be long enough to link two G-quadruplexes, eventually enough G-quadruplexes are tied together and the polymer crashes out of solution.

4.4.4 Unimolecular G-Quadruplex **61** is More Stable than the Noncovalent G-Quadruplex **60**.

Investigations on unimolecular G-quadruplex **61** showed that it was much more stable than its noncovalent counterpart **60**. Immediately after dissolving unimolecular G-quadruplex **61** into DMSO- d_6 , the ^1H NMR spectrum shows evidence that the structure is still organized into a G-quadruplex (**Figure 4.24a**). Noncovalent G-quadruplexes, such as precursor G-quadruplex **60**, fall apart in the polar solvent conditions of DMSO into “monomer.” This ^1H NMR spectrum shows the hydrogen bonded, although broadened, region of the N1H and N2H_A signals along with “unfolded” G-quadruplex in roughly a 1:1 ratio. Upon heating, these peaks disappear. **Figure 4.24b** shows the ^1H NMR spectrum of unimolecular G-quadruplex **61** after about one week as it is completely “unfolded” G-quadruplex. This shows that the unimolecular G-quadruplex is a kinetically stable structure that slowly unfolds, even in very polar solvent conditions (**Scheme 4.10**).

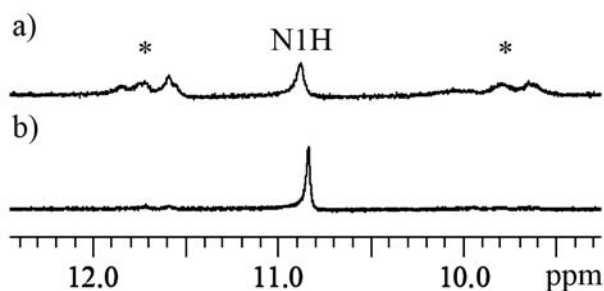
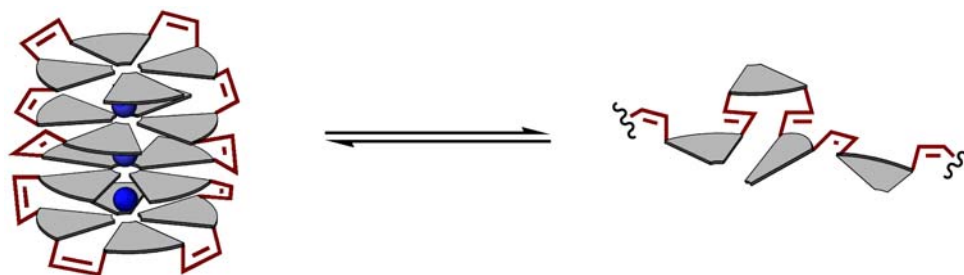


Figure 4.24. A region of the 400 MHz ^1H NMR spectra (DMSO- d_6) of unimolecular G-quadruplex **61** a) 10 minutes and b) one week after dissolving into DMSO- d_6 . The spectra shows what appears to be the additional hydrogen bonded signals for the N1H and N2H_A signals (*).



Scheme 4.10. Equilibrium between structured unimolecular G-quadruplex **61** (left) and “unfolded” unimolecular G-quadruplex **61** (right).

Additional evidence for this increased stability came from melting studies in DMF-d₇. DMF-d₇, a hydrogen bond competing solvent, is still polar enough to partially unfold unimolecular G-quadruplex **61** at rt and has a much lower melting point (-6 °C) than DMSO-d₆ (18.5 °C). At rt, the sample is mainly folded (61 % folded), after annealing at 100 °C. At higher temperatures (92 °C), the sample is mainly unfolded (19 % folded) after annealing at 100 °C (**Figure 4.25**).

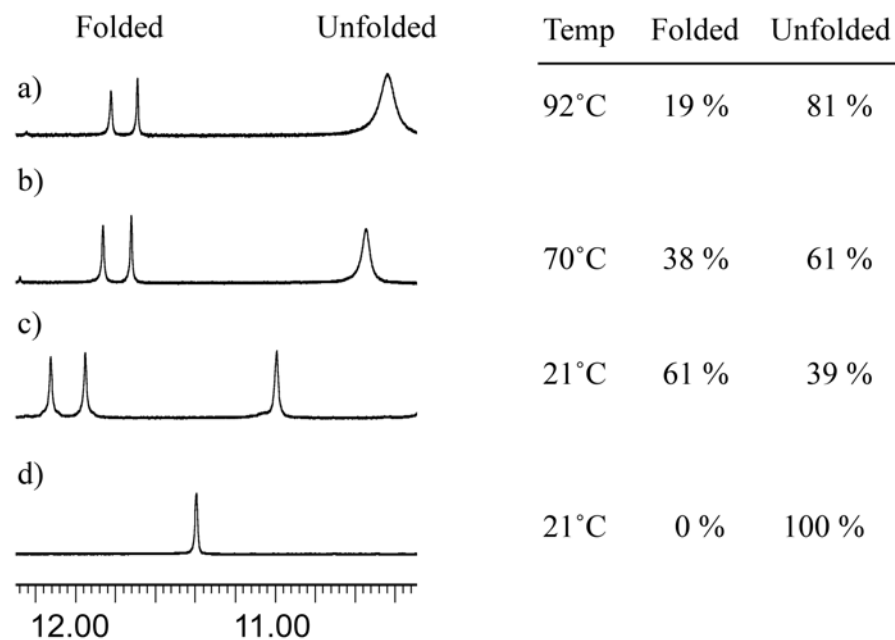


Figure 4.25. Selected N1H region of the 400 MHz ^1H NMR spectra (DMF- d_7) of a) unimolecular G-quadruplex **61** at 92 °C, b) 70 °C, c) 21 °C, and d) noncovalent G-quadruplex **60** at 21 °C. The percentage of folded to unfolded structures are also shown. The ^1H NMR spectra were generated by heating the sample up to 100 °C for 4 h, cooling down to the desired temperature, and waiting until the sample comes to equilibrium. Folded-unfolded ratios are ballpark numbers, since it takes a significant amount of time for the sample to come to equilibrium at low temperatures.

It should be noted that the sample takes a significant amount of time to come to equilibrium. After 30 minutes at 103 °C, the ^1H NMR spectrum of unimolecular G-quadruplex **61** is still significantly folded (41 %). After 220 min, the sample had come to equilibrium at 7 % folded (**Figure 4.26**). At lower temperatures, the sample takes significantly more time, weeks, to come to equilibrium between folded and unfolded species. Due to this kinetic stability, measuring the ratio of folded to unfolded at lower temperatures proved to be a daunting task. The slow kinetics of the unimolecular G-quadruplex **61** are associated with both the unfolding and refolding processes.

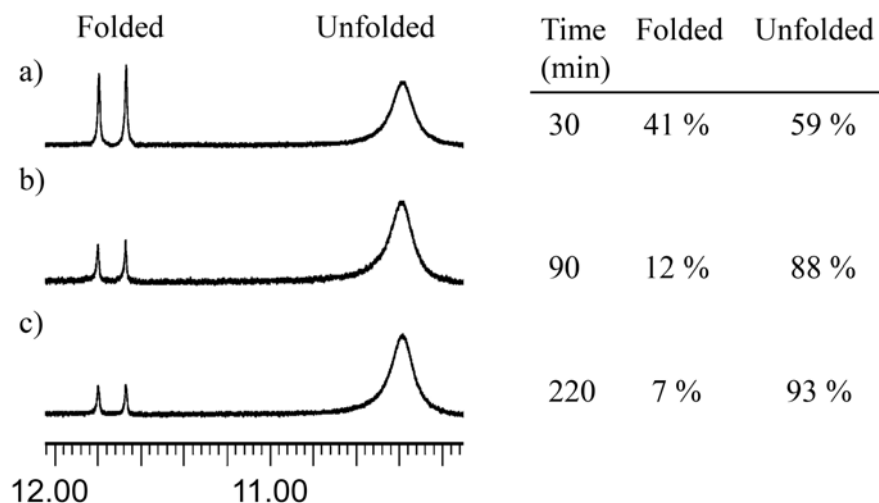
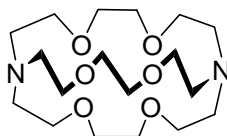


Figure 4.26. Selected N1H region of the 400 MHz ^1H NMR spectra (DMF- d_7) of unimolecular G-quadruplex **61** at 103 °C after a) 30 min, b) 90 min, and c) 220 min.

To shift this equilibrium, [2.2.2]cryptand **21**, a Na^+ scavenger, was used to remove metal from the G-quadruplex. An “empty” G-quadruplex should be substantially less stable than the Na^+ filled unimolecular G-quadruplex **61** because of the C6 oxygens being in close proximity without a stabilizing cation. **Figure 4.27a** shows a region of the 400 MHz ^1H NMR spectrum (DMF- d_7) of unimolecular G-quadruplex **61** at rt. After addition of [2.2.2]cryptand **21** (**Figure 4.27b**), the folded structures become less ordered as multiple new peaks arise that are downfield to the “unfolded” structure. Heating the sample to 100 °C completely unfolds the structure (**Figure 4.27c**). After annealing the sample, a new N1H signal arises downfield to the “unfolded” peak at rt (**Figure 4.27d**). Cooling the sample further to -43 °C (**Figure 4.27e**) results in the growth of the new “folded” signal (34 % new signal).



21

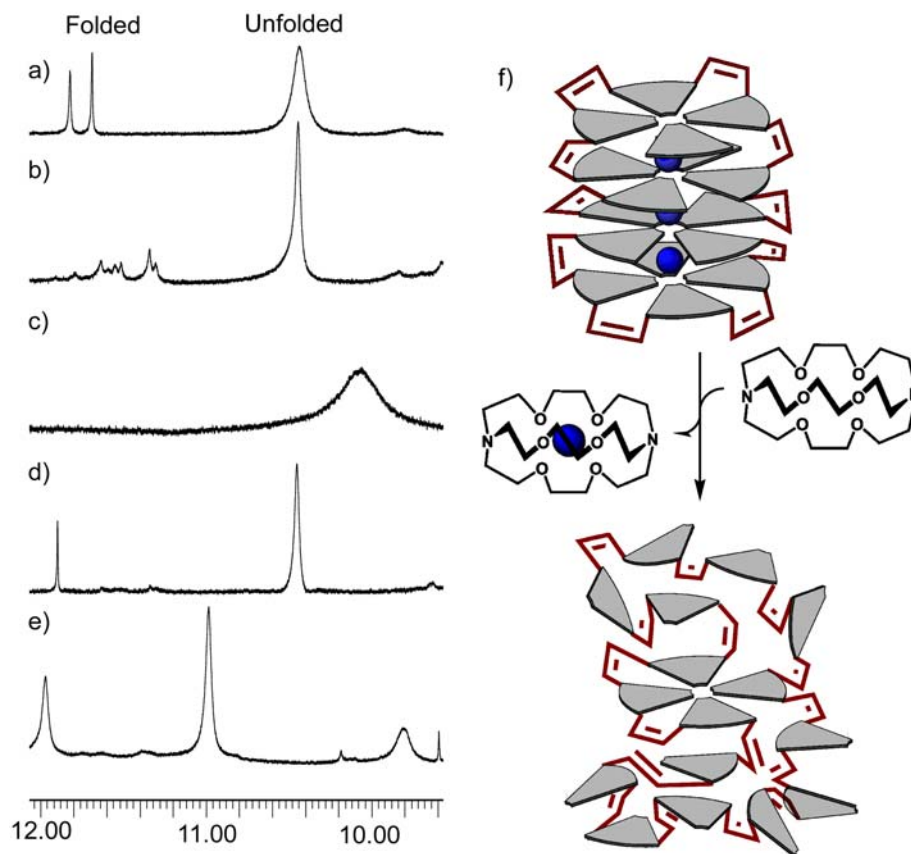
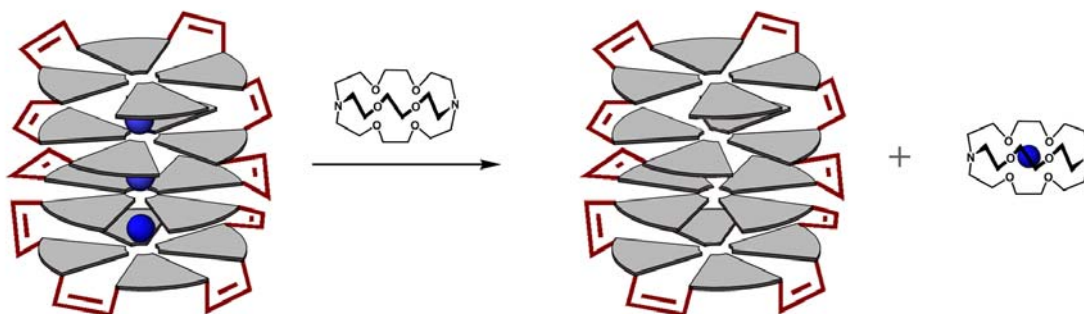


Figure 4.27. Selected N1H region of the 400 MHz ^1H NMR spectra (DMF- d_7) of unimolecular G-quadruplex **61** at a) 21 °C, b) at 21 °C with 4 equiv. [2.2.2]cryptand **21**, c) b at 103 °C, d) after annealing (100 °C) b, e) at -43 °C, and f) schematic showing a possible intermediate after the addition of [2.2.2]cryptand **21**.

This single set of signals could be an isolated tetramer or a symmetric octamer. It was previously shown that symmetric octameric G-quadruplexes give a single set of signals in this region downfield to the “unfolded” peaks.¹²¹ **Figure 4.27f** shows a possible structure of the intermediate observed in the spectra shown in **Figure 4.27d** and **e**. The possible structure in **Figure 4.27f** shows an isolated G-quartet with the rest of the structure “unfolded.” Further investigation into this intermediate is needed to fully characterize it.

Upon addition of [2.2.2]cryptand **21** to unimolecular G-quadruplex **61** in a more

nonpolar solvent (CD_2Cl_2) (**Scheme 4.11**), the unimolecular G-quadruplex **61** appears to remain folded (**Figure 4.28a and b**). The N1H signals show a significant downfield shift ($\Delta\delta = 0.5$ ppm) after the addition of [2.2.2]cryptand **21**. This downfield shift of the N1H signals is likely due to the removal of the Na^+ cations from the unimolecular G-quadruplex **61**. After removing these cations, the hydrogen bonds between the N1 protons and the C6 oxygens should be stronger, since the bound M^+ pull electron density from the oxygens (**Figure 4.29**). This stronger hydrogen bond should shift the N1 protons further downfield. Furthermore, ^{23}Na NMR spectra showed that the [2.2.2]cryptand extracted Na^+ from the unimolecular G-quadruplex **61**. The unimolecular G-quadruplex $[\text{G } \mathbf{61}] \cdot 3\text{Na}^+$ doesn't show any signals for bound Na^+ (**Figure 4.28c**). This is most likely due to the fact that the bound Na^+ in **61** are in intermediate exchange in the NMR chemical shift timescale. Upon addition of [2.2.2]cryptand **21** to unimolecular G-quadruplex **61**, a ^{23}Na signal arises for the [2.2.2]cryptate $\cdot \text{Na}^+$ complex.



Scheme 4.11. Schematic showing removal of cation in nonpolar solvent. Proposed structure of cation “free” unimolecular G-quadruplex in nonpolar solvents.

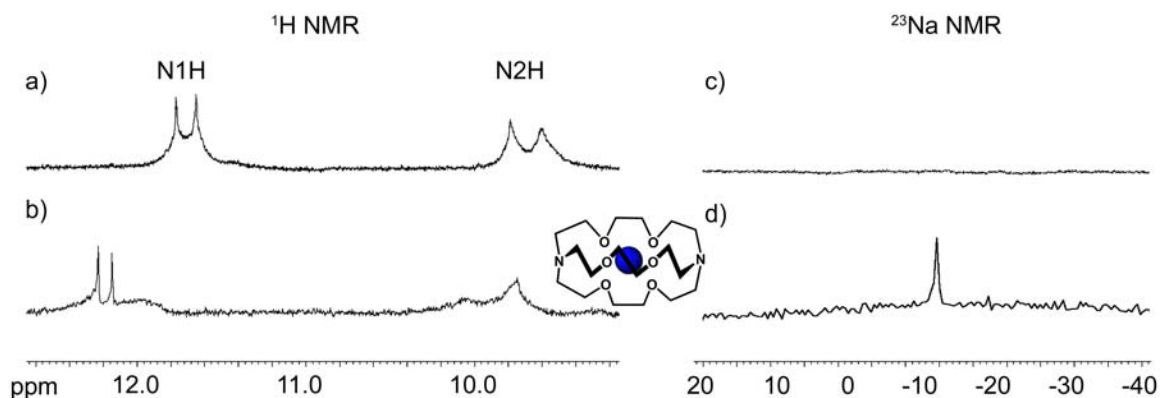


Figure 4.28. Selected N1H region of the ^1H NMR spectra (CD_2Cl_2) of a) unimolecular G-quadruplex **61** and b) with 16 eq [2.2.2]cryptand **21**. Additional ^{23}Na NMR spectra of c) unimolecular G-quadruplex **61** and d) with 16 eq [2.2.2]cryptand **21**.

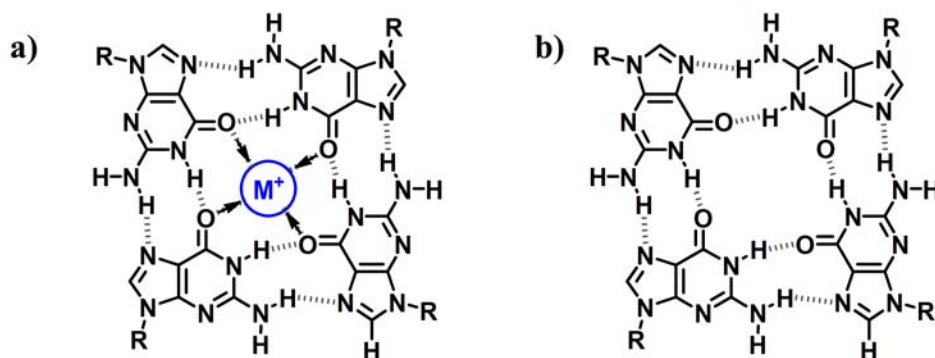


Figure 4.29. G-quartet a) with bound M^+ cation and b) without cation.

To gain more insight about the stability of the unimolecular G-quadruplex **61**, CD spectroscopy was again used to study the solution structure. As mentioned before the noncovalent G-quadruplex **60** is CD active. Upon addition of 3 equiv of [2.2.2]cryptand **21** to noncovalent G-quadruplex **60** in CH_2Cl_2 , no CD signal is observed (**Figure 4.30**). On the other hand, even with the addition of 160 equiv of [2.2.2]cryptand **21**, unimolecular G-quadruplex **61** is still CD active (**Figure 4.31**). With the exception of a slight shift in the CD spectrum, the two CD spectra of unimolecular G-quadruplex **61** with and without [2.2.2]cryptand are similar.

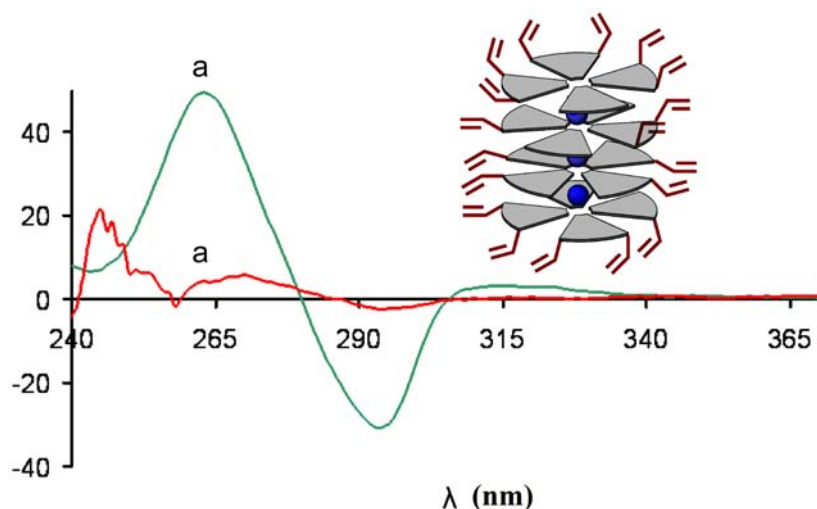


Figure 4.30. CD spectra of a) noncovalent G-quadruplex **60** (0.011 mM) (green line) and b) with 3 equiv. [2.2.2]cryptand **21** (red line) in CH_2Cl_2 using a 1.0 cm path length quartz cuvette.

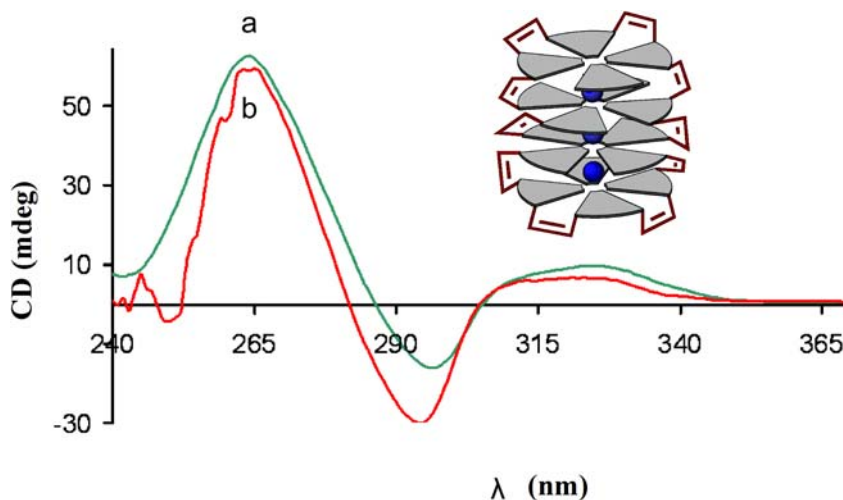


Figure 4.31. CD spectra of a) unimolecular G-quadruplex **61** (0.011 mM) (green line) and b) with 160 equiv. [2.2.2]cryptand **21** (red line) in CH_2Cl_2 using a 1.0 cm path length quartz cuvette.

These studies show the remarkable stability of the unimolecular G-quadruplex **60**. These studies show that the unimolecular G-quadruplex slowly unfolds and folds even in polar solvents. The addition of [2.2.2]cryptand appears to remove the M^+ . We,⁶² and others,⁶¹ have previously reported stable G-quartets without the presence of cations.

Furthermore, different intermediates are observed depending on the polarity of the solvent. In more polar solvents, DMF-d₇, a new intermediate is observed while in more nonpolar solvents, CD₂Cl₂, a cation “free” G-quadruplex is proposed.

4.4.5 Unimolecular G-quadruplex **61 is a Transmembrane Na⁺ Transporter**

The studies presented in this section used egg yolk phosphatidylcholine (EYPC) liposomes. A liposome is a spherical lipid bilayer that acts as a cell model. The liposome contains an aqueous intravesicular compartment. Both the intravesicular and extravesicular solution can be altered differently for specific assays.

The unimolecular G-quadruplex **61** showed remarkable stability in EYPC liposomes. Unimolecular G-quadruplex **61** gave the diagnostic CD spectrum for a G-quadruplex when added to an aqueous solution of EYPC liposomes (**Figure 4.32**), indicating that unimolecular G-quadruplex **61** can fold into this secondary structure within the phospholipid bilayer.²⁸⁷ As with other noncovalent lipophilic G-quadruplexes, noncovalent G-quadruplex **60** showed no CD activity under these conditions. In contrast, no active CD bands were observed for unimolecular G-quadruplex **61** when it was added to a solution of 10 mM sodium phosphate that did not contain liposomes, indicating that G-quadruplex **61** is either unstructured or insoluble in aqueous solution.

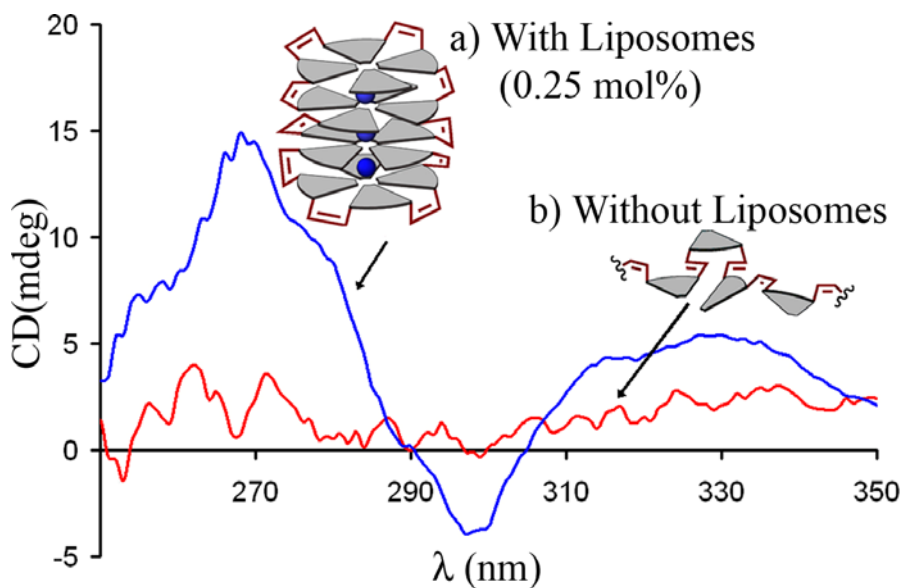


Figure 4.32. CD spectra of unimolecular G-quadruplex **61** (0.05 mM) in 10 mM sodium phosphate (pH 6.4) with a) and without b) EYPC liposomes (100 nm).

Having shown that unimolecular G-quadruplex **61** forms a G-quadruplex in phospholipid liposomes; its ability to function as a transmembrane ion transporter was evaluated. Initial studies used a standard base-pulse assay to indirectly measure Na^+ transport across liposomal membranes.^{216,314} Liposomes (100 nm) containing the pH-sensitive dye (**71**), HPTS, were suspended in a solution of 75 mM Na_2SO_4 , 10 mM sodium phosphate (pH=6.0). As shown in **Figure 4.33**, addition of exogenous base led to a rapid increase in the internal pH of these liposomes when they were in the presence of unimolecular G-quadruplex **61** (1 mol %). In sharp contrast, no pH change occurred when either G **59** or the non-covalent assembly $[\text{G } \mathbf{59}]_{16} \cdot 4\text{K}^+ \cdot 4\text{DNP}^-$ was added to the HPTS-loaded liposomes. The pH increase mediated by unimolecular G-quadruplex **61** is consistent with Na^+ influx across the phospholipid bilayer. Gramicidin was a positive control in these experiments. Gramicidin, a linear pentadecapeptide, forms elongated dimers that span phospholipid membranes. These dimers are potent cation channels that

are selective for monovalent cations.³¹⁵

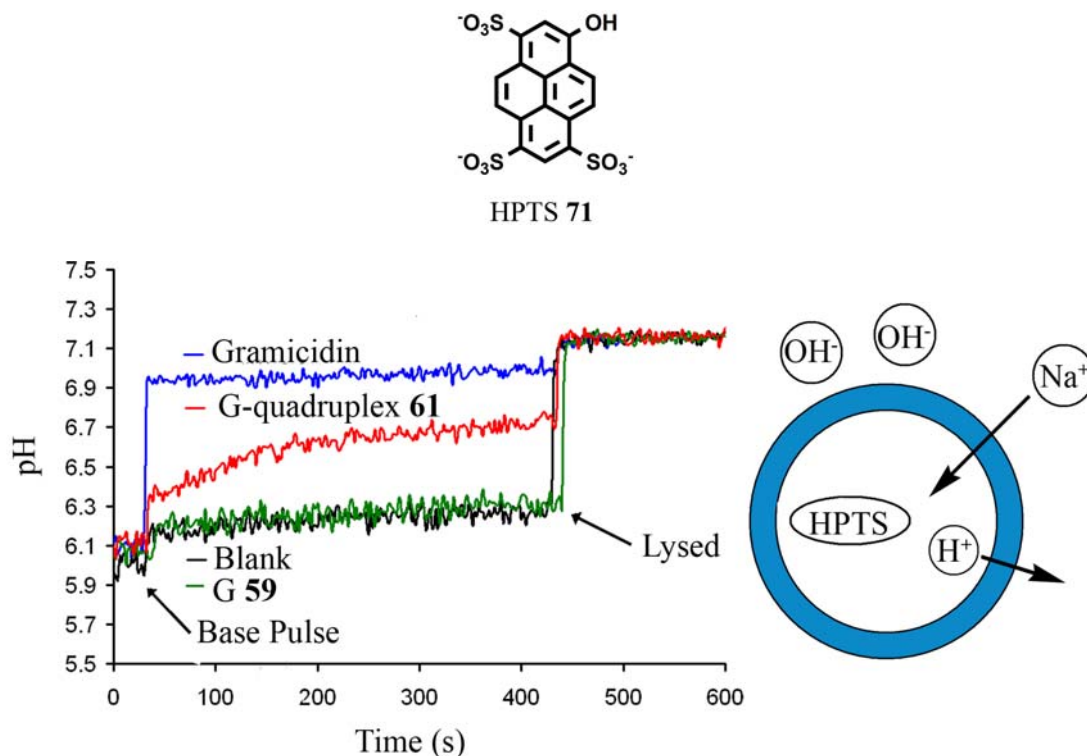


Figure 4.33. Transport of Na⁺ as determined in a pH gradient assay. EYPC liposomes (100 nm) containing HPTS dye **71** (0.1 mM) in 100 mM NaCl, 10 mM sodium phosphate (pH 6.1) were suspended in 100 mM NaCl, 10 mM sodium phosphate (pH 6.1). The compounds, G **59**, G-quadruplex **61** or gramicidin, were added at t = 0 s as DMSO solutions to give a 1:100 ligand to lipid ratio. The addition of NaOH solution at t = 40 s established a pH gradient of about 1 pH unit. At t = 430 s the liposomes were destroyed with Triton-X detergent. Measurement of the fluorescence of the trianionic and tetraanionic forms of HPTS dye **71** allowed determination of the liposomal pH.

Direct evidence for transmembrane cation transport down a Na⁺ gradient, as facilitated by unimolecular G-quadruplex **61**, was obtained from ²³Na NMR experiments. EYPC liposomes (200 nm) containing 130 mM LiCl in 10 mM lithium phosphate (pH=6.4) were suspended in a solution containing 100 mM NaCl, 10 mM sodium phosphate (pH = 6.4). Addition of the NMR shift reagent, Dy(PPPi)₂⁻⁷, caused the “outer” ²³Na peak to move upfield to δ -7.00, distinguishing it from any “internal” ²³Na at δ 0.24. After incubation of the LiCl-filled liposomes with the metathesis product unimolecular

G-quadruplex **61** (0.1 mol %) for 10 minutes, ^{23}Na NMR analysis showed that equilibrium had been achieved between the internal and external Na^+ populations (**Figure 4.34**). Importantly, under the same conditions no Na^+ transport was mediated by the precursor G **59** or the non-covalent assembly **60** $[\text{G } \mathbf{59}]_{16} \cdot 4\text{K}^+ \cdot 4\text{DNP}^-$ (1 mol %). Again, gramicidin served as a positive control in these Na^+ transport experiments.

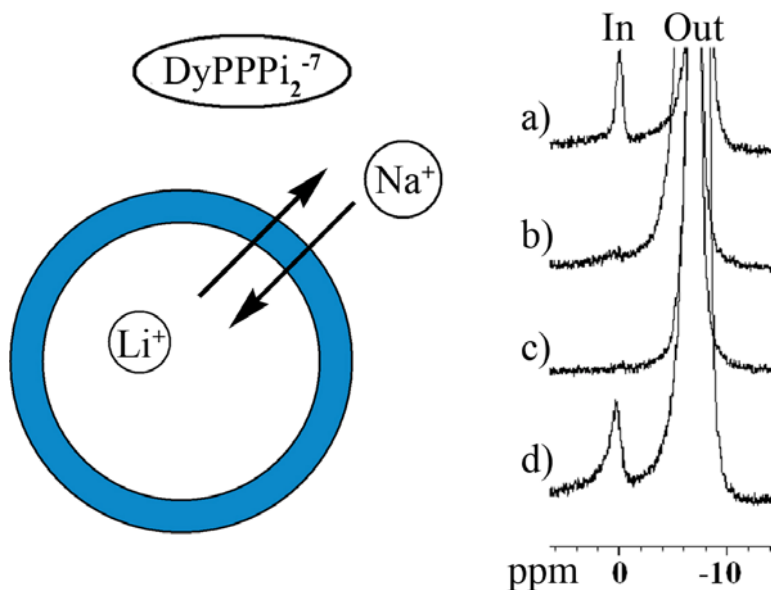


Figure 4.34. A series of ^{23}Na NMR spectra 10 min after addition of a) metathesis product **61**, b) G **59**, c) DMSO blank and d) gramicidin to a solution of EYPC liposomes (200 nm) that initially contained 100 mM LiCl, 10 mM lithium phosphate suspended in an extravesicular buffer containing 100 mM NaCl, 10 mM sodium phosphate. Transport of Na^+ across the bilayer is indicated by a ^{23}Na NMR peak at δ 0.24 ppm.

4.4.6 Unimolecular G-quadruplex Transports Li^+ and K^+ Across EYPC Liposomes.

Initial studies on the selectivity of the unimolecular G-quadruplex **61** showed that it is not Na^+ specific. HPTS base-pulse assays, similar to the Na^+ studies, showed that unimolecular G-quadruplex also transports Li^+ and K^+ . **Figure 4.35** shows the HPTS base-pulse assays with Li^+ and **Figure 4.36** shows the HPTS base-pulse assays with K^+ . These studies suggest that unimolecular G-quadruplex **61** transports all three monovalent

cations. Although recent calculations have predicted that smaller monovalent cations move through DNA G-quadruplexes with lower activation barriers as compared to larger cations, further studies are needed to confirm this selectivity.³¹⁶

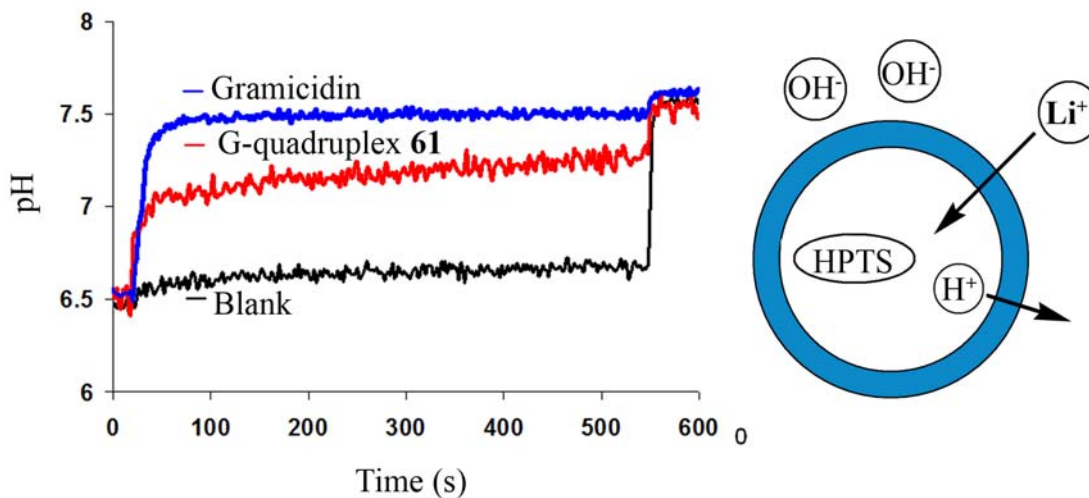


Figure 4.35. Transport of Li^+ as determined in a pH gradient assay. EYPC liposomes (100 nm) containing HPTS dye (0.1 mM) in 100 mM LiCl, 10 mM lithium phosphate (pH 6.5) were suspended in 100 mM LiCl, 10 mM lithium phosphate (pH 6.5). The compounds, G **59**, G-quadruplex **61** or gramicidin, were added at $t = 0$ s as DMSO solutions to give a 1:100 ligand to lipid ratio. The addition of LiOH solution at $t = 40$ s established a pH gradient of about 1 pH unit. At $t = 430$ s the liposomes were destroyed with Triton-X detergent. Measurement of the fluorescence of the trianionic and tetraanionic forms of HPTS dye allowed determination of the liposomal pH.

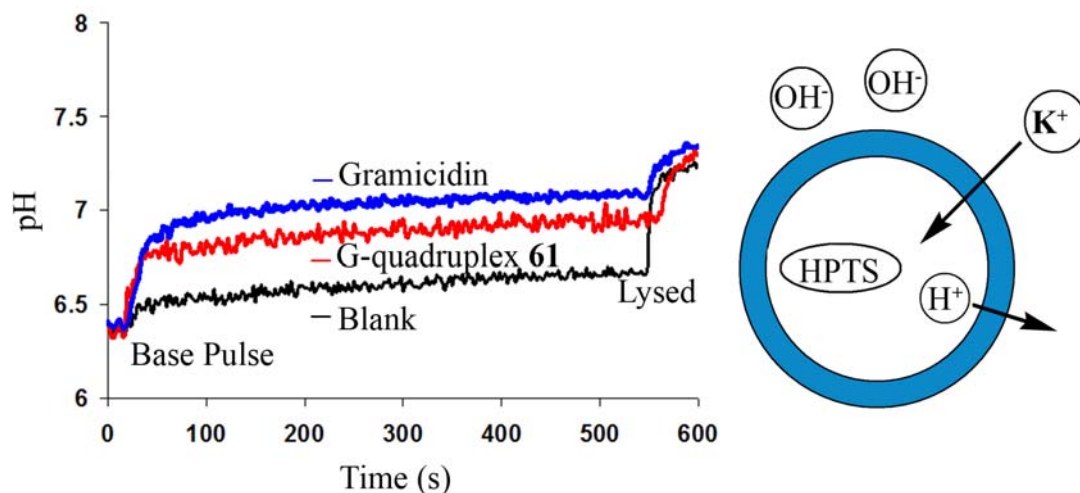


Figure 4.36. Transport of K^+ as determined in a pH gradient assay. EYPC liposomes (100 nm) containing HPTS dye (0.1 mM) in 100 mM KCl, 10 mM potassium phosphate (pH 6.4) were suspended in 100 mM KCl, 10 mM potassium phosphate (pH 6.4). The compounds, G **59**, G-quadruplex **61** or gramicidin, were added at $t = 0$ s as DMSO solutions to give a 1:100 ligand to lipid ratio. The addition of KOH solution at $t = 40$ s established a pH gradient of about 1 pH unit. At $t = 430$ s the liposomes were destroyed with Triton-X detergent. Measurement of the fluorescence of the trianionic and tetraanionic forms of HPTS dye allowed determination of the liposomal pH.

4.5 Conclusion

In conclusion, it was shown that N2-C8-guanosine derivatives **51** can form G-quartets. These G-quartets have the substituents on the N2 and C8 positions in close proximity, which could be used to covalently capture the G-quartet. This strategy that combines non-covalent synthesis and covalent capture to prepare a functional supramolecular assembly, unimolecular G-quadruplex **61**, in just a two steps from a guanosine derivative is described. This unimolecular G-quadruplex is remarkably stable when compared with its noncovalent G-quadruplex **60**. The unimolecular G-quadruplex **61** apparently folds into a conformation that allows it to bind and transport Na^+ ions across phospholipid bilayer membranes. Additionally, this unimolecular G-quadruplex **61** is selective for monovalent cations. Further studies could elucidate the order of

selectivity of these transporters. Additionally, further studies are needed to show if this unimolecular G-quadruplex is indeed an ion channel.

Chapter 5. Future Directions

Diffusion NMR was demonstrated as a valuable technique in characterizing the size of lipophilic G-quadruplexes (**Chapter 2**). The solution structure of $[G \mathbf{8}]_{16} \cdot 4K^+ \cdot 4pic^-$ is determined to be a hexadecamer using diffusion NMR. Additionally, G **24** is also shown to form a hexadecamer G-quadruplex, which has an octameric intermediate structure. Two different octamers, a singly and doubly charged octamer, formed by G **29** are elucidated by diffusion NMR. The information gained from the diffusion NMR technique allowed for a better understanding of the self-assembly processes, especially regarding the roles of cation, anion and solvent.

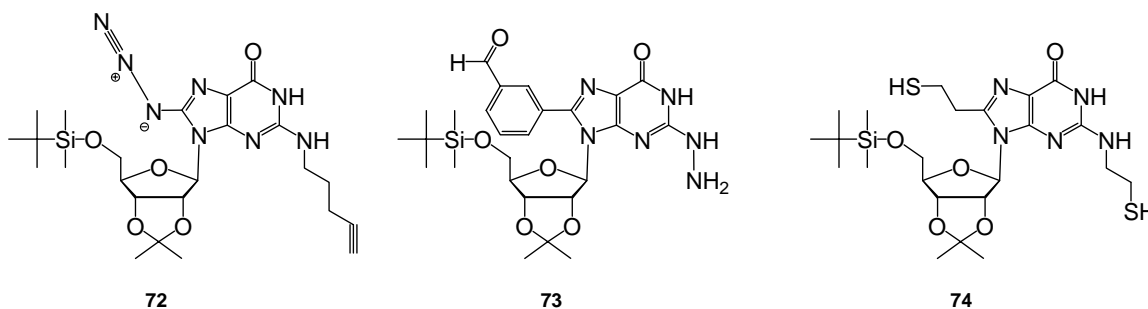
Chapter 3 utilized demonstrated pseudo-regioselective exchange of isotopically labeled G **35-d** into $[G \mathbf{8-h}]_{16} \cdot 4K^+ \cdot 4pic^-$ is demonstrated. Both the bound anion and cation can control the exchange of ligand into the different layers of a synthetic G-quadruplex.

The covalent capture of lipophilic G-quadruplex **60** with reactive groups on the periphery generated a unimolecular G-quadruplex **61** (**Chapter 4**). This unimolecular G-quadruplex **61** shows exceptional stability in nonpolar and polar solvents, even without the presence of cations. Furthermore, this unimolecular G-quadruplex transports monovalent cation across phospholipid membranes.

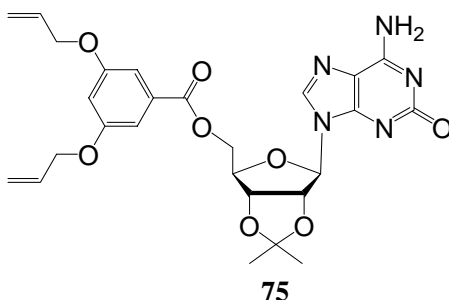
The research discussed in this thesis has a significant bearing on the application of the G-quadruplex as a nanostructure and biomaterial. The characterization and manipulation of the lipophilic G-quadruplexes can be broadly applied to the self-assembled G-quadruplex structures discussed in the introduction. Furthermore, the functionalization of discrete regions of G-quadruplexes has not been fully exploited. To

date, most G-quadruplex biomaterials have relied on the TBA scaffold. Due to the unimolecular G-quadruplex's (**61**) enhanced stability over noncovalent structures, the unimolecular G-quadruplex **61** would be an ideal candidate as a cation sensor.

Covalent capture of a single G-quartet, similar to that of G **51**, is of great interest. Alternative strategies include 1,3-dipolar cycloaddition **72**, disulfide **73** or hydrazone bonds **74**. These alternative strategies may be more successful in covalently capturing a single G-quartet.



Both lipophilic guanosine and isoguanosine, a guanosine isomer, are selective in removing radioactive $^{226}\text{Ra}^{2+}$.^{261,317} Covalent capture techniques with isoguanosine **75** may lead to covalently captured pentamers or decamers. Radioactive $^{226}\text{Ra}^{2+}$ can cause cancer and other problems through replacing Ca^{2+} in the bone. Although both of these noncovalent structures of guanosine and isoguanosine are selective for Ra^{2+} , the noncovalent structures form unorganized structures in the presence of other hydrogen bonding species.²⁶¹ One way to alleviate this obstacle is to use the covalent capture approach described in this thesis to build unimolecular structures. These structures are more stable and should still form stable organized structures even in the presence of other hydrogen bonding species, thus extracting Ra^{2+} .



Further manipulation of the unimolecular G-quadruplex **61** may lead to materials with diverse properties. For example, hydrogenation of the double bond may yield a less rigid unimolecular G-quadruplex that would have different cation selectivity. Additionally, regioselective exchange of more polar guanosine ligands into the outer layers, followed by covalent capture may lead to more amphiphilic structures. Furthermore, transesterification with methanol of the benzoate ester in G-quadruplex **61** may lead to a large 144-membered macrocycle.

The unfolding and folding properties of the unimolecular G-quadruplex **61** need to be explored further. In particular, the intermediate that arises in polar solvents in the absence of cations needs to be further characterized.

The ion selectivity properties of G-quadruplex **61** need to be carefully studied. Channel conductance studies are needed to verify that G-quadruplex **61** clearly functions as an ion channel.²⁸⁰ Studies on liposomes comprised of phospholipids of different sizes and charges may allow for better insight into the mechanism of transport.²⁰⁵

Lastly, the binding properties of unimolecular G-quadruplex **61** with both 5'GMP and small G-rich DNA strands in DMF are of particular interest. Interactions between these two species could be monitored through diffusion NMR. Compounds that bind G-rich DNA strands, such as telomeres, are of increased interest as drug targets.³⁴⁻⁴¹ Studies

on both unimolecular G-quadruplex **61** and more hydrophilic derivatives may lead to promising results in this area.

Chapter 6. Experimental and References.

6.1 General Experimental

All ^1H NMR spectra were recorded on a Bruker DRX-400, a Bruker Avance 400 instrument operating at 400.13 MHz, or on a Bruker DRX-500 operating at 500.13 MHz. The ^{13}C NMR spectra were recorded on a Bruker DRX-400 and Bruker Avance 400 instrument operating at 100.61 MHz. Chemical shifts are reported in ppm relative to the residual protonated solvent peak. Variable temperature ^1H NMR experiments were controlled to ± 0.1 °C and calibrated with methanol at low temperatures and ethylene glycol at high temperature. All NMR spectra were recorded at 20-25 °C (room temperature) unless otherwise specified. Two dimensional ^1H - ^1H COSY (^1H - ^1H three-bond coupling), ^1H - ^1H NOESY (^1H - ^1H through space magnetization transfer), ^1H - ^{13}C HSQC (^1H - ^{13}C one-bond coupling) and ^1H - ^{13}C HMQC (^1H - ^{13}C multibond coupling) experiments were run using previously published standard protocols.⁵² Fast atom bombardment (FAB) mass spectra were recorded on a JEOL SX-102A magnetic sector mass spectrometer. ESI-MS experiments, except when noted, were recorded on a JEOL AccuTOF CS. All fluorimetric experiments were carried out on an Hitachi F4500 fluorescence spectrophotometer. The pH of solutions was monitored with a Fisher Scientific AR25 dual channel pH/ion meter. Circular dichroism (CD) spectra were recorded on a JASCO-810 spectropolarimeter with a 1.0 cm and 1.0 mm path length quartz cuvette. Variable temperature CD experiments were controlled by an attached PFD425S Peltier system with a 1.0 cm and 1.0 mm path length quartz cuvette. Deuterated solvents were purchased from Cambridge Isotope Laboratories. Chromatography was performed using 60-200 mesh silica purchased from Baker and 40-120 μ Sephadex G-10

purchased from Pharmacia Fine Chemicals. Thin layer chromatography was performed on Kieselgel 60 F254 and UniplatTM Silica Gel GF silica-coated glass plates and visualized by UV or by staining with I₂ or an aqueous solution of ceric ammonium molybdate (CAM). All chemicals and solvents were purchased from Sigma, Fluka, Aldrich, or Acros. Guanosine **8**,^{53,318} adenosine **23**,³¹⁸ G-quadruplex **22**,^{59,182} guanosine **29**,³¹⁹ 3,5-(allyloxy)benzoic acid **64**,³¹² 3,5-(but-3-enyloxy)benzoic acid **68**,³¹³ and the potassium and sodium phenolates⁵⁸ were prepared following published methods. All solvents were dried and distilled following standard procedures.

6.2 Synthesis

2',3'-O-Isopropylidene-5'-O-(3,5-bis(methoxy)benzoyl)-guanosine (G 24): 3,5-Dimethoxy benzoyl chloride (465 mg, 1.5 mmol) was added to a solution of 2',3'-O-isopropylidene guanosine **25** (500 mg, 1 mmol) and 4-dimethylaminopyridine (5 mg) in distilled pyridine (7.5 mL). The resulting solution was stirred at rt under a N₂ atmosphere for 4 h. The solvent was evaporated under reduced pressure. The remaining white solid was dissolved in CH₂Cl₂ (40 mL) and washed with 0.1 N HCl (10 mL), sat NaHCO₃ (10 mL), and H₂O (2×10 mL). After removal of the solvent, trituration with Et₂O gave G **24** as a white powder (630 mg, 84 %). ¹H NMR (400 MHz, DMSO-d₆): δ= 10.84 (s, 1 H, NH1), 7.82 (s, 1 H, H8), 7.00 (d, 1 H, *J*=2.3 Hz, H8^{*}), 6.76 (t, 1 H, *J*=2.3 Hz, H10^{*}), 6.61 (br s, 2 H, NH₂), 6.05 (d, 1 H, *J*=1.5 Hz, H1^{*}), 5.26 (dd, 1 H, *J*=6.0, 1.5 Hz, H2^{*}), 5.24 (dd, 1 H, *J*=6.0, 2.5 Hz, H3^{*}), 4.37-4.51 (m, 2 H, H5^{*}), 4.41 (br s, 1 H, H4^{*}), 3.77 (br s, 6 H, OCH₃), 1.52 (s, 3 H, CH₃), 1.32 (s, 3 H, CH₃); ¹³C NMR (100 MHz, DMSO-d₆): δ= 165.1, 160.5, 156.9, 153.9, 150.4, 136.0, 131.3, 117.0, 113.3, 106.9, 105.2, 88.5, 84.3,

83.9, 81.2, 65.0, 55.5, 27.0, 25.3; HRMS (FAB): m/z : calcd for $C_{22}H_{25}O_8N_5Li$: 494.186, found 494.186 $[M+Li]^+$.

Octamer $[G\ 24]_8\text{-K}^+\text{-DNP}^-$ (27): A solution of **G 24** (5.0 mg, 10.3 mmol) in CH_2Cl_2 (1 mL) was added to a solution of K^+ 2,6-DNP in water (2 mL, 0.65 mM). The resulting biphasic mixture was stirred at rt for 12 h. The organic layer was then separated and concentrated. 1H NMR (400 MHz, CD_2Cl_2): δ = 12.23 (s, 8 H, NH1), 7.88 (d, 2 H, $J=8.1$ Hz, *m*DNP), 7.21 (s, 8 H, H8), 7.17 (d, 16 H, $J=2.3$ Hz, $H8^f$), 6.65 (t, 8 H, $J=2.3$ Hz, $H10^f$), 5.90 (s, 8 H, $H1'$), 5.90 (t, 1 H, $J=8.1$ Hz, *p*DNP), 5.62 (dd, 8 H, $J=6.3, 2.9$ Hz, $H3^f$), 5.24 (d, 8 H, $J=6.3$ Hz, $H2'$), 4.88 (dd, 8 H, $J=14.1, 8.5$ Hz, $H5^f_A$), 4.80-4.74 (m, 16 H, $H4^f, H5^f_B$), 3.80 (s, 48 H, OCH_3), 1.68 (s, 24 H, CH_3), 1.44 (s, 24 H, CH_3).

Hexadecamer $[G\ 24]_{16}\text{-4 K}^+\text{-4 DNP}^-$ (28): A K^+ 2,6-DNP solution in water (1 mL, 10.3 mM) was added to a solution of **G 24** (5.0 mg, 10.3 mmol) in CH_2Cl_2 (1 mL). The resulting biphasic mixture was stirred at rt for 12 h. The organic layer was then separated and concentrated. The designations a (outer G-quartet) and b (inner G-quartet) in the 1H NMR data refer to the two sets of signals for the hexadecamer. 1H NMR (400 MHz, CD_2Cl_2): δ = 11.76 (s, 8 H, NH1a), 11.70 (s, 8 H, NH1b), 9.72 (s, 8 H, $NH_{2A}a$), 9.56 (br s, 8 H, $NH_{2A}b$), 7.86 (d, 8 H, $J=7.6$ Hz, *m*DNP), 7.17 (s, 8 H, H8b), 6.97 (s, 8 H, H8a), 6.94 (s, 8 H, $NH_{2B}b$), 6.81 (d, 16 H, $J=2.2$ Hz, $H8^f_b$), 6.80 (d, 16 H, $J=2.2$ Hz, $H8^f_a$), 6.55 (t, 8 H, $J=2.0$ Hz, $H10^f_a$), 6.33 (br s, 8 H, $NH_{2B}a$), 6.26 (t, $J=2.0$ Hz, $H10^f_b$), 5.95 (dd, 8 H, $J=5.9, 3.5$ Hz, $H2^f_b$), 5.90 (t, 4 H, $J=7.6$ Hz, *p*DNP), 5.85 (s, 8 H, $H1^f_b$), 5.74 (dd, 8 H, $J=6.3, 2.4$ Hz, $H3^f_b$), 5.53 (d, 8 H, $J=3.5$ Hz, $H1^f_a$), 5.33 (br s, 8 H, $H2^f_b$), 5.23 (d, 8 H,

$J=5.9$ Hz, H3'a), 5.04 (t, 8 H, $J=10.2$ Hz, H5'A_b), 4.79-4.68 (m, 16 H, H4'a, H4'b), 4.54 (dd, 8 H, $J=11.0, 8.4$ Hz, H5'A_a), 4.34 (m, 8 H, H5'B_b), 4.17 (dd, 8 H, $J=11.0, 4.1$ Hz, H5'_{Ba}), 3.74 (s, 48 H, OCH_{3a}), 3.38 (s, 48 H, OCH_{3b}), 1.77 (s, 24 H, CH_{3a}), 1.65 (s, 24 H, CH_{3b}), 1.50 (s, 24 H, CH_{3a}), 1.43 (s, 24 H, CH_{3b}).

Octamer [G 29]₈-2 Na⁺-2 pic⁻ (31): Na⁺Pic⁻ (2.0 mg, 8.0 mmol) was added to a solution of G 29 (5.0 mg, 13.7 mmol) in CH₂Cl₂ (1 mL). The resulting suspension was stirred at rt for 12 h. After centrifuging, the organic layer was decanted and concentrated. ¹H NMR (400 MHz, CDCl₃): δ = 11.86 (s, 4 H, NH1), 8.58 (s, 2 H, picrate), 7.12 (s, 4 H, H8), 5.86 (s, 4 H, H1'), 5.39 (dd, 4 H, $J=5.4, 3.4$ Hz, H3'), 5.25 (d, 4 H, $J=5.4$ Hz, H2'), 4.63 (dd, 4 H, $J=10.8, 5.9$ Hz, H5'A), 4.58 (ddd, 4 H, $J=6.9, 5.9, 3.4$ Hz, H4'), 4.41 (dd, 4 H, $J=10.8, 6.9$ Hz, H5'B), 2.23 (s, 12 H, Ac), 1.62 (s, 12 H, CH₃), 1.42 (s, 12 H, CH₃).

Octamer [G 29]₈-Na⁺-pic⁻ (33): A Na⁺Pic⁻ solution in water (2 mL, 0.6 mM) was added to a solution of G 29 (5.0 mg, 13.7 mmol) in CH₂Cl₂ (1 mL). The biphasic mixture was stirred at rt for 12 h. The organic layer was then separated and concentrated. ¹H NMR (400 MHz, CDCl₃): δ = 12.38 (s, 8 H, NH1), 9.66 (s, 8 H, NH_{2A}), 8.85 (s, 2 H, picrate), 7.10 (s, 8 H, H8), 6.21 (s, 8 H, NH_{2B}), 5.85 (s, 8 H, H1'), 5.25 (dd, 8 H, $J=5.9, 3.4$ Hz, H3'), 5.25 (d, 8 H, $J=5.9$ Hz, H2'), 4.64 (dd, 8 H, $J=10.3, 5.9$ Hz, H5'A), 4.58 (ddd, 8 H, $J=6.9, 5.9, 3.4$ Hz, H4'), 4.42 (dd, 8 H, $J=10.3, 6.9$ Hz, H5'B), 2.21 (s, 24 H, Ac), 1.61 (s, 24 H, CH₃), 1.38 (s, 24 H, CH₃).

[8-²H]guanosine G 36. A suspension of guanosine (5.0 g) in 100 mL of 99.9% D₂O was

refluxed under N₂ for 15 h. The product, which separated as a crystalline solid upon cooling, was collected and washed with water to give 4.61 g (92%) of [8-²H]guanosine **36**. The intensity of the H8 singlet at δ 7.85 in the ¹H NMR spectrum was reduced to 2 % of that of the H1' singlet at δ 5.66, corresponding to 98 % deuterium incorporation at C8.

2',3'-O-isopropylidene-5'-*t*-butyl-dimethylsilyl-[8-²H]guanosine G 35-*d*. To a suspension of [8-²H]guanosine **36** (1.00 g, 3.53 mmol) in acetone (100 mL) was added *p*-TsOH-H₂O (1.34 g, 7.06 mmol) and 2,2-dimethoxypropane (4.42 g, 42.4 mmol). The resulting solution was stirred for 3 h at rt. Triethylamine (1.07 g, 10.6 mmol) was added to neutralize the solution. A precipitate formed, and the solvent was removed *in vacuo*. To a suspension of the residue and imidazole (0.41 g, 6.0 mmol) in CH₂Cl₂ (40 ml) was added *t*-butyl dimethylsilyl chloride (0.91 g, 6.0 mmol). The reaction mixture was stirred for 20 h, after which time TLC analysis indicated the reaction was complete. The reaction mixture was washed with 0.1 N HCl, sat NaHCO₃ and sat NaCl and concentrated *in vacuo*. Crystallization from isopropanol gave G **35-*d*** as a white solid (0.803 g, 52 %). It was important to be cautious in the recrystallization process since vigorous heating in isopropanol leads to the reprotonation of the C8 position. ¹H NMR (400 MHz, CD₂Cl₂): δ 12.08, (s, 1H, NH1), 6.58 (s, 2H, N2), 5.99 (d, 1H, H1', J = 2.0 Hz), 5.15 (dd, 1H, H2', J = 2.2, 6.0 Hz), 4.91 (dd, 1H, H3', J = 2.7, 6.0 Hz), 4.33 (m, 1H, H4', J = 2.7 Hz, 10.0 Hz), 3.78 (m, 2H, H5', H5'', J = 6.0, 10.0 Hz, 6.0 Hz), 1.38 (s, 3H, CH₃), 1.28 (s, 3H, CH₃), 0.89 (s, 9H, *t*-Bu), 0.01 (s, 3H, Si (CH₃)), 0.00 (s, 3H, Si (CH₃)).

Hexadecamer of the Deuterated G-quadruplex [G 35-*d*]₁₆ • 2Ba²⁺ • 4DNP⁻. A

suspension of G **35-d** (100 mg, 229 μmol) in 5 mL of CHCl_3 was stirred with a solution BaDNP_2 solution in water (5 mL, 6 mM) at rt for 5 h. The organic layer was separated and dried under vacuum. The residue was dissolved in 1 mL of CHCl_3 and 4 mL of CH_3CN . The resulting clear solution was allowed to evaporate slowly at rt in a N_2 -filled desiccator. Yellow, needle-like crystals of $[\text{G } \mathbf{35-d}]_{16} \cdot 2\text{Ba}^{2+} \cdot 4\text{DNP}^-$ formed after 2 days. The ^1H NMR spectrum for this deuterated complex was identical to that for the isotopomer $[\text{G } \mathbf{8-h}]_{16} \cdot 2\text{Ba}^{2+} \cdot 4\text{DNP}^-$,⁵⁸ except that the H8 signals were reduced to < 3 % relative intensity, indicating that the complex was > 97 % deuterated. The a (outside layer) and b (inside layer) designations refer to the 2 sets of signals observed for this D_4 -symmetric hexadecamer. ^1H NMR (400 MHz, CD_2Cl_2): δ 11.32 (s, 1H, NH1_a), 11.01 (s, 1H, NH1_b), 9.65 (s, 1H, N2 H_{Aa}), 8.72 (s, 1H, N2 H_{Ab}), 8.11 (s, 1H, N2 H_{Bb}), 8.10 (d, 2H, DNP anion *m*-H, $J = 8.1$ Hz), 6.48 (s, 1H, $\text{H1}'_a$), 6.25 (t, 1H, anion *p*-H, $J = 8.1$ Hz), 6.17 (d, 1H, $\text{H2}'_a$, $J = 6.0$ Hz), 5.85 (s, 1H, N2 H_{Ba}), 5.83 (t, 1H, $\text{H2}'_b$, $J = 4.0$ Hz), 5.56 (d, 1H, $\text{H1}'_b$, $J = 3.7$ Hz), 4.80 (d, 1H, $\text{H3}'_a$, $J = 6.0$ Hz), 4.28-4.16 (m, 4H, $\text{H4}'$, $\text{H5}'$), 3.64 (d, 1H, $\text{H3}'_b$, $J = 6.4$ Hz), 3.62 (d, 1H, $\text{H5}'_b$, $J = 9.3$ Hz), 3.19-3.11 (m, 2H, $\text{H5}'$), 1.58 (s, 3H, CH_{3a}), 1.56 (s, 3H, CH_{3b}), 1.53 (s, 3H, CH_{3b}), 1.27 (s, 3H, CH_{3a}), 0.87 (s, 9H, Si-*t*Bu_a), 0.55 (s, 9H, Si-*t*Bu_b), 0.17 (s, 3H, Si- CH_{3a}), 0.15 (s, 3H, Si- CH_{3b}), -0.34 (s, 3H, Si- CH_{3b}), -0.37 (s, 3H, Si- CH_{3a}).

2',3'-O-isopropylidene-5'-triisopropylsilyl-guanosine G 45. To a suspension of the 2',3'-O-isopropylidene-guanosine **25** (2.68 g, 8.58mmol) and imidazole (1.0 g, 14.5 mmol) in DMF (150 ml) was added triisopropylsilyl chloride (2.10 g, 10.9 mmol). The reaction mixture was stirred for 20 h, after which time TLC analysis indicated the

reaction was complete. The reaction mixture was concentrated and the residue was redissolved in CH₂Cl₂. The solution was washed with 0.1 N HCl, sat NaHCO₃ and sat NaCl and concentrated *in vacuo*. Crystallization from isopropanol gave TIPS-G **45** as a white solid (1.16 g, 28 %). ¹H NMR (400 MHz, DMSO-d₆): δ 10.68 (s, 1H, NH1), 7.81 (s, 1H, H8), 6.52 (s, 2H, N2), 5.98 (d, 1H, H1', J = 1.8 Hz), 5.23 (dd, 1H, H2', J = 1.8, 6.0 Hz), 5.02 (dd, 1H, H3', J = 3.5, 6.0 Hz), 4.11 (m, 1H, H4'), 3.78 (d, 1H, H5', J = 2.5 Hz), 3.76 (d, 1H, H5'', J = 1.5 Hz), 1.50 (s, 3H, CH₃), 1.30 (s, 3H, CH₃), 0.94 (m, 21H, *i*Pr-Si). δ = 156.6, 153.6, 150.4, 135.8, 116.8, 112.9, 88.2, 87.3, 83.6, 80.8, 63.8, 28.9, 25.2, 17.6, 17.6, 11.2. ESI-MS: *m/z*: calcd for C₂₂H₃₈O₅N₅Si: 480.2462, found 480.2491 [*M*+H]⁺.

Hexadecamer of the G-quadruplex [TIPS-G **45**]₁₆ • 2Ba²⁺ • 4DNP⁻. A suspension of TIPS-G **45** (100 mg, 208 μmol) in 5 mL of CH₂Cl₂ was stirred with a solution BaDNP₂ solution in water (5 mL, 6 mM) at rt for 24 h. The organic layer was separated and dried under vacuum. The residue was dissolved in 1 mL of CH₂Cl₂ and 4 mL of CH₃CN. The resulting yellow solution was allowed to evaporate slowly at rt in a N₂-filled desiccator. Yellow, needle-like crystals of [G **45**]₁₆ • 2Ba²⁺ • 4DNP⁻ formed after 2 days. The a (outside layer) and b (inside layer) designations refer to the 2 sets of signals observed for this D₄-symmetric hexadecamer. ¹H NMR (400 MHz, CD₂Cl₂)*: δ 11.24 (s, 1H, NH1_a), 10.96 (s, 1H, NH1_b), 9.57 (s, 1H, N2 H_{Aa}), 8.64 (s, 1H, N2 H_{Ab}), 8.12 (s, 1H, N2 H_{Bb}), 8.10 (d, 2H, DNP anion *m*-H, J = 8.5 Hz), 7.83 (s, 1H, H8_a), 7.07 (s, 1H, H8_b), 6.59 (s, 1H, H1'_a), 6.20 (t, 1H, anion *p*-H, J = 8.5 Hz), 6.11 (d, 1H, H2'_a, J = 5.5 Hz), 5.70 (t, 1H, H2'_b, J = 4.3 Hz), 5.50 (d, 1H, H1'_b, J = 1.8 Hz), 5.44 (s, 1H, N2 H_{Ba}), 4.82 (d, 1H, H3'_a, J = 4.9 Hz), 4.26-4.17 (m, 3H, H4'_a, H5'_b, H5''_b), 4.10 (t, 1H, H4'_b, J = 11.6 Hz), 3.82 (d,

1H, H3'_b, J = 11.6 Hz), 3.21 (dd, 1H, H5'_a, J = 7.3, 9.7 Hz), 3.10 (dd, 1H, H5''_a, J = 6.0, 9.7 Hz), 1.60 (s, 3H, CH_{3a}), 1.56 (s, 3H, CH_{3b}), 1.50 (s, 3H, CH_{3a}), 1.31 (s, 3H, CH_{3b}), 1.10 (s, 21H, *i*Pr-Si_a), 0.74 (s, 21H, *i*Pr-Si_b), 0.17 (s, 3H, Si-CH_{3a}), 0.15 (s, 3H, Si-CH_{3b}), -0.34 (s, 3H, Si-CH_{3b}), -0.37 (s, 3H, Si-CH_{3a}).

* The two different layers, a and b, were distinguished by COSY, HMBC, and HSQC 2D NMR experiments. Layer a and layer b were distinguished to be outer and inner layers respectively by 2D NOESY experiments shown in **Figure 6.1**.

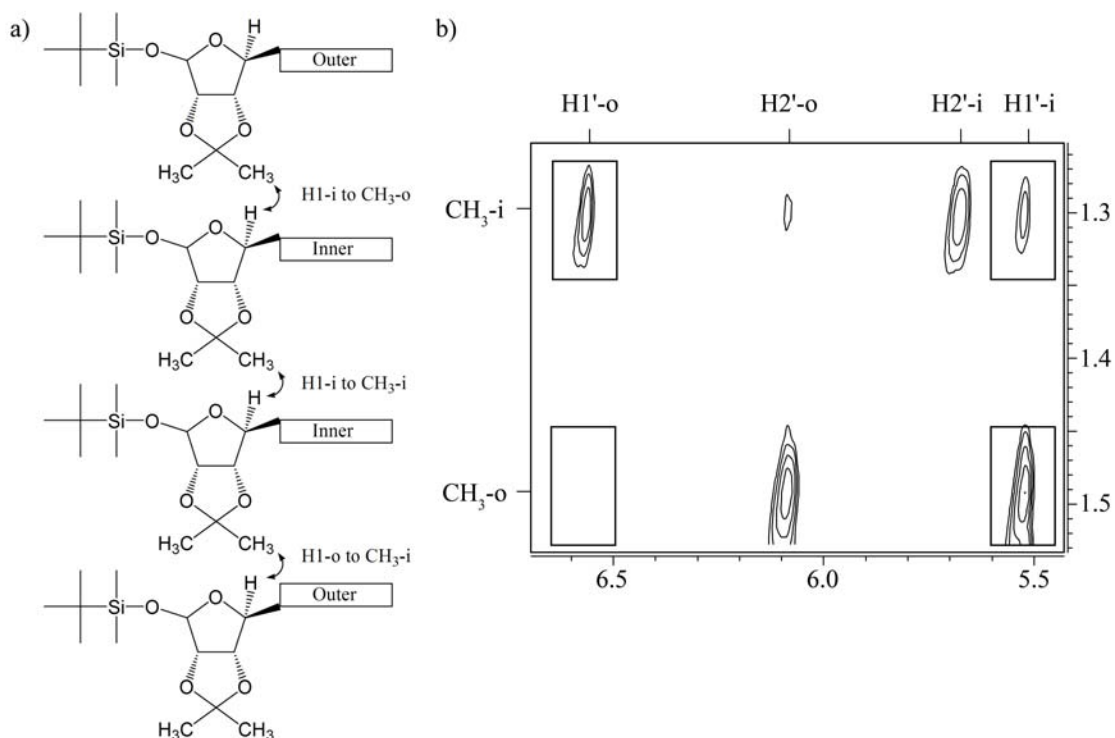


Figure 6.1. a) Schematic of G-quadruplex with a focus on the sugar moiety. b) Selected region of ¹H-¹H NOESY spectrum at 400 MHz of G-quadruplex TIPS-G **45**]₁₆ • 2Ba²⁺ • 4DNP⁻. The signal for inner CH₃ has NOE's to both the inner and outer H1' signals, while the outer CH₃ only has an NOE to the inner H1'.⁵³

8-bromo-2',3'-O-isopropylidene-5'- *t*-BDMS-guanosine 55. To a solution of G **54** (2.4 g, 6.0 mmol) and imidazole (0.61 g, 8.0 mmol) in DMF (100 mL) was added *t*-

butyldimethylsilylchloride (1.4 g, 9.0 mmol). The reaction mixture was stirred at rt under N₂ for 8 h. The mixture was poured into water (1 L) and filtered to yield 0.57 mg (73 %) of a white precipitate. ¹H NMR (400 MHz, DMSO-d₆) δ 10.86 (s, 1 H, N1 H), 6.65 (br s, 2 H, N2 H2), 5.89 (d, 1 H, H1', J = 0.59 Hz), 5.47 (dd, 1 H, H2', J = 6.26, 0.59 Hz), 5.13 (dd, 1 H, H3', J = 6.26, 3.52 Hz), 4.07 (ddd, 1 H, H4', J = 5.48, 3.52, 2.54 Hz), 3.69 (d, 1 H, H5'a, J = 5.48 Hz), 3.65 (d, 1 H, H5'b, J = 2.54 Hz), 1.49 (s, 3 H, CH₃), 1.31 (s, 3 H, CH₃), 0.75 (s, 9 H, Si-*t*-butyl), -0.14 (s, 3 H, Si-CH₃), -0.16 (s, 3 H, Si-CH₃); ¹³C NMR (125.77 MHz, DMSO-d₆): δ= 155.4, 153.6, 151.3, 150.5, 112.9, 88.3, 86.9, 82.9, 80.9, 63.4, 26.9, 25.6, 25.3, 17.9, -5.6, -5.7. ESI-MS, calcd for C₁₉H₃₁BrN₅O₅Si [M+H]⁺: 516.1278, found: 516.1273.

N2-(4-pentenyl)-8-bromo-2',3'-O-isopropylidene-5'-*t*-BDMS-guanosine 56. This reaction was conducted similarly to previously known transformations as described by Sako *et al.*³⁰⁷ To a solution of **55** (4 g, 7.8 mmol) and 4-pentanal (2.5 mL, 31 mmol) in 1:1 H₂O-MeOH (300 mL) was added sodium cyanoborohydride (2.9 g, 46.5 mmol). The reaction mixture was stirred at 50 °C under N₂ for 8 h (Reaction beyond this period gave N2 dialkylation). After removal of the solvent, 200 mL of H₂O was added and the pH was adjusted to 7.0. After extraction with CH₂Cl₂, the organic layer was washed with sat. NaHCO₃, 0.1 N HCl, and water. Following evaporation of the solvent, the resulting brown solid was purified by flash chromatography (2 % MeOH in CH₂Cl₂) to give 3.0 g (67 %) of a white solid. ¹H NMR (400 MHz, DMSO-d₆) δ 10.77 (s, 1 H, N1 H), 6.65 (br s, 1 H, N2 H), 5.91 (d, 1 H, H1', J = 1.17 Hz), 5.81 (ddt, 1 H, H13, J = 17.22, 10.37, 6.65 Hz), 5.68 (dd, 1 H, H2', J = 6.26, 1.17 Hz), 5.03 (dq, 1 H, H14a, J = 17.22, 1.96 Hz), 4.96

(dq, 1 H, H14b, J = 10.33, 2.15 Hz), 4.96 (dd, 1 H, H3', J = 6.65, 3.33 Hz), 4.07 (dt, 1 H, H4', J = 6.65, 3.33 Hz), 3.62 (d, 2 H, H5', J = 6.65 Hz), 3.19 (m, 2 H, H10), 2.07 (m, 2 H, H12), 1.64 (p, 2 H, H11, J = 7.24 Hz) 1.51 (s, 3 H, CH₃), 1.30 (s, 3 H, CH₃), 0.76 (s, 9 H, Si-*t*-butyl), -0.11 (s, 3 H, Si-CH₃), -0.14 (s, 3 H, Si-CH₃); ¹³C NMR (125.77 MHz, DMSO-d₆): δ= 155.5, 151.8, 149.1, 148.2, 138.7, 114.6, 113.0, 112.7, 87.0, 86.8, 82.7, 80.8, 63.5, 52.9, 31.0, 27.0, 26.0 25.8, 25.3, 18.0, -5.5, -5.6. ESI-MS, calcd for C₂₄H₃₉BrN₅O₅Si [M+H]⁺: 584.1904, found: 584.2024.

N2-(4-pentenyl)-8-vinyl-2',3'-O-isopropylidene-5'- *t*-BDMS guanosine 51. This reaction was conducted as described by Sessler.³²⁰ To a solution of **56** (1 g, 7.8 mmol) and vinyltributyltin (1.25 mL, 4.3 mmol) in freshly distilled toluene (30 mL, 3 freeze-pump thaw cycles) was added tetrakis(triphenyl-phosphine)palladium(0) (0.32 g, 0.27 mmol). The mixture was stirred at reflux under N₂ for 24 h. The solvent was removed and the residue redissolved in CH₂Cl₂. The organic layer was washed with sat. NaHCO₃, 0.1 N HCl, and water. Following evaporation of the solvent, the resulting solid was purified by flash chromatography (1:2:98 NEt₃-MeOH-CH₂Cl₂) to give 0.35 g (38 %) of a white solid. ¹H NMR (400 MHz, DMSO-d₆) δ 10.85 (br s, 1 H, N1 H), 6.87 (dd, 1 H, H15, J = 17.02, 11.15 Hz), 6.76 (br s, 1 H, N2 H), 6.14 (dd, 1 H, H16a, J = 17.02, 1.76), 6.08 (d, 1 H, H1', J = 1.96 Hz), 5.80 (ddt, 1 H, H13, J = 17.22, 10.37, 6.65 Hz), 5.60 (dd, 1 H, H2', J = 6.26, 1.96 Hz), 5.46 (dd, 1 H, H16b, J = 11.15, 1.76 Hz), 5.02 (dq, 2 H, H14a, J = 17.22, 1.76 Hz), 4.96 (m, 1 H, H14b, H3'), 4.08 (dt, 1 H, H4', J = 6.06, 3.52 Hz), 3.62 (d, 2 H, H5', J = 6.06 Hz), 3.21 (m, 2 H, H10), 2.06 (m, 2 H, H12), 1.62 (p, 2 H, H11, J = 7.24 Hz) 1.51 (s, 3 H, CH₃), 1.30 (s, 3 H, CH₃), 0.78 (s, 9 H, Si-*t*-butyl), -0.09

(s, 3 H, Si-CH₃), -0.11 (s, 3 H, Si-CH₃; ¹³C NMR (125.77 MHz, DMSO-d₆): δ=156.6, 152.2, 150.6, 144.0, 137.7, 123.7, 120.0, 115.2, 115.1, 113.0, 88.0, 86.7, 82.4, 81.0, 62.8, 30.5, 27.8, 26.7, 25.6, 25.4, 24.9, 17.8, -5.6, -5.8. ESI-MS, calcd for C₂₆H₄₂N₅O₅Si [M+H]⁺: 532.2955, found: 532.3411.

G-quadruplex [G 51]₈ • Ba²⁺ • DNP⁻. To a solution of G **51** (100 mg, 0.19 mmol) in CH₂Cl₂ (20 mL) was added barium 2,6-dinitrophenolate, Ba²⁺(DNP⁻)₂, (50.35 mg, 0.10 mmol). The resulting mixture was stirred at rt for 24 h. After centrifuging, the organic layer was separated and concentrated to give an orange solid. ¹H NMR (400 MHz, CDCl₃)*: δ= 12.27 (s, 8 H, NH1), 10.27 (s, 8 H, NH_{2A}), 8.01 (d, 4H, DNP anion *m*-H, J = 8.1 Hz), 6.77 (dd, 8 H, , J=17.2, 11.4 Hz, H15), 6.40 (d, 8 H, J= 17.2 Hz, H16a), 6.05 (d, 8 H, J=2 Hz, H1'), 5.78 (m, 10 H, H13, DNP anion *p*-H), 5.54 (d, 8 H, J=9.95 Hz, H16b), 5.54 (m, 8 H, H2'), 4.98 (dd, 24 H, H14, H3'), 4.19 (dt, 8 H, J=5.2, 3.3 Hz, H4'), 3.71 (m, 16 H, H5'_A), 3.38 (m, 16 H, H10), 2.12 (dt, 16 H, J=7.5, 6.6 Hz, H12), 1.75 (p, 16 H, J=7.5 Hz, H11), 1.58 (s, 24 H, CH₃), 1.35 (s, 24 H, CH₃), 0.84 (s, 72 H, Si-*t*Bu), -0.02 (s, 48 H, Si-CH₃).

* The COSY shown in **Figure 6.2** was used to identify the proton signals for the NOE experiment.

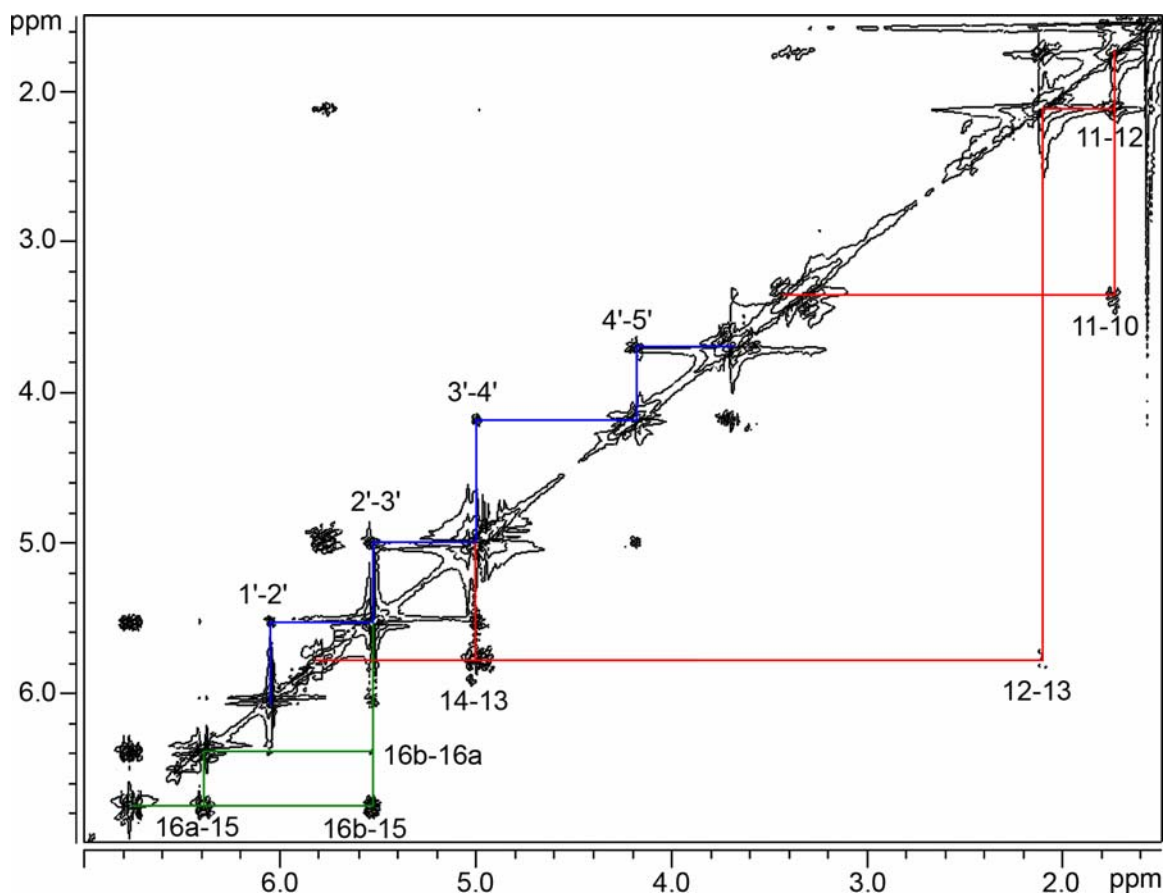


Figure 6.2. Selected region of 2D COSY spectrum of sample of G-quadruplex [G **51**]₈ • Ba²⁺•DNP⁻.

N²-(4-pentenyl)-8-(1-(*E*)-propenyl)-2',3'-O-isopropylidene-5'-*t*-butyldimethylsilyl-guanosine **58.** To a solution of **56** (1 g, 1.7 mmol) and allyltributyltin (1.35 mL, 4.3 mmol) in freshly distilled toluene (30 mL, 3 freeze-pump thaw cycles) was added tetrakis(triphenyl-phosphine)palladium(0) (0.32 g, 0.27 mmol). The resulting solution was stirred at reflux under a N₂ atmosphere for 24 h. The solvent was subsequently removed and the residue was redissolved in CH₂Cl₂. The organic layer was washed with sat. NaHCO₃, 0.1 N HCl, and water. Following evaporation of the solvent, the resulting solid was purified by flash chromatography (1:2:98 NEt₃-MeOH-CH₂Cl₂) to give a white precipitate **58** (170 mg, 18 %). ¹H NMR (*d*₆-DMSO) δ 10.85 (br s, 1H, N1H), 6.65 (dd,

1H, H16, J = 15.26, 6.46 Hz), 6.55 (dd, 1H, H15, J = 15.26, 1.17), 6.53 (br s, 1H, N2H), 6.04 (d, 1H, H1', J = 0.98 Hz), 5.81 (ddt, 1H, H13, J = 17.22, 10.37, 6.65 Hz), 5.68 (dd, 1H, H2', J = 6.26, 0.98 Hz), 5.03 (dq, 1H, H14a, J = 17.22, 1.76 Hz), 4.96 (m, 2H, H14b, H3'), 4.06 (dt, 1H, H4', J = 6.06, 3.52 Hz), 3.58 (d, 2H, H5', J = 6.06 Hz), 3.20 (m, 2H, H10), 2.07 (m, 2H, H12), 1.89 (dd, 3H, H17, J = 6.46, 1.17 Hz) 1.65 (m, 2H, H11) 1.50 (s, 3H, CH3), 1.30 (s, 3H, CH3), 0.77 (s, 9H, Si-*t*-butyl), -0.10 (s, 3H, Si-CH3), -0.13 (s, 3H, Si-CH3); HRMS, calcd for C₂₇H₄₄N₅O₅Si [M+H]⁺: 546.3112, found: 546.3126.

3,5-bis(allyloxy) benzoic acid chloride 65. Thionyl chloride (10.93 ml, 56.3 mmol) was added to a solution of 3,5-bis(allyloxy) benzoic acid **64**³¹² (1.10 g, 4.7 mmol) in distilled toluene and the resulting mixture was refluxed for 2.5 h. The solvent was evaporated under reduced pressure to give a green solid, which was immediately used without purification.

2',3'-isopropylidene-5'-(3,5-bis(allyloxy)benzoyl)- guanosine (G 59). To a solution of 2',3'-O-isopropylidene guanosine⁵⁸ (970 mg, 3.0 mmol) and 4-dimethylaminopyridine (10 mg) in distilled pyridine (15 mL) was added 3,5-bis(allyloxy) benzoyl acid chloride **65** (1.10 g, 4.35 mmol). The resulting solution was stirred at rt under a N₂ atmosphere for 4 h. The solvent was evaporated under reduced pressure. The remaining white solid was dissolved in CH₂Cl₂ (100 mL) and washed with 0.1 N HCl (10 mL), sat NaHCO₃ (3 x 10 mL), and H₂O (3 x 10 mL). After removal of the solvent, trituration with *i*-Pr₂O gave a solid that was purified by flash chromatography (5 % MeOH in CH₂Cl₂) to give G **59** (1.05 g, 72%). ¹H NMR (400 MHz, DMSO-*d*₆): δ 10.79 (s, 1H, N1H), 7.82 (s, 1H, H8),

7.02 (d, 2H, H8', J = 2.3 Hz), 6.81 (t, 1H, H10', J = 2.3 Hz), 6.59 (br s, 2H, NH₂), 6.05 (s, 1H, H1'), 6.01 (ddt, 2H, H12', J = 17.3, 10.5, 5.0), 5.38 (ddd, 2H, H13', J = 17.3, 3.4, 1.0 Hz), 5.25 (m, 1H, H3'), 5.25 (m, 1H, H2'), 5.25 (ddd, 2H, H13'', J = 10.5, 3.4, 1.5 Hz), 4.59 (ddd, 4H, H11', J = 5.0, 1.5, 1.0 Hz), 4.42 (m, 2H, H5'), 4.40 (m, 1H, H4'), 1.52 (s, 3H, CH₃), 1.32 (s, 3H, CH₃); ¹³C NMR (100 MHz, DMSO-d₆): δ 165.0, 159.3, 156.7, 153.8, 150.4, 136.1, 133.4, 131.2, 117.7, 117.0, 113.3, 107.8, 106.6, 88.5, 84.3, 83.9, 81.2, 68.5, 65.0, 27.0, 25.3; HRMS (FAB) [M+H]⁺ calcd for C₂₆H₃₀N₅O₈ 540.2094, found 540.2069.

G-quadruplex 60 [G 59]₁₆·4K⁺·4DNP⁻: To a solution of G 59 (200 mg, 0.37 mmol) in CH₂Cl₂ (20 mL) was added potassium 2,6-dinitrophenolate (K⁺DNP⁻) (40 mg, 0.18 mmol). The resulting mixture was stirred at rt for 24 h. After centrifuging, the organic layer was separated and concentrated to give an orange solid. The a (outside layer) and b (inside layer) designations refer to the 2 sets of signals observed for this D₄-symmetric hexadecamer. ¹H NMR (400 MHz, CD₂Cl₂): δ 11.87 (s, 8H, NH1_a), 11.75 (s, 8H, NH1_b), 9.77 (s, 8H, N2 H_{Aa}), 9.62 (br s, 8H, N2 H_{Ab}), 7.97 (br s, 8H, DNP anion *m*-H), 7.25 (br s, 8H, N2 H_{Bb}), 7.21 (s, 8H, H8_b), 7.03 (br s, 8H, H8_a), 7.00 (d, 16H, H8'_b, J = 2.0 Hz), 6.90 (d, 16H, H8'_a, J = 2.0 Hz), 6.62 (t, 8H, H10'_b, J = 2.0 Hz), 6.41 (t, 8H, H10'_a, J = 2.0 Hz), 6.50 (dq, 8H, H12'_a, J = 5.0, 17.3 Hz), 5.96-5.81 (m, 36H, H12'_b, H2'_b, H1'_b, H3'_b, *p*-DNP), 5.53 (d, 8H, H1'_a, J = 3.0 Hz), 5.45-5.29 (m, 32H, H2'_a, H3'_a, H13'), 5.07 (t, 8H, H5'_{Ab}, J = 7.8 Hz), 4.76 (m, 8H, H4'_b), 4.62-4.42 (m, 24H, H5'_{Aa}, H11'), 4.15 (dd, 8H, H5'_{Bb}, J = 5.5, 12.8 Hz), 4.0 (dd, 4H, H5'_{Ba}, J = 4.3, 11.3 Hz), 1.78 (s, 3H, CH_{3a}), 1.69 (s, 3H, CH_{3b}), 1.54 (s, 3H, CH_{3b}), 1.50 (br s, 3H, CH_{3a}).

Unimolecular G-quadruplex 61. To a solution of precursor G-quadruplex **60** (80 mg, 0.0068 mmol) in distilled, degassed CH₂Cl₂ (90 mL) was added Grubb's second-generation catalyst ((H₂IMes)(PCy₃)(Cl₂)Ru=CHPh) (9.3 mg, 0.011 mmol, 5 mol% per alkene).³¹⁰ The resulting solution was stirred at 35 °C under a N₂ atmosphere for 48 h. The resulting solution was then washed with 0.1 N HCl (10 mL), sat NaHCO₃ (3 x 10 mL), and H₂O (3 x 10 mL). After removal of the solvent, the black solid was purified by flash chromatography (5 % MeOH in CH₂Cl₂) to give G-quadruplex **61** as an off-white solid (32 mg, 57%). ¹H NMR (400 MHz, DMSO-d₆): δ10.78 (br s, 1H, N1H), 7.81 (s, 1H, H8), 6.88 (d, 2H, H8', J = 1.6 Hz), 6.65 (t, 1H, H10', J = 1.6 Hz), 6.60 (br s, 2H, NH₂), 6.05 (d, 1H, H1', J = 1.6 Hz), 5.71 (br s, 2H, H12'), 5.26 (dd, 1H, H2', J = 1.6, 6.3 Hz), 5.22 (dd, 1H, H3', J = 3.0, 6.3 Hz), 4.73 (br s, 1H, H11'), 4.45-4.33 (m, 3H, H4', H5', H5''), 1.52 (s, 3H, CH₃), 1.32 (s, 3H, CH₃); ESI-MS [M+3K]³⁺ calcd for C₃₈₄H₄₀₀K₃N₈₀O₁₂₈ 2766.5, found. 2766.3.

3,5-bis(but-3-enyloxy) benzoic acid chloride 69. Thionyl chloride (10.93 ml, 56.3 mmol) was added to a solution of 3,5-bis(but-3-enyloxy) benzoic acid **68**³¹³ (1.23 g, 4.7 mmol) in distilled toluene and the resulting mixture was refluxed for 2.5 h. The solvent was evaporated under reduced pressure to give a green solid, which was immediately used without purification.

2',3'-isopropylidene-5'-(3,5-bis(but-3-enyloxy)benzoyl)- guanosine (G 66). To a solution of 2',3'-O-isopropylidene guanosine⁵⁸ (970 mg, 3.0 mmol) and 4-

dimethylaminopyridine (10 mg) in distilled pyridine (15 mL) was added 3,5-bis(*but*-3-enyloxy) benzoyl acid chloride **69** (1.22 g, 4.35 mmol). The resulting solution was stirred at rt under a N₂ atmosphere for 4 h. The solvent was evaporated under reduced pressure. The remaining white solid was dissolved in CH₂Cl₂ (100 mL) and washed with 0.1 N HCl (10 mL), sat NaHCO₃ (3 x 10 mL), and H₂O (3 x 10 mL). After removal of the solvent, trituration with *i*-Pr₂O gave a solid that was purified by flash chromatography (5 % MeOH in CH₂Cl₂) to give G **66** (1.60 g, 94%). ¹H NMR (400 MHz, DMSO-d₆): δ 10.69 (s, 1H, N1H), 7.82 (s, 1H, H8), 6.99 (d, 2H, H8', J = 2.3 Hz), 6.76 (t, 1H, H10', J = 2.3 Hz), 6.55 (br s, 2H, N2H), 6.05 (s, 1H, H1'), 5.87 (ddt, 2H, H13', J = 17.4, 10.6, 6.6), 5.24 (m, 2H, H2', H3'), 5.15 (dq, 2H, H14', J = 17.4, 1.7 Hz), 5.07 (dq, 2H, H14'', J = 10.6, 2.0 Hz), 4.44 (m, 3H, H4',H5'), 4.03 (t, 4H, H11', J = 6.6 Hz), 2.46 (m, 4H, H12'), 1.52 (s, 3H, CH₃), 1.32 (s, 3H, CH₃); ¹³C NMR (125.77 MHz, DMSO-d₆): δ 165.5, 159.6, 156.6, 153.6, 150.3, 136.0, 134.7, 131.1, 117.0, 116.9, 113.2, 107.5, 106.0, 88.4, 84.3, 83.8, 81.2, 70.0, 64.9, 26.9, 25.3; HRMS (FAB) [M+H]⁺ calcd for C₂₈H₃₄N₅O₈ 568.2407, found 568.2388.

G-quadruplex 28 [G 66]₁₆·4K⁺·4DNP⁻: To a solution of G **66** (213 mg, 0.37 mmol) in CH₂Cl₂ (20 mL) was added potassium 2,6-dinitrophenolate (Na⁺BPh₄⁻) (65 mg, 0.19 mmol). The resulting mixture was stirred at rt for 24 h. After centrifuging, the organic layer was separated and concentrated to give a white solid. The ¹H NMR spectrum was consistent with G-quadruplex formation.

6.3 ESI-MS Experiments on G 29.

Electrospray mass spectra were recorded with a ZMD Micromass single quadrupole mass spectrometer, operating at m/z 4000. A Hamilton syringe driven by a Harvard pump was used for direct injection of the sample at a rate of 10 L min^{-1} ; a capillary voltage of 3.2 kV and a cone voltage of 40 V were applied, and a desolvation temperature of $120 \text{ }^\circ\text{C}$ was used. The charge of the species observed was deduced directly from the spacing of the isotope peaks, apart from the less resolved m/z 2945 signal. The space between the principal peak and the minor adjacent peak at 2961 corresponds to the mass difference between K^+ and Na^+ , indicating a monocharged species. Sample a) was prepared by a solid-liquid extraction experiment: a 5 mM chloroform solution of G 29 (2 mL, 0.01 mmol) was stirred overnight in the presence of sodium picrate (4 mg, 16 mmol), and the organic layer was then decanted. Sample b) was obtained by washing twice 1 mL of sample a with an equal amount of water: the organic phase was then recovered and injected into the mass spectrometer.

6.4 PFG-NMR Experiments.

Diffusion experiments were carried out with a Bruker DRX-500 spectrometer, using the Stimulated Echo Pulse Gradient sequence in FT mode.¹⁸⁰ To improve homogeneity a “13 interval pulse sequence” was used with two pairs of bipolar gradients.¹⁸¹ All samples for the diffusion measurements were prepared in Shigemi tubes (Shigemi, Inc., Allison Park, PA) and the temperature was actively controlled at $21.0 \pm 0.5 \text{ }^\circ\text{C}$. Diffusion coefficients were derived using integration of the desired peaks to a single exponential decay, using the “Simfit (Bruker XWINNMR v3.1)” software. The diffusion coefficients reported are

the mean \pm standard deviation at least 4 separate measurements.

Hexadecamer 22 and adenosine 23 in CD₃CN: Experiments consisted of 24 points with gradient strengths (g) ranging from 0.687-30.91 G cm⁻¹. All experiments comprised 256 scans with a pulse delay of 4 s and δ value of 2.8 ms, Δ value of 99.8 ms, and γ value of 4258 Hz per G. Quadruplex **22** and A **23** were at concentrations of 0.059 and 0.16 mM, respectively.

Guanosine 8 and adenosine 23 in DMSO-d₆: Experiments consisted of 24 points with gradient strengths (g) ranging from 0.687-30.91 G cm⁻¹. All experiments comprised 64 scans with a pulse delay of 4 s and δ value of 4.6 ms, Δ value of 199.8 ms, and γ value of 4258 Hz per G. Both G **8** and A **23** were at concentrations of 10.0 mM.

Octamer 27 and hexadecamer 28 in CDCl₃: Experiments consisted of 32 points with gradient strengths (g) ranging from 3.420-61.560 G cm⁻¹. All experiments comprised 256 scans with a pulse delay of 4 s and δ value of 2.6 ms, Δ value of 59.9 ms, and γ value of 4258 Hz per G. Octamer **27** and hexadecamer **28** were at concentrations of 0.64 and 0.32 mM, respectively.

Octamer 31, octamer 33 and adenosine 23 in CDCl₃: Experiments consisted of 24 points with gradient strengths (g) ranging from 0.687-30.91 G cm⁻¹. All experiments comprised 128 scans with a pulse delay of 4 s and δ value of 2.6 ms, Δ value of 59.8 ms, and γ value of 4258 Hz per G. Octamers (**31** and **33**) and monomer **23** were at concentrations of 1.7

and 6.4 mM, respectively.

Hexadecamer 34 and adenosine 23 in CDCl₃: Experiments consisted of 24 points with gradient strengths (g) ranging from 0.687-30.91 G cm⁻¹. All experiments comprised 128 scans with a pulse delay of 4 s and δ value of 2.6 ms, Δ value of 59.8 ms, and γ value of 4258 Hz per G. Hexadecamer **34** and monomer **23** were at concentrations of 0.52 and 4.0 mM, respectively.

G-quadruplex [G 51]₈ • Ba²⁺ and adenosine 23. Experiments consisted of measuring 24 points with gradient strengths (g) ranging from 3.420–61.560 G cm⁻¹. All experiments comprised 256 scans with a pulse delay of 4 s and δ value of 2.6 ms, Δ value of 130 ms, and γ value of 4258 Hz per G. The complex [G **51**]₈ • Ba²⁺ and the internal standard 5'-*t*-BDMS-2',3'-isopropylidene A **23** were present at concentrations of 2.0 mM and 1.1 mM, respectively.

Hexadecamer 60 and adenosine 23 in CD₂Cl₂: Experiments consisted of 24 points with gradient strengths (g) ranging from 0.687-30.91 G cm⁻¹. All experiments comprised 128 scans with a pulse delay of 4 s and δ value of 2.6 ms, Δ value of 59.8 ms, and γ value of 4258 Hz per G. Hexadecamer **60** and monomer **23** were at concentrations of 0.52 and 4.0 mM, respectively.

*G-quadruplex 61 and adenosine 23 in DMSO-*d*₆*: Experiments consisted of 24 points with gradient strengths (g) ranging from 0.687-30.91 G cm⁻¹. All experiments comprised 64

scans with a pulse delay of 4 s and γ value of 4.6 ms, δ value of 199.8 ms, and Δ value of 4258 Hz per G. Both G **61** and A **23** were at concentrations of 10.0 mM.

6.5 Determination of DNP Anion Exchange Rates.

A solution of $[G \text{ 8-h}]_{16} \cdot 4K^+ \cdot 4DNP^-$ (1 mM), $Ba(DNP)_2$ (2 mM), and 2 mM [2.2.2]cryptand, to solubilize $Ba(DNP)_2$, was prepared in 50:50% CD_2Cl_2 - CD_3CN . The coalescence point of the $[G \text{ 8-h}]_{16} \cdot 4K^+ \cdot 4DNP^-$ quadruplex was measured by observing signals for the “free” anion (7.83 ppm) and bound anion (8.11 ppm) coalesce at -8 °C. Using the difference in the frequencies of the “free” anion and the complexed anion, the coalescence rate was calculated to be 588 s^{-1} by the equation $\text{exchange rate} = 2\pi \times \Delta\nu$. The activation energy (ΔG^\ddagger) was calculated to be 12.0 kcal/mol using this equation. A solution of $[G \text{ 8-h}]_{16} \cdot 4Ba^{2+} \cdot 4DNP^-$ (1 mM), $Ba(DNP)_2$ (1 mM), and 1 mM [2.2.2]cryptand (used to solubilize $Ba(DNP)_2$) was prepared in 50:50% CD_2Cl_2 - CD_3CN . The coalescence point of the $[G \text{ 8-h}]_{16} \cdot 2Ba^{2+} \cdot 4DNP^-$ quadruplex was measured by observing signals for the “free” anion (7.83 ppm) and bound anion (8.11 ppm) coalesce at -52 °C. Using this difference in the frequencies of the “free” anion and the bound anion, the exchange rate at coalescence was calculated to be 687 s^{-1} . The ΔG^\ddagger rate was calculated to be 10.0 kcal/mol.

6.6 Liposome Preparation. Liposomes were prepared by previously published methods.²⁷⁹ High pressure extrusion was performed on the AvantiTM mini-extruder with a 0.1 μm or 0.2 μm polycarbonate membrane. EYPC was purchased from Avanti Polar Lipids. Egg yolk L- α -phosphatidylcholine (EYPC ethanol solution, 70 μL , 92 μmol)

was dissolved in CHCl_3 (3 mL), the solution was slowly evaporated under reduced pressure followed by drying under high vacuum for 2 h. The resulting thin lipid film was hydrated in 1.4 mL of 10 mM phosphate buffer for 1 h. During hydration, the suspension was submitted to 5 freeze-thaw cycles. The large multilamellar liposome suspension (1.0 mL) was submitted to high-pressure extrusion at rt (21 extrusions) through a 0.1 μm polycarbonate membrane afforded a suspension of large unicellular vesicles (LUVs) with an average diameter of 100 nm unless noted. The following LUV suspension was 65 mM lipid.

6.7 HPTS Assay.²⁷⁹

HPTS (8-hydroxypyrene-1,3,6-trisulfonic acid) is a pH sensitive dye that can be monitored by fluorescence. HPTS-loaded vesicles (100 μL of the stock solution), filled with a saline phosphate buffer (10 mM sodium phosphate, pH 6.4, 75 mM Na_2SO_4) were suspended in 1.9 mL of an corresponding phosphate sulfate buffer and placed into a fluorimetric cell. The emission of HPTS at 510 nm was monitored with excitation wavelengths at 403 and 460 nm simultaneously. During the experiment, 4 μL of a 2.5 mM DMSO solution of the compound of interest was added (through an injection port), followed by injection of 20 μL of 0.5 M aqueous NaOH. Addition of the M^+OH resulted in a pH increase of approximately 1 pH unit in the extravesicular buffer. Maximal possible changes in dye emission were obtained at the end of each experiment by lysis of the liposomes with detergent (40 μL of 5% aqueous Triton X100). The final transport trace was obtained as a ratio of the emission intensities monitored at 460 and 403 nm and normalized to 100% of transport. Li^+ and K^+ experiments were run similarly with the

exception of the respective alkali metal replacing Na⁺.

6.8 DMF-d₇ Folding-Unfolding Experiments on Unimolecular G-quadruplex 61.

Unimolecular G-quadruplex **61** • 4Na⁺ • 4BPh₄⁻ (0.5 mM) was dissolved into DMF-d₇. ¹H NMR spectra were taken at temperatures indicated. Annealing was performed through heating the sample in the NMR spectrometer to 103 °C for 0.5 h and cooling down to the desired temperature. Equilibrium studies were performed by maintaining the sample at a given temperature and obtaining ¹H NMR spectra every 0.5 h until the sample had reached equilibrium. Equilibrium was determined through the measurement of the integration for the peaks of “folded” and “unfolded” G-quadruplex.

6.9 ²³Na NMR Experiments.³²¹

Lithium filled vesicles were prepared by previously published methods.²⁷⁹ High pressure extrusion was performed on the AvantiTM mini-extruder with a 0.5 μm polycarbonate membrane. EYPC was purchased from Avanti Polar Lipids. Egg yolk L-α-phosphatidylcholine (EYPC ethanol solution, 140 μL, 184 μmol) was dissolved in CHCl₃ (3 mL), the solution was slowly evaporated under reduced pressure followed by drying under high vacuum for 2 h. The resulting thin lipid film was hydrated in 1.4 mL of 10 mM phosphate buffer (10 mM lithium phosphate, pH 6.4, 130 mM LiCl) for 1 h. During hydration, the suspension was submitted to 5 freeze-thaw cycles. The large multilamellar liposome suspension (1.0 mL) was submitted to high-pressure extrusion at rt (21 extrusions) through a 0.5 μm polycarbonate membrane afforded a suspension of large unicellular vesicles (LUVs) with an average diameter of 500 nm. This liposome

suspension contained Li^+ on the inside and outside of the liposomes.

Lithium filled vesicles (250 μL of the stock solution) containing phosphate buffer (10 mM lithium phosphate, pH 6.4, 130 mM LiCl) were suspended in 250 μL of phosphate buffer (10 mM sodium phosphate, pH 6.4, 100 mM NaCl, 30 mM Na_5PPPi). To this solution was added 2 μL of 1 M DyCl_3 (enough to shift extravascular ^{23}Na peak upfield by ~ 10 ppm). After monitoring vesicles by ^{23}Na NMR, 25-50 μL of compound (2.5 mM in DMSO) was added to the vesicles and the subsequent ^{23}Na NMR was taken 10 minutes later (508 scans). Spectra taken at $t=15$ min and $t=60$ min were identical to $t=10$ min, ensuring that equilibrium had been achieved.

References

- (1) Kaucher, M. S.; Harrell Jr., W. A.; Davis, J. T., "Chapter 10: The G-quartet in supramolecular chemistry and nanoscience." In *Quadruplex Nucleic Acids*, Ed.: Neidle, S.; Balasubramanian, S., Royal Society of Chemistry: Cambridge, **2007**, In Press.
- (2) Lehn, J. M. "Supramolecular chemistry - Scope and perspectives molecules, supermolecules, and molecular devices." *Angew. Chem. Int. Ed.* **1988**, *27*, 89-112.
- (3) Reinhoudt, D. N.; Crego-Calama, M. "Synthesis beyond the molecule." *Science* **2002**, *295*, 2403-2407.
- (4) Whitesides, G. M.; Simanek, E. E.; Mathias, J. P.; Seto, C. T.; Chin, D. N.; Mammen, M.; Gordon, D. M. "Noncovalent synthesis - Using physical-organic chemistry to make aggregates." *Acc. Chem. Res.* **1995**, *28*, 37-44.
- (5) de Wild, M.; Berner, S.; Suzuki, H.; Ramoino, L.; Baratoff, A.; Jung, T. A. "Molecular assembly and self-assembly: Molecular nanoscience for future technologies." *Chimia* **2002**, *56*, 500-505.
- (6) Zhang, S. G. "Fabrication of novel biomaterials through molecular self-assembly." *Nat. Biotechnol.* **2003**, *21*, 1171-1178.
- (7) Kato, T., "Hydrogen-bonded liquid crystals: Molecular self-assembly for dynamically functional materials." *Struct. Bond.* **2000**, *96*, 95-146.
- (8) Barron, A. E.; Zuckermann, R. N. "Bioinspired polymeric materials: in-between proteins and plastics." *Curr. Opin. Chem. Biol.* **1999**, *3*, 681-687.
- (9) Hammond, P. T. "Form and function in multilayer assembly: New applications at the nanoscale." *Adv. Mater.* **2004**, *16*, 1271-1293.

- (10) Armstrong, G.; Buggy, M. "Hydrogen-bonded supramolecular polymers: A literature review." *J. Mater. Sci.* **2005**, *40*, 547-559.
- (11) Faul, C. F. J.; Antonietti, M. "Ionic self-assembly: Facile synthesis of supramolecular materials." *Adv. Mater.* **2003**, *15*, 673-683.
- (12) Matile, S.; Som, A.; Sorde, N. "Recent synthetic ion channels and pores." *Tetrahedron* **2004**, *60*, 6405-6435.
- (13) Saenger, W., *Principles of Nucleic Acid Structure*. Springer-Verlag: New York, **1984**.
- (14) Davis, J. T. "G-quartets 40 years later: From 5'-GMP to molecular biology and supramolecular chemistry." *Angew. Chem. Int. Ed.* **2004**, *43*, 668-698.
- (15) Guschlbauer, W.; Chantot, J. F.; Thiele, D. "4-stranded nucleic-acid structures 25 years later - from guanosine gels to telomer dna." *J. Biomol. Struct. Dyn.* **1990**, *8*, 491-511.
- (16) Spada, G. P.; Gottarelli, G. "The disclosure of the stepwise supramolecular organization of guanosine derivatives: Serendipity or programmed design?" *Synlett* **2004**, 596-602.
- (17) Simonsson, T. "G-quadruplex DNA structures - Variations on a theme." *Biol. Chem.* **2001**, *382*, 621-628.
- (18) Williamson, J. R. "G-quartet structures in telomeric dna." *Annu. Rev. Biophys. Biomolec. Struct.* **1994**, *23*, 703-730.
- (19) Gellert, M.; Lipsett, M. N.; Davies, D. R. "Helix formation by guanylic acid." *Proc. Natl. Acad. Sci. U. S. A.* **1962**, *48*, 2013-2018.

- (20) Fresco, J. R.; Massoulié, J. "Polynucleotides.5. Helix-coil transition of polyriboguanilyc acid." *J. Am. Chem. Soc.* **1963**, *85*, 1352-1353.
- (21) Pinnavaia, T. J.; Miles, H. T.; Becker, E. D. "Self-assembled 5'-guanosine monophosphate - Nuclear magnetic-resonance evidence for a regular, ordered structure and slow chemical exchange." *J. Am. Chem. Soc.* **1975**, *97*, 7198-7200.
- (22) Pinnavaia, T. J.; Marshall, C. L.; Mettler, C. M.; Fisk, C. I.; Miles, H. T.; Becker, E. D. "Alkali-metal ion specificity in solution ordering of a nucleotide, 5'-guanosine monophosphate." *J. Am. Chem. Soc.* **1978**, *100*, 3625-3627.
- (23) Wong, A.; Ida, R.; Spindler, L.; Wu, G. "Disodium guanosine 5'-monophosphate self-associates into nanoscale cylinders at pH 8: A combined diffusion NMR spectroscopy and dynamic light scattering study." *J. Am. Chem. Soc.* **2005**, *127*, 6990-6998.
- (24) Zhou, S. Y.; Liu, D. "Inside the mammalian telomere interactome: Regulation and regulatory activities of telomeres." *Crit. Rev. Eukaryot. Gene Expr.* **2006**, *16*, 103-118.
- (25) McEachern, M. J.; Krauskopf, A.; Blackburn, E. H. "Telomeres and their control." *Annu. Rev. Genet.* **2000**, *34*, 331-358.
- (26) Collins, K. "Mammalian telomeres and telomerase." *Curr. Opin. Cell Biol.* **2000**, *12*, 378-383.
- (27) Greider, C. W. "Telomere length regulation." *Annu. Rev. Biochem.* **1996**, *65*, 337-365.
- (28) Bailey, S. M.; Murnane, J. P. "Telomeres, chromosome instability and cancer." *Nucleic Acids Res.* **2006**, *34*, 2408-2417.
- (29) Blackburn, E. H. "Switching and signaling at the telomere." *Cell* **2001**, *106*, 661-

673.

- (30) Cech, T. R. "Life at the end of the chromosome: Telomeres and telomerase." *Angew. Chem. Int. Ed.* **2000**, *39*, 34-43.
- (31) Bryan, T. M.; Cech, T. R. "Telomerase and the maintenance of chromosome ends." *Curr. Opin. Cell Biol.* **1999**, *11*, 318-324.
- (32) Rhodes, D.; Giraldo, R. "Telomere structure and function." *Curr. Opin. Struct. Biol.* **1995**, *5*, 311-322.
- (33) Hahn, W. C.; Counter, C. M.; Lundberg, A. S.; Beijersbergen, R. L.; Brooks, M. W.; Weinberg, R. A. "Creation of human tumour cells with defined genetic elements." *Nature* **1999**, *400*, 464-468.
- (34) Olausson, K. A.; Dubrana, K.; Dornont, J.; Spano, J. P.; Sabatier, L.; Soria, J. C. "Telomeres and telomerase as targets for anticancer drug development." *Crit. Rev. Oncol./Hematol.* **2006**, *57*, 191-214.
- (35) Jing, N. J.; Sha, W.; Li, Y. D.; Xiong, W. J.; Tweardy, D. J. "Rational drug design of G-quartet DNA as anti-cancer agents." *Curr. Pharm. Design* **2005**, *11*, 2841-2854.
- (36) Chen, Z.; Corey, D. R., "Telomerase inhibitors: A new option for chemotherapy." In *Advances In Cancer Research, Vol 87*, **2003**, 31-58.
- (37) Neidle, S.; Parkinson, G. "Telomere maintenance as a target for anticancer drug discovery." *Nat. Rev. Drug Discov.* **2002**, *1*, 383-393.
- (38) Perry, P. J.; Arnold, J. R. P.; Jenkins, T. C. "Telomerase inhibitors for the treatment of cancer: the current perspective." *Expert Opin. Investig. Drugs* **2001**, *10*, 2141-2156.

- (39) Han, H. Y.; Hurley, L. H. "G-quadruplex DNA: a potential target for anti-cancer drug design." *Trends Pharmacol. Sci.* **2000**, *21*, 136-142.
- (40) Kerwin, S. M. "G-quadruplex DNA as a target for drug design." *Curr. Pharm. Design* **2000**, *6*, 441-471.
- (41) Hurley, L. H.; Wheelhouse, R. T.; Sun, D.; Kerwin, S. M.; Salazar, M.; Fedoroff, O. Y.; Han, F. X.; Han, H. Y.; Izbicka, E.; Von Hoff, D. D. "G-quadruplexes as targets for drug design." *Pharmacol. Ther.* **2000**, *85*, 141-158.
- (42) Famulok, M.; Mayer, G.; Blind, M. "Nucleic acid aptamers - From selection in vitro to applications in vivo." *Acc. Chem. Res.* **2000**, *33*, 591-599.
- (43) Bock, L. C.; Griffin, L. C.; Latham, J. A.; Vermaas, E. H.; Toole, J. J. "Selection of single-stranded-DNA molecules that bind and inhibit human thrombin." *Nature* **1992**, *355*, 564-566.
- (44) Macaya, R. F.; Schultze, P.; Smith, F. W.; Roe, J. A.; Feigon, J. "Thrombin-binding DNA aptamer forms a unimolecular quadruplex structure in solution." *Proc. Natl. Acad. Sci. U. S. A.* **1993**, *90*, 3745-3749.
- (45) Marathias, V. M.; Bolton, P. H. "Determinants of DNA quadruplex structural type: Sequence and potassium binding." *Biochemistry* **1999**, *38*, 4355-4364.
- (46) Vairamani, M.; Gross, M. L. "G-quadruplex formation of thrombin-binding aptamer detected by electrospray ionization mass spectrometry." *J. Am. Chem. Soc.* **2003**, *125*, 42-43.
- (47) Padmanabhan, K.; Padmanabhan, K. P.; Ferrara, J. D.; Sadler, J. E.; Tulinsky, A. "The structure of alpha-thrombin inhibited by a 15-mer single-stranded-DNA aptamer." *J. Biol. Chem.* **1993**, *268*, 17651-17654.
- (48) Tasset, D. M.; Kubik, M. F.; Steiner, W. "Oligonucleotide inhibitors of human

thrombin that bind distinct epitopes." *J. Mol. Biol.* **1997**, 272, 688-698.

- (49) Gottarelli, G.; Masiero, S.; Spada, G. P. "Self-assembly in organic solvents of a deoxyguanosine derivative induced by alkali metal picrates." *Chem. Commun.* **1995**, 2555-2557.
- (50) Giorgi, T.; Grepioni, F.; Manet, I.; Mariani, P.; Masiero, S.; Mezzina, E.; Pieraccini, S.; Saturni, L.; Spada, G. P.; Gottarelli, G. "Gel-like lyomesophases formed in organic solvents by self-assembled guanine ribbons." *Chem.-Eur. J.* **2002**, 8, 2143-2152.
- (51) Rinaldi, R.; Maruccio, G.; Biasco, A.; Arima, V.; Cingolani, R.; Giorgi, T.; Masiero, S.; Spada, G. P.; Gottarelli, G. "Hybrid molecular electronic devices based on modified deoxyguanosines." *Nanotechnology* **2002**, 13, 398-403.
- (52) Marlow, A. L.; Mezzina, E.; Spada, G. P.; Masiero, S.; Davis, J. T.; Gottarelli, G. "Cation-templated self-assembly of a lipophilic deoxyguanosine: Solution structure of a K^+ -dG(8) octamer." *J. Org. Chem.* **1999**, 64, 5116-5123.
- (53) Forman, S. L.; Fettingter, J. C.; Pieraccini, S.; Gottarelli, G.; Davis, J. T. "Toward artificial ion channels: A lipophilic G-quadruplex." *J. Am. Chem. Soc.* **2000**, 122, 4060-4067.
- (54) Wong, A.; Fettingter, J. C.; Forman, S. L.; Davis, J. T.; Wu, G. "The sodium ions inside a lipophilic G-quadruplex channel as probed by solid-state Na-23 NMR." *J. Am. Chem. Soc.* **2002**, 124, 742-743.
- (55) Wu, G.; Wong, A.; Gan, Z. H.; Davis, J. T. "Direct detection of potassium cations bound to G-quadruplex structures by solid-state K-39 NMR at 19.6 T." *J. Am. Chem. Soc.* **2003**, 125, 7182-7183.
- (56) Kotch, F. W.; Fettingter, J. C.; Davis, J. T. "A lead-filled G-quadruplex: Insight into the G-quartet's selectivity for Pb^{2+} over K^+ ." *Org. Lett.* **2000**, 2, 3277-3280.

- (57) Cai, M.; Sidorov, V.; Lam, Y. F.; Flowers, R. A., II; Davis, J. T. "Guest and subunit exchange in self-assembled ionophores." *Org. Lett.* **2000**, *2*, 1665-8.
- (58) Shi, X. D.; Mullaugh, K. M.; Fettinger, J. C.; Jiang, Y.; Hofstadler, S. A.; Davis, J. T. "Lipophilic G-quadruplexes are self-assembled ion pair receptors, and the bound anion modulates the kinetic stability of these complexes." *J. Am. Chem. Soc.* **2003**, *125*, 10830-10841.
- (59) Shi, X. D.; Fettinger, J. C.; Davis, J. T. "Homochiral G-quadruplexes with Ba²⁺ but not with K⁺: The cation programs enantiomeric self-recognition." *J. Am. Chem. Soc.* **2001**, *123*, 6738-6739.
- (60) Andrisano, V.; Gottarelli, G.; Masiero, S.; Heijne, E. H.; Pieraccini, S.; Spada, G. P. "Enantioselective extraction of dinitrophenyl amino acids mediated by lipophilic deoxyguanosine derivatives: Chiral discrimination by self-assembly." *Angew. Chem. Int. Ed.* **1999**, *38*, 2386-2388.
- (61) Sessler, J. L.; Sathiosatham, M.; Doerr, K.; Lynch, V.; Abboud, K. A. "A G-quartet formed in the absence of a templating metal cation: A new 8-(N,N-dimethylaniline)guanosine derivative." *Angew. Chem. Int. Ed.* **2000**, *39*, 1300-1302.
- (62) Kotch, F. W.; Sidorov, V.; Lam, Y. F.; Kayser, K. J.; Li, H.; Kaucher, M. S.; Davis, J. T. "Water-mediated association provides an ion pair receptor." *J. Am. Chem. Soc.* **2003**, *125*, 15140-15150.
- (63) Otero, R.; Schock, M.; Molina, L. M.; Laegsgaard, E.; Stensgaard, I.; Hammer, B.; Besenbacher, F. "Guanine quartet networks stabilized by cooperative hydrogen bonds." *Angew. Chem. Int. Ed.* **2005**, *44*, 2270-2275.
- (64) Gubala, V.; Betancourt, J. E.; Rivera, J. M. "Expanding the Hoogsteen edge of 2'-deoxyguanosine: Consequences for G-quadruplex formation." *Org. Lett.* **2004**, *6*, 4735-4738.

- (65) Otto, W. H.; Keefe, M. H.; Splan, K. E.; Hupp, J. T.; Larive, C. K. "Analysis of molecular square size and purity via pulsed-field gradient NMR spectroscopy." *Inorg. Chem.* **2002**, *41*, 6172-6174.
- (66) Rowan, S. J.; Cantrill, S. J.; Cousins, G. R. L.; Sanders, J. K. M.; Stoddart, J. F. "Dynamic covalent chemistry." *Angew. Chem. Int. Ed.* **2002**, *41*, 898-952.
- (67) Schouten, J. A.; Ladame, S.; Mason, S. J.; Cooper, M. A.; Balasubramanian, S. "G-quadruplex-specific peptide-hemicyanine ligands by partial combinatorial selection." *J. Am. Chem. Soc.* **2003**, *125*, 5594-5595.
- (68) Clark, G. R.; Pytel, P. D.; Squire, C. J.; Neidle, S. "Structure of the first parallel DNA quadruplex-drug complex." *J. Am. Chem. Soc.* **2003**, *125*, 4066-4067.
- (69) Haider, S. M.; Parkinson, G. N.; Neidle, S. "Structure of a G-quadruplex-ligand complex." *J. Mol. Biol.* **2003**, *326*, 117-125.
- (70) Gowan, S. M.; Harrison, J. R.; Patterson, L.; Valenti, M.; Read, M. A.; Neidle, S.; Kelland, L. R. "A G-quadruplex-interactive potent small-molecule inhibitor of telomerase exhibiting in vitro and in vivo antitumor activity." *Mol. Pharmacol.* **2002**, *61*, 1154-1162.
- (71) Whitney, A. M.; Ladame, S.; Balasubramanian, S. "Templated ligand assembly by using G-quadruplex DNA and dynamic covalent chemistry." *Angew. Chem. Int. Ed.* **2004**, *43*, 1143-1146.
- (72) Ladame, S.; Whitney, A. M.; Balasubramanian, S. "Targeting nucleic acid secondary structures with polyamides using an optimized dynamic combinatorial approach." *Angew. Chem. Int. Ed.* **2005**, *44*, 5736-5739.
- (73) Sreenivasachary, N.; Lehn, J. M. "Gelation-driven component selection in the generation of constitutional dynamic hydrogels based on guanine-quartet formation." *Proc. Natl. Acad. Sci. U. S. A.* **2005**, *102*, 5938-5943.

- (74) Krishnan-Ghosh, Y.; Whitney, A. M.; Balasubramanian, S. "Dynamic covalent chemistry on self-templating PNA oligomers: formation of a bimolecular PNA quadruplex." *Chem. Commun.* **2005**, 3068-3070.
- (75) Ghossoub, A.; Lehn, J. M. "Dynamic sol-gel interconversion by reversible cation binding and release in G-quartet-based supramolecular polymers." *Chem. Commun.* **2005**, 5763-5765.
- (76) Nagatoishi, S.; Nojima, T.; Juskowiak, B.; Takenaka, S. "A pyrene-labeled G-quadruplex oligonucleotide as a fluorescent probe for potassium ion detection in biological applications." *Angew. Chem. Int. Ed.* **2005**, *44*, 5067-5070.
- (77) Ueyama, H.; Takagi, M.; Takenaka, S. "A novel potassium sensing in aqueous media with a synthetic oligonucleotide derivative. Fluorescence resonance energy transfer associated with guanine quartet-potassium ion complex formation." *J. Am. Chem. Soc.* **2002**, *124*, 14286-14287.
- (78) Ho, H. A.; Bera-Aberem, M.; Leclerc, M. "Optical sensors based on hybrid DNA/conjugated polymer complexes." *Chem.-Eur. J.* **2005**, *11*, 1718-1724.
- (79) Ho, H. A.; Leclerc, M. "Optical sensors based on hybrid aptamer/conjugated polymer complexes." *J. Am. Chem. Soc.* **2004**, *126*, 1384-1387.
- (80) He, F.; Tang, Y. L.; Wang, S.; Li, Y. L.; Zhu, D. B. "Fluorescent amplifying recognition for DNA G-quadruplex folding with a cationic conjugated polymer: A platform for homogeneous potassium detection." *J. Am. Chem. Soc.* **2005**, *127*, 12343-12346.
- (81) Potyrailo, R. A.; Conrad, R. C.; Ellington, A. D.; Hieftje, G. M. "Adapting selected nucleic acid ligands (aptamers) to biosensors." *Anal. Chem.* **1998**, *70*, 3419-3425.
- (82) Lee, M.; Walt, D. R. "A fiber-optic microarray biosensor using aptamers as

- receptors." *Anal. Biochem.* **2000**, 282, 142-146.
- (83) Hamaguchi, N.; Ellington, A.; Stanton, M. "Aptamer beacons for the direct detection of proteins." *Anal. Biochem.* **2001**, 294, 126-131.
- (84) Li, J. W. J.; Fang, X. H.; Tan, W. H. "Molecular aptamer beacons for real-time protein recognition." *Biochem. Biophys. Res. Commun.* **2002**, 292, 31-40.
- (85) Yang, C. J.; Jockusch, S.; Vicens, M.; Turro, N. J.; Tan, W. H. "Light-switching excimer probes for rapid protein monitoring in complex biological fluids." *Proc. Natl. Acad. Sci. U. S. A.* **2005**, 102, 17278-17283.
- (86) Nutiu, R.; Li, Y. F. "Structure-switching signaling aptamers." *J. Am. Chem. Soc.* **2003**, 125, 4771-4778.
- (87) Nutiu, R.; Li, Y. F. "Structure-switching signaling aptamers: Transducing molecular recognition into fluorescence signaling." *Chem.-Eur. J.* **2004**, 10, 1868-1876.
- (88) Heyduk, E.; Heyduk, T. "Nucleic acid-based fluorescence sensors for detecting proteins." *Anal. Chem.* **2005**, 77, 1147-1156.
- (89) Pavlov, V.; Xiao, Y.; Shlyahovsky, B.; Willner, I. "Aptamer-functionalized Au nanoparticles for the amplified optical detection of thrombin." *J. Am. Chem. Soc.* **2004**, 126, 11768-11769.
- (90) Seela, F.; Jawalekar, A. M.; Chi, L. F.; Zhong, D. Y. "Ion-specific aggregation of gold-DNA nanoparticles using the dG quartet hairpin 5'-d(G(4)T(4)G(4))." *Chem. Biodivers.* **2005**, 2, 84-91.
- (91) Li, Z.; Mirkin, C. A. "G-quartet-induced nanoparticle assembly." *J. Am. Chem. Soc.* **2005**, 127, 11568-11569.

- (92) Ikebukuro, K.; Kiyohara, C.; Sode, K. "Electrochemical detection of protein using a double aptamer sandwich." *Anal. Lett.* **2004**, *37*, 2901-2909.
- (93) Hianik, T.; Ostatna, V.; Zajacova, Z.; Stoikova, E.; Evtugyn, G. "Detection of aptamer-protein interactions using QCM and electrochemical indicator methods." *Bioorg. Med. Chem. Lett.* **2005**, *15*, 291-295.
- (94) Xiao, Y.; Lubin, A. A.; Heeger, A. J.; Plaxco, K. W. "Label-free electronic detection of thrombin in blood serum by using an aptamer-based sensor." *Angew. Chem. Int. Ed.* **2005**, *44*, 5456-5459.
- (95) Xiao, Y.; Piorek, B. D.; Plaxco, K. W.; Heeger, A. J. "A reagentless signal-on architecture for electronic, aptamer-based sensors via target-induced strand displacement." *J. Am. Chem. Soc.* **2005**, *127*, 17990-17991.
- (96) So, H. M.; Won, K.; Kim, Y. H.; Kim, B. K.; Ryu, B. H.; Na, P. S.; Kim, H.; Lee, J. O. "Single-walled carbon nanotube biosensors using aptamers as molecular recognition elements." *J. Am. Chem. Soc.* **2005**, *127*, 11906-11907.
- (97) Radi, A. E.; Sanchez, J. L. A.; Baldrich, E.; O'Sullivan, C. K. "Reagentless, reusable, ultrasensitive electrochemical molecular beacon aptasensor." *J. Am. Chem. Soc.* **2006**, *128*, 117-124.
- (98) Xiao, Y.; Pavlov, V.; Niazov, T.; Dishon, A.; Kotler, M.; Willner, I. "Catalytic beacons for the detection of DNA and telomerase activity." *J. Am. Chem. Soc.* **2004**, *126*, 7430-7431.
- (99) Pavlov, V.; Shlyahovsky, B.; Willner, I. "Fluorescence detection of DNA by the catalytic activation of an aptamer/thrombin complex." *J. Am. Chem. Soc.* **2005**, *127*, 6522-6523.
- (100) Fan, C. H.; Plaxco, K. W.; Heeger, A. J. "Electrochemical interrogation of conformational changes as a reagentless method for the sequence-specific

- detection of DNA." *Proc. Natl. Acad. Sci. U. S. A.* **2003**, *100*, 9134-9137.
- (101) Li, J. W. J.; Tan, W. H. "A single DNA molecule nanomotor." *Nano Lett.* **2002**, *2*, 315-318.
- (102) Alberti, P.; Mergny, J. L. "DNA duplex-quadruplex exchange as the basis for a nanomolecular machine." *Proc. Natl. Acad. Sci. U. S. A.* **2003**, *100*, 1569-1573.
- (103) Dittmer, W. U.; Reuter, A.; Simmel, F. C. "A DNA-based machine that can cyclically bind and release thrombin." *Angew. Chem. Int. Ed.* **2004**, *43*, 3550-3553.
- (104) Koshkin, A. A.; Rajwanshi, V. K.; Wengel, J. "Novel convenient syntheses of LNA [2.2.1]bicyclo nucleosides." *Tetrahedron Lett.* **1998**, *39*, 4381-4384.
- (105) Obika, S.; Nanbu, D.; Hari, Y.; Andoh, J.; Morio, K.; Doi, T.; Imanishi, T. "Stability and structural features of the duplexes containing nucleoside analogous with a fixed N-type conformation, 2'-O,4'-C-methyleneribonucleosides." *Tetrahedron Lett.* **1998**, *39*, 5401-5404.
- (106) Dominick, P. K.; Jarstfer, M. B. "A conformationally constrained nucleotide analogue controls the folding topology of a DNA G-quadruplex." *J. Am. Chem. Soc.* **2004**, *126*, 5050-5051.
- (107) Randazzo, A.; Esposito, V.; Ohlenschlager, O.; Ramachandran, R.; Mayol, L. "NMR solution structure of a parallel LNA quadruplex." *Nucleic Acids Res.* **2004**, *32*, 3083-3092.
- (108) Mergny, J. L.; De Cian, A.; Ghelab, A.; Sacca, B.; Lacroix, L. "Kinetics of tetramolecular quadruplexes." *Nucleic Acids Res.* **2005**, *33*, 81-94.
- (109) Datta, B.; Schmitt, C.; Armitage, B. A. "Formation of a PNA(2)-DNA(2) hybrid quadruplex." *J. Am. Chem. Soc.* **2003**, *125*, 4111-4118.

- (110) Marin, V. L.; Armitage, B. A. "RNA guanine quadruplex invasion by complementary and homologous PNA probes." *J. Am. Chem. Soc.* **2005**, *127*, 8032-8033.
- (111) Krishnan-Ghosh, Y.; Stephens, E.; Balasubramanian, S. "A PNA(4) quadruplex." *J. Am. Chem. Soc.* **2004**, *126*, 5944-5945.
- (112) Datta, B.; Bier, M. E.; Roy, S.; Armitage, B. A. "Quadruplex formation by a guanine-rich PNA oligomer." *J. Am. Chem. Soc.* **2005**, *127*, 4199-4207.
- (113) Petraccone, L.; Pagano, B.; Esposito, V.; Randazzo, A.; Piccialli, G.; Barone, G.; Mattia, C. A.; Giancola, C. "Thermodynamics and kinetics of PNA-DNA quadruplex-forming chimeras." *J. Am. Chem. Soc.* **2005**, *127*, 16215-16223.
- (114) Wyatt, J. R.; Davis, P. W.; Freier, S. M. "Kinetics of G-quartet-mediated tetramer formation." *Biochemistry* **1996**, *35*, 8002-8008.
- (115) Li, Y. F.; Sen, D. "Toward an efficient DNAzyme." *Biochemistry* **1997**, *36*, 5589-5599.
- (116) Li, Y. F.; Sen, D. "The modus operandi of a DNA enzyme: enhancement of substrate basicity." *Chem. Biol.* **1998**, *5*, 1-12.
- (117) Geyer, C. R.; Sen, D. "Use of intrinsic binding energy for catalysis by a cofactor-independent DNA enzyme." *J. Mol. Biol.* **2000**, *299*, 1387-1398.
- (118) Travascio, P.; Li, Y. F.; Sen, D. "DNA-enhanced peroxidase activity of a DNA aptamer-hemin complex." *Chem. Biol.* **1998**, *5*, 505-517.
- (119) Travascio, P.; Witting, P. K.; Mauk, A. G.; Sen, D. "The peroxidase activity of a hemin-DNA oligonucleotide complex: Free radical damage to specific guanine bases of the DNA." *J. Am. Chem. Soc.* **2001**, *123*, 1337-1348.

- (120) Chinnapen, D. J. F.; Sen, D. "A deoxyribozyme that harnesses light to repair thymine dimers in DNA." *Proc. Natl. Acad. Sci. U. S. A.* **2004**, *101*, 65-69.
- (121) Kaucher, M. S.; Lam, Y. F.; Pieraccini, S.; Gottarelli, G.; Davis, J. T. "Using diffusion NMR to characterize guanosine self-association: Insights into structure and mechanism." *Chem.-Eur. J.* **2004**, *11*, 164-173.
- (122) Prins, L. J.; Reinhoudt, D. N.; Timmerman, P. "Noncovalent synthesis using hydrogen bonding." *Angew. Chem. Int. Ed.* **2001**, *40*, 2383-2426.
- (123) Schalley, C. A. "Molecular recognition and supramolecular chemistry in the gas phase." *Mass Spectrom. Rev.* **2001**, *20*, 253-309.
- (124) Isaacs, L.; Witt, D.; Lagona, J. "Self-association of facially amphiphilic methylene bridged glycoluril dimers." *Org. Lett.* **2001**, *3*, 3221-3224.
- (125) Michels, J. J.; O'Connell, M. J.; Taylor, P. N.; Wilson, J. S.; Cacialli, F.; Anderson, H. L. "Synthesis of conjugated polyrotaxanes." *Chem.-Eur. J.* **2003**, *9*, 6167-6176.
- (126) Schubert, D.; Tziatzios, C.; Schuck, P.; Schubert, U. S. "Characterizing the solution properties of supramolecular systems by analytical ultracentrifugation." *Chem.-Eur. J.* **1999**, *5*, 1377-1383.
- (127) Fenniri, H.; Deng, B. L.; Ribbe, A. E. "Helical rosette nanotubes with tunable chiroptical properties." *J. Am. Chem. Soc.* **2002**, *124*, 11064-11072.
- (128) Price, W. S., In *New Advances in Anal. Chem.*, Ed.: Atta-ur-Rahman, E., Gordon and Breach Science Pub: Amsterdam, **2000**, 31-72.
- (129) Stilbs, P. "Fourier transform pulsed-gradient spin-echo studies of molecular diffusion." *Prog. NMR Spectrosc.* **1987**, *19*, 1-45.

- (130) Price, W. S. "Pulsed-field gradient nuclear magnetic resonance as a tool for studying translational diffusion.1. Basic theory." *Concepts Magn. Resonan.* **1997**, *9*, 299-336.
- (131) Price, W. S. "Pulsed-field gradient nuclear magnetic resonance as a tool for studying translational diffusion: Part II. Experimental aspects." *Concepts Magn. Reson.* **1998**, *10*, 197-237.
- (132) Johnson, C. S. "Diffusion ordered nuclear magnetic resonance spectroscopy: principles and applications." *Prog. Nucl. Magn. Reson. Spectrosc.* **1999**, *34*, 203-256.
- (133) Lo, M. C.; Helm, J. S.; Sarngadharan, G.; Pelczer, I.; Walker, S. "A new structure for the substrate-binding antibiotic ramoplanin." *J. Am. Chem. Soc.* **2001**, *123*, 8640-8641.
- (134) Daranas, A. H.; Fernandez, J. J.; Morales, E. Q.; Norte, M.; Gavin, J. A. "Self-association of okadaic acid upon complexation with potassium ion." *J. Med. Chem.* **2004**, *47*, 10-13.
- (135) Shikii, K.; Sakamoto, S.; Seki, H.; Utsumi, H.; Yamaguchi, K. "Narcissistic aggregation of steroid compounds in diluted solution elucidated by CSI-MS, PFG NMR and X-ray analysis." *Tetrahedron* **2004**, *60*, 3487-3492.
- (136) Mayo, K. H.; Ilyina, E.; Park, H. "A recipe for designing water-soluble, beta-sheet-forming peptides." *Protein Sci.* **1996**, *5*, 1301-1315.
- (137) Yao, S. G.; Howlett, G. J.; Norton, R. S. "Peptide self-association in aqueous trifluoroethanol monitored by pulsed field gradient NMR diffusion measurements." *J. Biomol. NMR* **2000**, *16*, 109-119.
- (138) Altieri, A. S.; Hinton, D. P.; Byrd, R. A. "Association of biomolecular systems via pulsed-field gradient NMR self-diffusion measurements." *J. Am. Chem. Soc.*

1995, *117*, 7566-7567.

- (139) Ilyina, E.; Roongta, V.; Pan, H.; Woodward, C.; Mayo, K. H. "A pulsed-field gradient NMR study of bovine pancreatic trypsin inhibitor self-association." *Biochemistry* **1997**, *36*, 3383-3388.
- (140) Krishnan, V. V. "Determination of oligomeric state of proteins in solution from pulsed-field-gradient self-diffusion coefficient measurements. A comparison of experimental, theoretical, and hard-sphere approximated values." *J. Magn. Reson.* **1997**, *124*, 468-473.
- (141) Price, W. S.; Tsuchiya, F.; Arata, Y. "Lysozyme aggregation and solution properties studied using PGSE NMR diffusion measurements." *J. Am. Chem. Soc.* **1999**, *121*, 11503-11512.
- (142) Wills, P. R.; Georgalis, Y. "Concentration-dependence of the diffusion-coefficient of a dimerizing protein - Bovine pancreatic trypsin-inhibitor." *J. Phys. Chem.* **1981**, *85*, 3978-3984.
- (143) Beck, S.; Geyer, A.; Brintzinger, H. H. "Diffusion coefficients of zirconocene-borate ion pairs studied by pulsed field-gradient NMR - evidence for ion quadruples in benzene solutions." *Chem. Commun.* **1999**, 2477-2478.
- (144) Keresztes, I.; Williard, P. G. "Diffusion-ordered NMR spectroscopy (DOSY) of THF solvated n-butyllithium aggregates." *J. Am. Chem. Soc.* **2000**, *122*, 10228-10229.
- (145) Martinez-Viviente, E.; Pregosin, P. S.; Vial, L.; Herse, C.; Lacour, J. "H-1 F-19, and P-31 PGSE NMR diffusion studies on chiral organic salts: Ion pairing and the dependence of a diffusion value on diastereomeric structure." *Chem.-Eur. J.* **2004**, *10*, 2912-2918.
- (146) Valentini, M.; Ruegger, H.; Pregosin, P. S. "Applications of pulsed-gradient spin-

- echo (PGSE) diffusion measurements in organometallic chemistry." *Helv. Chim. Acta* **2001**, *84*, 2833-2853.
- (147) Gorman, C. B.; Smith, J. C.; Hager, M. W.; Parkhurst, B. L.; Sierzputowska-Gracz, H.; Haney, C. A. "Molecular structure-property relationships for electron-transfer rate attenuation in redox-active core dendrimers." *J. Am. Chem. Soc.* **1999**, *121*, 9958-9966.
- (148) Kohlmann, O.; Steinmetz, W. E.; Mao, X. A.; Wuelfing, W. P.; Templeton, A. C.; Murray, R. W.; Johnson, C. S. "NMR diffusion, relaxation, and spectroscopic studies of water soluble, monolayer-protected gold nanoclusters." *J. Phys. Chem. B* **2001**, *105*, 8801-8809.
- (149) ten Cate, A. T.; Dankers, P. Y. W.; Kooijman, H.; Spek, A. L.; Sijbesma, R. P.; Meijer, E. W. "Enantioselective cyclization of racemic supramolecular polymers." *J. Am. Chem. Soc.* **2003**, *125*, 6860-6861.
- (150) Valentini, M.; Vaccaro, A.; Rehor, A.; Napoli, A.; Hubbell, J. A.; Tirelli, N. "Diffusion NMR spectroscopy for the characterization of the size and interactions of colloidal matter: The case of vesicles and nanoparticles." *J. Am. Chem. Soc.* **2004**, *126*, 2142-2147.
- (151) Cohen, Y.; Avram, L.; Frish, L. "Diffusion NMR spectroscopy in supramolecular and combinatorial chemistry: An old parameter - New insights." *Angew. Chem. Int. Ed.* **2005**, *44*, 520-554.
- (152) Avram, L.; Cohen, Y. "Complexation in pseudorotaxanes based on alpha-cyclodextrin and different alpha,omega-diaminoalkanes by NMR diffusion measurements." *J. Org. Chem.* **2002**, *67*, 2639-2644.
- (153) Frish, L.; Sansone, F.; Casnati, A.; Ungaro, R.; Cohen, Y. "Complexation of a peptidocalix[4]arene, a vancomycin mimic, with alanine-containing guests by NMR diffusion measurements." *J. Org. Chem.* **2000**, *65*, 5026-5030.

- (154) Frish, L.; Vysotsky, M. O.; Matthews, S. E.; Bohmer, V.; Cohen, Y. "Tropylium cation capsule of hydrogen-bonded tetraurea calix[4]arene dimers." *J. Chem. Soc.-Perkin Trans. 2* **2002**, 88-93.
- (155) Gafni, A.; Cohen, Y. "Complexes of macrocycles with gamma-cyclodextrin as deduced from NMR diffusion measurements." *J. Org. Chem.* **1997**, 62, 120-125.
- (156) Shenhar, R.; Wang, H.; Hoffman, R. E.; Frish, L.; Avram, L.; Willner, I.; Rajca, A.; Rabinovitz, M. "Self-assembled, helically stacked anionic aggregates of 2,5,8,11-tetra-tert-butylcycloocta[1,2,3,4-def,5,6,7,8-d'e'f]bisbiphenylene, stabilized by electrostatic interactions." *J. Am. Chem. Soc.* **2002**, 124, 4685-4692.
- (157) Timmerman, P.; Weidmann, J. L.; Jolliffe, K. A.; Prins, L. J.; Reinhoudt, D. N.; Shinkai, S.; Frish, L.; Cohen, Y. "NMR diffusion spectroscopy for the characterization of multicomponent hydrogen-bonded assemblies in solution." *J. Chem. Soc.-Perkin Trans. 2* **2000**, 2077-2089.
- (158) Avram, L.; Cohen, Y. "Spontaneous formation of hexameric resorcinarene capsule in chloroform solution as detected by diffusion NMR." *J. Am. Chem. Soc.* **2002**, 124, 15148-15149.
- (159) Avram, L.; Cohen, Y. "The role of water molecules in a resorcinarene capsule as probed by NMR diffusion measurements." *Org. Lett.* **2002**, 4, 4365-4368.
- (160) Avram, L.; Cohen, Y. "Effect of a cationic guest on the characteristics of the molecular capsule of resorcinarene: A diffusion NMR study." *Org. Lett.* **2003**, 5, 1099-1102.
- (161) Cabrita, E. J.; Berger, S. "HR-DOSY as a new tool for the study of chemical exchange phenomena." *Magn. Reson. Chem.* **2002**, 40, S122-S127.
- (162) Johnson, C. S. "Effects of chemical-exchange in diffusion-ordered 2D NMR-spectra." *J. Magn. Reson. Ser. A* **1993**, 102, 214-218.

- (163) Lin, M. F.; Larive, C. K. "Detection of insulin aggregates with pulsed-field gradient nuclear-magnetic-resonance spectroscopy." *Anal. Biochem.* **1995**, *229*, 214-220.
- (164) Regan, D. G.; Chapman, B. E.; Kuchel, P. W. "PGSE NMR diffusion study of the self-association of N-methylacetamide in carbon tetrachloride." *Magn. Reson. Chem.* **2002**, *40*, S115-S121.
- (165) Stejskal, E. O.; Tanner, J. E. "Spin diffusion measurements - Spin echoes in presence of a time-dependent field gradient." *J. Chem. Phys.* **1965**, *42*, 288-192.
- (166) Crank, J., *The Mathematics of Diffusion*. 2nd Ed., Claxendon Press: Oxford, **1975**.
- (167) Cussler, E. L., *Diffusion: Mass Transfer in Fluid Systems*. Cambridge University Press: Cambridge, **1984**.
- (168) Mayzel, O.; Gafni, A.; Cohen, Y. "Water hydration of macrocyclic systems in organic solvents: An NMR diffusion and chemical shift study." *Chem. Commun.* **1996**, 911-912.
- (169) Halle, B.; Denisov, V. P., "Magnetic relaxation dispersion studies of biomolecular solutions." *Methods Enzymol.* **2001**, *338*, 178-201.
- (170) Otting, G. "NMR studies of water bound to biological molecules." *Prog. Nucl. Magn. Reson. Spectrosc.* **1997**, *31*, 259-285.
- (171) Gerothanassis, I. P. "Multinuclear and multidimensional NMR methodology for studying individual water-molecules bound to peptides and proteins in solution - Principles and applications." *Prog. Nucl. Magn. Reson. Spectrosc.* **1994**, *26*, 171-237.
- (172) Hahn, E. L. "Spin echoes." *Phys. Rev.* **1950**, *80*, 580.

- (173) Price, W. S.; Walchli, M. "NMR diffusion measurements of strong signals: the PGSE-Q-switch experiment." *Magn. Reson. Chem.* **2002**, *40*, S128-S132.
- (174) Price, W. S.; Stilbs, P.; Jonsson, B.; Soderman, O. "Macroscopic background gradient and radiation damping effects on high-field PGSE NMR diffusion measurements." *J. Magn. Reson.* **2001**, *150*, 49-56.
- (175) Pregosin, P. S.; Kumar, P. G. A.; Fernandez, I. "Pulsed gradient spin-echo (PGSE) diffusion and H-1,F-19 heteronuclear overhauser spectroscopy (HOESY) NMR methods in inorganic and organometallic chemistry: Something old and something new." *Chem. Rev.* **2005**, *105*, 2977-2998.
- (176) Martin, G. E.; Crouch, R. C.; Zens, A. P. "Gradient submicro inverse detection: rapid acquisition of inverse-detected heteronuclear chemical shift correlation data on submicromole quantities of material." *Magn. Reson. Chem.* **1998**, *36*, 551-557.
- (177) Reynolds, W. F.; Yu, M.; Enriquez, R. G.; Leon, I. "Investigation of the advantages and limitations of forward linear prediction for processing 2D data sets." *Magn. Reson. Chem.* **1997**, *35*, 505-519.
- (178) Crouch, R. C.; Martin, G. E.; Musser, S. M.; Grenade, H. R.; Dickey, R. W. "Improvements in the sensitivity of inverse-detected heteronuclear correlation spectra using micro inverse probes and micro cells - HMQC and HMBC spectra of caribbean ciguatoxin - Preliminary structural inferences." *Tetrahedron Lett.* **1995**, *36*, 6827-6830.
- (179) Lapham, J.; Rife, J. P.; Moore, P. B.; Crothers, D. M. "Measurement of diffusion constants for nucleic acids by NMR." *J. Biomol. NMR* **1997**, *10*, 255-262.
- (180) Tanner, J. E. "Use of stimulated echo in NMR diffusion studies." *J. Chem. Phys.* **1970**, *52*, 2523-2526.
- (181) Cotts, R. M.; Hoch, M. J. R.; Sun, T.; Markert, J. T. "Pulsed field gradient

stimulated echo methods for improved NMR diffusion measurements in heterogeneous systems." *J. Magn. Reson.* **1989**, *83*, 252-266.

- (182) Shi, X.; Fettinger, J. C.; Davis, J. T. "Ion-pair recognition by nucleoside self-assembly: Guanosine hexadecamers bind cations and anions." *Angew. Chem. Int. Ed.* **2001**, *40*, 2827-2831.
- (183) Gottarelli, G.; Masiero, S.; Mezzina, E.; Spada, G. P.; Mariani, P.; Recanatini, M. "The self-assembly of a lipophilic deoxyguanosine derivative and the formation of a liquid-crystalline phase in hydrocarbon solvents." *Helv. Chim. Acta* **1998**, *81*, 2078-2092.
- (184) Pranata, J.; Wierschke, S. G.; Jorgensen, W. L. "Opls potential functions for nucleotide bases - Relative association constants of hydrogen-bonded base-pairs in chloroform." *J. Am. Chem. Soc.* **1991**, *113*, 2810-2819.
- (185) Sartorius, J.; Schneider, H. J. "A general scheme based on empirical increments for the prediction of hydrogen-bond associations of nucleobases and of synthetic host-guest complexes." *Chem.-Eur. J.* **1996**, *2*, 1446-1452.
- (186) Fettinger, J. C.; Sidorov, V.; Davis, J. T. *Unpublished Results*.
- (187) Teller, D. C.; Swanson, E.; DeHaen, C., "The translation frictional coefficient of proteins." In *Methods Enzymol.*, Ed.: Hirs, C. H. W.; Timasheff, S. N., Academic Press: New York, **1979**, 103-124.
- (188) Newmark, R. A.; Cantor, C. R. "Nuclear magnetic resonance study of interactions of guanosine and cytidine in dimethyl sulfoxide." *J. Am. Chem. Soc.* **1968**, *90*, 5010-5017.
- (189) Simic, V.; Bouteiller, L.; Jalabert, M. "Highly cooperative formation of bis-urea based supramolecular polymers." *J. Am. Chem. Soc.* **2003**, *125*, 13148-13154.

- (190) Zhao, D. H.; Moore, J. S. "Nucleation-elongation: a mechanism for cooperative supramolecular polymerization." *Org. Biomol. Chem.* **2003**, *1*, 3471-3491.
- (191) Gottarelli, G.; Masiero, S.; Spada, G. P. "The use of CD spectroscopy for the study of the self-assembly of guanine derivatives." *Enantiomer* **1998**, *3*, 429-436.
- (192) Taylor, P. N.; Anderson, H. L. "Cooperative self-assembly of double-strand conjugated porphyrin ladders." *J. Am. Chem. Soc.* **1999**, *121*, 11538-11545.
- (193) Pfeil, A.; Lehn, J. M. "Helicate self-organization - Positive cooperativity in the self-assembly of double-helical metal-complexes." *J. Chem. Soc.-Chem. Commun.* **1992**, 838-840.
- (194) Ercolani, G. "Assessment of cooperativity in self-assembly." *J. Am. Chem. Soc.* **2003**, *125*, 16097-16103.
- (195) Ercolani, G. "A model for self-assembly in solution." *J. Phys. Chem. B* **2003**, *107*, 5052-5057.
- (196) Badjic, J. D.; Nelson, A.; Cantrill, S. J.; Turnbull, W. B.; Stoddart, J. F. "Multivalency and cooperativity in supramolecular chemistry." *Acc. Chem. Res.* **2005**, *38*, 723-732.
- (197) Wang, Y.; Patel, D. J. "Guanine residues in D(T2ag3) And D(T2g4) form parallel-stranded potassium cation stabilized G-quadruplexes with antiglycosidic torsion angles in solution." *Biochemistry* **1992**, *31*, 8112-8119.
- (198) Pieraccini, S. "Self-assembly induced by alkali metal ions in organic solutions: NMR study." *Unpublished*. **2000**.
- (199) Fukushima, K.; Iwahashi, H. "1: 1 Complex of guanine quartet with alkali metal cations detected by electrospray ionization mass spectrometry." *Chem. Commun.* **2000**, 895-896.

- (200) Aggerholm, T.; Nanita, S. C.; Koch, K. J.; Cooks, R. G. "Clustering of nucleosides in the presence of alkali metals: Biologically relevant quartets of guanosine, deoxyguanosine and uridine observed by ESI-MS/MS." *J. Mass Spectrom.* **2003**, *38*, 87-97.
- (201) Manet, I.; Francini, L.; Masiero, S.; Pieraccini, S.; Spada, G. P.; Gottarelli, G. "An ESI-MS and NMR study of the self-assembly of guanosine derivatives." *Helv. Chim. Acta* **2001**, *84*, 2096-2107.
- (202) Wong, A.; Ida, R.; Spindler, L.; Wu, G. "Disodium guanosine 5'-monophosphate self-associates into nanoscale cylinders at pH 8: A combined diffusion NMR spectroscopy and dynamic light scattering study." *J. Am. Chem. Soc.* **2005**, *127*, 6990-6998.
- (203) Harrowfield, J. "pi stacking and the co-ordinate bond: Sometimes conflicting factors in molecular recognition, as revealed in the structures of metal picrates." *J. Chem. Soc.-Dalton Trans.* **1996**, 3165-3171.
- (204) Talanova, G. G.; Elkarim, N. S. A.; Talanov, V. S.; Hanes, R. E.; Hwang, H. S.; Bartsch, R. A.; Rogers, R. D. "The "picrate effect" on extraction selectivities of aromatic group-containing crown ethers for alkali metal cations." *J. Am. Chem. Soc.* **1999**, *121*, 11281-11290.
- (205) Gokel, G. W.; Mukhopadhyay, A. "Synthetic models of cation-conducting channels." *Chem. Soc. Rev.* **2001**, *30*, 274-286.
- (206) Davis, J. T.; Kaucher, M. S.; Kotch, F. W.; Iezzi, M. A.; Clover, B. C.; Mullaugh, K. M. "Kinetic control in noncovalent synthesis: Regioselective ligand exchange into a hydrogen bonded assembly." *Org. Lett.* **2004**, *6*, 4265-4268.
- (207) Gao, X. Y.; Matsui, H. "Peptide-based nanotubes and their applications in bionanotechnology." *Adv. Mater.* **2005**, *17*, 2037-2050.

- (208) Rajagopal, K.; Schneider, J. P. "Self-assembling peptides and proteins for nanotechnological applications." *Curr. Opin. Struct. Biol.* **2004**, *14*, 480-486.
- (209) Law, M.; Goldberger, J.; Yang, P. D. "Semiconductor nanowires and nanotubes." *Ann. Rev. Mater. Res.* **2004**, *34*, 83-122.
- (210) Ito, Y.; Fukusaki, E. "DNA as a 'nanomaterial'." *J. Mol. Catal. B-Enzym.* **2004**, *28*, 155-166.
- (211) Baughman, R. H.; Zakhidov, A. A.; de Heer, W. A. "Carbon nanotubes - the route toward applications." *Science* **2002**, *297*, 787-792.
- (212) Hu, J. T.; Odom, T. W.; Lieber, C. M. "Chemistry and physics in one dimension: Synthesis and properties of nanowires and nanotubes." *Acc. Chem. Res.* **1999**, *32*, 435-445.
- (213) Terrones, M.; Hsu, W. K.; Kroto, H. W.; Walton, D. R. M., "Nanotubes: A revolution in materials science and electronics." In *Fullerenes And Related Structures* **1999**, 189-234.
- (214) Marsh, T. C.; Henderson, E. "G-wires - Self-assembly of a telomeric oligonucleotide, D(Ggggttgggg), into large superstructures." *Biochemistry* **1994**, *33*, 10718-10724.
- (215) Marsh, T. C.; Vesenska, J.; Henderson, E. "A new DNA nanostructure, the G-wire, imaged by scanning probe microscopy." *Nucleic Acids Res.* **1995**, *23*, 696-700.
- (216) Sakai, N.; Mareda, J.; Matile, S. "Rigid-rod molecules in biomembrane models: From hydrogen-bonded chains to synthetic multifunctional pores." *Acc. Chem. Res.* **2005**, *38*, 79-87.
- (217) Gokel, G. W.; Schlesinger, P. H.; Djedovic, N. K.; Ferdani, R.; Harder, E. C.; Hu, J. X.; Leevy, W. M.; Pajewska, J.; Pajewski, R.; Weber, M. E. "Functional,

- synthetic organic chemical models of cellular ion channels." *Bioorg. Med. Chem.* **2004**, *12*, 1291-1304.
- (218) Gokel, G. W.; Murillo, O. "Synthetic organic chemical models for transmembrane channels." *Acc. Chem. Res.* **1996**, *29*, 425-432.
- (219) Archer, E. A.; Gong, H. G.; Krische, M. J. "Hydrogen bonding in noncovalent synthesis: selectivity and the directed organization of molecular strands." *Tetrahedron* **2001**, *57*, 1139-1159.
- (220) Badjic, J. D.; Cantrill, S. J.; Stoddart, J. F. "Can multivalency be expressed kinetically? The answer is yes." *J. Am. Chem. Soc.* **2004**, *126*, 2288-2289.
- (221) Davis, A. V.; Yeh, R. M.; Raymond, K. N. "Supramolecular assembly dynamics." *Proc. Natl. Acad. Sci. U. S. A.* **2002**, *99*, 4793-4796.
- (222) Hasenknopf, B.; Lehn, J. M.; Boumediene, N.; Leize, E.; Van Dorsselaer, A. "Kinetic and thermodynamic control in self-assembly: Sequential formation of linear and circular helicates." *Angew. Chem. Int. Ed.* **1998**, *37*, 3265-3268.
- (223) Hori, A.; Yamashita, K.; Fujita, M. "Kinetic self-assembly: Selective cross-catenation of two sterically differentiated Pd-II-coordination rings." *Angew. Chem. Int. Ed.* **2004**, *43*, 5016-5019.
- (224) Horn, M.; Ihringer, J.; Glink, P. T.; Stoddart, J. F. "Kinetic versus thermodynamic control during the formation of [2]rotaxanes by a dynamic template-directed clipping process." *Chem.-Eur. J.* **2003**, *9*, 4046-4054.
- (225) Leung, D. H.; Fiedler, D.; Bergman, R. G.; Raymond, K. N. "Selective C-H bond activation by a supramolecular host-guest assembly." *Angew. Chem. Int. Ed.* **2004**, *43*, 963-966.
- (226) Litvinchuk, S.; Bollot, G.; Mareda, J.; Som, A.; Ronan, D.; Shah, M. R.; Perrottet,

- P.; Sakai, N.; Matile, S. "Thermodynamic and kinetic stability of synthetic multifunctional rigid-rod beta-barrel pores: Evidence for supramolecular catalysis." *J. Am. Chem. Soc.* **2004**, *126*, 10067-10075.
- (227) Yount, W. C.; Juwarker, H.; Craig, S. L. "Orthogonal control of dissociation dynamics relative to thermodynamics in a main-chain reversible polymer." *J. Am. Chem. Soc.* **2003**, *125*, 15302-15303.
- (228) Maslak, V.; Yan, Z.; Xia, S.; Gallucci, J.; Hadad, C. M.; Badjic, J. D. "Design, synthesis, and conformational dynamics of a gated molecular basket." *J. Am. Chem. Soc.* **2006**, *128*, 5887-5894.
- (229) Yount, W. C.; Loveless, D. M.; Craig, S. L. "Small-molecule dynamics and mechanisms underlying the macroscopic mechanical properties of coordinatively cross-linked polymer networks." *J. Am. Chem. Soc.* **2005**, *127*, 14488-14496.
- (230) Yount, W. C.; Loveless, D. M.; Craig, S. L. "Strong means slow: Dynamic contributions to the bulk mechanical properties of supramolecular networks." *Angew. Chem. Int. Ed.* **2005**, *44*, 2746-2748.
- (231) Levin, M. D.; Stang, P. J. "Insights into the mechanism of coordination-directed self-assembly." *J. Am. Chem. Soc.* **2000**, *122*, 7428-7429.
- (232) Desiraju, G. R. "Supramolecular synthons in crystal engineering - A new organic-synthesis." *Angew. Chem. Int. Ed.* **1995**, *34*, 2311-2327.
- (233) Huc, I.; Lehn, J. M. "Virtual combinatorial libraries: Dynamic generation of molecular and supramolecular diversity by self-assembly." *Proc. Natl. Acad. Sci. U. S. A.* **1997**, *94*, 2106-2110.
- (234) Kerckhoffs, J.; van Leeuwen, F. W. R.; Spek, A. L.; Kooijman, H.; Crego-Calama, M.; Reinhoudt, D. N. "Regulatory strategies in the complexation and release of a noncovalent guest trimer by a self-assembled molecular cage." *Angew. Chem. Int.*

Ed. **2003**, *42*, 5717-5722.

- (235) Lehn, J. M.; Eliseev, A. V. "Chemistry - Dynamic combinatorial chemistry." *Science* **2001**, *291*, 2331-2332.
- (236) Moulton, B.; Zaworotko, M. J. "From molecules to crystal engineering: Supramolecular isomerism and polymorphism in network solids." *Chem. Rev.* **2001**, *101*, 1629-1658.
- (237) Paraschiv, V.; Crego-Calama, M.; Ishi-i, T.; Padberg, C. J.; Timmerman, P.; Reinhoudt, D. N. "Molecular 'chaperones' guide the spontaneous formation of a 15-component hydrogen-bonded assembly." *J. Am. Chem. Soc.* **2002**, *124*, 7638-7639.
- (238) Clark, T. D.; Ghadiri, M. R. "Supramolecular design by covalent capture - Design of a peptide cylinder via hydrogen-bond-promoted intermolecular olefin metathesis." *J. Am. Chem. Soc.* **1995**, *117*, 12364-12365.
- (239) Kidd, T. J.; Loontjens, T. J. A.; Leigh, D. A.; Wong, J. K. Y. "Rotaxane building blocks bearing blocked isocyanate stoppers: Polyrotaxanes through post-assembly chain extension." *Angew. Chem. Int. Ed.* **2003**, *42*, 3379-3383.
- (240) Kuehl, C. J.; Huang, S. D.; Stang, P. J. "Self-assembly with postmodification: Kinetically stabilized metalla-supramolecular rectangles." *J. Am. Chem. Soc.* **2001**, *123*, 9634-9641.
- (241) Rowan, S. J.; Stoddart, J. F. "Precision molecular grafting: Exchanging surrogate stoppers in [2]rotaxanes." *J. Am. Chem. Soc.* **2000**, *122*, 164-165.
- (242) Prins, L. J.; Neuteboom, E. E.; Paraschiv, V.; Crego-Calama, M.; Timmerman, P.; Reinhoudt, D. N. "Kinetic stabilities of double, tetra-, and hexarosette hydrogen-bonded assemblies." *J. Org. Chem.* **2002**, *67*, 4808-4820.

- (243) Philip, I. E.; Kaifer, A. E. "Electrochemically driven formation of a molecular capsule around the ferrocenium ion." *J. Am. Chem. Soc.* **2002**, *124*, 12678-12679.
- (244) Rivera, J. M.; Craig, S. L.; Martin, T.; Rebek, J. "Chiral guests and their ghosts in reversibly assembled hosts." *Angew. Chem. Int. Ed.* **2000**, *39*, 2130-2132.
- (245) Vysotsky, M. O.; Thondorf, I.; Bohmer, V. "Hydrogen bonded calixarene capsules kinetically stable in DMSO." *Chem. Commun.* **2001**, 1890-1891.
- (246) Hirschberg, J.; Brunsveld, L.; Ramzi, A.; Vekemans, J.; Sijbesma, R. P.; Meijer, E. W. "Helical self-assembled polymers from cooperative stacking of hydrogen-bonded pairs." *Nature* **2000**, *407*, 167-170.
- (247) Fenniri, H.; Packiarajan, M.; Vidale, K. L.; Sherman, D. M.; Hallenga, K.; Wood, K. V.; Stowell, J. G. "Helical rosette nanotubes: Design, self-assembly, and characterization." *J. Am. Chem. Soc.* **2001**, *123*, 3854-3855.
- (248) Schaak, R. E.; Mallouk, T. E. "Perovskites by design: A toolbox of solid-state reactions." *Chem. Mat.* **2002**, *14*, 1455-1471.
- (249) Agasimundin, Y. S.; Oakes, F. T.; Kostuba, L. J.; Leonard, N. J. "Annulation of guanosine by reaction with methyl n-cyanomethanimidate and sodium methoxide to give a tricyclic, fluorescent analog of adenosine." *J. Org. Chem.* **1985**, *50*, 2468-2474.
- (250) Lagier, C. M.; Olivieri, A. C.; Harris, R. K. "NMR studies of proton transfer in 1:1 tris(trimethoxyphenyl)-phosphine oxide-phenol complexes." *J. Chem. Soc.-Perkin Trans. 2* **1998**, 1791-1796.
- (251) Walmsley, J. A.; Sagan, B. L. "The effect of monovalent cations on the association behavior of guanosine 5'-monophosphate, cytidine 5'-monophosphate, and their equimolar mixture in aqueous solution." *Biopolymers* **1986**, *25*, 2149-2172.

- (252) Hud, N. V.; Schultze, P.; Sklenar, V.; Feigon, J. "Binding sites and dynamics of ammonium ions in a telomere repeat DNA quadruplex." *J. Mol. Biol.* **1999**, *285*, 233-243.
- (253) Deng, H.; Braunlin, W. H. "Kinetics of sodium ion binding to DNA quadruplexes." *J. Mol. Biol.* **1996**, *255*, 476-483.
- (254) Wong, A.; Wu, G. "Selective binding of monovalent cations to the stacking G-quartet structure formed by guanosine 5'-monophosphate: A solid-state NMR study." *J. Am. Chem. Soc.* **2003**, *125*, 13895-13905.
- (255) Wlodarczyk, A.; Patkowski, A.; Grzybowski, P.; Dobek, A. "The effect of mono- and divalent cations on *Tetrahymena thermophila* telomeric repeat fragment. A photon correlation spectroscopy study." *Acta Biochim. Pol.* **2004**, *51*, 971-981.
- (256) Miyoshi, D.; Nakao, A.; Sugimoto, N. "Structural transition from antiparallel to parallel G-quadruplex of d(G(4)T(4)G(4)) induced by Ca²⁺." *Nucleic Acids Res.* **2003**, *31*, 1156-1163.
- (257) Kankia, B. I.; Marky, L. A. "Folding of the thrombin aptamer into a G-quadruplex with Sr²⁺: Stability, heat, and hydration." *J. Am. Chem. Soc.* **2001**, *123*, 10799-10804.
- (258) Smirnov, I.; Shafer, R. H. "Lead is unusually effective in sequence-specific folding of DNA." *J. Mol. Biol.* **2000**, *296*, 1-5.
- (259) Chen, F. M. "Sr²⁺ facilitates intermolecular g-quadruplex formation of telomeric sequences." *Biochemistry* **1992**, *31*, 3769-3776.
- (260) Fahlman, R. P.; Sen, D. "Cation-regulated self-association of "synapsable" DNA duplexes." *J. Mol. Biol.* **1998**, *280*, 237-244.
- (261) van Leeuwen, F. W. B.; Verboom, W.; Shi, X. D.; Davis, J. T.; Reinhoudt, D. N.

- "Selective $^{226}\text{Ra}^{2+}$ ionophores provided by self-assembly of guanosine and isoguanosine derivatives." *J. Am. Chem. Soc.* **2004**, *126*, 16575-16581.
- (262) Cai, M. M.; Shi, X. D.; Sidorov, V.; Fabris, D.; Lam, Y. F.; Davis, J. T. "Cation-directed self-assembly of lipophilic nucleosides: the cation's central role in the structure and dynamics of a hydrogen-bonded assembly." *Tetrahedron* **2002**, *58*, 661-671.
- (263) Shi, X. D.; Fettinger, J. C.; Cai, M. M.; Davis, J. T. "Enantiomeric self-recognition: Cation-templated formation of homochiral isoguanosine pentamers." *Angew. Chem. Int. Ed.* **2000**, *39*, 3124-3127.
- (264) Rebek, J. "Molecular recognition and the development of self-replicating systems." *Experientia* **1991**, *47*, 1096-1104.
- (265) Wintner, E. A.; Rebek, J. "Autocatalysis and the generation of self-replicating systems." *Acta Chem. Scand.* **1996**, *50*, 469-485.
- (266) Soai, K.; Shibata, T.; Sato, I. "Enantioselective automultiplication of chiral molecules by asymmetric autocatalysis." *Acc. Chem. Res.* **2000**, *33*, 382-390.
- (267) Kondepudi, D. K.; Asakura, K. "Chiral autocatalysis, spontaneous symmetry breaking, and stochastic behavior." *Acc. Chem. Res.* **2001**, *34*, 946-954.
- (268) Sidorov, V.; Kotch, F. W.; El-Khouedi, M.; Davis, J. T. "Toward artificial ion channels: self-assembled nanotubes from calix 4 arene-guanosine conjugates." *Chem. Commun.* **2000**, 2369-2370.
- (269) Liu, H.; Matsugami, A.; Katahira, M.; Uesugi, S. "A dimeric RNA quadruplex architecture comprised of two G: G(A): G: G(A) hexads, G: G: G: G tetrads and UUUU loops." *J. Mol. Biol.* **2002**, *322*, 955-970.
- (270) Rucker, C. "The triisopropylsilyl group in organic-chemistry - just a protective

group, or more." *Chem. Rev.* **1995**, *95*, 1009-1064.

- (271) Landschulz, W. H.; Johnson, P. F.; McKnight, S. L. "The leucine zipper - A hypothetical structure common to a new class of DNA-binding proteins." *Science* **1988**, *240*, 1759-1764.
- (272) Since the TIPS G-quadruplex is not stable, the regioselective ligand exchange with TBDMS-G into TIPS G-quadruplex yields results similar to those of the control experiments.
- (273) Kaucher, M. S.; Davis, J. T. "N2, C8-disubstituted guanosine derivatives can form G-quartets." *Tetrahedron Lett.* **2006**, *47*, 6381-6384.
- (274) Kaucher, M. S.; Harrell, W. A.; Davis, J. T. "A unimolecular G-quadruplex that functions as a synthetic transmembrane Na⁺ transporter." *J. Am. Chem. Soc.* **2006**, *128*, 38-39.
- (275) Chen, L.; Sakai, N.; Moshiri, S. T.; Matile, S. "Toward supramolecular ion channels formed by oligonucleotide analogs: Hydrophobic guanine dimers." *Tetrahedron Lett.* **1998**, *39*, 3627-3630.
- (276) Smith, B. D.; Lambert, T. N. "Molecular ferries: membrane carriers that promote phospholipid flip-flop and chloride transport." *Chem. Commun.* **2003**, 2261-2268.
- (277) Doyle, D. A.; Cabral, J. M.; Pfuetzner, R. A.; Kuo, A. L.; Gulbis, J. M.; Cohen, S. L.; Chait, B. T.; MacKinnon, R. "The structure of the potassium channel: Molecular basis of K⁺ conduction and selectivity." *Science* **1998**, *280*, 69-77.
- (278) Sakai, N.; Brennan, K. C.; Weiss, L. A.; Matile, S. "Toward biomimetic ion channels formed by rigid-rod molecules: Length-dependent ion-transport activity of substituted oligo(p-phenylene)s." *J. Am. Chem. Soc.* **1997**, *119*, 8726-8727.
- (279) Sidorov, V.; Kotch, F. W.; Kuebler, J. L.; Lam, Y. F.; Davis, J. T. "Chloride

transport across lipid bilayers and transmembrane potential induction by an oligophenoxyacetamide." *J. Am. Chem. Soc.* **2003**, *125*, 2840-2841.

- (280) Sakai, N.; Kamikawa, Y.; Nishii, M.; Matsuoka, T.; Kato, T.; Matile, S. "Dendritic folate rosettes as ion channels in lipid bilayers." *J. Am. Chem. Soc.* **2006**, *128*, 2218-2219.
- (281) Talukdar, P.; Bollot, G.; Mareda, J.; Sakai, N.; Matile, S. "Ligand-gated synthetic ion channels." *Chem. -Eur. J.* **2005**, *11*, 6525-6532.
- (282) Gorteau, V.; Bollot, G.; Mareda, J.; Pasini, D.; Tran, D. H.; Lazar, A. N.; Coleman, A. W.; Sakai, N.; Matile, S. "Synthetic multifunctional pores that open and close in response to chemical stimulation." *Bioorg. Med. Chem.* **2005**, *13*, 5171-5180.
- (283) Talukdar, P.; Bollot, G.; Mareda, J.; Sakai, N.; Matile, S. "Synthetic ion channels with rigid-rod pi-stack architecture that open in response to charge-transfer complex formation." *J. Am. Chem. Soc.* **2005**, *127*, 6528-6529.
- (284) Qu, Z. Q.; Hartzell, H. C. "Anion permeation in Ca²⁺-activated Cl(-) channels." *J. Gen. Physiol.* **2000**, *116*, 825-844.
- (285) Smart, O. S.; Breed, J.; Smith, G. R.; Sansom, M. S. P. "A novel method for structure-based prediction of ion channel conductance properties." *Biophys. J.* **1997**, *72*, 1109-1126.
- (286) Eisenman, G.; Horn, R. "Ionic selectivity revisited - The role of kinetic and equilibrium processes in ion permeation through channels." *J. Membr. Biol.* **1983**, *76*, 197-225.
- (287) ten Cate, M. G. J.; Crego-Calama, M.; Reinhoudt, D. N. "Formation of a hydrogen-bonded receptor assembly in niosomal membranes." *J. Am. Chem. Soc.* **2004**, *126*, 10840-10841.

- (288) Stankiewicz, T.; Jurczak, J. "Self-assembly in organic synthesis." *Pol. J. Chem.* **1992**, *66*, 1743-79.
- (289) Diederich, F.; Stang, P. J., *Templated Organic Synthesis*. Wiley-VCH: Weinheim, **2000**.
- (290) Pedersen, C. J. "Cyclic polyethers and their complexes with metal salts." *J. Am. Chem. Soc.* **1967**, *89*, 7017-7036.
- (291) Liu, F.; J., S. R.; Seeman, N. C. "Self-assembly and modification of two-dimensional DNA crystals." *J. Am. Chem. Soc.* **1999**, *121*, 917-922.
- (292) Clark, T. D.; Buriak, J. M.; Kobayashi, K.; Isler, M. P.; McRee, D. E.; Ghadiri, M. R. "Cylindrical β -sheet peptide assemblies." *J. Am. Chem. Soc.* **1998**, *120*, 8949-8962.
- (293) Clark, T. D.; Kobayashi, K.; Ghadiri, M. R. "Covalent capture and stabilization of cylindrical beta-sheet peptide assemblies." *Chem.-Eur. J.* **1999**, *5*, 782-792.
- (294) Paraschiv, V.; Crego-Calama, M.; Fokkens, R. H.; Padberg, C. J.; Timmerman, P.; Reinhoudt, D. N. "Nanostructures via noncovalent synthesis: 144 hydrogen bonds bring together 27 components." *J. Org. Chem.* **2001**, *66*, 8297-8301.
- (295) Cardullo, F.; Calama, M. C.; Snellink-Ruel, B. H. M.; Weidmann, J. L.; Bielejewska, A.; Fokkens, R.; Nibbering, N. M. M.; Timmerman, P.; Reinhoudt, D. N. "Covalent capture of dynamic hydrogen-bonded assemblies." *Chem. Commun.* **2000**, 367-368.
- (296) Arico, F.; Badjic, J. D.; Cantrill, S. J.; Flood, A. H.; Leung, K. C. F.; Liu, Y.; Stoddart, J. F., "Templated synthesis of interlocked molecules." *Top. Curr. Chem.* **2005**, *249*, 203-259.
- (297) Gibson, H. W.; Bheda, M. C.; Engen, P. T. "Rotaxanes, catenanes, polyrotaxanes,

polycatenanes and related materials." *Prog. Polym. Sci.* **1994**, *19*, 843-945.

- (298) Zhang, Q.; Hamilton, D. G.; Feeder, N.; Teat, S. J.; Goodman, J. M.; Sanders, J. K. M. "Synthesis and post-assembly modification of some functionalized, neutral π -associated [2]catenanes." *New J. Chem.* **1999**, *23*, 897-903.
- (299) Rowan, S. J.; Stoddart, J. F. "Precision molecular grafting: Exchanging surrogate stoppers in [2]rotaxanes." *J. Am. Chem. Soc.* **2000**, *122*, 164.
- (300) Gubala, V.; De Jesus, D.; Rivera, J. M. "Self-assembled ionophores based on 8-phenyl-2'-deoxyguanosine analogous." *Tetrahedron Lett.* **2006**, *47*, 1413-1416.
- (301) Koizumi, M.; Akahori, K.; Ohmine, T.; Tsutsumi, S.; Sone, J.; Kosaka, T.; Kaneko, M.; Kimura, S.; Shimada, K. "Biologically active oligodeoxyribonucleotides. Part 12: N-2-methylation of 2'-deoxyguanosines enhances stability of parallel G-quadruplex and anti-HIV-1 activity." *Bioorg. Med. Chem. Lett.* **2000**, *10*, 2213-2216.
- (302) He, G. X.; Krawczyk, S. H.; Swaminathan, S.; Shea, R. G.; Dougherty, J. P.; Terhorst, T.; Law, V. S.; Griffin, L. C.; Coutre, S.; Bischofberger, N. "N-2- and C-8-substituted oligodeoxynucleotides with enhanced thrombin inhibitory activity in vitro and in vivo." *J. Med. Chem.* **1998**, *41*, 2234-2242.
- (303) Chantot, J. F.; Guschlbauer, W. "Physicochemical properties of nucleosides 3. Gel formation by 8-bromoguanosine." *FEBS Lett.* **1969**, *4*, 173-176.
- (304) Wang, L. Y.; Vysotsky, M. O.; Bogdan, A.; Bolte, M.; Bohmer, V. "Multiple catenanes derived from calix[4]arenes." *Science* **2004**, *304*, 1312-1314.
- (305) Liu, X.; Kwan, I. C. M.; Wang, S.; Wu, G. "G-Quartet formation from an N2-modified guanosine derivative." *Org. Lett.* **2006**, *8*, 3685-3688
- (306) Amer, M. S.; Amer, A. M.; Ahmed, A. F. S.; Farouk, W. M. "Synthesis of some

modified guanosine derivatives." *Indian J. Chem. Sect B-Org. Chem. Incl. Med. Chem.* **2001**, *40*, 382-385.

- (307) Sako, M.; Kawada, H.; Hirota, K. "A convenient method for the preparation of N-2-ethylguanine nucleosides and nucleotides." *J. Org. Chem.* **1999**, *64*, 5719-5721.
- (308) Bouhoutsosbrown, E.; Marshall, C. L.; Pinnavaia, T. J. "Structure-directing properties of Na⁺ in the solution ordering of guanosine 5'-monophosphate - Stoichiometry of aggregation, binding to ethidium, and modes of Na⁺ complexation." *J. Am. Chem. Soc.* **1982**, *104*, 6576-6584.
- (309) Borzo, M.; Detellier, C.; Laszlo, P.; Paris, A. "H-1, Na-23, and P-31 NMR-studies of the self-assembly of the 5'-guanosine monophosphate dianion in neutral aqueous-solution in the presence of sodium-cations." *J. Am. Chem. Soc.* **1980**, *102*, 1124-1134.
- (310) Scholl, M.; Ding, S.; Lee, C. W.; Grubbs, R. H. "Synthesis and activity of a new generation of ruthenium-based olefin metathesis catalysts coordinated with 1,3-dimesityl-4,5-dihydroimidazol-2-ylidene ligands." *Org. Lett.* **1999**, *1*, 953-956.
- (311) Grubbs, R. H. "Olefin metathesis." *Tetrahedron* **2004**, *60*, 7117-7140.
- (312) Elmer, S. L.; Zimmerman, S. C. "Cross-linking dendrimers with allyl ether end-groups using the ring-closing metathesis reaction." *J. Org. Chem.* **2004**, *69*, 7363-7366.
- (313) Wendland, M. S.; Zimmerman, S. C. "Synthesis of cored dendrimers." *J. Am. Chem. Soc.* **1999**, *121*, 1389-1390.
- (314) Kano, K.; Fendler, J. H. "Pyranine as a sensitive pH probe for liposome interiors and surfaces - pH gradients across phospholipid vesicles." *Biochim. Biophys. Acta* **1978**, *509*, 289-299.

- (315) Wallace, B. A. "Gramicidin channels and pores." *Ann. Rev. Biophys. Biophys. Chem.* **1990**, *19*, 127-157.
- (316) van Mourik, T.; Dingley, A. J. "Characterization of the monovalent ion position and hydrogen-bond network in guanine quartets by DFT calculations of NMR parameters." *Chem. -Eur. J.* **2005**, *11*, 6064-6079.
- (317) Van Leeuwen, F. W. B.; Miermans, C. J. H.; Beijleveld, H.; Tomasberger, T.; Davis, J. T.; Verboom, W.; Reinhoudt, D. N. "Selective removal of $^{226}\text{Ra}^{2+}$ from gas-field-produced waters." *Environ. Sci. Technol.* **2005**, *39*, 5455-5459.
- (318) Davis, J. T.; Tirumala, S.; Jenssen, J. R.; Radler, E.; Fabris, D. "Self-assembled ionophores from isoguanosine." *J. Org. Chem.* **1995**, *60*, 4167-4176.
- (319) Nowak, I.; Robins, M. J. "Protection of the amino group of adenosine and guanosine derivatives by elaboration into a 2,5-dimethylpyrrole moiety." *Org. Lett.* **2003**, *5*, 3345-3348.
- (320) Sessler, J. L.; Jayawickramarajah, J.; Sathiosatham, M.; Sherman, C. L.; Brodbelt, J. S. "Novel guanosine-cytidine dinucleoside that self-assembles into a trimeric supramolecule." *Org. Lett.* **2003**, *5*, 2627-2630.
- (321) Pike, M. M.; Simon, S. R.; Balschi, J. A.; Springer, C. S. "High-resolution NMR-studies of transmembrane cation-transport - Use of an aqueous shift-reagent for Na-23." *Proc. Natl. Acad. Sci. U.S.A.* **1982**, *79*, 810-814.